UNIVERSITÉ DU QUÉBEC

THÈSE

PRÉSENTÉE À

L'UNIVERSITÉ DU QUÉBEC À CHICOUTIMI

COMME EXIGENCE PARTIELLE

DU DOCTORAT EN RESSOURCES MINÉRALES

PAR

YONGZHANG ZHOU

GÉOCHIMIE ET MÉCANISME MÉTALLOGÉNIQUE

DU DISTRICT AURIFERE DE HETAI, SUD DE LA CHINE

JUIN 1992

Mise en garde/Advice

GEOCHEMISTRY AND METALLOGENETIC MECHANISM OF THE HETAI GOLD FIELD, SOUTHERN CHINA

BY

YONGZHANG ZHOU

UNIVERSITÉ DU QUÉBEC À CHICOUTIMI

AND

INSTITUTE OF GEOCHEMISTRY, ACADEMIA SINICA

JUNE 1992

ABSTRACT

The Hetai gold field, located in western Guangdong Province, is the biggest found in the Yunkai Terrain, southern China. The objective of this study is to characterize the geological and geochemical features of the Hetai gold field, to understand the geochemical behavior of gold in the history of mineralization, and to establish a reasonable metallogenetic model.

The country rocks are principally metamorphosed Sinian (Late Precambrian) series, which developed in a medium or medium-low pressure metamorphic facies series during the Caledonian period. The protolith is mainly pelitic or semi-pelitic rocks, intercalated with bedded cherts. Petrographic evidence suggests that the bedded cherts within the Sinian strata are the product of a fossil geothermal system, which is favored by geochemical analysis. The cherts have a geochemical affinity to typical hydrothermal cherts.

The migration pattern of impurity trace elements in source rocks can be described by a fractal structure of entrapment paths. Ideally there are two migration tendencies for trace elements. One is from within bulk solid cells toward various entrapment paths. The other is from a high temperature field to a lower one. High temperature accelerates the realization of these two tendencies. Diffusion is an important type of element reactivation, which is essentially a kind of oriented short-range mass transport within bulk solid cells and low rank entrapment paths.

The ore is predominantly auriferous altered mylonites within hydrothermally altered ductile shear zones. At all scales, the characteristic pattern of shear deformation is anastomosing domains of higher deformation separating rhomboid domains of lower deformation. Hydrothermal alteration is both spatially and temporally associated with the development of the shear deformation system. The alteration products are principally quartz and sulfides. Gold precipitation is an integral part of the hydrothermal alteration system, and culminated during the formation of the second generation of sulfidation.

Fluid inclusion study demonstrates that the primary ore-forming hydrothermal solution is a H_2O-$NaCl$-CO_2-dominated system, characterized by a low-salinity (about 1.5 - 6 equiv. wt.% $NaCl$) and bearing CO_2. Moderate-salinity aqueous fluid and CO_2-

dominated fluid were caused by CO_2 effervescence and an unmixing of the primary hydrothermal fluid.

The Hetai gold deposits are the result of the integration of polystage geological and geochemical processes. Sedimentation, regional metamorphism, granitic magmatism, deformation and hydrothermal activities, have all contributed to the formation of the gold deposits. During the Precambrian to Cambrian period, a thick potential source strata was deposited. Coeval hydrothermal activity may have participated in the preliminary enrichment of gold in the source rock. The Caledonian regional metamorphism played a basic role to redistribute the gold in the source strata. There are two general tendencies for gold to migrate during metamorphism. One is from within host minerals toward the weaknesses of rocks, where gold is more accessible in subsequent events. The other tendency is from higher grade metamorphic domains toward low ones.

The Hercyno-Indosinian period is the main stage of the gold mineralization history of the Hetai gold field. Gold emplacement occurred along altered shear deformation zones. The temperature drop, sudden release of pressure, and the accompanying unmixing of the primary low salinity hydrothermal fluid are key factors leading gold precipitation out of the hydrothermal solution. The Yunluogan and Wucun granites are not the main source of gold, but provided the heat source necessary for the circulation of the hydrothermal fluid, which is a mixture of meteoric water and metamorphic water.

Géochimie et Mécanisme Métallogénique du District Aurifère de Hetai, Sud de la Chine

(Résumé en Français)

Le district aurifère de Hetai est situé au sud de la Chine, dans le terrain métamorphique de Yunkai, qui est limité à l'est par le système de failles de Wuchuan - Sihui, et à l'ouest par le système de failles de Bobai - Wuzhou. Il représente le plus grand camp minier aurifère découvert à l'ouest de la province de Guangdong. Les dépôts aurifères avec des réserves prouvées incluent les gîtes de Gaocun, Yunxi, Taipingding, Shangtai, Kangmei, Taozhishan, Huojing et Hehai. À part le gîte de Hehai, tous ces gîtes sont de type hydrothermale dans une zone de mylonite. Le gîte de Hehai est constitué de veines de quartz.

L'encaissant principal des gisements d'or est la strate Sinienne. Cette unité est composée de roches métamorphiques variées, avec les schistes, les quartzites schisteuses et les migmatites constituant les roches encaissantes immédiates des dépôts aurifères. Les intrusions granitiques de Wucun et de Yunluogan se rencontrent au nord et à l'ouest, alors que les granites (migmatitiques) de Shidong en occupent l'extrémité Nord - Ouest.

1. Métamorphisme régional et granites

Les roches métamorphiques de la région de Hetai consistent principalement en des schistes, des quartzites schisteux, ainsi que de migmatites. On retrouve aussi des métasédiments de bas degré de métamorphisme au sud-est des dépôts aurifères. La paragenèse minérale caractéristique des schistes dominant est quartz + muscovite + biotite ± staurolite ± sillimanite ± almandine. Ces minéraux se sont développés dans des séries de faciès métamorphiques de moyenne à basse pression, au cours de l'orogénie Calédonienne. La température et la pression auxquelles les schistes se sont formés varient respectivement entre 550° - 670°C et 230 - 600 MPa. Les protolithes sont principalement des roches pélitiques avec des cherts intercalés.

Les migmatites font partie intégrante des séries métamorphiques de Hetai et représentent les roches les plus intensément métamorphisées de la région. La formation des migmatites est caractérisée par une introduction graduelle de SiO2, de K2O et probablement de Na2O. En général, les migmatites de Hetai sont appauvries en la plupart des éléments métalliques, particulièrement les éléments "chalcophiles", en comparaison avec les schistes de Hetai. Seuls quelques éléments incompatibles, tels Rb, Ta, Nb, Hf, Zr et Sc, sont restés inchangés ou se sont enrichis. La concentration des éléments traces était contrôlée par deux processus différents: la tendance naturelle de la migration des éléments traces des domaines de haute température vers les domaines de basse température et l'introduction des éléments incompatibles accompagnant l'injection du magma dérivé de la fusion partielle du protolithe. En général, les migmatites ont hérité du patron de la distribution de ETR des schistes, avec une légère préférence en Terres Rares Lourdes plutôt qu'en Terres Rares Légères.

L'occurrence des granites est spectaculaire dans la région de Hetai. Les granites de Shidong, Yunluongan et Wucun représentent une séquence complète d'évolution du granitisme de l'autochtone au parautochtone jusqu'aux intrusions magmatiques. Le granite de Shidong s'est développé au cours de la période Calédonienne et a la même origine que les migmatites du même âge. Les granites de Yunluogan et de Wucun se sont formés durant la période Hercyno-Indosinienne. Les isotopes stables de Sr et de O suggèrent que ces granites sont dérivés de la croûte supérieure. Le granite de Wucun contiendrait probablement certains matériaux d'une source plus profonde.

2. Les cherts lités: caractéristiques pétrologiques et géochimiques et origine

Les cherts lités étudiés se trouvent dans la section de Gusui et font partie du membre supérieur (Z^d) des strates du système Sinien (Précambrien). Le quartz microcristallin prédomine. Les minéraux accessoires incluent les minéraux argileux, l'hématite, la barite et occasionnellement la pyrite. Les structures litées, laminées, massives et pseudobréchiques ont été identifiées. Les caractéristiques pétrographiques suggèrent une origine hydrothermale pour la formation des cherts. La structure pseudobréchique non-déformée ainsi que le faible degré de compaction, résulteraient de la précipitation rapide de la silice opaline et de la transformation de la silice opaline en quartz microcristallin.

Les cherts lités sont caractérisés par des valeurs régulièrement faibles de TiO2, Al2O3, K2O, et de la plupart des éléments métalliques. Cependant, ils sont enrichis en Ba,

As, Sb, Hg et Se, lesquels éléments sont diagnostiques des dépôts hydrothermaux. Dans le diagramme ternaire Al - Fe - Mn, ils tombent dans le "champ hydrothermal". Ces évidences géochimiques sont également en faveur d'une origine hydrothermale pour les cherts de la section Gusui.

Les associations caractéristiques d'éléments sont effectivement reconnues par l'analyse factorielle et l'analyse de correspondance. Parmi les associations caractéristiques, {As, Cu, -Cr}, {Ba, Hg, -Sn} et {Ba, Pb} sont diagnostiques des dépôts hydrothermaux. La plupart des éléments en traces trouvent leur réflexion dans le facteur de lessivage de la solution hydrothermale à travers les roches encaissantes pendant l'ascension. En plus des faibles teneurs en MnO, les facteurs d'éléments majeurs, {MnO, FeO, MgO} et {Fe2O3}, indiquent que la formation des cherts résulteraient de l'environment sédimentaire oxydant, avec une réduction épisodique et locale.

Considérant la teneur totale en terres rares, on distingue deux membres extrêmes: le chert hydrothermal pur et le shale hydrogéné. Le premier est caractérisé par une teneur totale faible en ETR. La teneur totale en ETR des cherts impurs varie selon la contribution de shale hydrogéné aux cherts hydrothermaux. Le patron de distribution des teneurs moyennes en terres rares (normalisées par rapport à NASC) des cherts de Gusui varie entre les limites supérieures et inférieures des dépôts hydrothermaux typiques connus. L'anomalie ambiguë de Ce et la teneur très élevée en terres rares de certains échantillons sont attribuées à la contamination des dépôts hydrothermaux par les dépôts hydrogénés. Deux modes de contamination sont plus probables: d'une part, l'alternance des processuss hydrothermaux et hydrogénés; d'autre part, leur présence commune dans le même domaine de temps et espace, avec divers taux de contribution.

Un mécanisme de formation est proposé. D'abord, l'eau de mer froide et dense s'infiltrait le long de fractures qui recoupaient l'ancien sousbassement tectonique et les strates du géosynclinal marginal pré-Calédonien du sud de la Chine. Dans sa marche descendante, l'eau de mer pénétrante était réchauffée et réduite par réaction avec des roches encaissantes près d'une source de chaleur inconnue située à une certaine profondeur. En continuant d'évoluer, les solutions hydrothermales ont lessivé les roches encaissantes qu'elles traversaient, et gagées ainsi la masse. Finalement, les solutions hydrothermales "primaires" riches en silice remontèrent. Près de la sortie, elles sont déchargées et mélangées avec l'eau de mer ambiante. Une partie de la silice est précipitée sous forme de silice amorphe ou de calcédoine. L'autre est perdue dans les eaux du fond marin local, et transportée assez loin pour se déposer ultérieurement, associée aux processus hydrogénés. Le quartz microcristallin est le résultat de la recristallisation de la phase silice amorphe et de la calcédoine précipitées initialement.

3. Migration des éléments traces pendant les événements thermaux: modèle de mosaïque incrusté de pièges

La relation entre l'infiltration, le flux de fluides et la diffusion n'en est pas une de substitution, mais de superposition. Malgré la grande efficacité de l'infiltration et du flux de fluides dans le transport des éléments, la diffusion reste vitale pour la migration des éléments traces, particulièrement lorsqu'un solide parfait est considéré, là où il n'y a pas de convection du fluide.

Le concept de piège est une abstraction mathématique de l'imperfection de l'ensemble des solides, et du comportement différent des éléments traces dans les solides et leurs imperfections. En réalité, les imperfections, telles les surfaces subgranulaires ou granulaires, les micro-fissures, les fractures, etc., existent dans toutes les roches et les domaines géologiques. Elles sont souvent remplies de solutions, donc sont beaucoup plus efficaces pour la diffusion des éléments traces que les cellules des solides hôtes, qui sont parfaits au point de vue structural.

Les pièges peuvent être profonds de plusieurs couches ou niveaux, correspondant à une séries des coefficients de diffusion entre les limites du solide et du fluide. À chaque niveaux, plusieurs pièges et cellules de solides forment une mosaïque. Le modèle de mosaïque incrusté de pièges est une référence d'ordre hiérarchique des différents lits du mosaïque (mosaïques sont incrustés dans une mosaïque plus grande). Il a une structure de self-similarité, et donc est une structure fractale.

Selon le modèle de mosaïque incrusté de pièges, il y a deux tendances de migration des éléments traces. La première est que les éléments traces tendent d'émigrer à la sortie des cellules des solides et s'enrichissent dans les zones de faiblesse. A travers divers grades de pièges, les éléments traces rejoindront finalement une solution aqueuse qui remplit les fractures suffisamment grandes. L'autre tendance est celle de la migration des éléments des champs de haute température vers les domaines de basse température. Les hautes températures et le gradient croissant de température favorisent l'établissement de ces tendances.

La réactivation des éléments par diffusion est un transport de masses orienté de courte distance à l'intérieur des solides et des pièges des rangs inférieurs. La trajectoire est en accord avec la tendance de migration des éléments traces dans le modèle de mosaïque incrusté de pièges.

La conjugaison des anomalies géochimiques est une conséquence inévitable d'un système géochimique fermé. Deux environnements géologiques sont particulièrement favorables au développement à grande échelle d'anomalies géochimiques conjuguées, e.g., les régions avec un grand contraste de distribution des températures, et un système de grandes failles. De telles conjugaisons d'anomalies, lorsqu'elles se superposent à l'anomalie géochimique régionale, pourraient devenir un excellent guide pour l'exploration et l'évaluation des gisements.

4. Déformation de cisaillement ductile et l'altération hydrothermale liée à la formation des minerais

Les minerais du camp minier de Hetai sont souvent constitués de mylonites aurifères altérées. Les zones de cisaillement ductile Hercyno-Indosinienne et les altérations hydrothermales associées contrôlent la formation et l'occurrence des dépôts aurifères de Hetai.

La géométrie des structures internes des zones individuelles de cisaillement sont similaires aux patrons des zones de cisaillement dans le système de cisaillement. À toutes les échelles, le patron caractéristique est constitué de domaines anastomosés fortement déformés, séparant les domaines rhomboïdes de faible déformation. À travers une seule zone de cisaillement ductile, la déformation s'accroît graduellement de l'extérieur vers l'intérieur de la zone, et les roches déformées varient des roches primaires non-déformées aux mylonites et, localement, aux ultramylonites, en passant par les protomylonites.

L'altération hydrothermale de la roche encaissante est spatialement et temporellement associée au développement du système de cisaillement ductile. L'altération produit principalement la chlorite, la séricite, le quartz, les sulfures et l'ankérite. Dans les roches altérées, on distingue au moins trois générations de quartz: un quartz pré-mylonitisation, le quartz hydrothermal de premier stade et le quartz hydrothermal associé aux sulfures. De plus, il y a deux générations des sulfures. La première consiste en pyrite idiomorphe à gros grains, et l'autre, en chalcopyrite et pyrite xenomorphes à grains fins.

La précipitation de l'or est essentiellement un type spécial d'altération hydrothermale. L'or natif, la chalcopyrite, la pyrite sont parmi les minéraux économiques les plus importants. Ils sont disséminés dans la roche minéralisée.

Le calcul de bilan de masses montre un gain de masse durant l'altération, avec un facteur de masse moyen de 1 : 0.92. Le gain de masse arrive à son maximum dans le minerai (les roches intensément altérées qui sont caractérisées par la présence de sulfures et

le quartz associé), avec un facteur de masse moyen de 1 : 0.84. La silice, les métaux précieux et la plupart des éléments chalcophiles, comme Bi, Cu, Hg, Sb, Se, Te, Zn, Co et probablement As, font partie des constituants ajoutés. La soude ainssi que la plupart des éléments lithophiles caractéristiques du socle de la Chine méridionale, comme Cs, Hf, Zr, Nb, Sc, Th, Ba et Terre Rares, sont appauvris durant l'altération et la minéralisation. D'autres éléments, comme K_2O, Rb, U, Ta et W, ont été d'abord ajoutés, puis lessivés par la suite lors de l'étape tardive d'intense minéralisation.

Le patron de distribution (normalisé par rapport aux chondrites) des terres rares des strates hôtes altérées est comparable à celui du minerai, avec un faible déplacement vers le bas et peu de différentiation interne entre les terres rares, comparé à la moyenne des strates non-altérées. Ce déplacement cohérent vers le bas est attribué en partie à la dilution résultant de l'introduction de masse comme la silicification, ainsi qu'au lessivage des terres rares.

Les pegmatites granitiques altérées ont un patron de distribution des ETR complètement différent de celui du minerai. Elles sont caractérisées par un patron irrégulier en forme de W, une très faible teneur totale en ETR et des terres rares lourdes relativement enrichies par rapport aux terres rares légères.

5. Géochimie des inclusions fluides

La plupart des inclusions fluides sont d'origine secondaire en relation avec le quartz hôte, et se situent le long des fractures cicatrisées. Cependant, les évidences minéralogiques indiquent qu'elles se sont formées pas plus tard que la dernière épisode de minéralisation aurifère. La précipitation de l'or est étroitement associée dans le temps et dans l'espace avec le piégeage de ces inclusions fluides.

On distingue trois types de composition dans ces inclusions fluides: des fluides aqueux contenant au CO_2 à basse salinité (environ 1.5 - 6 poids% équivalent de NaCl), des fluides aqueux à salinité modérée (environ 6 - 14 poids% équivalent de NaCl) et des inclusions très riches en CO_2. Tous ces types d'inclusions fluides sont contemporaines. Leur température d'homogénéisation varie entre 130° et 310°C, avec deux modes statistiques autour de 245° et 170°C. Les inclusions fluides à basse salinité sont considérées comme des solutions hydrothermales primaires. Il s'agit d'un système hydrothermal dominé par de H_2O-NaCl-CO_2, avec une présence probable de Ca^{2+} et H_2S.

L'effervescence de CO_2 et la séparation des phases ont alternativement pris place pendant l'évolution de la solution hydrothermale primaire. Dans les deux cas, le CO_2

s'échappait de la solution hydrothermale, avec presque tous les métaux restant dans la phase aqueuse résultante. Deux événements de séparation des phases à grande échelle sont supposés avoir pris place à 245° et 170°C.

6. Mécanisme métallogénique

Les dépôts aurifères de Hetai sont un produit cumulatif d'étapes multiples de processuss géologiques et géochimiques. La sédimentation, le métamorphisme régional, le magmatisme granitique, la déformation et les activités hydrothermales ont contribué à la formation des dépôts aurifères.

Les strates Sinienne et Cambrienne sont la principale source de l'or, comme l'indique les évidences des éléments en traces, des terres rares et des isotopes. La présence d'un système hydrothermal fossile, indiqué par l'existence des cherts lités hydrothermale de Z^d, suggère la possibilité que des activités hydrothermales de géosystème fossile ont contribué à la concentration préliminaire de l'or durant les périodes Sinienne et Cambrienne.

Le métamorphisme régional Calédonien a joué un rôle principal dans la remobilisation et le transport de l'or existant dans les strates hôtes. Il y a eu deux tendances générales de migration de l'or durant le métamorphisme. L'une consiste en la migration de l'or à partir des cellules des solides vers les zones de faiblesse des roches. L'autre tendance de migration est celle des champs de haute température vers ceux de basse température.

La période Hercyno-Indosinienne représente l'étape principale de la minéralisation aurifère du camp de Hetai. La mise en place de l'or était contrôlée par les zones de déformation et l'altération hydrothermale associée. La baisse de la température, la libération soudaine de la pression, la séparation des phases de la solution hydrothermal primaire de basse salinité en une phase à dominance de CO_2 et une phase aqueuse à salinité modéré, ainsi que l'interaction des fluides avec du fer des roches encaissantes, constituent les facteurs clés de précipitation de l'or de la solution hydrothermale. Sur la base des observations pétrographiques et minéralogiques, la déposition de l'or a connu son point culminant durant la déposition de la seconde génération des sulfures.

Les granites de Yunluogan et de Wucun ne constituent pas la principale source de l'or, mais ils ont fourni la source de chaleur nécessaire à la circulation des fluides hydrothermaux. Ces fluides consistent en eaux météoriques et métamorphiques, comme l'indique les évidences d'inclusions fluides et l'étude des isotopes d'oxygène et d'hydrogène.

ACKNOWLEDGEMENTS

TABLE OF CONTENTS

Chapter 1

Chapter 2

Chapter 3

BEDDED CHERTS: PETROLOGIC AND GEOCHEMICAL CHARACTERISTICS
AND ORIGIN 53...

Chapter 4

MIGRATION OF TRACE ELEMENTS DURING THERMAL EVENTS 100

Chapter 5

DUCTILE SHEAR DEFORMATION AND HYDROTHERMAL ALTERATION
RELATED TO ORE FORMATION 120

Chapter 6

GEOCHEMISTRY OF HYDROTHERMAL FLUID INCLUSIONS................... 165

§ 1 Occurrence of Fluid Inclusions **165**

Chapter 8

LIST OF FIGURES

LIST OF TABLES

LIST OF PLATES

INTRODUCTION

Of all elements, gold has been the most esteemed by man since earliest times (Boyle, 1979). It is used in many aspects. Traditionally, it is used in ornamentation and as a monetary unit. Today, it finds more and more use in industrial fields, and the world's demand for gold seems never to decrease.

The recent wave of gold exploration started in the early 1970s (Craigie, 1986). The wave was further motivated by the rise of the price of gold from about U.S.$200 an ounce in 1979 to nearly $700 an ounce by the end of the same year, and finally led to the gold rush of the 1980s (Keays and Skinner, 1988). It is estimated that 75 to 85 percent of the present world's exploration dollars are invested in the search for precious metals, with gold as the principal target (Barber, 1985).

With the exploration wave, new concepts of geological and geochemical environments favorable for gold, and improved exploration methodology were put forward and have borne fruit, as summarized in a series of volumes and papers, including *Gold '82: The Geology, Geochemistry and Genesis of Gold Deposits* (Foster, 1984), *Proceedings of Gold '86,* (Macdonald, 1986), *Archean Lode Gold Deposits in Ontario* (Colvine et al., 1988), *The Geology of Gold Deposits: The Perspective in 1988* (Keays et al., 1989) and others (e.g., Groves and Phillips, 1987; Colvine et al., 1984; Guha et al, 1988; Hugon, 1986; Kerrich, 1989; Phillips and DeNooy, 1988; Rogers, 1979; Spooner et al., 1987).

The major contributors to the 1980s' increased stream of gold have been Australia, Canada, Brazil and United States on the base of statistics from available data (Keays and Skinner, 1988). The discovery and geological setting of gold deposits in China, one of the largest countries, is less well known outside this country. Therefore significant gold deposits of this country should be introduced to the world, which will enrich the study of gold deposits in general.

Previous Work

Western Guangdong Province (including part of southeastern Guangxi Zhang Autonomous Region) is one of the traditional gold-producing areas of China. Gold deposits and showings are widely scattered throughout this area. These deposits, however, are mostly small in terms of proven gold reserves and are not suitable for mining at a large industrial scale. This situation has changed radically since the Hetai gold field was first discovered in 1982 by two peasants and then proved by geological exploration teams.

The Hetai gold field is the biggest so far discovered in the western Guangdong area. The proven gold reserves are more than 30 tonnes. Its discovery enhanced the early 1980s' gold rush in southern China, and encouraged geological exploration for similar types of gold mineralization in pre-Devonian metamorphic strata of similar tectonic units.

Regional geological investigations, concentrating on paleontology, stratigraphy, petrology and tectonics, had been carried out over the whole western Guangdong area before the discovery of the Hetai gold field, and several recent geological maps (1/200,000) and reports on the area are available (Guangdong Bureau of Geology, 1977; Institute of Geochemistry, 1979; Mo and Ye, 1980; Fu, 1985; Guangxi Bureau of Geology and Resources, 1985; Liu, 1989; Nan, 1989). A general idea of the geological setting of the area under study may be derived from these publications.

Individual representative deposits of the Hetai gold field have been studied on the deposit scale, and several major geological factors controlling the localization of ores proposed. The basic geological features of the Gaocun gold deposit were described by No.719 Geology Team (1987) and Dai (1986). The geological features of the Yunxi gold deposit, as well as the difference of host rocks between the Gaocun and Yunxi ore deposits, were described by Xiao (1990). In comparison to the Gaocun ore deposit, where schists are the major country rock, the Yunxi ore deposit has more migmatite as its host rock. The Sinian and Cambrian strata were considered the favorable source strata of gold by Chen et al. (1988), whereas it was argued (Fu, 1988; 1989; Huang, 1988) that Yunluogan and Wucun granites be involved in the formation of the Hetai gold deposits. The shear zone that controlled the emplacement of gold was described by Ling (1988), Yuan and Huang (1990), Duan (1986, unpublished), Ye (1988, unpublished) and Ma (1989).

Proposed Study

Despite the previous work, however, there are still many geological and geochemical problems to be solved, e.g., the initial source of gold, the geochemical behavior of gold during metamorphism, and the role of granites, the interdependence of geological factors controlling the formation of the gold deposits. The solution of these problems and establishment of a sound deposit model appears essential for evaluating the potential of gold and further gold prospecting in the Hetai gold field. It may also affect the philosophy of the choice of target district in similar geological units, and contribute to the understanding of the emplacement of gold deposits.

Gold is many things to many men. To the geochemist and economic geologist, it is a rare element, whose geochemistry is intricate and complex. It presents a challenge of both prospecting philosophy and mineralization theory (Boyle, 1979). The general objective of the present thesis is to characterize the geological and geochemical features of the Hetai gold field, to understand the geochemical behavior of gold in the history of mineralization, and to establish a detailed and plausible metallogenetic model, which explains the factors controlling the ore emplacement. During the realization of the thesis, the following problems are carefully addressed.

Regional Geological Setting

This part includes the description of tectonic background, strata, regional metamorphic rocks, granites, as well as the spatial distribution of gold deposits. It is the basis to understand the gold deposits and to further study gold mineralization.

Source of Gold: Related to a Fossil Geothermal System?

One problem in the study of gold deposits is the primary source of gold. Several possible sources have been argued for the Hetai gold field. Chen et al. (1988) proposed that the favorable source of gold be the Sinian and Cambrian strata, because of their great thickness and high gold content, while Fu (1988; 1989) noted the affinity of the Yunluogan and Wucun granites to the gold deposits, and argued that these Hercyno-Indosinian granites be the major gold sources. Aside from the possibility that the ore-forming hydrothermal

solution may have been driven by the heat of granitic magmatism, trace element and isotopic evidence favors the Sinian and Cambrian strata as the major source of gold. However, it may be considered that such a gold source may be related to a particular type of sedimentation, such as that related to submarine hydrothermal activity.

It is interesting that a suite of unmetamorphosed bedded cherts, which are probably equivalent to the protolith of the schistose quartzites intercalated within the ore-hosting metamorphic rock series, was found within the Sinian strata. These bedded cherts from the Hetai area may have formed as a consequence of the hydrothermal activity of a fossil geothermal system. If it is proven that these bedded cherts resulted from hydrothermal activity, it is possible that the activity of a fossil geothermal system has participated in the preliminary enrichment of gold during the formation of the source strata.

Geochemical Behavior of Gold as an Impurity Trace Element in Metamorphism

Much gold occurs as an impurity trace component of rock-forming minerals, although it may occur as an independent mineral and a significant component of some minerals. Gold is a trace element in source rocks as a whole. Later gold mineralization often requires the extraction of gold from rock-forming minerals and subsequent transports to favorable geochemical locations. During this process, the transport of gold along visible fractures, especially along those with moving aqueous fluid, is relatively simple and rapid. In contrast, the migration from within rock-forming minerals to visible fractures is usually less efficient although this distance may be very short, and thus becomes the bottleneck of the migration of gold from its initial position in source rocks to ore sites.

The redistribution of gold in source rocks may be driven by regional metamorphism (Boyle, 1979; Tu, 1984). The present study recognizes the need to consider the ideal geochemical behavior of impurity trace elements in a thermal field in order to understand the mechanism of their remobilization and migration in source rocks during metamorphism.

Role of Shear Deformation System

The importance of deformation in controlling the location of the gold ores was acknowledged by previous researches (No.719 Geol. Team, 1987). Both the mining district

and individual mineral orebodies are strictly controlled by deformation zones in the Hetai area, and gold concentration commonly increases to a peak in dynamically deformed zones, regardless of the lithology of original undeformed rocks. The present thesis attempts to unveil the role of deformation in gold mineralization, and to consider whether elements have changed their spatial distribution, and how such changes may have taken place.

Fluid Inclusions and Hydrothermal Wall-rock Alteration

Extensive intense alteration is a visible feature of the Hetai gold field. Many successful case studies in other areas have demonstrated (Colvine et al., 1988; Franklin et al., 1981; Guha et al., 1991; Davies et al., 1982; Fyon et al., 1986; Fyfe et al., 1978; Helgeson et al., 1987; Kuhns, 1986; McInnes et al., 1986; Roedder, 1984; Bickle et al., 1987) that hydrothermal wall-rock alteration and fluid inclusions within minerals of the ore zone were a key to the mineralization history of ore deposits. The study of fluid inclusions and hydrothermal alteration of this thesis aims at recognizing the composition and physio-chemical conditions of the ore-forming hydrothermal solution.

Metallogenetic Model

The metallogenetic model is a summary of the entire study, which should link the gold deposit to its geological environment and tectonic setting. The metallogenetic model is expected to aid in guiding the choice of significant prospecting indicators.

Methodology

To realize the aims described above, a specific research program of field and laboratory investigations has been proposed. The field investigations concentrate on observation and analysis of the occurrence of gold mineral deposits and the relationship between the ores, host strata (including bedded cherts), deformation zones, hydrothermal alteration and granitic rocks. Systematically sampling is also an integral part of the field investigations.

Following the field investigations, laboratory studies of the research program cover:

(1) Petrographic and mineragraphic examination of the ores and wall rocks occurring

in the Hetai gold field: This is a key for establishing a temporal sequence of mineralization, and for further explanation of all geochemical data.

(2) Chemical composition determination of major and trace elements of the ores and major types of rocks: The trace elements analyzed include Cu, Zn, Pb; Ni, Co, Cr; Nb, Ta, W, Sn; Au, Ag; As, Sb, Bi, Se, Hg, Te; REE (instrumental neutron activation method).

(3) Multivariate statistical analysis of geochemical data: The applied methods include factor analysis, correspondence analysis and correlation analysis. Such multivariate statistical methods may provide insight into the intrinsic textures of the available geochemical data, and extract eigen element associations representing the information end-members of the involved geological and geochemical processes.

(4) Fluid inclusion microthermometry: The examined items include the homogenization temperature, salinity, and composition of the ore-forming hydrothermal solution preserved in fluid inclusions.

(5) Mathematical modelling: This attempts to establish a general pattern of element remobilization and migration using mathematical-physical tools.

Chapter I

GEOLOGICAL SETTING

§1 Yunkai Metamorphic Terrain (Gold Province)

1.1 Geographic Location

The Yunkai Metamorphic Terrain, named after the Yunkai Mountainous Area, is located in southern China and has a surface area of about 30,000 km^2. It includes western Guangdong Province and part of southeastern Guangxi Zhang Autonomous Region (Fig. 1.1), limited on the southeast by Qingyuan, Gaoyao (Zhaoqing), Xinxing and Dianbai counties of Guangdong Province and on the northwest by Bobai and Yülin counties of Guangxi Autonomous Region.

1.2 Distribution of Gold Deposits

The Yunkai Metamorphic Terrain is an excellent gold province, which consists of two neighboring traditional gold producing areas of China, the western Guangdong area and the southeastern Guangxi area. Gold deposits and showings are widely scattered over this terrain as shown in Figure 1.2. A series of recent discoveries of large scale gold and silver-gold deposits within the terrain makes it even more attractive.
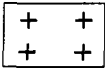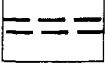
One prominent characteristic of the distribution of the gold deposits in this terrain is their clustering along certain tectonic zones. For example, the Pangxidong (Ag + Au), the Jinshan (Ag + Au), the Zhangmutang (Ag + Au) and the Zhongsu (Ag + Au) ore deposits occur along the northeasterly striking Pangxidong fault zone on the west of the terrain, while the Hetai gold field does along the Luoding - Guangning fault zone on the east. The Hetai gold

Figure 1.1
GEOGRAPHIC MAP OF
WESTERN GUANGDONG PROVINCE

9

Figure 1.2
Tectonic Outline and Distribution of
Gold Ore Deposits
of Western Guangdong Province

0   60   120km
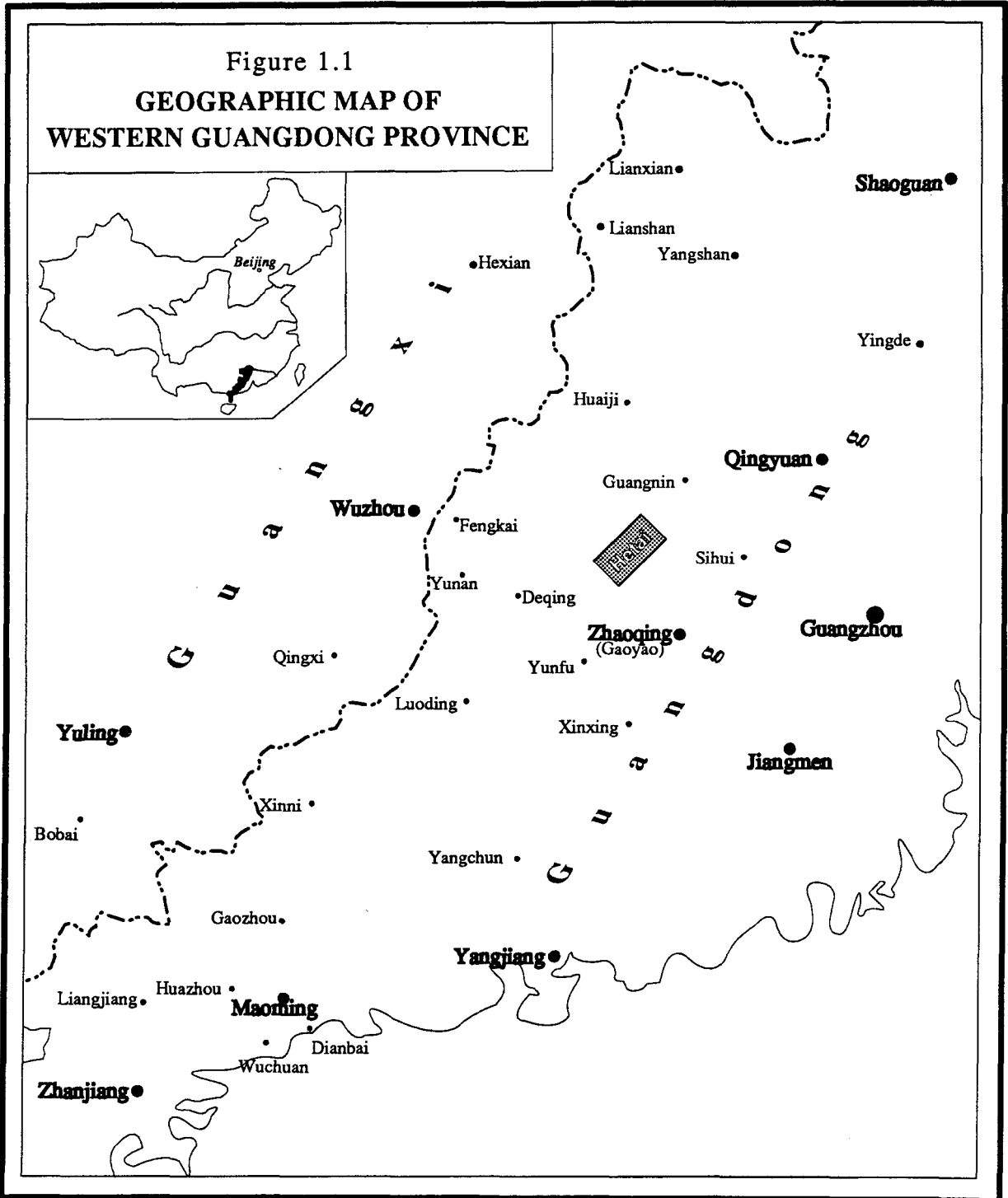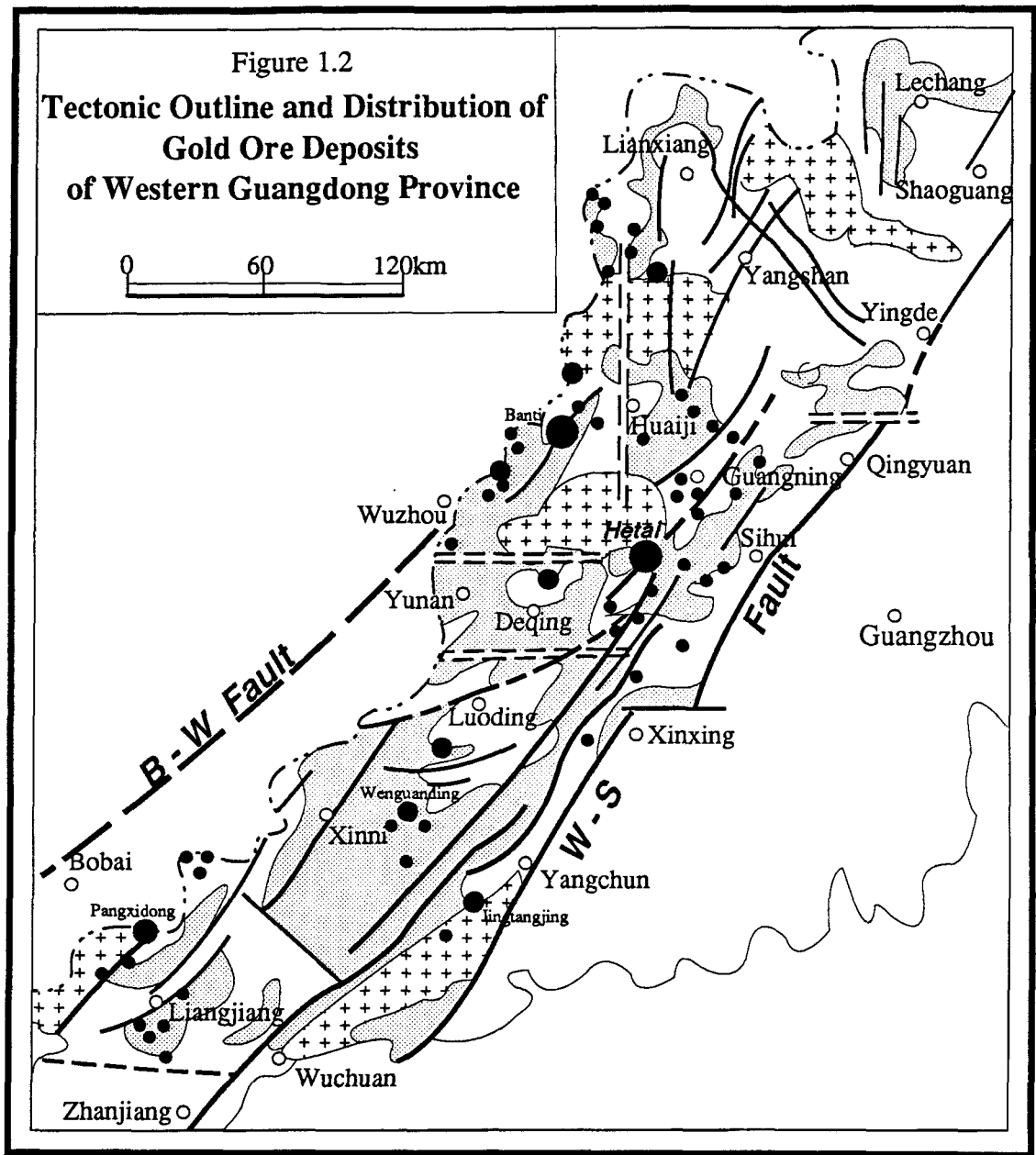
Drawn based on Guangdong Bureau of Geology (1977) and Ye (1988)

Sinian meta-morphic strata	Large-scale gold deposits
Granites	Medium- to small-scale gold deposits
Faults	clusters of gold showing
Faults suggested by exploration geophysics	

field consists of several individual ore deposits.

The major deformation zones, such as the Luoding - Guangning fault zone and the Pangxidong fault zone, are regional scale features. Within these regional deformation zones, small scale structures play a direct role in localizing gold deposits. Orebodies, and ore shoots at a still smaller scale, occupy specific structural features.

The primary gold deposits occurring in the Yunkai terrain may be classified into four major types (No. 719 and 704 Geol. Teams, 1983): (a) the disseminated hydrothermally altered mylonite-hosted type, (b) the auriferous quartz vein type, (c) the metasediment gneiss type, and (d) the base metal-associated type. Significant gold deposits representative of the Yunkai terrain are listed in Table 1.1.

The disseminated hydrothermally altered mylonite-hosted type is at present the most important type of gold deposits in the Yunkai area. It is distinguished from the other types in that its elongate ore bodies are localized in deformation zones, composed of mylonites and phyllonites, which are tied to intense hydrothermal alteration. The altered deformation zones are several centimeters to about a kilometer wide. The main alterations include sericitization, chloritization, silicification, pyritization and carbonatization. The auriferous minerals are disseminated in the altered, deformed rocks. The economic elements are gold or silver or both. Representative of this type are the Hetai deposits (Au) in Gaoyao county and the Pangxidong deposit (Au, Ag) in Lianjiang county.

The auriferous quartz vein type is also common in the Yunkai area. The ore minerals are mainly fine-grained native gold and electrum, disseminated heterogeneously in quartz veins, without or with minor amounts of sulfides. The macroscopic or mesoscopic quartz veins are usually developed along extension or extension-shear fractures, filled either in open space or in breccia mode. Locally, the wall rocks may be silicified. This type of gold deposits often occurs near the outer contact zone of granitic massifs or around multi-metal deposits. The Xinzhou ore deposit in Qingyuan county and the Banti ore deposit in Fengkai county are representative examples of this type.

The metasedimentary gneiss type of gold deposit is known at the township of Silun of Luoding county (the Jinniu ore deposit). It occurs within the auriferous gneiss facies strata of the Sinian migmatitic metamorphic series, whose lithology is mainly fine grained biotite-

Table 1.1 Genetic classification of the primary Au (Ag) ore deposits occurring the Yunkai metamorphic terrain

Types	Representative examples	Modes of gold emplacement
Mylonite-hosted hydrothermal replacement	Gaocun (Au), Yunxi (Au), Dapingding (Au), Pangxidong (Ag, Au), Jinshan (Ag, Au), Zhangmutang (Au, Ag), Zhongsu (Au, Ag)	hydrothermal wall-rock alteration, superimposed on ductile shear zones
Auriferous quartz vein	Banti (Au), Xinzhou (Au), Quanpai (Au), Jitian (Au)	open space fill in dilational fractures
Metasediment gneiss	Jinniu (Au), Niutao (Au)	gold enrichment through metamorphism
Base metal sulfide-associated	Chadong (Ag, Au), Qibeishan (Ag, Au), Heshangan (Au, Ag)	by-product of base or polymetallic mineralization

plagioclase gneiss, interbedded with hornblende-rich quartziferous beds. The auriferous layers lie concordantly within the host metamorphic strata. The main ore mineral is very fine-grained disseminated native gold, which is scattered along the gneissosity planes. There is no absolute boundary between the ore and country rock, but only an economic cut-off. The ore possesses typical metamorphic textures and structures, and no traces of overprinting by hydrothermal replacement (No. 719 and 704 Teams, 1983).

In addition to the three types of gold deposits described above, there are also numerous auriferous skarn or hydrothermal base metal sulfide deposits, in which gold is a profitable associated element which may be extracted as a by-product. These make up the gold deposits of the base metal-sulfide-deposit-associated type.

1.3 General Geology

1. Tectonic Background

The Yunkai terrain is an anticlinorium in metamorphic rocks. It is bounded on the east by the NE-striking Wuchuan - Sihui fault system; and on the west by the Bobai - Wuzhou fault system which also strikes NE (Fig. 1.2; Guangdong Bureau of Geology, 1977; Guangxi Bureau of Geology and Mineral Resources, 1985). The terrain is mainly composed of metamorphic and/or migmatitic complexes. As the remnant of a marginal geosyncline which received thick sediments during the Precambrian and Early Paleozoic periods, the terrain was shaped as an orogenic belt for the first time during the Caledonian orogeny (Guangdong Bureau of Geology, 1977; Guangxi Bureau of Geology and Mineral Resources, 1985).

2. Strata and Non-magmatic Rocks

The Sinian (Precambrian) and Lower Paleozoic strata are widely exposed in the terrain. They are mainly composed of marine flysch formations, with intercalated cherts (Fig. 1.3; Table 1.2; Nan, 1989). Because of the Caledonian regional metamorphism, the lithology is mainly slates, schists, metaquartzite and gneisses. Migmatitic rocks occur in several metamorphic centers and uplifted dynamothermal deformation zones. In such areas, agmatite, metatexite and diatexite are observed. Examples may be found from Shijian of Guangning county to Hetai of Gaoyao county, in Daganshan Mount of Yunfu county, from Silun of Luoding county to Datianding of Xinni county, and from Beijie of Xinni county to Tangpeng
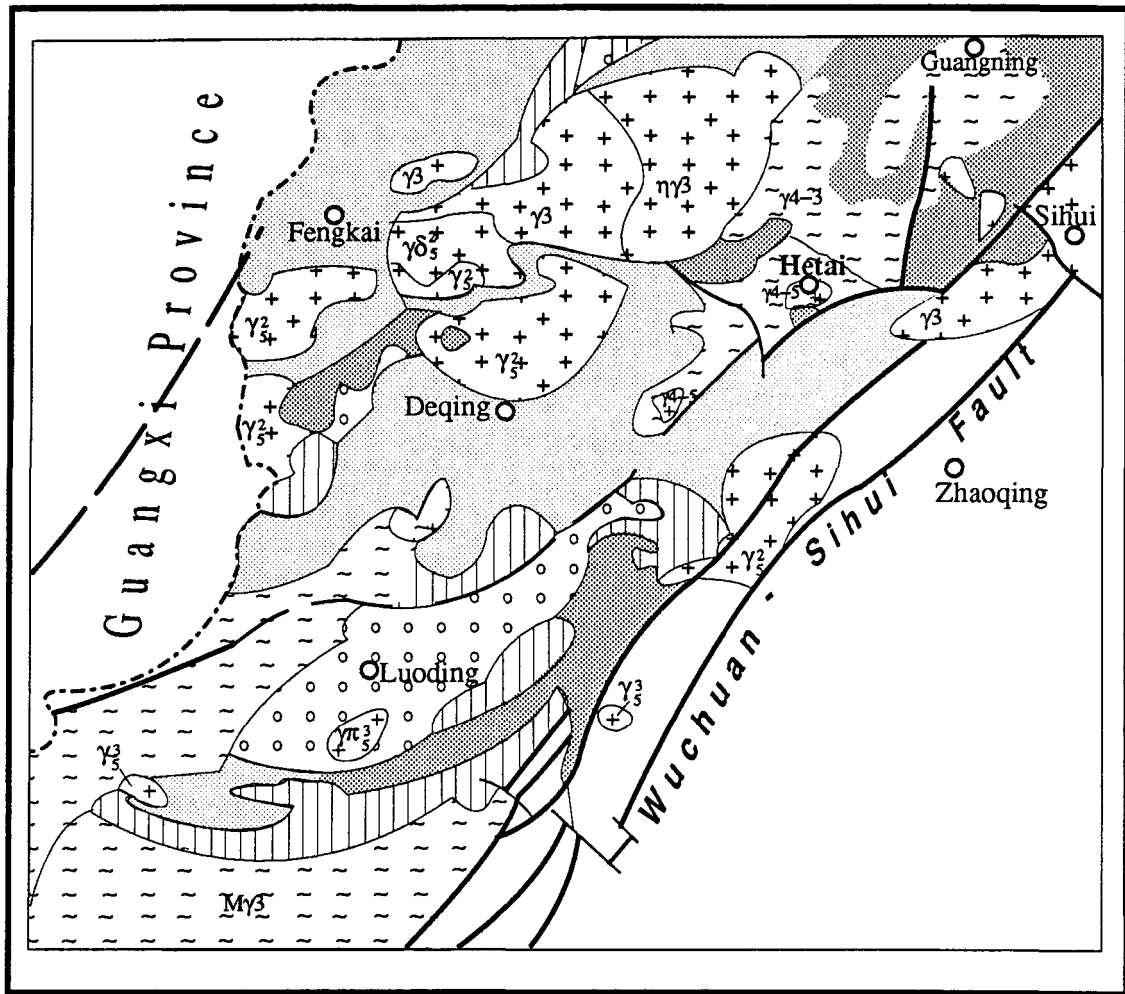
Figure 1.3 Tectonic Background of the Hetai Gold Field
(Redrawn after No. 719 Geol. Team, 1987)
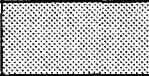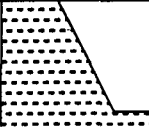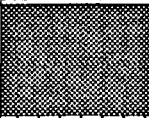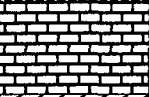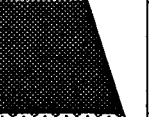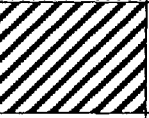
Mz or later sediments	Caledonian migmatites
Pz $_2$ sediments	Hercynian-Indosinian and Yanshanian granites
Pz $_1$ low-grade metasediments	Caledonian granites
Sinian metamorphic rocks	Faults

Table 1.2 Simplified stratigraphic and tectonic column of western Guangdong Province

	Erathem/ System	Units of strata	Column (not to scale)	Sedimentary facies and lithology	Tectonic events and ages
	Cenozoic			Terrestrial clastic sediments	
	Mesozoic			Terrigenous clastic facies (red bed), intercalated with intermediate to acidic terrestrial volcanic rocks	*Yanshanian (210-70 Ma)* *Indosinian (230-210 Ma)*
Upper Palaeozoic	Permian	Longtan formation (P2)		Alternating marine-continental coal-bearing clastic facies. Quartz sandstone, siltstone, carbonaceous shale	*Hercynian (280-230 Ma)*
		Gufeng formation (P1)		Shallow marine carbonate facies.	
	Carboniferous	Hutian group (C2+3)		Shallow marine carbonate facies.	
		Datang formation (C1D)		Shallow sea to swamp coal-bearing clastic facies. Quartz sandstone, siltstone, carbonaceous shale and coal.	
		Yanguan formation (C1Y)		Shallow marine carbonate facies, intercalated with fine-grained clastic rocks	
	Devonian	Liujiang formation (D3)		Shallow marine carbonate and terrigenous fine-grained clastic facies, with Mn-, P-bearing rocks, and cherts	
		Quzhiqiao (D2q) and Guitiao member (D2g)		Terrigenous clastic facies	
Lower Palaeozoic	Silurian	Lingsha group Wenshan group Liangtan group		Abyssal graptolite shale facies	*Caledonian (500-400 Ma)*
	Ordovician	Shanjian group (O2-3) Suwei formation (O1)		Abyssal graptolite shale facies and terrigenous fine-grained clastic facies	
	Cambrian	Bacun group		Marine flyschoid formation. Graywacke, feldspathic sandstone, carbonaceous and siliceous shale.	
Precambrian .	Sinian			Metamorphosed flysch formation intercalated with volcaniclastic rocks and bedded cherts	

Sources: Nan (1989); Guangdong Bureau of Geology (1977); No.719 Geol. Team (1987)

of Lianjiang county (Mo and Ye, 1980; Liu, 1989; Guangdong Bureau of Geology, 1977).

The Upper Paleozoic and lower-middle Triassic strata are a suite of platformal sediments, consisting mainly of shallow marine carbonate facies and terrigenous clastic facies. Conglomerates are found at the base of Devonian system, which are in discordant contact with the older strata. These strata are usually unmetamorphosed.

Younger strata, including the upper Triassic to Quaternary, are less abundant than those above, usually occurring as patches in fault-basins. Continental intermediate to acidic volcaniclastic sediments are locally developed.

3. Granites

The Yunkai terrain is part of the south China granite belt, and numerous granitic bodies have been identified within it (Institute of Geochemistry, 1979; Mo and Ye, 1980; Guangdong Bureau of Geology, 1977; Guangxi Bureau of Geology and Mineral Resources, 1985). Based on the cross-cutting relationship and geochronological data, the granites can be divided into three distinct episodes: the Caledonian, the Hercyno-Indosinian and the Yanshanian.

Many of the Caledonian granitic rocks bear close relationships with the metamorphic rock series. Field observations and laboratory work (Mo and Ye, 1980; Huang, 1988) indicate that they are the product of syntectonic partial melting or anatexis of high-grade metamorphic paragneisses and migmatites. Three types of Caledonian granitic rocks can be recognized on the basis of their relationship to the surrounding metamorphic rocks and strata: the autochthonous, the parautochthonous and the intrusive. The first two groups have the appearance of the coeval migmatite, and are spatially associated with the latter.

In contrast with the Caledonian granites, the Hercyno-Indosinian and Yanshanian granites are characterized by clear intrusive features.

1.3 Tectonic Evolution

The Yunkai terrain was a marginal geosyncline during the Precambrian and early Paleozoic periods. The earlier formed Yangtze platform (Proterozoic orogen) lies to the

northwest. Before the Caledonian orogeny, thick flysch formations, mainly of terrigenous clastic sediments and cherts intercalated with volcanic sediments, accumulated. The Caledonian orogeny took place during the Cambrian to Silurian period, depending on geographic location. The last area to experience the Caledonian movement is the southwest section of the terrain, where Ordovician shelly clastic facies and Silurian graptolitic shale facies deposits are identified (Fu, 1985). Broad folding and regional metamorphism accompanied the Caledonian orogeny. Migmatites and coeval batholithic granites developed in several high-grade regional metamorphic centers.

After a period of erosion following the Caledonian orogeny, a new sedimentary cycle began. From the Devonian through to early-middle Triassic period, lithofacies characteristic of platformal sedimentation was developed. The base of these platformal strata may be locally absent due to the difference of the onset of younger sedimentary cycle depending on geographic location.

Hercynian tectonic movement is not common, and has not been clearly distinguished from the stronger Indosinian tectonic movement. Sedimentation continued from the Permian to the Triassic in most sections, but unconformities are common between the middle and the upper Triassic, and many granite intrusions have an Indosinian radiometric age. Therefore, the name *Hercyo-Indosinian* has been used to characterize this tectonism. The most significant product of the Hercyo-Indosinian movement is the granite magmatism. Fault-related metamorphism may also be observed within some major deformation zones.

The Yanshanian is the last important tectonic event in southern China. It caused strong tectonic remobilization, accompanied by granitic magmatism and volcanic eruption in many areas of southern China. Its influence, however, appears less important than the Hercyno-Indosinian movement in the Hetai area.

§2 Hetai Gold Field

The Hetai gold field (Figs. 1.3 and 1.4) is situated in the northeast section of the Luoding - Guangning deformation system, which occurs near and subparallel to the northeasterly trending Wuchuan - Sihui fault system. It is also part of the southern margin of the Shidong - Wuhe - Shijian - Hetai migmatite district. As a whole, this gold field has a
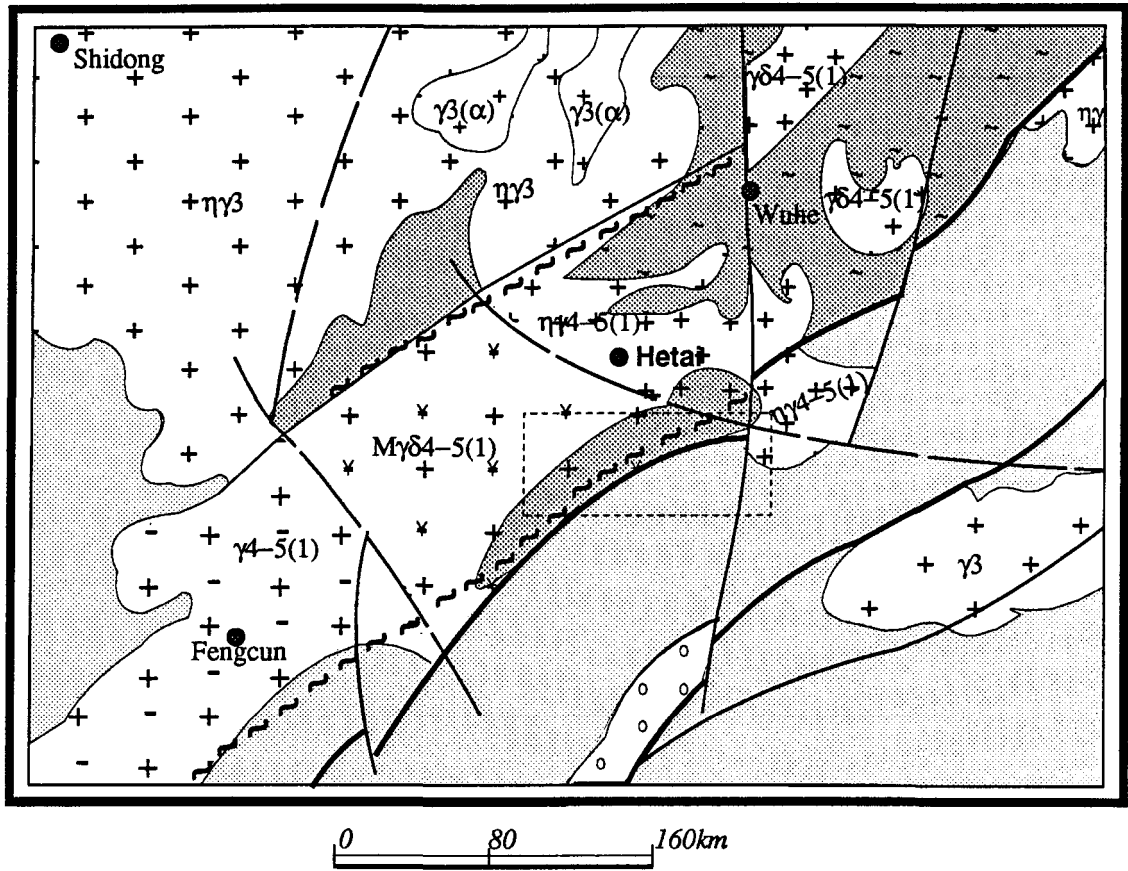
Figure 1.4 Regional Geological Map of the Hetai Area

(after No.719 Geol. Team, 1987)

Triassic Fault Basin

Lower Paleozoic Folded Belt

Sinian Metamorphic Belt

Caledonian Migmatite

Main Shear Deformation Zone

Wucun Granite

Fengcun Granite

Yunluogan Granite

Shidong Migmatitic Granite *(Caledonian)*

(Hercynian-Indosinian)
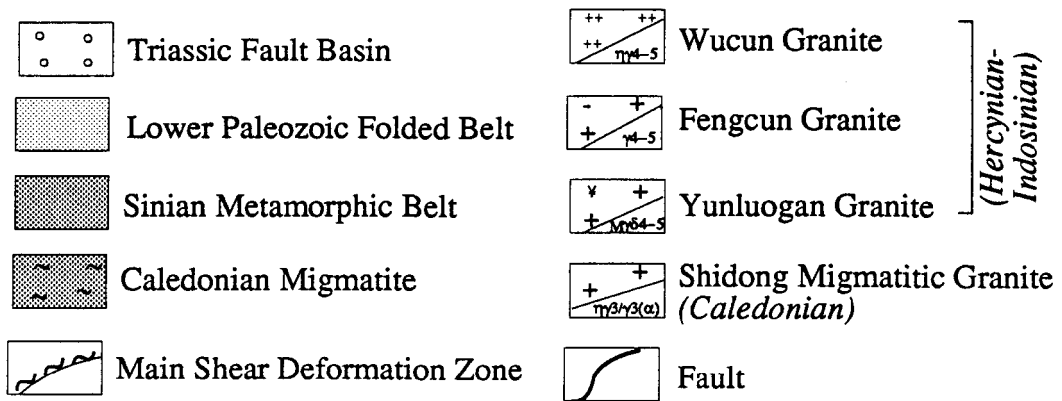
Fault

The dot line rectangle domain is the Hetai gold field (see Fig. 1.5)

Figure 1.5

**Distribution of Shear Zones and Gold
Ore Deposits in the Hetai Gold Field**
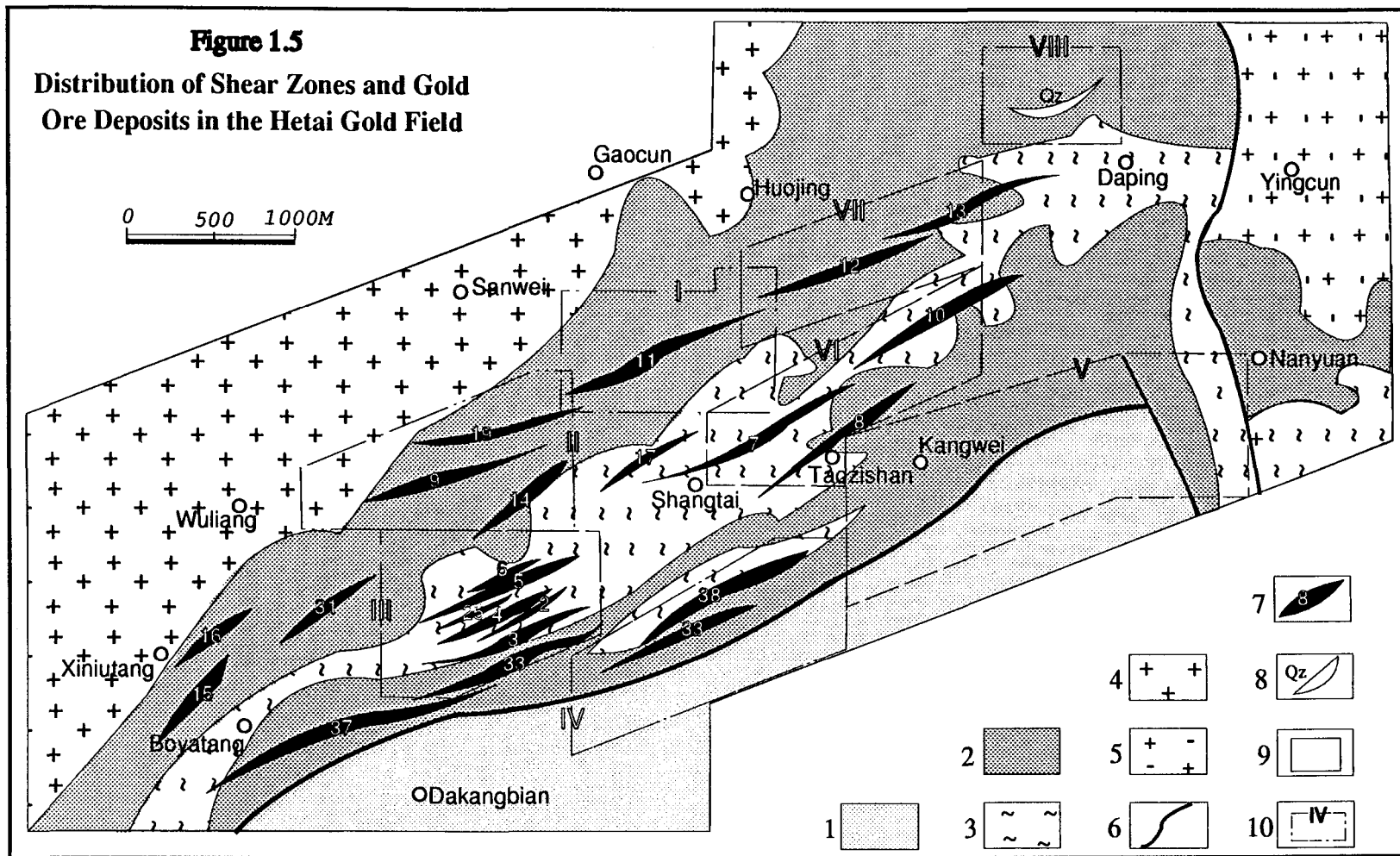
(after No.719 Geological Team, 1987)

1. Ordovician low-grade metasediments
2. Sinian medium-high grade metamorphic rocks
3. Migmatites
4. Yunluogan granodiorite
5. Wucun porphyritic monzonitic granite

6. Major faults
7. Ductile shear zones
8. Quartz veins
9. Range of the gold field

10. Ore deposits and its exploration extension
(I) Gaocun; (II) Yunxi
(III) Taipingding; (IV) Shangtai
(V) Kangwei; (VI) Taozishan
(VII) Huojing; (VIII) Hehai

18
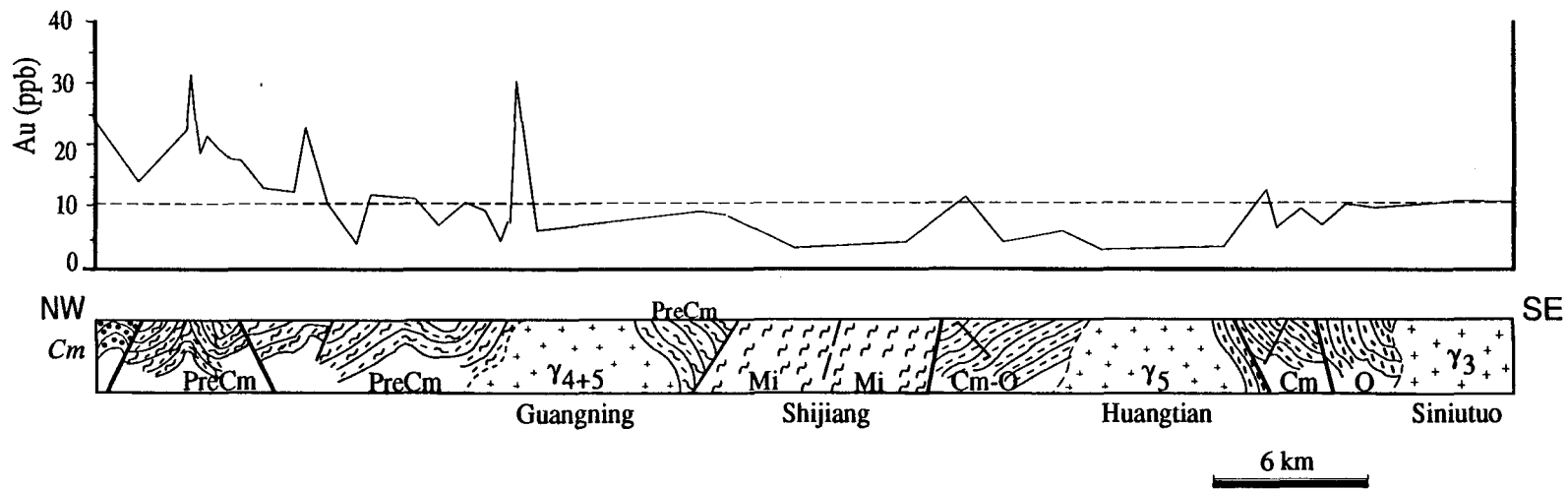
Figure 1.6 The Sihui - Gusui geological and geochemical profile

After Chen et al. (1988)

O — Ordovician, Cm — Cambrian, PreCm — Precambrian;

γ — granites, Mi — migmatites

Table 1.3 Au concentrations (ppb) in the strata of the regional Hetai area

Geological profiles	Hebao - Tianliudong			Shihui - Gusui			Zaoqing -Baozhi -Mocun			Overall
	N.S.	Range	Average	N.S.	Range	Average	N.S.	Range	Average	Average
Upper Triassic				4	11.2 -28.5	18.5	10	1.5 -2	1.8	6.5
Carboniferous							13	1 -11.0	2.2	2.2
Devonian							19	<1 -1.5	1	1
Silurian	10	1 -7.0	2.5				29	1 -8.0	2.2	2.3
Ordovician	5	1.5 -10	4.3	11	3 -11.5	8.2	21	<1 -6	1.9	4.1
Cambrian				16	1.0 -25	16.3	2	1.5 -2	1.7	14.7
Sinian (Precambrian)	15	1 -17.5	6.3	34	2.0 -36	12.3	1	2.5		10.3

N.S stands for the number of samples. Sources: Chen et al. (1988)

tectonic context consistent with that of the entire Yunkai terrain.

The proven gold deposits include Gaocun, Yunxi, Taipingding, Shangtai, Kangmei, Taozhishan, Huojing and Hehai (Fig. 1.5). All but the Hehai belong to the disseminated hydrothermal replacement mylonite-hosted type. The Hehai ore deposit belongs to the quartz vein type.

The country rocks of the gold ore deposits are various schists and migmatitic rocks. The Hercyno- Indosinian period Yunluogan and Wucun granites are prominent in the Hetai area, but do not make up the immediate country rock of gold ore bodies.

The exposed strata in the Hetai area are principally Sinian (Precambrian) and Lower Paleozoic. They are originally terrigenous marine flysch formations intercalated with submarine hydrothermal sediments, and most of them have been metamorphosed during the Caledonian orogeny. The metamorphic Sinian strata have a great thickness, and are the most important host of gold deposits occurring in the area.

Detailed investigations have been carried out along three regional geological profiles by local geological teams, to determine whether a regional geochemical gold anomaly is present in the studied area (No. 719 and 704 Geol. Teams, 1983). Systematical sampling and gold analysis of particular interest are made along the Sihui - Gusui geological profile, which passes, from NW to SE, through Gusui, Guangning, Shijian, Huangtian and Sihui (Fig. 1.6). To establish the reliability of the data, only those samples distant from known gold deposits were analyzed. Gold abundance of various strata is listed in Table 1.3. This table shows that the gold abundance is highest in the Sinian and Cambrian strata, with average at about 10 and 15 ppb, respectively.

Chapter II

REGIONAL METAMORPHIC ROCKS AND GRANITES

§1 Metamorphic Petrology and Facies

Schists and migmatitic rocks, which may have been deformed in late tectonic events, are predominant country rocks of the Hetai gold deposits. The Hetai gold field is in fact part of the southeast margin of the greater Caledonian Shidong - Wuhe - Shijian - Hetai (SWSH) migmatitic metamorphic district (Fig. 2.1), which is one of the metamorphic centers of the Yunkai Terrain. On a regional scale the metamorphic rocks occurring in the SWSH area forms a complete series, from low grade metasediments, through various schists and quartzite, to gneisses and migmatites. They were derived mainly from the Sinian and Cambrian strata (Liu, 1989; Fu, 1985). Metamorphosed post-Cambrian strata occur to the southeast of the Luoding - Guangning fault zone, but are usually of low metamorphic grade. A description of the regional metamorphic rocks and their geochemical characteristics is necessary to understand the geological setting of the studied area.

1.1 Major Rock Types

The metamorphic rocks occurring in the SWSH area may be classified into the following groups, based on the lithologic characteristics and metamorphic grade.

Fine-Grained Clastic Metasedimentary Rocks

This group of rocks consists of phyllites and slates. The main minerals are muscovite, chlorite, albite and quartz. Fine-grained phyllitic structure and slaty cleavage are common.
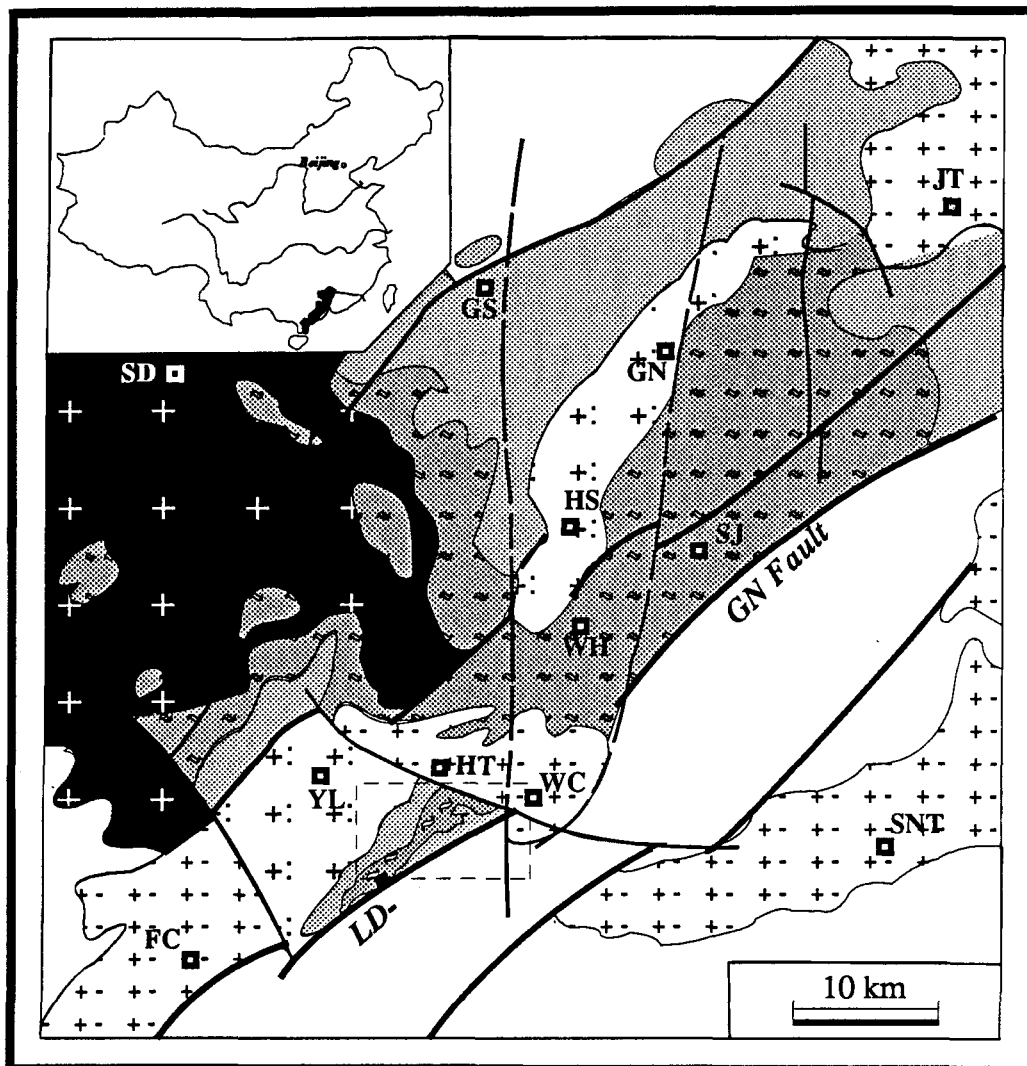
Figure 2.1 Distribution map of regional metamorphic (and migmatitic) rocks in the Shidong - Wuhe - Shijiang - Hetai district

☐	Post-Cambrian metasediments	⊞	Hercynian or later granites
▦	Cambrian and Precambrian metamorphic rocks	■	Caledonian granites
▨	Precambrian migmatites	⬚	Faults
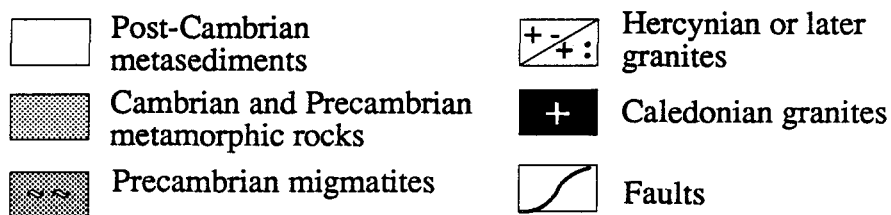
SD = Shidong; WH = Wuhe; SJ = Shijian; HT = Hetai; GS = Gusui;
GN = Guangning; WC = Wucun; YL = Yunluogan; FC = Fengcun;
SNT = Shiniutou; JT = Jiangtun; HS = Hengshan
LD-GN = Luoding-Guangning

The fine-grained platy minerals, such as muscovite, gives an overall silky sheen to the slaty planes. Relict minerals and palimpest structures of original rocks are easily identified. They indicate that the original rock was a fine grained sedimentary clastic rock, mainly pelitic and semi-pelitic. This group of rocks occurs mainly in the lower Paleozoic strata in the southeast block of the Luoding - Guangning fault zone, and the Sinian strata in the central north of SWSH area.

Metacherts and Schistose Quartzites

Metacherts are characterized by their predominant microcrystalline quartz and the good preservation of primary sedimentary bedded and laminated structures. The microcrystalline quartz is the product of recrystallization of other silica phases (c.f. Chapter 3). At the Gusui section, situated north to the main Hetai gold deposits, unmetamorphosed bedded cherts with thin shaly partings are identified. Hematite is also common.

Schistose quartzites are basically a monomineralic rock consisting essentially of interlocking grains of quartz, showing no trace of the original grains and breaking with a conchoidal fracture. Minor constituents include sillimanite, feldspar and biotite. This group of rocks are interbedded with schists. It distinguished from the metachert mentioned above by its coarser granulometry. Although they have lost almost every petrographic trace of their origin, they may be equivalent to the metacherts.

Schists

This group of metamorphic rocks has a well developed schistosity defined by the orientation of micas. Quartz, muscovite and biotite are abundant. Staurolite (Plate 2.1), sillimanite and almandine are characteristic metamorphic minerals. Sillimanite commonly occurs as needles, and staurolite and almandine, as porphyroblasts. Almandine porphyroblasts are equant, occasionally with rotated texture, locally interrupting the schistosity. The schists are often associated with banded schistose quartzites, but their contact relationship are usually sharp instead of gradual one.

Gneisses

This group of rocks is characterized by a marked gneissosity structure and coarse grained texture. The gneissosity is formed either by alternating concentrations of dark and
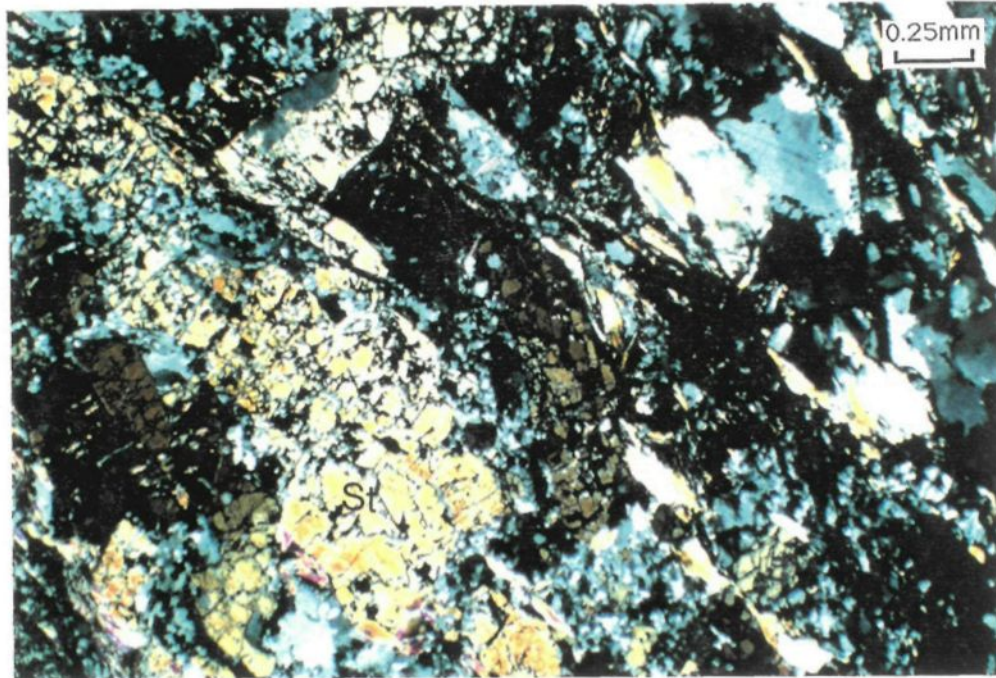
Plate 2.1 Staurolite porphyroblast occurring in the dominant schists of the Hetai area
Cross polarized light

light minerals or by variations in grain size. Quartz, oligoclase and biotite are the main constituents, with the presence of sillimanite. The gneisses often occur as the paleosome of a migmatite. They may be the high grade equivalent of fine-grained clastic metasedimentary rocks described earlier.

Granulites

Granulites are characterized by their granoblastic texture and massive structure, without or with very weak preferred orientation. They commonly occur as enclaves or paleosomes of a migmatite, but are not abundant in the studied area, mainly found in the northwest portion, where migmatites and migmatitic granites occupy a large proportion of exposed surface. The major constituents are quartz, plagioclase and biotite, with the presence of hypersthene and sillimanite. The alkali felspar is typically mesoperthitic, with Ab component up to 50%. The plagioclase is mainly andesine or labradorite. Most granulites occurring in the SWSH area are of charnockitic composition (quartzo-feldspathic granulite).

1.2 Mineral Parageneses and Facies

The mineral assemblages listed below are identified in the metamorphic rocks of the SWSH area:

(Ia) quartz + muscovite

(Ib) quartz + muscovite + chlorite + albite

(IIa) quartz + muscovite + biotite

(IIb) quartz + muscovite + biotite + plagioclase

(IIc) quartz + plagioclase

(IIIa) quartz + muscovite +staurolite

(IIIb) quartz + muscovite + biotite + staurolite

(IIIc) quartz + muscovite + biotite + plagioclase

(IIId) quartz + biotite + plagioclase

(IIIe) quartz + muscovite + biotite +almandine

(IIIf) quartz + muscovite + biotite + K-feldspar (microcline)

(IIIg) quartz + biotite + almandine

(IVa) quartz + biotite + plagioclase + orthoclase + sillimanite

(IVb) quartz + biotite + plagioclase + orthoclase + sillimanite + almandine

(Va) quartz + plagioclase + orthoclase + hypersthene

These assemblages are stable, and each represents a mineral paragenesis. It should be pointed out that some of the mineral assemblages are incomplete. Among them, (Ix) is defined as the muscovite - chlorite zone, characterized by the presence of muscovite and/or chlorite with no biotite (Fu, 1985; Liu, 1989). (IIx) is the biotite zone, characterized by the disappearance of sericite and chlorite, and the appearance of biotite. The paragenesis of muscovite and biotite is common; (IIIx), the staurolite zone; (IVx), the sillimanite - potassium feldspar zone; and (Vx), the regional hypersthene zone, characterized by the appearance by hypersthene.

§2 Protolith and Possible P - T Conditions

2.1 Protolith

The relict minerals and palimpest structures of the low grade metasedimentary rocks indicate that the protolith of the regional metamorphic rocks occurring in the Hetai area are mainly pelitic and/or semi-pelitic fine grained sedimentary clastic rocks, intercalated with less abundant bedded cherts. The abundant occurrence of sillimanite and staurolite in schists and more higher grade metamorphic rocks also suggests a pelitic and/or semi-pelitic protolith. It was demonstrated (Best, 1982) that such highly aluminous minerals are mainly derived from clay minerals-rich pelitic or semi-pelitic rocks. The presence of metacherts and schistose quartzites argues that sedimentary siliceous rocks also occurred as part of the protolith.

A pelitic and/or semi-pelitic protolith is also favored by geochemical evidence. The major chemical compositions are generally considered to behave as a closed system during metamorphism until a significant amount of anatexis or metasomatic modification takes place. If so, the content of major element oxides of the schists may be compared to that of the protolith.

The chemical compositions of the Hetai schists are listed in Appendix III-2.1. Correlation coefficient (Table 2.1) and factor analysis (Appendix III-2.2) demonstrates that the most significant element association of the Hetai schist is {-SiO_2, Al_2O_3, TiO_2, K_2O, MgO, Fe_2O_3, FeO}. This factor is characteristic of clay minerals (Zhou, 1987), which are usually the main constituent of pelitic rocks. However, only pelites are unlikely to account for the high SiO_2 content (see comparison with the average shale and the North America Shale Composite (NASC)). In other words, the protolith must be a semi-pelite, or a "pure" pelite plus something else. Taking into consideration that CaO is consistently low, the other element is probably a quartz-rich sediment, such as cherts.

2.2 Metamorphic Temperature and Pressure

Metamorphic rocks are developed in response to the rise of temperature and pressure. The high-grade facies of a progressive metamorphic belt must pass through lower P - T fields in the course of prograde metamorphism. It is difficult to determine a single P - T field for the whole evolution process. So estimates of P - T condition are given only for the schist, which is the most abundant country rock of the Hetai gold deposits. Such estimates may be expected to provide an approximate idea of the main temperature and pressure range that the Hetai metamorphic area experienced during the regional metamorphism.

The use of index minerals and mineral assemblages may give a general idea of the metamorphic P - T conditions with the help of experimentally determined mineral stability diagrams (Ehlers and Blatt, 1982). The index minerals contained in the schists from the Hetai area include staurolite, sillimanite and almandine, with the presence of quartz, plagioclase, muscovite and biotite, but neither kyanite nor andalusite has been reported.

When the mineral assemblages of the Hetai schist are projected to the experimentally determined stability field of selected mineral assemblages (Fig 2.2), it is found that the Hetai

Table 2.1 Correlation coefficients between major elements of the schists occurring in the Hetai Area

(N = 15)

	SiO2	TiO2	Al2O3	Fe2O3	FeO	MnO	MgO	CaO	Na2O	K2O	P2O5
SiO2	1.00	-0.82	-0.99	-0.54	-0.84	-0.32	-0.91	0.33	0.33	-0.93	-0.01
TiO2	-0.82	1.00	0.76	0.49	0.84	0.53	0.90	-0.18	-0.56	0.70	-0.20
Al2O3	-0.99	0.76	1.00	0.50	0.81	0.26	0.85	-0.43	-0.29	0.93	0.05
Fe2O3	-0.54	0.49	0.50	1.00	0.36	0.17	0.55	-0.21	-0.48	0.33	-0.43
FeO	-0.84	0.84	0.81	0.36	1.00	0.45	0.94	-0.45	-0.50	0.66	-0.28
MnO	-0.32	0.53	0.26	0.17	0.45	1.00	0.47	0.07	-0.20	0.28	-0.51
MgO	-0.91	0.90	0.85	0.55	0.94	0.47	1.00	-0.27	-0.60	0.73	-0.24
CaO	0.33	-0.18	-0.43	-0.21	-0.45	0.07	-0.27	1.00	0.17	-0.19	0.12
Na2O	0.33	-0.56	-0.29	-0.48	-0.50	-0.20	-0.60	0.17	1.00	-0.09	0.40
K2O	-0.93	0.70	0.93	0.33	0.66	0.28	0.73	-0.19	-0.09	1.00	0.25
P2O5	-0.01	-0.20	0.05	-0.43	-0.28	-0.51	-0.24	0.12	0.40	0.25	1.00
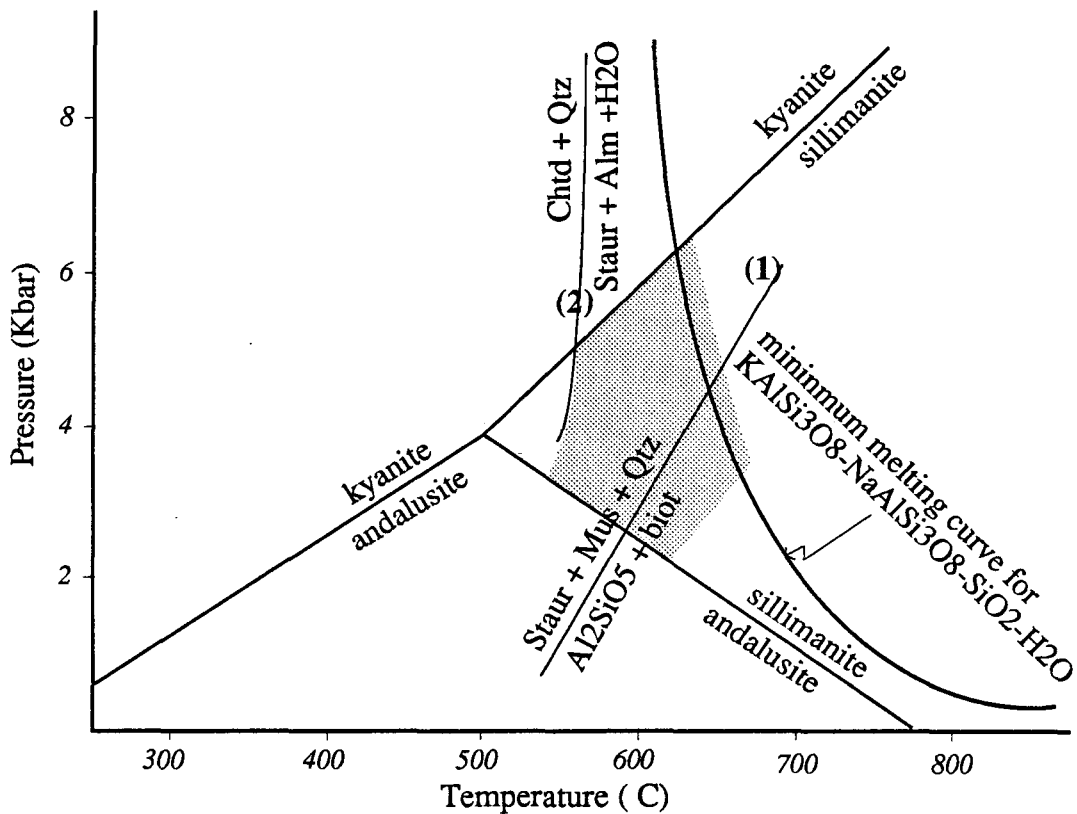
Figure 2.2 The stability field diagram of minerals as a function of T and P

[After Ehlers and Blatt (1982): Univariant lines for the polymorphs of Al2SiO5 from Holdaway (1971); Minimum melting curve from Luth et al. (1964); Curve 1 from Hoschek (1969); Curve 2 from Richardson (1968)] Chtd = chloritoid, Qtz = quartz, Bio =biotite, Alm = almandine, Mus = muscovite, Staur = staurolite.

The shadowed area indicates the approximate P - T range of the Hetai metamorphic rocks

schist formed approximately in the 550 to 670°C and 230 to 600 MPa range. The practical temperature and pressure range that the Hetai area has suffered during the regional metamorphism may be somewhat higher than the estimate above, if the presence of migmatitic rocks and local granulite facies is taken into account.

2.3 Fossil Geothermal Gradient

Three metamorphic facies series are generally recognized (Miyashiro, 1961; 1973). The high pressure one is developed where temperature increases slowly with depth, characterized by a low geothermal gradient, and a high P/T ratio. In contrast, the low pressure facies series occurs in regions of high geothermal gradients with a low P/T ratio. An intermediate pressure facies series lies between the high and low pressure facies series.

The progressive change series observed in the SWSH district is greenschist facies (muscovite-chlorite zone and biotite zone) — lower amphibolite facies (staurolite zone) — upper amphibolite facies (sillimanite zone) — granulite facies (regional hypersthene zone) or migmatite. Staurolite, almandine and sillimanite are common, but without high or low pressure-diagnostic minerals such as kyanite and andalusite. In a general sense, the SWSH area resembles the Barrovian zones of the Scottish Highlands (Harte and Johnson, 1969), which has been assigned as a "standard" intermediate pressure facies series (Miyashiro, 1973), i.e., the SWSH metamorphic rocks belongs to an intermediate or intermediate-low pressure facies series. They were probably developed in an area with a geothermal gradient of about 30 - 50°C/km (Best, 1982).

§3 Migmatites

3.1 Occurrence and Petrologic Characteristics

Migmatitic rocks occur over a large surface in the central, the northwestern and the northeast portions of the SWSH area (Fig.2.1). They have a transitional relationship with ordinary metamorphic rocks. On the regional scale, a complete sequence of migmatite is evident from northwest toward southeast, consisting of homogeneous and nebulitic migmatites on the northwest (the central phase), through the streaky and striped varieties, to normal

gneisses and migmatitic schists around Hetai on the southeast (the marginal phase). Fabric elements preserved in the schlieren of migmatites indicate two preferential orientations, one of which parallel to the schistosity of the surrounding metamorphic rocks. The migmatites may contain gneiss or granulite enclaves locally.

The relationship between the central phase migmatite and the coeval granite is disputable. Around Shidong, homogeneous and nebulitic migmatites are clearly tied to Caledonian granites, and are, in principle, indistinguishable from the latter. Some refer these rocks as granite or migmatitic granite rather than homogeneous or nebulitic migmatite (Mo and Ye, 1980; Huang, 1988; Liu, 1989). This is a problem of nomenclature, but for practical purposes, their compositions are the same.

Three groups of migmatites can be distinguished in the studied area: homogeneous, gneissic and layered (vein). The typical homogeneous migmatites are medium- to coarse-grained, with nebulitic structure and granitic texture, consisting mainly of quartz, oligoclase and K-feldspar. Biotite forms about 5 - 15% of the rock. The gneissic migmatites are characterized by their gneissic structure, consisting of biotite-rich schlieren and quartz-feldspar leucosomes. The darked-colored schlieren are oriented, while the leucosomes are often sugary textured. The layered migmatites are gneisses containing quartz-feldspar layers or veins. The veins, about 1 cm thick. may be regular or irregular in shape. The paleosomes have a typical metamorphic texture. Sillimanite and staurolite are found in the paleosomes.

3.2 Geochemical Characteristics

The potential protolith of the metasediments in the Hetai area exhibits a range of chemical composition, although it is mainly pelitic or semi-pelitic, as discussed earlier. It is not clear which of the surrounding metasediments was the true protolith of the migmatites. Here the average composition of the Hetai schists is used as the initial composition of the protolith of the migmatites.

1. Major Elements

The bulk chemical composition of the migmatites occurring in the studied area is listed in Table 2.2, with their average and the average of the Hetai schist for comparison. At first glance, the major constituents SiO_2, Al_2O_3 and K_2O seem to be nearly unchanged with
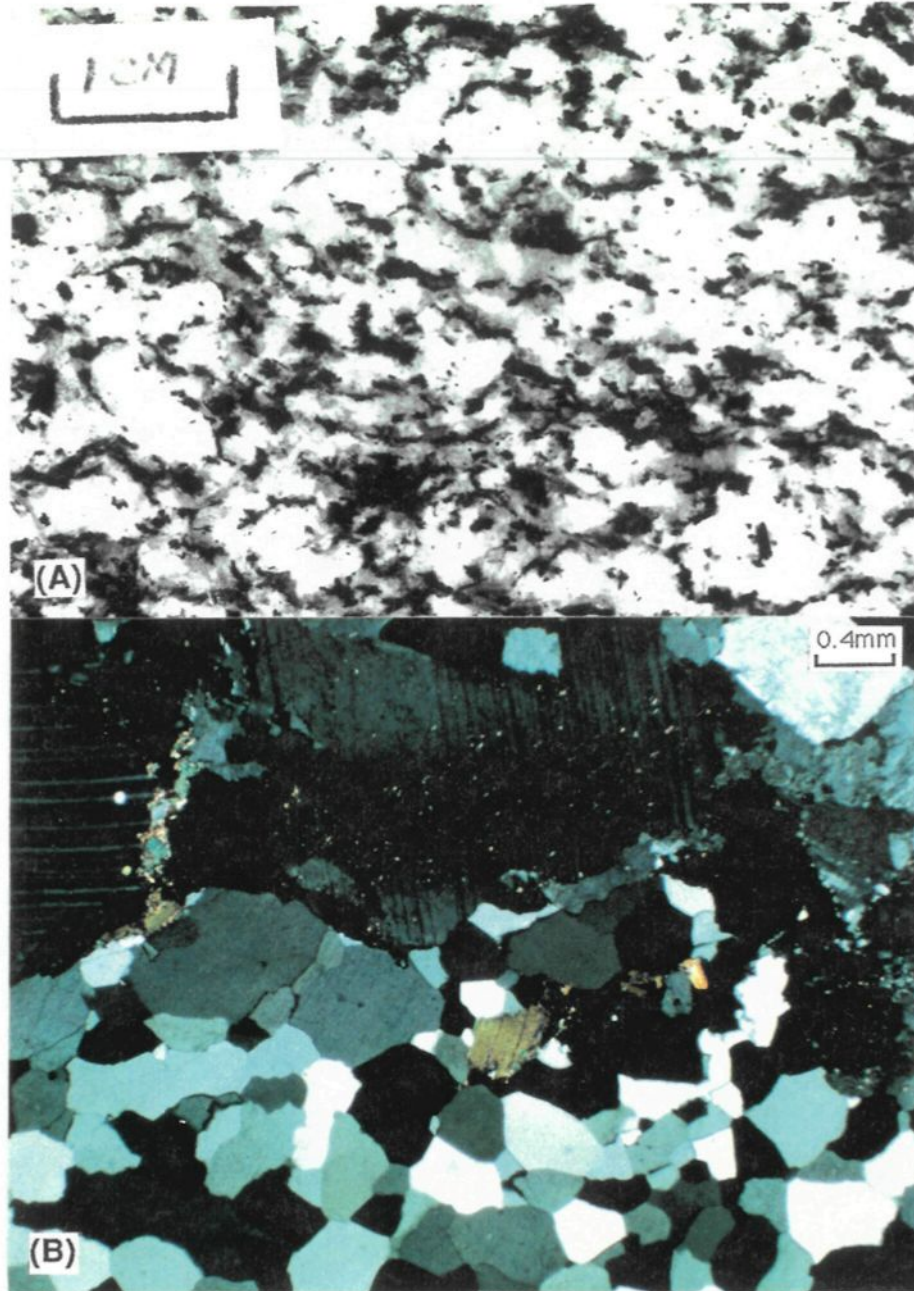
Plate 2.2 Biotite gneissic migmatite occurring in the Shidong - Wuhe - Shijian - Hetai area

(A) Gneissic structure, consisting of sub-oriented biotite-rich sclieren and quartz-feldspar leucosomes. The leucosomes are sugary textured. Polished slab. (B) The light-colored neosome (lower) and paleosome (upper) under the microscope. The paleosome has metasomatic texture, while the neosome has typical triple point texture, characteristic of crystallization. Cross polarized light.

Table 2.2 Chemical compositions of the migmatites occurring in the Hetai area

Sample	SiO2	TiO2	Al2O3	Fe2O3	FeO	MnO	MgO	CaO	Na2O	K2O	P2O5	K2O/Na2O
G93*	73.15	0.25	13.43	0.12	2.35	0.03	0.60	1.14	2.48	4.66	0.12	1.88
G94-1*	69.26	0.50	14.51	0.29	3.64	0.03	1.44	3.02	2.52	2.56	0.08	1.02
P4-4-1*	72.56	0.33	13.39	0.50	1.59	0.08	0.51	0.78	2.40	5.08	0.00	2.12
P4-4-3*	68.01	0.55	15.20	0.34	3.58	0.15	2.00	2.78	3.34	2.30	0.00	0.69
P4-4-5*	69.01	0.45	15.01	0.41	3.33	0.15	1.86	2.52	3.60	2.51	0.05	0.70
P4-4-6*	70.85	0.33	14.89	0.27	2.77	0.10	1.35	1.49	3.55	2.77	0.00	0.78
W51*	68.16	0.51	15.17	0.43	3.23	0.06	1.77	3.22	3.18	3.10	0.14	0.97
S-02	70.46	0.35	14.76	0.63	1.79	0.05	0.80	2.80	3.24	4.51	0.13	1.39
S-03	67.35	0.53	16.02	1.23	2.66	0.08	1.10	4.00	4.13	2.29	0.20	0.55
S-06	74.41	0.13	13.44	0.16	0.96	0.04	0.30	0.70	3.60	4.99	0.05	1.39
Average migmatite	70.32	0.39	14.58	0.44	2.59	0.08	1.17	2.25	3.20	3.48	0.08	1.09
Average schist	70.93	0.55	13.87	0.96	3.31	0.05	1.91	0.64	1.18	3.72	0.13	3.16
Migmatite/Schist	0.99	0.71	1.05	0.45	0.78	1.52	0.62	3.53	2.72	0.94	0.60	0.34
TiO2-normalized	1.40	1.00	1.48	0.64	1.10	2.14	0.87	4.98	3.83	1.32	0.85	

Sources: * from Huang (1988); Others from the present study

respect to the average Hetai schist, suggesting a chemically closed system for these elements during the formation of migmatite. However, this is not necessarily true, since it can also be caused by the closure of constant sum data. One of the methods to solve the constant sum problem is to make the constant sum data into an open one (Chayes, 1971).

TiO_2 is an immobile element in high grade metamorphism (Barbey and Cuney, 1982), and its concentration can be precisely determined. When selective melting takes place, it remains in the relict phase, especially in rutile, sphene, ilmenite, and biotite if not melted. So it is reasonable to assume that TiO_2 is conserved during the formation of migmatite, and the TiO_2-normalized value may be used as a measure of the enrichment and depletion of elements. Table 2.2 indicates that SiO_2, Al_2O_3, K_2O, Na_2O and CaO, the characteristic components of the leucocratic neosome, have TiO_2-normalized values greater than 1, implying that they are the introduced constituents during the formation of migmatite. So according to the mass balance, the leucocratic neosome, consisting of quartz and feldspars, must be partly allochthonous, such as deeper strata.

Correlation coefficients (Appendix III-2.3) and factor analysis (Appendix III-2.4) demonstrate that the most significant major element association of the migmatite is {$-SiO_2$, TiO_2, $-K_2O$, MgO, FeO, CaO}, instead of {$-SiO_2$, Al_2O_3, TiO_2, K_2O, MgO, Fe_2O_3, FeO} that characterizes the Hetai schist (c.f. Appendix III-2.2). Al_2O_3 is no longer part of the key element association, and the linear relationship between SiO_2 and K_2O changes from negative for the schists into positive for the migmatites. This is in line with the nature of the formation of migmatite, which means nearly in situ mineral and chemical adjustments. That the formation of migmatite is characterized by a gradual introduction of SiO_2 and K_2O (possibly plus Na_2O) is also well demonstrated by the elevation of SiO_2 and K_2O and the decrease of Al_2O_3, Fe_2O_3, FeO, MgO and CaO from less homogeneous migmatite (represented by Samples S-02 and S-03) to homogeneous migmatites (e.g., Sample S-06).

The discussion above is consistent with previous studies. The migmatites occurring in the SWSH area are believed to be a direct result of high grade metamorphism, with the light-colored neosome as the product of in situ selective melting (anatexis) of the medium or low grade metamorphic equivalents (Fu, 1985; Mo and Ye, 1980; Huang, 1988; Liu, 1989; Institute of Geochemistry, 1979). The relatively higher SiO_2, Al_2O_3, K_2O, Na_2O and CaO in the migmatites than in the schists may be explained if it is considered that the selective

melting has occurred in the Sinian strata at depth, and the resultant melt has move up slightly, injecting or mixing with the overlying gneisses.

2. Trace Elements

Trace element concentrations of the migmatites are listed in Table 2.3, as well as the ratio of the average migmatite to the average Hetai schist for comparison. This table indicates that many trace elements are depleted in the migmatite, but several remain almost unchanged or even enriched with respect to the average schist. Depletions may be explained by the fact that trace elements act as impurity constituents in the protolith, and tend to migrate toward low temperature domains from higher temperature ones.

The trace elements which are nearly unchanged or enriched are commonly incompatible those, including large ion lithophile element Rb and high field strength elements Nb, Ta, Th, U, Zr, Hf, REE and Sc. This phenomenon is the result of the balance between a general tendency for element migration from high temperature fields toward lower ones and an introduction of incompatible elements accompanied by the upward injection of the melt derived by anatexis at depth.

Further correspondence analysis (Appendix III-2.5 and Figure 2.3) of the Hetai migmatites together with the Hetai schists indicates that sulphophile elements such as As, Sb, Au, Cu, Bi and Hg are apparently antipathetic to migmatites. They do not cluster around the migmatite field, while lithophile elements, such as Hf, Zr and W, are linked to migmatite. Migmatite and schist are indistinguishable on their trace element associations in the Hetai area.

The discussion above demonstrates that a closed chemical system does not exist for trace elements during the formation of migmatite, and that the geochemical behavior of trace elements is mainly controlled and balanced by two different actions. One is that trace elements tend to migrate outwards to lower temperature domains when temperature rises. The other is that incompatible elements are introduced with the anatexis of original rocks at depth and the injection of the resultant melt.

3. Rare Earth Elements

Rare earth elements are considered immobile during metamorphism, even in

(continued)

	Se	Sn	Sr	Ta	Te	Th	U	V	W	Zn	Zr	La	LREE	HREE	REE	Rb/Sr	Nb/Ta	U/Th	Zr/Hf
For Schists																			
G-01	0.052	4		0.8	0.043	13.6	3.1	29	1	112.5	202	30	116.2	13.7	129.9		11.38	0.23	50.50
G-02	0.049	4		1.25	0.04	19.8	4.5	24	1	152.5	197	43	178.7	18.7	197.3		11.20	0.23	34.56
G-03	0.082	7		0.56	0.05	15.2	3.1	25	1.5	32.5	364	28	116.0	16.5	132.5		13.75	0.20	30.33
G-3-2	0.042	7		1.44	0.04	21.7	4.8	23	0.8	130	191	48	193.3	20.9	214.2		11.81	0.22	38.20
G-06	0.044	7		0.78	0.038	10.1	2.4	29	2	90	144	24	94.4	13.0	107.5		8.33	0.24	49.66
G-08	0.085	10		1.15	0.052	19.7	3.7	34	1	110	163	43	171.6	18.1	189.8		11.30	0.19	37.05
G-09	0.068	11		1.37	0.05	24	4.4	25	1	140	159	51	207.3	23.4	230.7		9.49	0.18	22.71
GZ-23	0.050	4.5		0.79	0.04	17.4	3.6	14	1.4	72.5	496	31	128.5	12.8	141.4		9.75	0.21	33.07
GZ-28	0.050	4.3		1.45	0.038	26.9	5.8	20	1.3	220	245	61	247.7	25.9	273.6		12.41	0.22	47.12
GZ-30	0.039	3.5		1.72	0.04	24	7.4	23	1	105	182	43	180.1	18.8	199.0		6.40	0.31	37.92
Average schist	0.056	6.2		1.13	0.0431	19.2	4.3	25	1.2	117	234	40	163.4	18.192	181.6		10.345	0.2225	35.5
For Migmatites																			
S-02	0.050	4		0.91	0.05	29	4.4	34	0.8	95	150	48	179	19.6	198.6		9.23	0.15	34.88
S-03	0.062	9		1.073	0.038	23.8	2.9	32	1	125	214	42	149.5	14.8	164		13.70	0.12	40.38
S-06	0.055	8		0.418	0.04	13	3.2	24	1.2	57.5	165	19	74.4	13	87		20.11	0.25	47.14
P4-4-1*		8.4	73	0.0				23	0.2	48		22	133.0	71.0	204.0	3.18	0.00		
P4-4-3*		10.1	88	1.0				75	0.1	89		20	106.0	29.1	135.0	2.14	0.08		
P4-4-6*		17.7	161	3.5				46	0.2	46							1.15	0.29	
Average migmatite	0.056	9.5	107	1.15	0.0	21.9	3.5	39	0.6	77	176	30	128.4	29.5	157.7	2.2	7.24	0.17	40.80
Migmatite/Schist	0.99	1.53		1.02	0.99	1.14	0.82	1.58	0.47	0.66	0.75	0.75	0.79	1.62	0.87		0.70	0.78	1.15
TiO2-normalized	1.40	2.16		1.43	1.39	1.61	1.15	2.23	0.67	0.93	1.06	1.06	1.11	2.28	1.22				

Table 2.3   Trace elements of the schists and migmatites occurring in the Hetai area

	Ag	As	Au	Ba	Bi	Co	Cr	Cs	Cu	Hf	Li	Hg	Nb	Ni	Pb	Rb	Sb	Sc
For Schists																		
G-01	90	7.2	2	448	5.5	10	67	11	30	4		0.73	9.1	75	38.5	154	0.084	7.6
G-02	136.6	7.5	39	445	8	15	96	17	53.9	5.7		0.55	14	66.7	38	201	0.077	13
G-03	36.6	1.6	2.5	213	1	5.5	56	4.3	10	12		4.05	7.7	41.7	38.5	70	0.075	5.3
G-3-2	136.6	8.5	1	766	8.3	17	101	31	35.9	5		1.21	17	75	38.5	299	0.012	16
G-06	90	16	0	667	10.4	8.8	54	10.5	41.9	2.9		4.96	6.5	50	76.9	176	0.124	8.3
G-08	126	13.3	1	513	5	13.3	90	13	61.9	4.4		5.00	13	75	38.5	186	0.035	15
G-09	160	237	1.5	620	12.6	18	105	26	12	7		5.30	13	83.3	38	238	0.35	14.5
GZ-23	30	3.2	2	106	1	3.9	58	8.5	10	15		3.42	7.7	33.3	19.2	87	0.105	5.5
GZ-28	213.3	14	2	527	3.6	19	122	27	22	5.2		1.10	18	83.3	38.5	291	0.078	19
GZ-30	90	6.2	1	506	0.3	4.3	33	10.5	16	4.8		21.88	11	41.7	57.7	242	0.067	4.5
Average schist	110.9	31.5	5.2	481	5.6	11.5	78	15.9	29.4	6.6		4.82	11.7	62.5	42.2	194	0.1007	10.9
For Migmatites																		
S-02	26.6	0.6	1	864	0.7	4.8	45	4.7	12	4.3		13.97	8.4	16.7	57.7	144	0.094	5.8
S-03	60	0.4	3	417	6.4	6.3	45	10	12	5.3		2.83	14.7	58.3	38	121	0.041	8.3
S-06	16.6	1	2	694	0.5	1.3	39	4.4	2	3.5		0.74	8.4	41.7	76.9	207	0.078	4.4
P4-4-1*						3.9	16.5		26.5		25.4		15.0	1.5	37.0	232		4.0
P4-4-3*						9.7	42.7		23.2		58.7		13.0	19.6	21.0	188		14.0
P4-4-6*						6.3	55.0		30.1		43.9		12.0	19.5	32.0	185		6.0
Average migmatite	34.4	0.7	2.0	658	2.5	5.4	41	6.4	17.6	4.4	42.7	5.85	11.9	26.2	43.8	180	0.071	7.1
Migmatite/Schist	0.31	0.02	0.38	1.37	0.45	0.47	0.52	0.40	0.60	0.66		1.21	1.02	0.42	1.04	0.92	0.71	0.65
TiO2-normalized	0.44	0.03	0.54	1.93	0.64	0.66	0.73	0.56	0.85	0.93		1.71	1.43	0.59	1.46	1.30	0.99	0.92

Sources: * from Huang (1988); Others from the present study
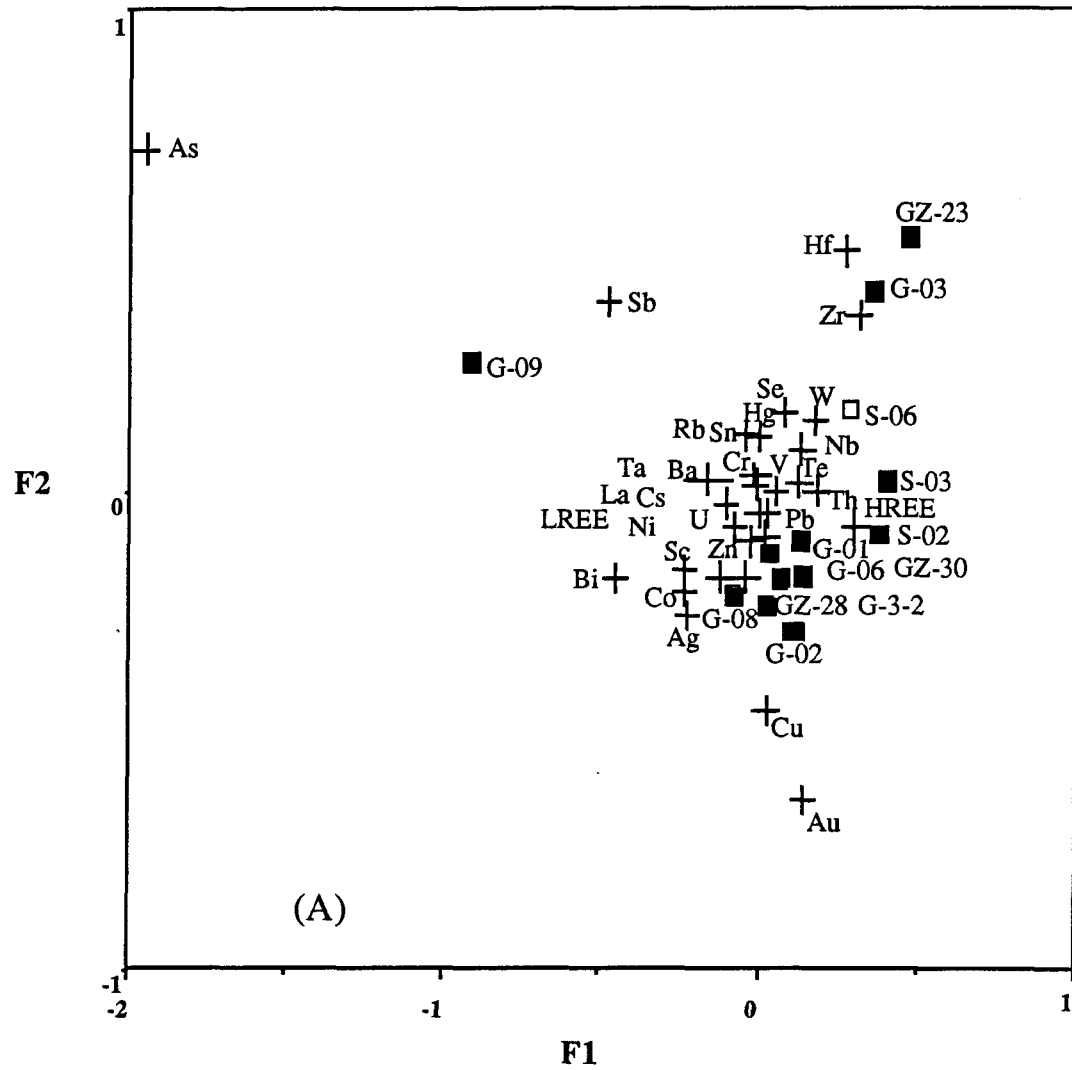
Figure 2.3 Correspondence analysis of the schists and migmatites occurring in the Hetai area, southern China
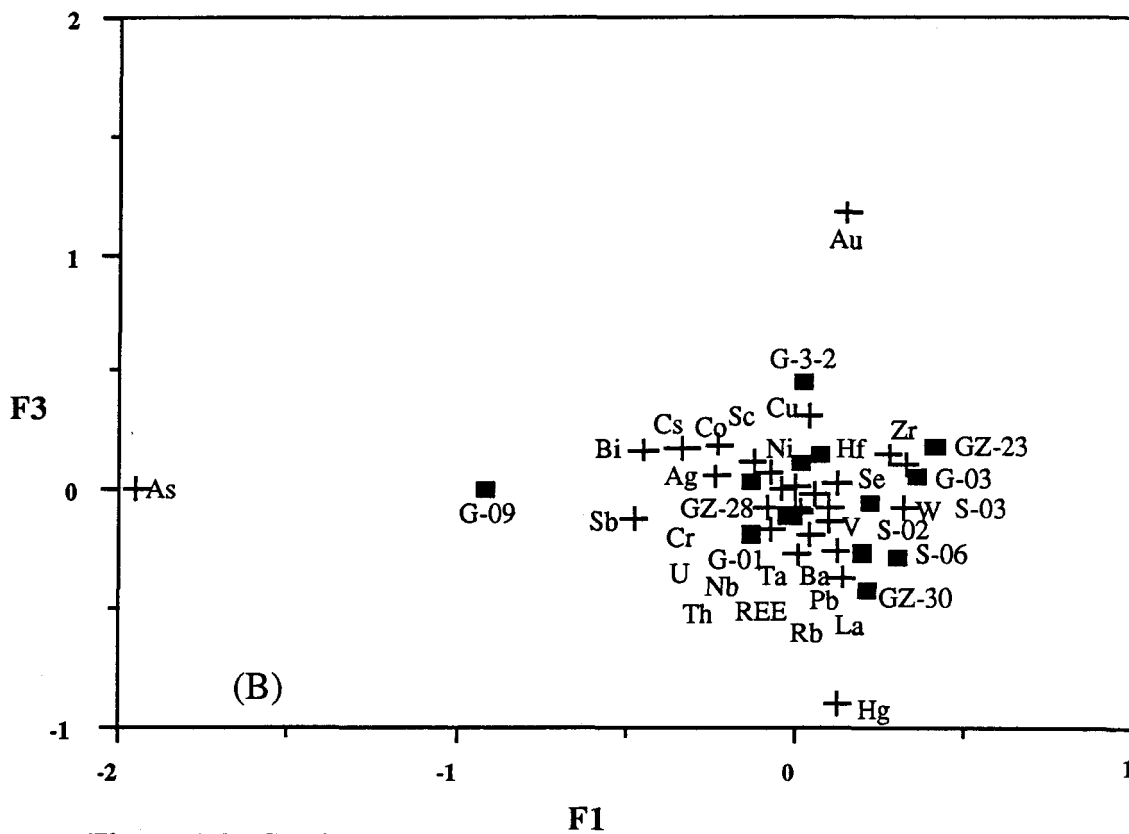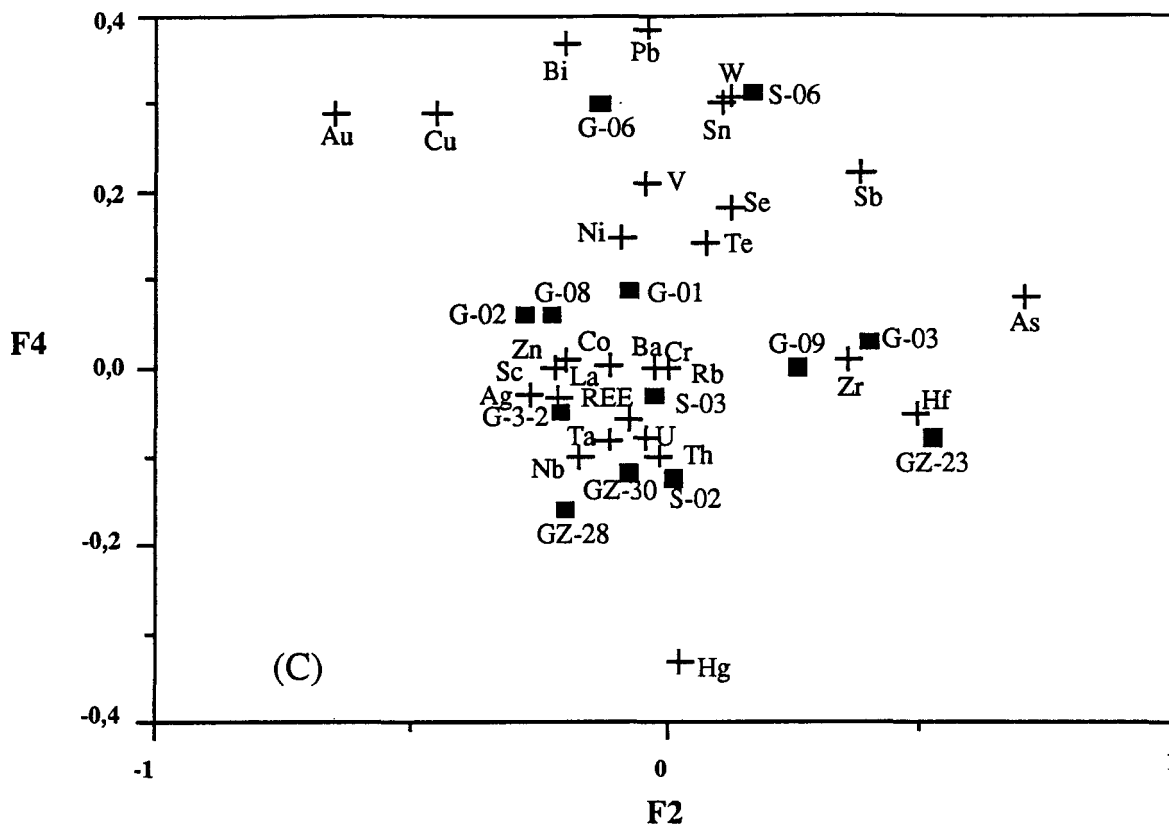
Figure 2.3 (Continued)

metasomatic processes, by a number of authors (Menzies and Seyfried, 1979; Helvaci and Griffin, 1983; Bernard-Griffiths et al, 1985; Hajash, 1984; Grauch, 1989). However, others (Church, 1987; Staudigel and Hart, 1983; Vocke et al., 1987; Stahle et al; 1987; MacLean, 1988) demonstrated that REE are mobile under certain conditions. The present study shows that REE were mobilized during the formation of the Hetai migmatite, but they moved coherently, with only slight fractionation within the group.

The analyzed REE data of the Hetai migmatites together with other involved reference data are listed in Appendices III-2.6 and 2.7 and displayed in Figures 2.4 and 2.5. Samples of the schists occurring in the same area are also listed for comparison. These show three points: (1) The REE abundance of the migmatites is nominally depleted on the average in comparison to the schist of the same area. However, after deleting the effect caused by the mass change of major elements, their abundance is in fact higher than that of the average Hetai schist. The total REE has an average TiO_2-normalized value of 1.17. (2) The change of individual REE during the formation of migmatite is nearly the same. After TiO_2-normalization, the REE ratios of the average migmatite to the average schist extend in a narrow range, with most between 1.1 and 1.4. This is also reflected on the the Masuda - Coryell diagram (Fig. 2.5), which displays that the average REE distribution pattern of the studied migmatites is approximately parallel to, but slightly lower than that of the schists; (3) The HREE are preferentially enriched slightly in the migmatite with respect to LREE. The ratio of LREE/HREE rises from an average of 6.1 for the schist to 8.9 for the migmatite. Such a rise is consistent with the fact that HREE are stronger incompatible elements than LREE (Table 2.4).

4. Partition Coefficients and Partial Melting

Compatible elements may be used as important chemical constraints on the genesis of migmatite (Sawyer, 1987). The partition coefficients of several elements between solid minerals and melt phase are listed in Table 2.4. This table shows that Rb, Cs and Sc are the compatible elements of biotite, while Sr and Ba are compatible with feldspars, principally of potassium feldspar formed through the breakdown of muscovite. By definition, compatible elements do not preferentially enter the melt phase (Allègre and Minster, 1978).

In the Hetai area, Ba, a compatible element of potassium feldspar, is enriched in the migmatite, whereas Cs and Sc, the compatible elements of biotite, are depleted. Since any
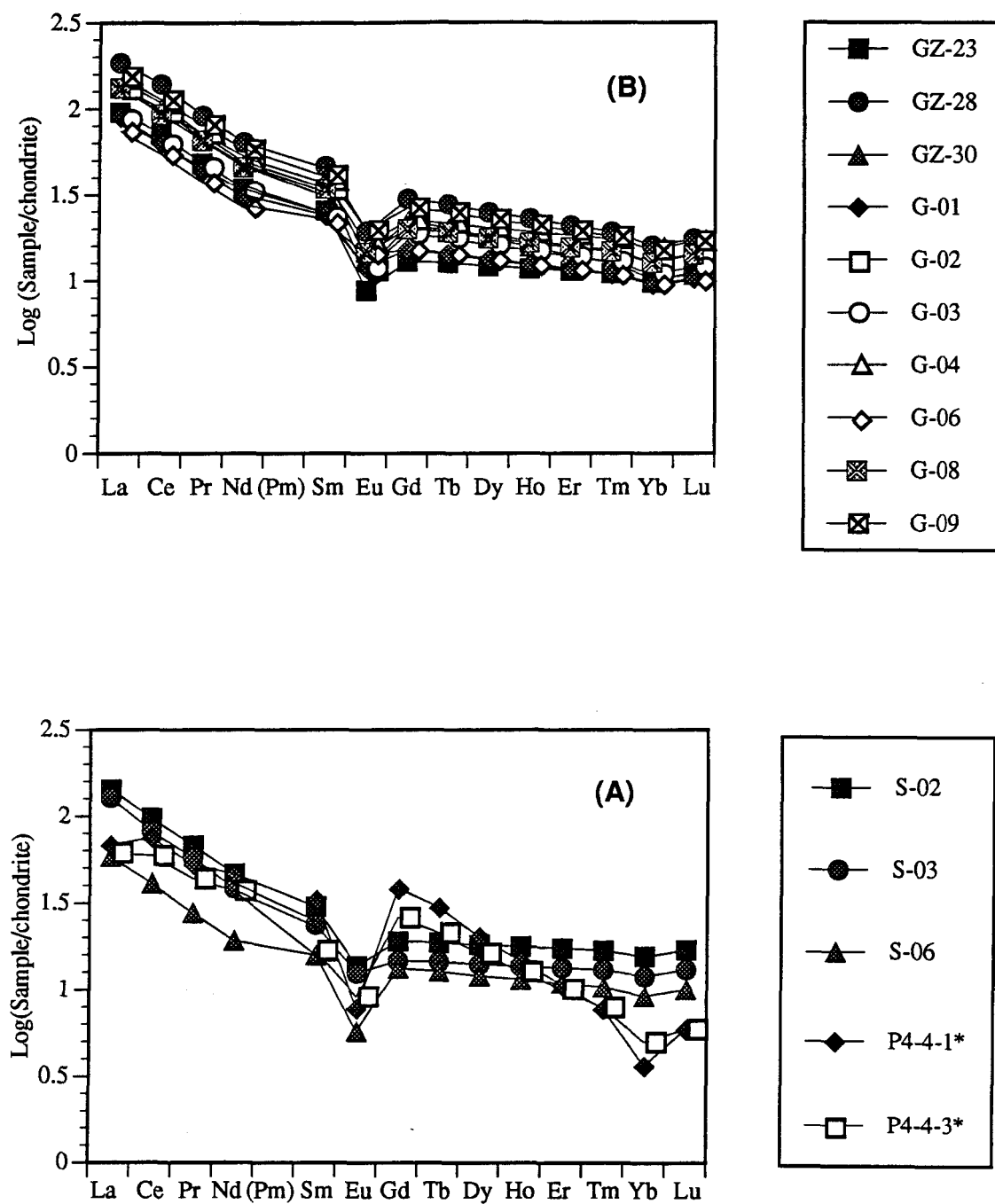
Figure 2.4 REE abundance distribution patterns (normalized to chondrite) of the schists (B) and migmatites (A) occurring in the Hetai area, southern China
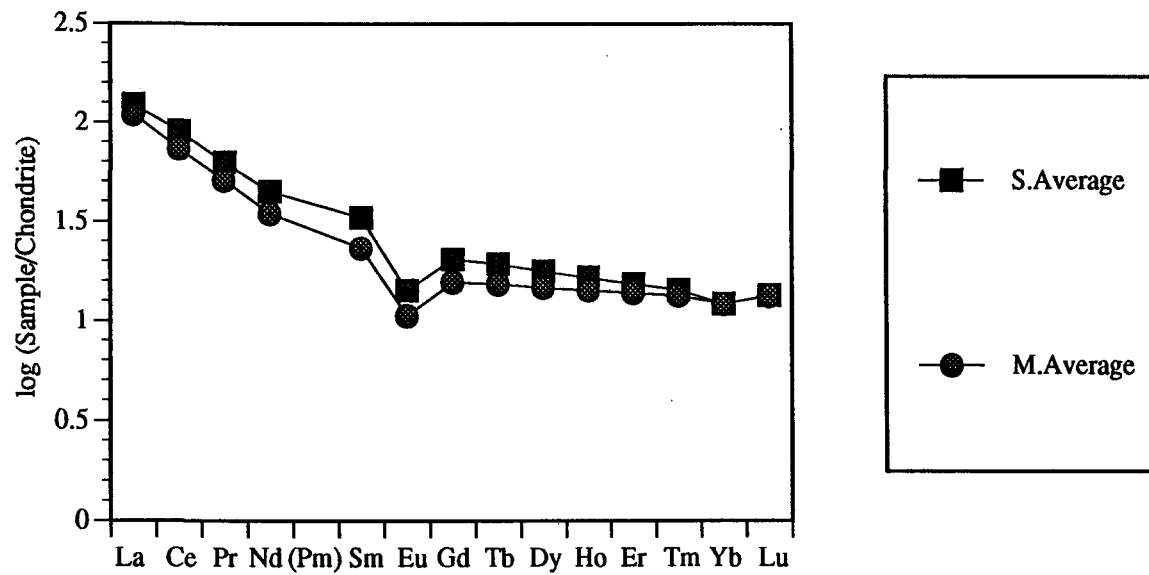
Figure 2.5 Comparison between the REE distribution patterns (normalized to chondrite) of the average migmatite and the average schist of the Hetai area, southern China

Table 2.4 Partition coefficients between mineral and melts used in partial melting and crystal fractionation model

Elements	Plagioclase	K Feldspar	Biotite	Garnet	Apatite
Ba	0.36	6	6.36	0.017*	
Ce	0.24	0.044	0.32	0.63	3-10***
Co	0.01***			1.9	
Cr	0.01***			13**	
Cs	0.04-0.31***	0.14	6		
Eu	2.15	1.13	0.24	5	5-30***
Hf	0.01-0.02***		0.01		
La	0.26		0.3	0.5	3-10***
Lu	0.062	0.006	0.33	50	
Mn				>1**	
Nd	0.04-0.13***				5-30***
Ni				0.8**	
Rb	0.048	0.8	3.26	0.0085*	
Sc	0.01***		11	27.6	
Sm	0.13	0.018	0.26	5.2	5-30***
Sr	2.84	3.87	0.12	0.015	1.1-2.4***
Tb	0.09	0.011	0.3	22	
Th	0.05	0.09	0.12		1-1.4***
U				<0.01**	
Y	0.01		0.4	40	
Yb	0.077	0.012	0.44	47	3-10***
Zn				about 1**	
Zr	0.01-0.02***			0.3**	

Data from Sawyer (1987) except: * from Hanson (1978); ** from Wedepohl (1985); *** from Grove et Donnelly-Nolan (1986)

deviation of the migmatite from the protolith, presumably the average Hetai schist, must be due to the introduction of leucocratic neosomes, this phenomenon is explainable only if it is supposed that biotite remains unmelted in the relict phase, while K feldspar and other felsic materials are exhausted by melting.

The geochemical analysis of elements argues that the migmatites in the Hetai area developed first through anatexis of pelitic or semi-pelitic gneisses at depth, and then the resultant melts moved upwards slightly and injected into the overlying gneisses which acted as the paleosome of the migmatite.

§4 Granites

4.1 Occurrence and Petrologic Characteristics

Three are three granite bodies present in the Hetai area (Fig. 1.4). They are Shidong, Yunluogan, and Wuncun granites.

Shidong (Migmatitic) Granite   Situated to the northwest of the gold field and with an surface area of more than 400 km^2, the Shidong granite is not in direct contact with the Hetai gold deposits. It intruded into Sinian to Cambrian strata, and has a gradational contact relationship with the surrounding migmatites. In some places, it is impossible to distinguish between the Shidong granite and the homogeneous migmatite. So the Shidong granite is sometimes called a migmatitic granite, and believed to have a origin similar to the surrounding migmatites, but with apparent upward intrusion of the melt (Mo and Ye, 1980; Liu, 1989; Huang, 1988; Fu, 1985).

Yunluogan Granite   Situated in the west of the Hetai gold field, the Yunluogan granite body has an exposed surface area of about 120 km^2. It consists of medium-grained biotite granodiorite, and locally of plagioclase granite and monzonitic granite. The major minerals of the biotite granodiorite are plagioclase (An = 25 - 40, 45 - 50%), K-feldspar (10 - 15%), quartz (20 - 25%) and biotite (about 10%). Zircon, apatite, sphene, ilmenite and magnetite are common accessory minerals.

Wucun Granite   The Wucun granite body is located in the north of the Hetai gold

Table 2.5 The ages of the granitic rocks in the Hetai area

Granites	Ages (Ma)	Methods
Pegmatite (Gaocun)	224	U - Pb
Wucun	210 ± 69	Rb - Sr isochron
Yunluogan	242 ± 3.3	Zircon U - Pb
Shidong	490 ± 62	Rb - Sr isochron

Source from No.719 Geological Team (1987) and Huang (1988)

field, and has a surface area of about 70 km². The lithology is mainly megacrystic biotite monzonitic granite and ordinary granite. The major mineral constituents consist of microcline (30 -40%), quartz (20 - 30%), plagioclase (oligoclase and andesine, 10 - 20%) and biotite (5 -10%). The megacrysts are commonly microcline, and the size ranges from 4 x 5 mm to 80 x 26 mm. Apatite, zircon, monazite, sphene and ilmenite are found among the common accessory minerals.

4.2 Chronology

Rb - Sr isochron and zircon U - Pb isotope methods were used to determine the age of the granitic rocks occurring in the Hetai area. Their ages of formation are listed the Table 2.5. This table shows that the Shidong granite formed the earliest (Caledonian), and then came the Yunluogan and Wucun intrusives during the Hercyno-Indosinian period.

4.3 Geochemical Characteristics

1. Major and Trace Elements

The chemical analysis data of major and trace elements of the granites occurring in the Hetai area are listed in Appendices III-2.8 and 2.9. It is shown that: (1) The Shidong granite is similar to the Caledonian migmatite of the same area in major chemical compositions; (2) Compared to the element abundance of the regional unmetamorphosed rock, the Wucun granite is enriched in large ion lithophile and high field strength elements, such as Cs, Nb, Rb, Ta, U, and W; (3) The Yunluogan granite is more basic than the other two. It contains less SiO_2, K_2O and Na_2O, but high CaO, MgO, MnO, TiO_2, TFe, Ag, Bi, Co, Cr, Cu, Hg, Sc, Sn, V, Zn, Zr, etc..

2. Rare Earth Elements

The REE distribution patterns (normalized to chondrite) of the Hetai granites are displayed in Figures 2.6 and 2.7, and the corresponding analysis data are listed in Appendix III-2.10. They illustrate that the REE patterns of these three granite bodies are similar to one another, and parallel to that of the regional basement rock (mainly metapelitic) of the area This may imply that they had a similar initial source area.
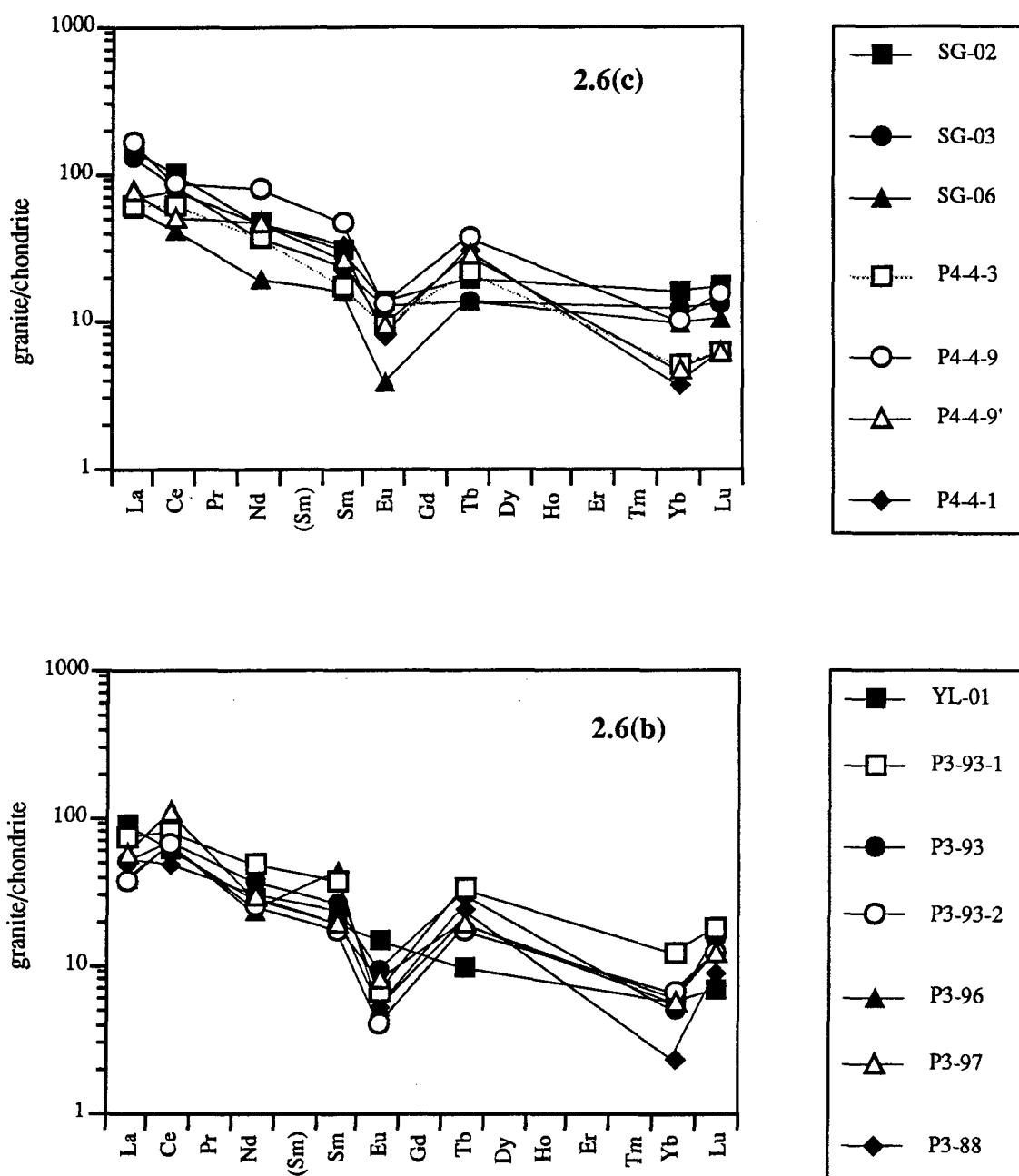
Figure 2.6 REE distribution patterns of the granitic rocks in the Hetai area
(a) Wucun granite; (b) Yunluogan granite; (c) Shidong granite

2.6(a)
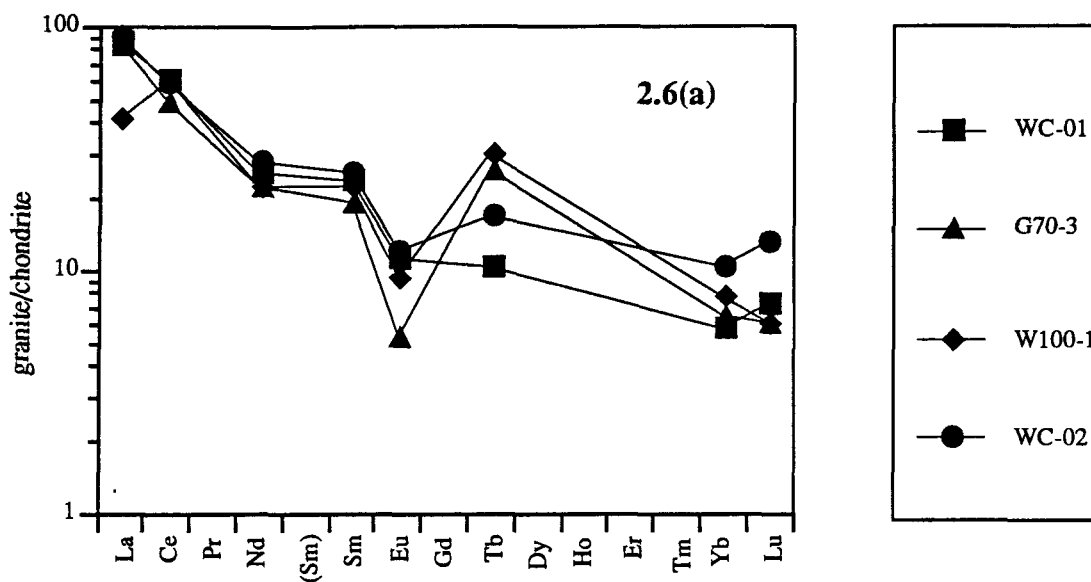
Figure 2.6 (Continued)
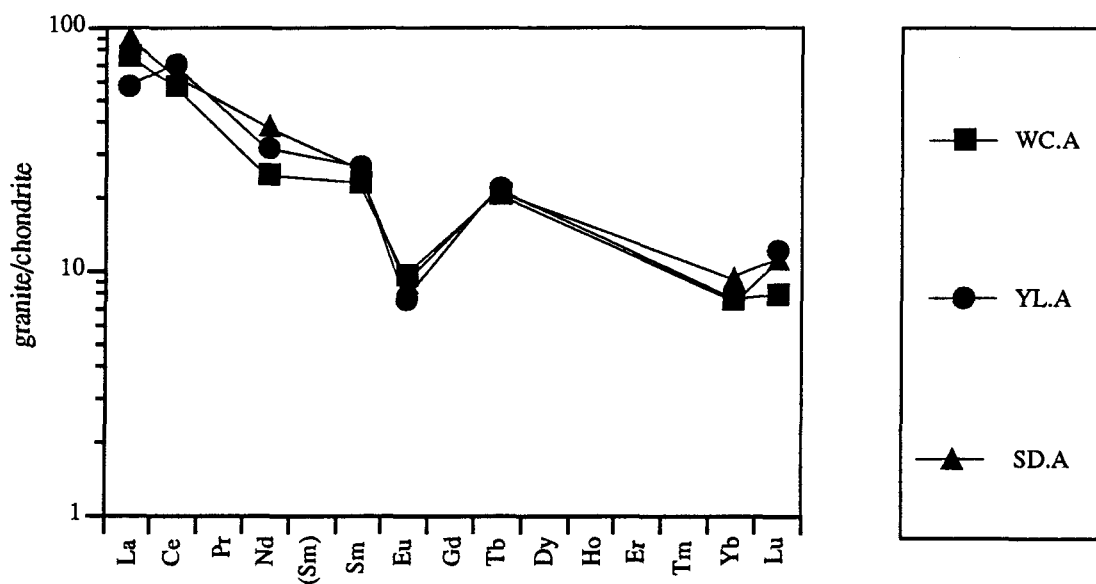
Figure 2.7 Comparison of the REE patterns of the granites in the Hetai area
WC.A stands for the average of the Wucun granite; YL, the Yunluogan granite;
SD, the Shidong granite

Table 2.6 Oxygen isotope of the granites occurring in the Hetai area

Samples	granites	Examined material	$\delta 18O$ *(per mil)*
G89-2	Shijiang	quartz	13.45
G-93	Shijiang	quartz	14.56
G95-2	Shijiang	quartz	9.90
W9	Shijiang	whole rock	9.70
W24	Shijiang	whole rock	10.39
W14	Shijiang	whole rock	11.65
H20	Yunluogan	quartz	10.24
H21	Yunluogan	quartz	11.05
G60	Yunluogan	quartz	14.30
G61	Yunluogan	whole rock	10.62
G70	Wucun	quartz	8.63
W88	Wucun	whole rock	10.06

Data from Huang (1988)

3. Strontium and Oxygen Isotopes

The initial ratio of $^{87}Sr/^{86}Sr$ is 0.713 for the Shidong granite, 0.7178 for the Yunluogan, and 0.7065 for the Wucun (Huang, 1988). The initial ratio of $^{87}Sr/^{86}Sr$ is a good indicator to the granite source (Faure, 1977). When this ratio is on the evolution curve of the upper mantle, the granite derived directly or indirectly from the upper mantle (I-type). High initial $^{87}Sr/^{86}Sr$ ratios are usually attributed to the introduction of radiogenic ^{87}Sr by rubidium of assimilated crustal rocks and/or long crustal residence time. When it is above the evolution curve, the granite is commonly of S-type. The apparently high observed initial ratio values of $^{87}Sr/^{86}Sr$ with the exception of the Wucun granite suggest that the granites occurring in the Hetai area have a S-type origin, derived from sediments. The Wucun granite may be either of I-type or of S-type.

The oxygen isotope data are listed in Table 2.6. It also shows that the Yunluogan and Shidong granites fall into the S-type granite field (>9.9%, O'Neil, 1979), while the Wucun can be either of S-type or of I-type.

§5 Summary

Schists are the main country rock of the Hetai gold deposits. The characteristic minerals include staurolite, sillimanite and almandine garnet. They were developed in a intermediate or intermediate-low pressure metamorphic facies series, with a geothermal gradient of about 30-50°C per kilometer. The main temperature and pressure at which the schists formed range from 550 to 670°C and from 250 to 600 MPa. The protolith is pelitic or semi-pelitic, intercalated with bedded cherts.

The formation of migmatites was an integral part of high grade regional metamorphism. It is characterized by the nearly in-situ adjustment of chemical compositions within the open metamorphic system. Many trace metals, especially the sulphophile, are depleted in the migmatites with respect to the schists. However, several incompatible elements (e.g., Rb, Ta, Nb, Hf, Zr and Sc) are unchanged or enriched. The migmatites inherits the REE distribution pattern of the schists, but HREE appear slightly more enriched than LREE in the migmatites.

Th Caledonian Shidong granite has an origin similar to the coeval migmatite. The Yunluogan and Wucun granites formed during the Hercyno-Indosinian period. They were derived from the upper crust, with the Wucun probably derived in part from the mantle.

Chapter III

BEDDED CHERTS: PETROLOGIC AND GEOCHEMICAL CHARACTERISTICS, AND ORIGIN

Petrographic and geochemical studies suggest that many bedded cherts have a hydrothermal origin (Iijima et al., 1983), as well as a biologic origin (Hesse, 1988). The presence of chert in the upper part of the Sinian sequence offers an excellent opportunity to evaluate a possible hydrothermal system in the potential source rocks of gold. Should the cherts prove to be of hydrothermal origin, two objectives may be analyzed. First, the potential of the Sinian strata to provide gold to a hydrothermal system may be evaluated, and second, if gold enrichment is attained by early hydrothermal activity, an important regional source rock may be produced.

Hydrothermally deposited cherts occur in various tectonic environments in past geological history. The late Jurassic to early Cretaceous Franciscan chert formation in California, for example, associated with an ophiolite complex, is apparently related to a fossil hydrothermal system (Crerar et al., 1982; Yamamoto, 1987). Similar chert formations were found in the Late Jurassic through Santonian Nicoya Complex along the Pacific coast of Costa Rica (relatively near-shore environment, Hein et al., 1983) and Panama (Kuijpers and Denyer, 1979), in the Mesozoic Kelp Bay Group of southeastern Alaska (Hein et al., 1983), in the Cretaceous Shimanto Terrain (Orogenic belt, originally hemipelagic marginal and inter-arc basin), southwest Japan (Yamamoto, 1987), in the Ordovician Munsungun Lake Formation (volcanic arc) of northwestern Maine (Pollock, 1987), and in Devonian intra-platformal basin of northwest Guangxi province, southern China, where bedded cherts were derived from hydrothermal emanations (Chen and Chen, 1990; Zhou, 1990).
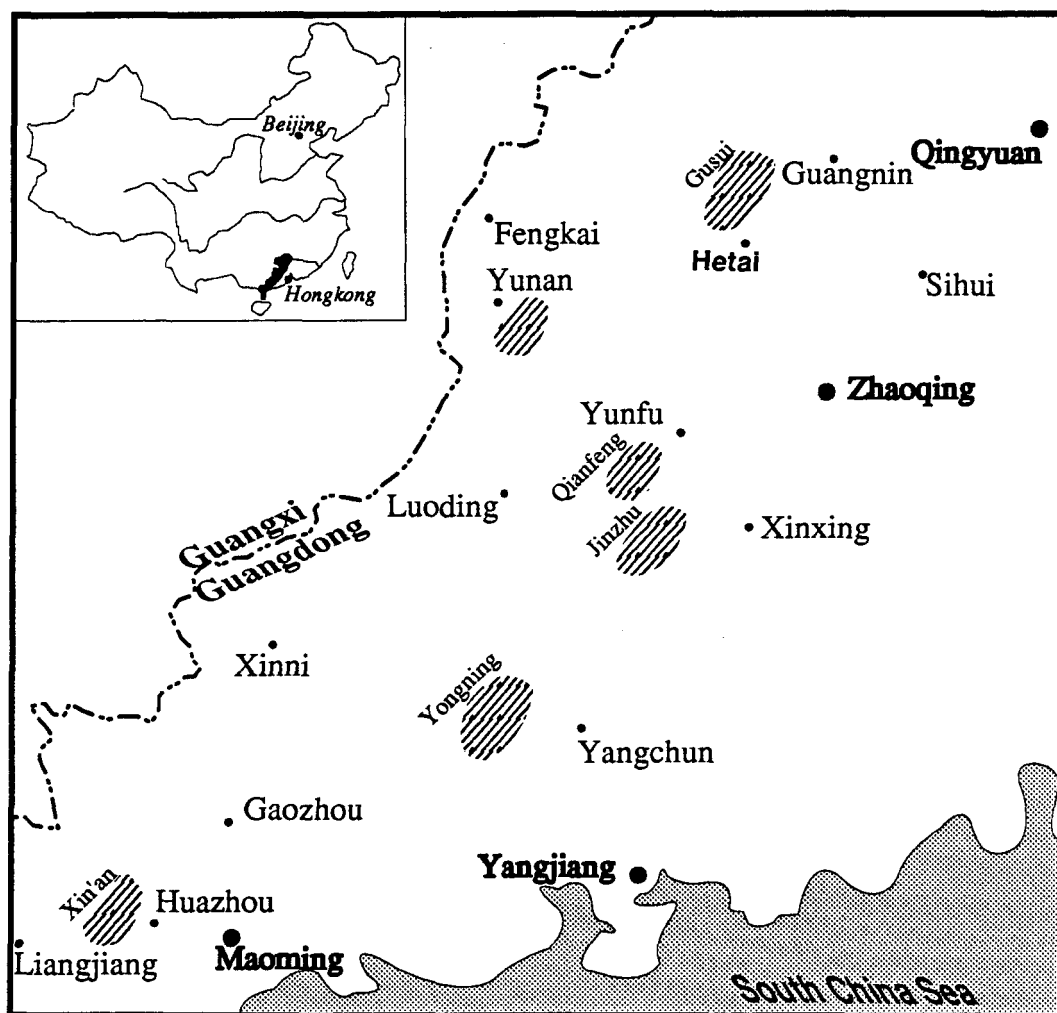
**Figure 3.1 Distribution of known Zd bedded chert formation
in western Guangdong Province**

The lined areas stand for the chert formation (not to scale)

Examples of hydrothermal cherts occurring in modern ocean floors and continental high geothermal areas include the DSDP Leg 32 in the northern Pacific (Adachi et al., 1986), the DSDP Leg 62 on Mid-Pacific Mountains and the Hesse Rise (Hein et al., 1982; Hein et al., 1983), Galapagos at 86°W (Herzig et al., 1988), Juan de Fuca ridge (Canadian American Seamount Expedition, 1985), the Mid-Atlantic Ridge (Crocket, 1990) and the Taupo Volcanic Zone at Rotokaua of New Zealand (Weissberg, 1969).

The following study focuses on the chert from the Gusui section, about 30 km to the north of the township of Hetai (Fig. 3.1).

§1 Regional Occurrence and Petrology

1.1 Regional Occurrence

The bedded chert formation examined is an independent stratigraphic unit (Z^d) and a marker horizon defining the top of the Sinian strata (Guangdong Bureau of Geology, 1977; Ji, 1988, personal communications). It occurs over the whole western Guangdong and southeast Guangxi provinces. In addition to the Gusui occurrence, the chert formation was also identified at Jinzhu of Xinxing county, Yunfu township of Yunfu county, Yongning of Yangchun county, Xin'an of Huazhou county, Yunan town of Yunan county.

The Z^d bedded chert formation varies in thickness depending on geographic location, but usually ranges from a few tens of meters to about a hundred meters. At the Gusui section, it is about 60 meters thick. It overlies the older Sinian strata, consisting mainly of fine-grained terrigenous sediments intercalated with chert bands, and underlies the dark carbonaceous and siliceous shales of the Cambrian strata. Both contacts are conformable. The Z^d bedded cherts at the Gusui section is particularly well exposed in a road-cut outcrop.

1.2 Mineralogy and Structures

The Z^d bedded cherts are very fine-grained rocks, predominantly composed of microcrystalline quartz (about 0.02 - 0.05 μm in diameter). Minor minerals include clay minerals, hematite, barite, and occasional pyrite, as well as carbonaceous and organic

materials. Barite is observed as a thin film along fracture surfaces of the chert. Barite is reported as a component of sea-floor hydrothermal sediments (Bonatti et al., 1972; Bertine and Keene, 1975; Laluo, 1983), and has been found in the Afar Rift, associated with opal, gypsum, nontronite, goethite and Mn-oxide, and the Laue basin, associated with opal and volcanic detritus.

Typical structures of the cherts include the following:

Bedded Structure: Bedded structure consists of layers ranging from 1 cm to some 30 cm, with the average about 3 cm. Layers are separated by films of dark clay and parallel discontinuous planes.

Laminated Structure (Plate 3.1): The layers (laminae) are much thinner than those of the bedded structure. Hairline or pinstripe laminae alternate rhythmically, and are parallel to bedding. The laminae are distinguished by color, mineral and chemical variation. Unlike the bedded chert, laminated cherts cannot be split along the lamination planes with a hammer. Under the microscope the alternation of a microcrystalline quartz phase and a hematite-rich phase (micronodules) is characteristic (Plate 3.2). A similar laminated structure is found in the upper Devonian chert formation of the Nandan-Hechi basin of Guangxi Autonomous Region, southern China, where it was suggested to be the product of intermittent or periodic hydrothermal activity, with the silica phase representing rapid precipitation during peak hydrothermal activity, and the iron and manganese oxide-rich phase representing slow deposition during quiescent periods (Zhou, 1987).

Massive Structure: Massive structure includes thick sequences of chert that are uniform. Because it is frequently brightly colored, the massive chert may be categorized as jasperoid. Lovering (1972) described the characteristics and distribution of jasperoids occurring in the United States, and other authors (Fournier, 1985) attributed them to massive replacement of limestone by silica. However, the replacement model is unlikely for the Gusui chert, since there is no evidence that limestone ever deposited in this area during the Sinian period. Instead, the Gusui jasperoid may have resulted either from mixing of hydrothermal solutions with cold seawater, or from decompressional boiling of the hydrothermal solutions. The favorable environment for its presence is near the exit point of hydrothermal solutions (Chen and Chen, 1990; Zhou, 1990).
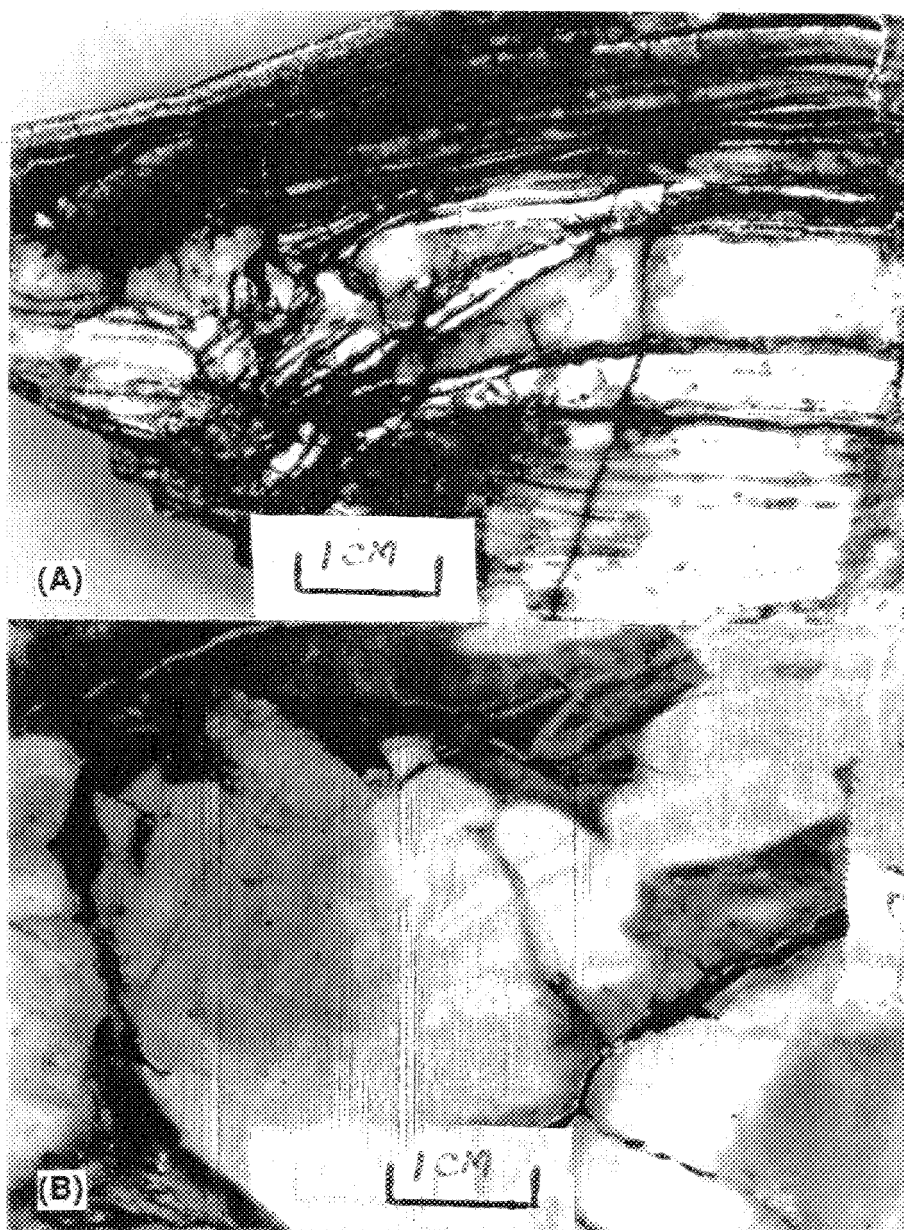
Plate 3.1 Sedimentary structures of the Gusui bedded cherts

(A) Laminated structure: Characterized by the alternation of "pure" microcrystalline quartz bed (laminae) and impure quartz laminae. Laminae are thinner than 1 cm, and parallel the bedding. Polished thin slab. (B) Pseudobrecciated structure: Pseudobreccias are centimeter-sized chunks of red to brown chert suspended in a white and green microcrystalline matrix. The margin is irregular veins and bleached zones. The pseudobreccias are well preserved, with little compaction or deformation. Polished thin slab.
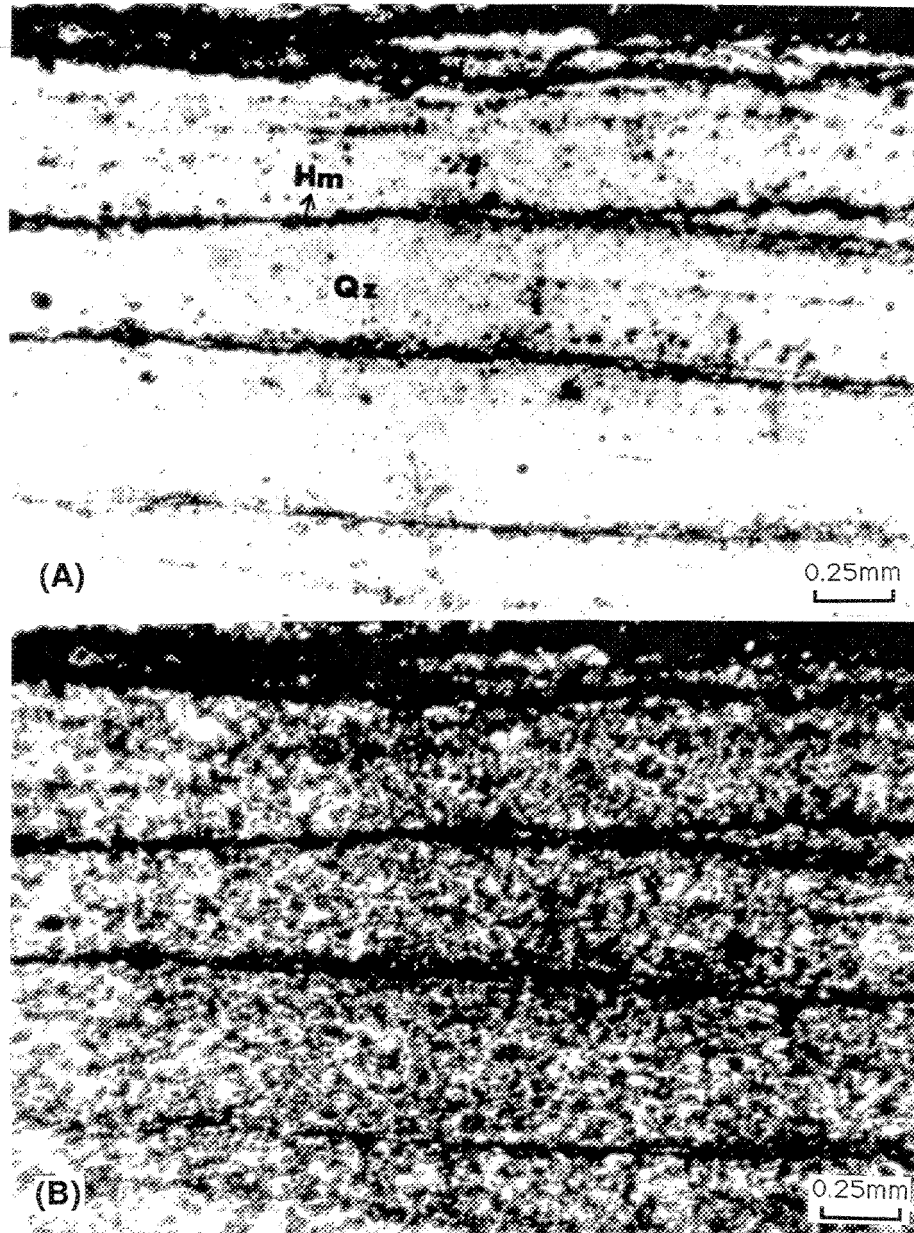
Plate 3.2 Microscopic laminated structure of the Gusui cherts

Hairline or pinstripe laminae parallel to bedding and alternate rhythmically. The alternation of microcrystalline quartz phase and hematite-rich phase is particularly characteristic. (A) in plane polarized light, and (B) in Nicols.

Vein and Pseudobrecciated Structures (Plates 3.1): Veining is well developed in the Gusui bedded cherts. The veins are associated with pseudobreccias and serve as the latter's boundaries. They may be used to distinguish between successive stages of hydrothermal activity. Both massive and bedded cherts are cut by a network of veins microns to millimeters thick. Three main veining stages — early, intermediate, and late — are observed on both the megascopic and microscopic scale. The first two generations are quasi-synsedimentation.

The early and intermediate veining stages are represented by a characteristic bleached zone and "pseudobreccia", being centimeter-sized chunks of red to brown chert suspended in a white and green microcrystalline matrix. This distinctive texture was also observed in Costa Rican cherts (Kuijpers and Denyer, 1979) and in Franciscan manganiferous cherts (Crerar et al., 1982). The veins and bleached zones that cause pseudobrecciation have vague and irregular margins, and contain clasts of the surrounding chert. These veins appear to represent fluid channels which disperse into the original silica sediments. The bleaching presumably results from reduction of red ferric oxides. Keith and Muffler (1978) suggested that simultaneous brecciation and deposition of amorphous silica occur as a result of self-sealing and sudden release of pressure, caused by fracturing accompanying resurgent doming.

Some early-stage veins have indistinct boundaries. It is suggested (Crerar et al., 1982) that such veins are originally chalcedonic. Such chalcedony is known to occur as a hydrothermal precipitate and recrystallization product in waters at 100° to 300°C, and represents the product of the first movement of hydrothermal solutions through the unconsolidated sediments at or near the sediment-seawater interface (White and Corwin, 1961; Crerar et al., 1982).

Late-stage veins are commonly inclusion free, thin and straight, display sharp margins, and crosscut early veins. They suggest either late hydrothermal pulses, feeding the upper level sediments through the deeper, consolidated sediment, or result from Caledonian deformation and metamorphism.

All stages of veins are at present composed of microcrystalline quartz. However, the grain size of microcrystalline quartz varies from stage to stage, generally the later-formed veins consist of coarser recrystallized quartz grains. In addition to microcrystalline quartz veins, pore spaces in surrounding sediments are filled and cemented with silica which may

have been either hydrothermal or diagenetic in origin.

1.3 Compaction and Recrystallization

A low degree of compaction, as indicated by good preservation of the pseudobreccia texture, is remarkable in the recrystallized Gusui cherts. The recrystallization may be responsible for the development of the observed coloring and mineralogy. Microcrystalline quartz may be derived from the transformation or recrystallization of amorphous silica (opal-A), cristobalite (opal-CT and opal-C), tridymite, chalcedony, or various combinations of these phases (Pollock, 1987). Quartz grains are commonly coarser in veins than in the groundmass. The low degree of compaction favors a rapid precipitation and transformation of opaline silica to microcrystalline quartz at a relatively high temperature.

1.4 Color

The cherts exhibit a wide range of color, from chocolate brown, reddish, green, to pale yellow, gray and white. Mottles, lamination and smeared-out coloration are common. Some colors seem to be specific to a component of certain structures. For example, chocolate brown and reddish color is characteristic of the Fe oxide-rich laminae of laminated cherts, while the pseudobrecciated chunks of jasperoid are characteristically brightly multicolored with white and pale yellow being the base color in the center, and green around the margins.

The difference of color indicates varying amounts and proportions of minerals and trace elements, and a formation process under various physiochemical conditions. Recent studies (Pollock, 1987; Hein et al., 1983) shown that the red coloration is caused by finely disseminated grains of anhedral to subhedral hematite, and characterized chemically by ferric iron, while the greenish color is due to clay- to silt-size chlorite, and higher in Ni and V; the white, due to higher SiO_2; and the black, due to very low FeO, and high Mn, Co, Cu, Ni and organic materials.

In summary, the petrographic characteristics described above suggest that the Gusui bedded cherts are of hydrothermal origin.

§2 Geochemistry of Major and Trace Elements

Cherts of different origin from different areas differ in chemical compositions. Various elements and element associations have been used to study the depositional environment and origin of cherts. Results show that characteristic element abundance and element associations are sensitive to the depositional environment and origin, and therefore may be used as an indicator of the latters.

2.1 Bulk Compositions

The Z^d bedded cherts at the Gusui profile are predominantly composed of SiO_2. The concentrations of conventional major element oxides (in weight %) and 26 trace elements (in ppm) are listed in Table 3.1. Their average and the ratio to the average crustal abundance are also shown in the same table for comparison. This table demonstrates that the major oxides, TiO_2, Al_2O_3 and MnO, are characteristically low in the studied cherts with the exception of Sample GS-11, which is a mudstone sandwiched between chert beds. Most trace elements are also apparently depleted with respect to the average crust. However, a few others, such as Ba, As, Sb, W, Sn, Hg, Ag, Se and Bi, appear to be preferentially enriched in the Gusui cherts. The abundance of gold is 8.7 ppb on the average, about twice that of the crust.

The features of element abundance described above are analogous to those of many other bedded cherts attributed to hydrothermal origin. It was suggested (Yamamoto, 1987) that low TiO_2 and Al_2O_3 is characteristic of hydrothermal cherts. Table 3.2 lists the average chemical compositions of typical hydrothermal cherts from the Franciscan Terrain, the Shimanto Terrain, the DSDP Leg 32 and northwestern Guangxi, compared to the Gusui chert. All hydrothermal cherts in this table are poor in TiO_2 and Al_2O_3. For this reason, a TiO_2-normalized value has been used as indication of the chemical characteristics and depositional environments of siliceous rocks, and is successful in distinguishing between hydrothermal and hydrogenous components (Yamamoto, 1987; Sugisaki, 1984). The TiO_2-normalized value of an element is obtained by dividing the content of the element by that of TiO_2 of the same sample. Hydrothermal cherts usually have greater TiO_2-normalized values than those of hydrogenous origin (Yamamoto, 1987).

The hydrothermal cherts occurring in the Munsungun Lake Formation of northwestern

Table 3.1 Major and trace element analysis of the Gusui bedded cherts, southern China

Samples	SiO2	TiO2	Al2O3	Fe2O3	FeO	MnO	MgO	CaO	Na2O	K2O	P2O5	LOI	Ag	As	Au	Ba	Bi	Co	Cr
GS-01	93.20	0.12	1.83	1.17	2.10	0.12	0.7	0.10	0.02	0.06	0.03	0.37	0.145	8.5	1	641	75	13	29
GS-02	94.04	0.11	1.83	0.34	1.19	0.07	0.4	0.30	0.01	0.38	0.24	0.50	0.332	2.4	3	8812	59	7	1
GS-03	95.94	0.05	0.69	1.50	0.51	0.08	0.001	0.10	0.01	0.16	0.08	0.44	0.314	65	25.5	9955	56	7	1
GS-04	91.55	0.05	2.29	2.94	0.69	0.06	0.4	0.01	0.01	0.34	0.03	0.74	0.612	67	29.8	470	61	13	2
GS-05	97.82	0.05	0.69	0.15	0.32	0.05	0.001	0.01	0.01	0.07	0.01	0.51	0.506	5.5	3	152	57	7	1
GS-06	97.39	0.03	0.09	0.36	0.45	0.09	0.001	0.02	0.01	0.06	0.04	0.69	0.737	8.2	9	197	47	1	1
GS-07	97.61	0.05	0.69	0.15	0.59	0.06	0.001	0.02	0.01	0.17	0.01	0.36	1.195	3	1	644	52	7	45
GS-08	98.52	0.07	0.14	0.14	0.30	0.05	0.001	0.03	0.01	0.05	0.00	0.34	0.103	1	2	288	60	7	1
GS-09	97.32	0.03	0.09	0.18	0.59	0.10	0.001	0.03	0.01	0.05	0.03	0.89	0.113	1.5	3	1924	60	7	29
GS-10	97.05	0.03	0.14	0.33	0.39	0.06	0.001	0.10	0.01	0.06	0.08	0.78	0.100	1.5	1	8295	65	7	1
GS-11	60.82	0.64	21.44	4.52	0.61	0.01	0.09	0.10	0.20	5.27	0.04	5.50	0.356	24	17.4	4293	92	51	44
Average(A)	92.84	0.11	2.72	1.07	0.70	0.07	0.1	0.07	0.03	0.61	0.05		0.4	17.1	8.7	3243	62.2	11.5	14.1
Crust(C)													0.07	1.8	4	425	0.17	25	100
A/C													5.9	9.5	1.9	7.6	365.8	0.5	0.1

Major element oxides in weight %; Trace elements in ppm except Au in ppb. The detection limit for gold is 1 ppb

The element abundances of the crust comes from Tayor (1964): Abundance of chemical elements in the continental

crust: a new table, Geochim. Cosmochim. Acta, v.28, pp.1273-1285

(continued)

Samples	Cs	Cu	Hf	Hg	Nb	Ni	Pb	Rb	Sb	Sc	Se	Sn	Ta	Th	U	V	W	Zn	Zr
GS-01	0.1	94	0.9	4	3.0	36	2	2.2	0.307	15	5.3	11	1.0	2	0.1	4	5.3	55	56
GS-02	1.2	6	0.1	10	2.0	1	2	19.6	0.405	9.2	1.8	7	0.5	1.7	0.6	8	1.8	20	58
GS-03	0.4	14	0.2	5	1.8	1	39	4	1.96	4.3	2.6	13	0.5	1.3	1.5	4	2.6	15	9.7
GS-04	0.8	22	0.5	6	1.8	18	2	16.2	0.812	14	6.6	12	0.5	1.8	0.1	4	6.6	15	72
GS-05	0.2	4	0.01	4	0.8	18	2	0.8	0.509	4.4	1.6	9	0.3	0.5	0.12	8	1.6	7	20
GS-06	0.1	12	0.1	3	2.6	1	2	2	0.504	1.7	2	11	0.6	0.2	0.07	4	2	5	8
GS-07	0.4	10	0.3	3	3.0	36	2	4.2	0.338	3.5	2.4	12	0.6	1.2	0.2	4	2.4	5	20
GS-08	0.1	4	0.1	3	1.3	2	2	1.6	0.24	2.7	1.2	54	0.5	0.3	0.04	8	1.2	3	19
GS-09	0.1	8	0.1	6	1.3	18	2	2	0.42	2	1.6	3	0.3	0.2	0.08	4	1.6	5	11
GS-10	0.2	8	0.1	7	1.0	1	2	1.9	0.28	3.7	1.3	5	0.3	0.8	0.45	4	1.3	20	38
GS-11	17.4	20	4.5	6	12.0	54	19	271	5.6	23	13.2	61	15.0	24	4.2	12	13.2	53	166
Average(A)	1.9	18.4	0.6	5.2	2.8	16.9	6.9	29.6	1.0	7.6	3.6	18.0	1.8	3.1	0.7	5.8	3.6	18.5	43.4
Crust(C)	3	55	3	0.08	20	75	12.5	90	0.2	22	0.05	2	2	9.6	2.7	135	1.5	70	165
A/C	0.6	0.3	0.2	64.8	0.1	0.2	0.6	0.3	5.2	0.3	72.0	9.0	0.9	0.3	0.3	0.04	2.4	0.3	0.3

Table 3.2 The average concentration of elements of representative hydrothermal cherts

Location	SiO2	TiO2	Al2O3	FeO	Fe2O3	MnO	MgO	CaO	Na2O	K2O	P2O5
1	92.30	0.09	1.31	0.27	2.36	0.53	0.28	0.11	0.16	0.35	0.03
2	87.87	0.05	1.09	0.52	2.52	1.08	0.86	1.05	0.35	0.24	0.12
3	91.92	0.07	0.82	(TFe)	2.16	0.45	0.43	0.29	0.52	0.37	0.16
4	93.10	0.10	1.80	0.40	0.90	0.10	0.10	0.20	0.10	0.50	
5	92.84	0.11	2.72	0.70	1.07	0.07	0.10	0.07	0.03	0.61	0.05

	Ba	Co	Ga	Mo	Nb	Ni	Pb	Rb	Sr	Th	Y	Zn	Zr
1	499	3	2	2	3	13	25	7	25	3	8	41	24
2	251	5	3	9	1	35	8	10	59	4	12	93	7
3	576	8	3	15	3	30	13	13	34	11	17	40	20
4		14	100			49	15		13	1.6	77	6	3

1: Fransican Chert Formation, from K. Yamamoto, 1987, Sedimemt. Geol., v.52, p52
2: Cherts of Shimanto Terrain, from K. Yamamoto, 1987, Sedimemt. Geol., v.52, p52
3: Cherts at Sites 303 and 304 of Leg 32, From M. Adachi et al.,1986, Sedimen. Geol.v.47, p125
4: Cherts of the upper Devonian of Nadan-Hechi basin, Guangxi, southern China, from Zhou, 1990, Acta Sedimen., v.8, p.77
5: Average Gusui cherts
Note: Non-cherts (SiO2<80% for Shimanto Terrain, <88% for others) do not enter the average

Maine, U.S.A, which were developed in an Ordovician volcanic arc, contain two distinct facies (Pollock, 1987). Facies 1 (thick sequences of uniformly bedded and laminated chert) is commonly low in alumina, alkalis and titania, and is similar to the cherts, also of hydrothermal origin, of western Costa Rica and the Japanese Geosyncline. Facies 2 (thin bedded chert interbedded with volcanoclastics) generally consists of two populations, one of which is consistent with the facies 1, and the other is characterized by higher alumina, alkalis and titania. Pollock (1987) interpreted the second population as being controlled by the deposition of suspended materials in the Td and Te divisions of a turbidite.

Most metallic elements are depleted in the Gusui cherts and have an antipathetic relationship with silica, implying that the silica crystalline phase is nearly "pure", and contains very minor amounts of metallic elements. This is comparable to the Franciscan cherts (Crerar et al., 1982), which are strongly depleted in metal elements relative to hydrogenous sediments.

The anomalous enrichment of Ba, As, Sb and Hg strongly indicates an affinity between the Gusui chert formation and typical known hydrothermal formations. Ba, As and Sb are considered to be characteristic elements of hydrothermal sediments. High barium contents were observed in many hydrothermal cherts, such as those of Costa Rica, and Guangxi, southern China (Hein et al., 1983; Chen and Chen, 1990). After studying modern ocean-floor hydrothermal sediments, Maxchiy (1982) suggested that high Sb and As are particularly characteristic of hydrothermal metalliferous sediments. A similar phenomenon was observed in the Devonian cherts related to hydrothermal activity occurring in northwestern Guangxi, southern China (Chen and Chen, 1990; Zhou, 1987; 1990), and in the siliceous muds which are deposited from the modern hot springs at Steamboat Spring, Nevada (White, 1981). It was concluded (White, 1981) that the hydrothermally deposited siliceous muds occurring at Steamboat Spring are characterized by high Ag (150 ppm), Sb (1.5%), As (700 ppm) and Au (150 ppb), with Cu (20 ppm), Pb (7 ppm), Zn (50 ppm).

2.2 Element Associations Obtained by Multivariate Statistics

Original raw data, such as chemical compositions of many samples from a geological unit, are frequently multi-dimensional, numerous, and seem sometimes confused. They are essentially a display of mixing-up of several geological and geochemical processes. It is often

difficult or even impossible to identify and distinguish the processes involved using only single elements instead of element associations. To obtain meaningful element associations or to highlight the end-members of geological and geochemical processes is, in the terms of statistics, equivalent to reducing the dimension number of original raw data sets reasonably. To do so, factor analysis and correspondence analysis are applied here. One of the advantages of multivariate statistic analyses is that they can reduce a set of original raw geochemical data, based on the intrinsic texture (a kind of linkage among data) into a few major factors, and therefore contribute to the explanation of the geological and geochemical history.

1. Results of Correspondence Analysis

The principal results of correspondence analysis calculations on the Gusui bedded cherts are listed in Appendices III-3.1 and 3.2, and displayed in Figures 3.2 and 3.3. They demonstrate that three distinct major element fields may be distinguished: Field [I-1], characterized by the presence of Al_2O_3, K_2O, (TiO_2) and (FeO), as well as sample GS-11; Field [I-2], characterized by MgO, Fe_2O_3 and FeO, and samples GS-01 and GS-04; and Field [I-3], representative of Fe_2O_3 and FeO, and samples GS-04 and GS-02. For trace elements, four fields are recognizable. They are: Field [II-1] — {Bi, Ni, Zr, Cu, Ba...} + {GS-01,GS-04, GS-05}; Field [II-2] — {Rb, Cs, Ta, Th, U, Zr, Cu...} + {GS-11, GS-01}; Field [II-4] − − {As, Au, Sn} + {GS-04, GS-08}; and Field [II-3] = Field [II-1] + Field [II-2].

Although in principle, the factors should be independent of one another, certain overlaps exist between the fields. Some have significant geological implications. For example, {SiO_2}, as shown in Figure 3.2, occurs at the intersection of all three fields of major elements. Its mass (contribution) to factor extraction is so great with respect to other major oxide components (c.f. Appendix III-3.1) that all fields of major elements show its influence. For trace elements, {Ba} behaves in a similar manner as {SiO_2}, while {Cu} occurs at the intersection of the fields [II-1] and [II-2].

2. Results of Factor Analysis

Appendices III-3.3 and 3.4 present the calculated results of factor analysis on the Gusui cherts. The following factors or element associations may be extracted.
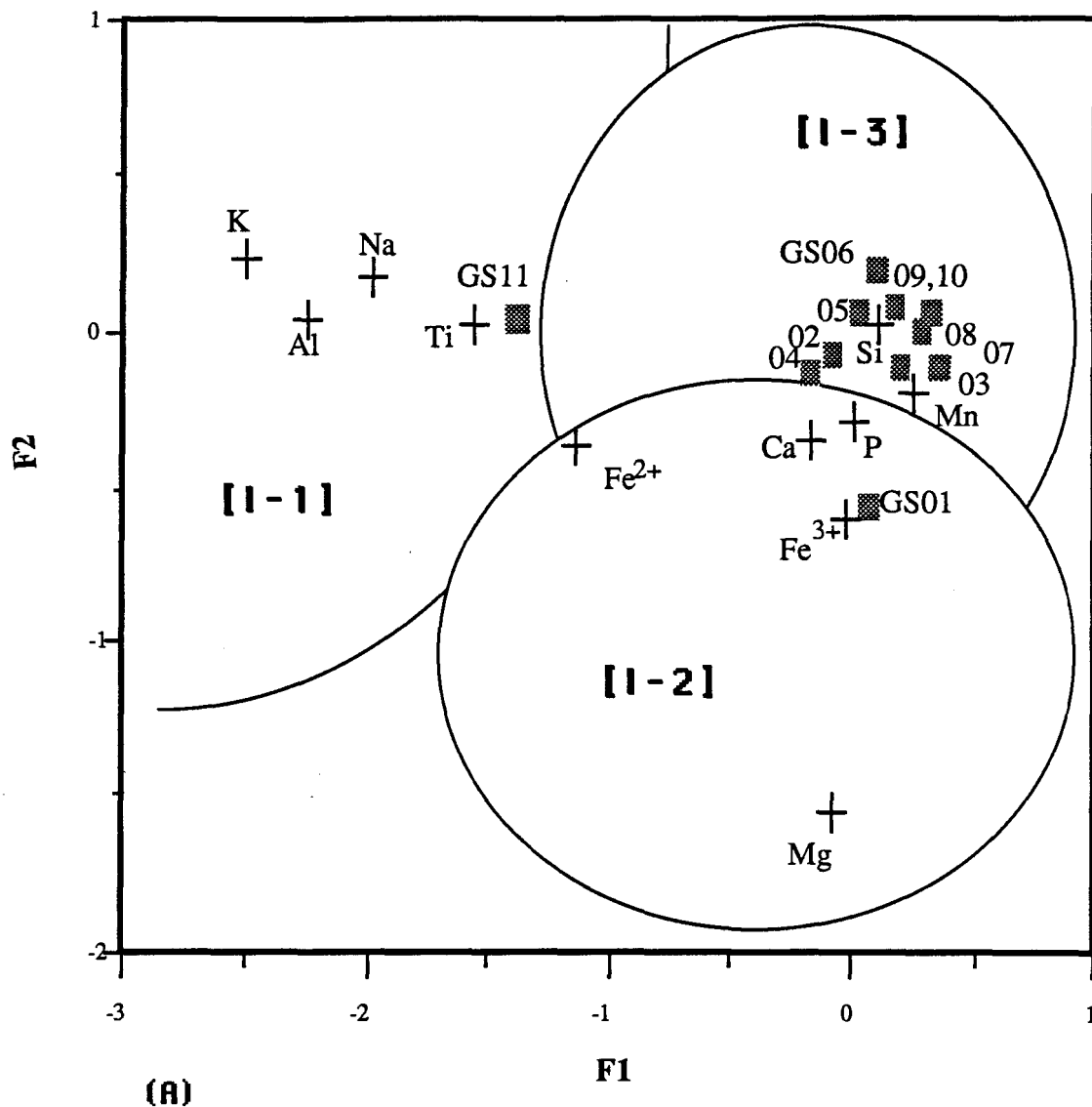
Figure 3.2 Correspondence Analysis of the Gusui Bedded Chert, Major Elements

Field [I-1], characterized by {Al2O3, K2O, TiO2, Na2O, -SiO2}, is related to potassium-bearing clay minerals, and was derived from hydrogenous sedimentation.

Field [I-2], characterized by {MgO, Fe2O3, FeO}, indicates an oxiding sedimentary environment.

Field [I-3], characterized by {Fe2O3, FeO}, is representative of the presence of Fe oxide micronodules, which make up the laminated alternation with microcrystalline quartz phase.
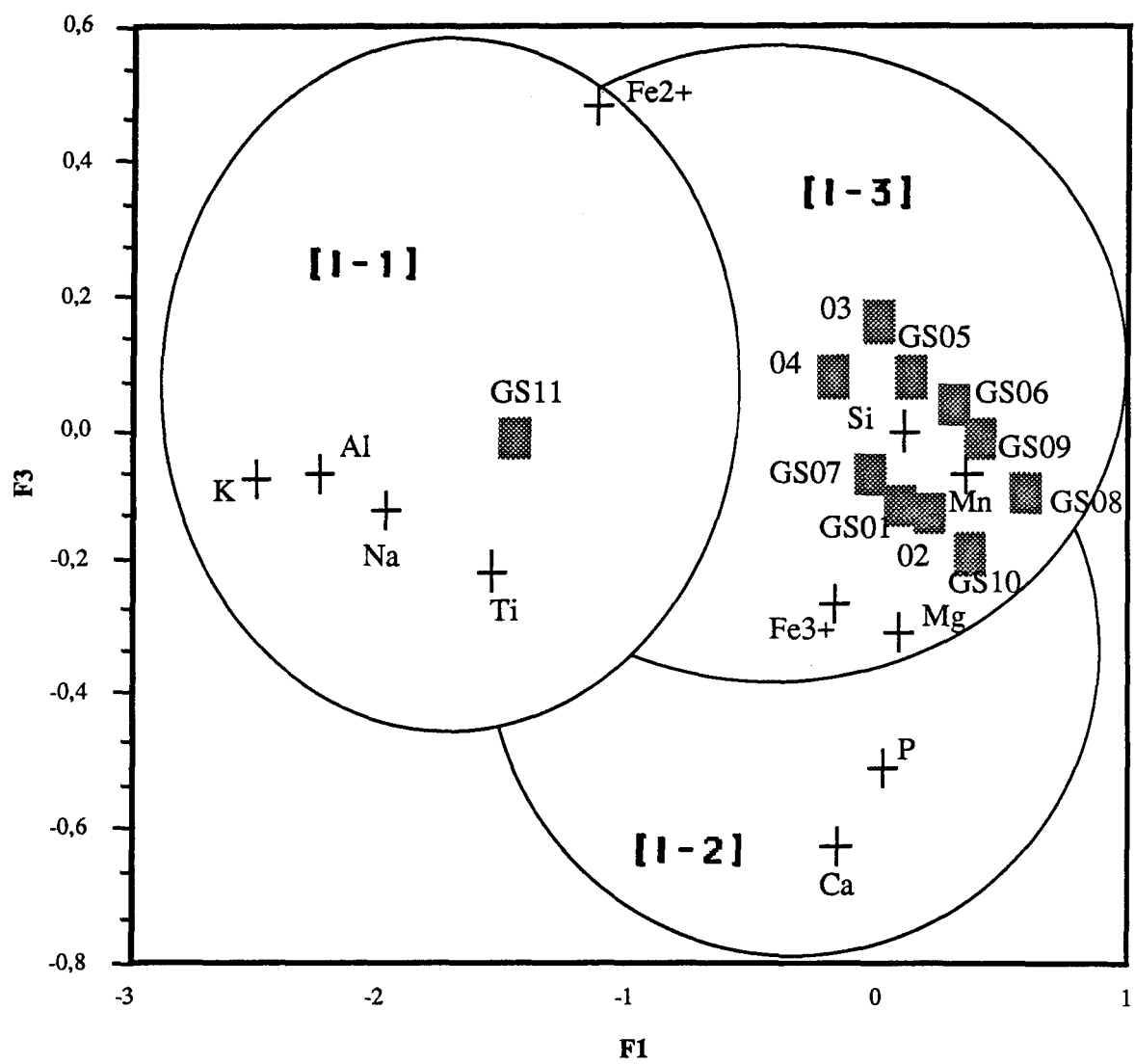
Figure 3.2 (Continued)
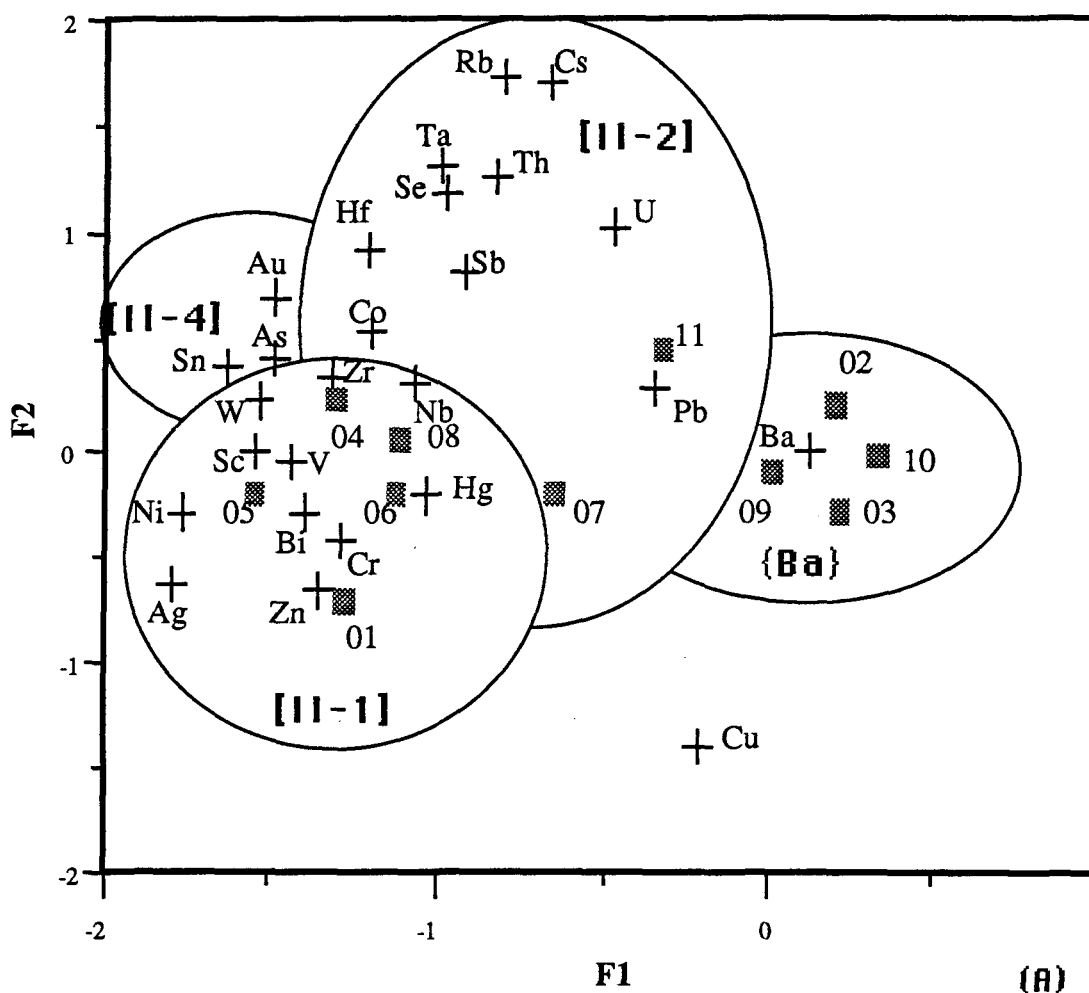
Figure 3.3 Correspondence Analysis of the Gusui Bedded Chert;
Trace Elements

Fields [II-1], {Bi, Ni, Zn, ...}, and [II-2], {Rb, Cs, Th, Ta, W, Nb, Sn, Hf, Sc, ...}, are equal to the first major factor <TF-1> of factor analysis, representing the leaching and extracting subsystem of a circulating geothermal system. [II-2] is the characteristic anomalous element association of southern China area.

Field [II-4], {As, Au, Sn}, is parallel to <TF-2> of factor analysis, and is a geochemical index for hydrothermal sediments.

{Ba}, the intersection of factors, also characterized by <TF-3> and <TF-6> of factor analysis, is diagnostic of hydrothermal deposit.
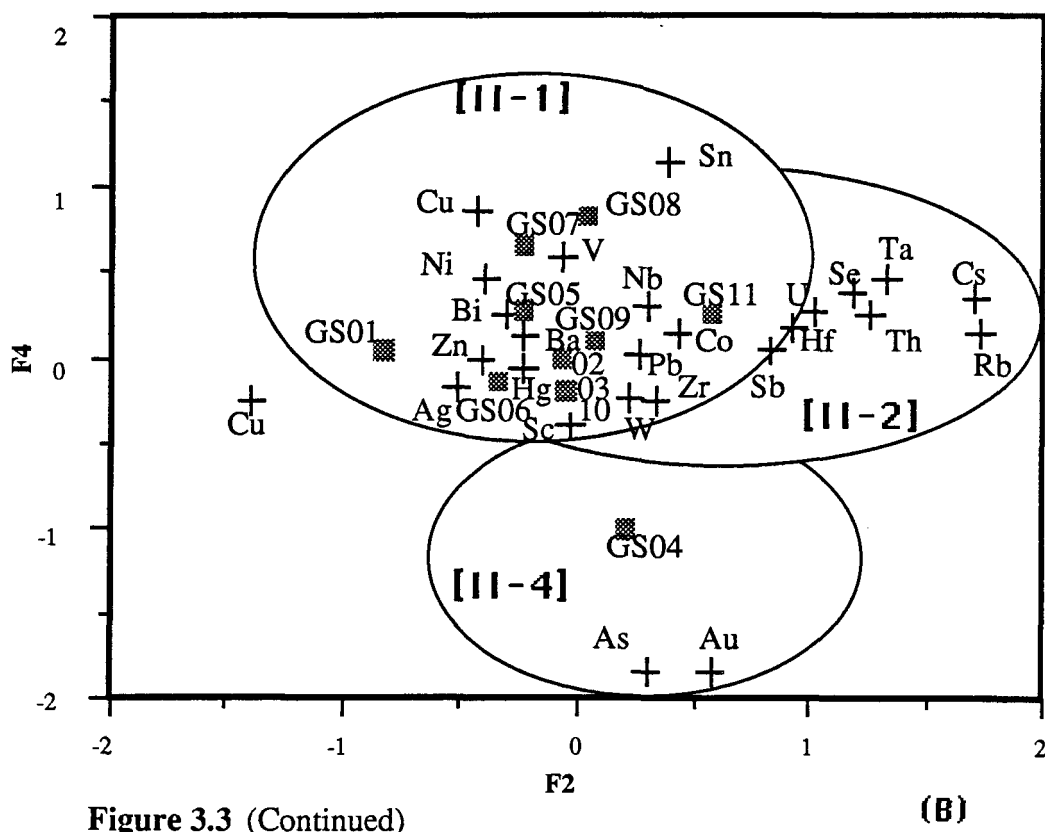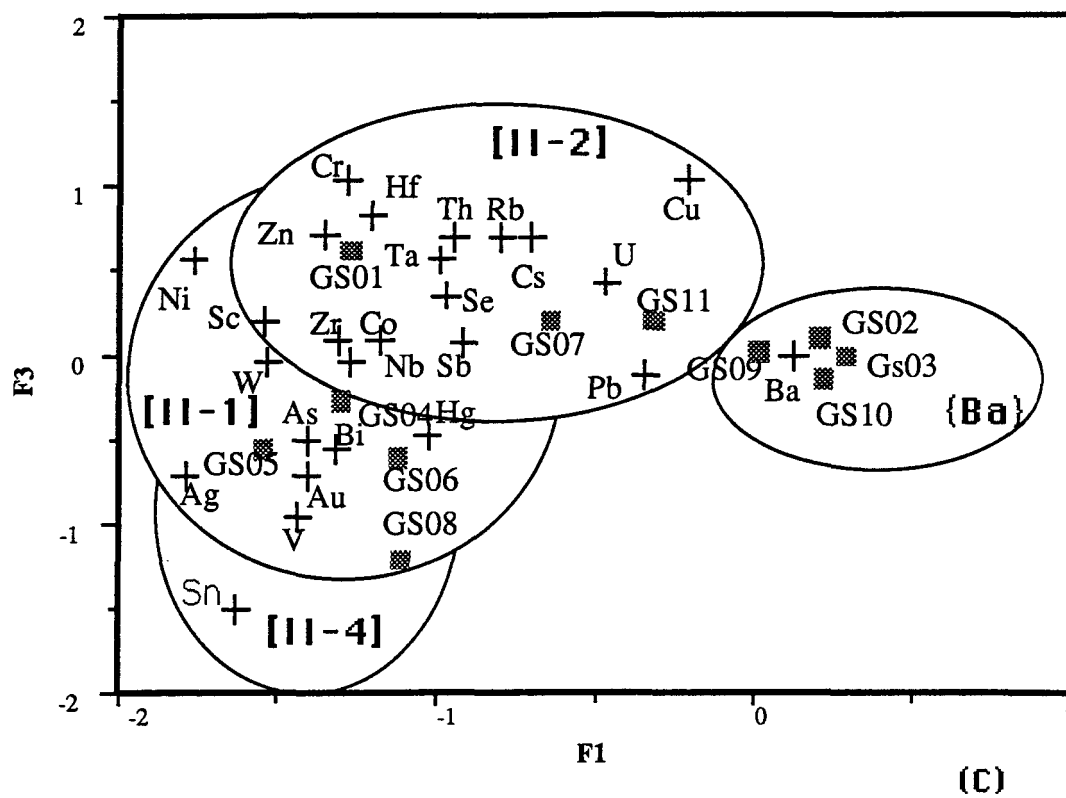
Figure 3.3 (Continued)

For major elements:

        <MF-1>:   *{-SiO2; TiO2, Al2O3, K2O, Na2O; Fe2O3}*

        <MF-2>:   *{FeO, MnO, MgO}*

        <MF-3>:   *{CaO, P2O5}*

For trace elements:

        <TF-1>:   *{Rb, Cs, Ta, Th, Nb, Th, U, Zr, Hf, W, Sn, Sc,*
                                        V, Co, Ni, Bi, Sb, Se}

        <TF-2>:   *{As, Au}*

        <TF-3>:   *{Hg, Ba, -Sn}*

        <TF-4>:   *{Zn, Cu, Ni, Cr, Bi}*

        <TF-5>:   *{Ag, Cr, Ni, -Sn}*

        <TF-6>:   *{Pb, Ba}*

3. Geochemical Implications

The results of factor analysis and correspondence analysis show the following:

The first major oxide factor <MF-1> of factor analysis is characterized by the element association {-SiO2; TiO2, Al2O3, K2O, Na2O; Fe2O3}. It is further divided into three parts: {SiO2}, {TiO2, Al2O3, K2O, Na2O}, and {Fe2O3},by correspondence analysis, .

{SiO2} is actually the intersection of all fields of Figure 3.2. That SiO2 occurs itself as an end-member is natural, since all cherts are characterized by high silica. Most of the samples studied cluster around SiO2.

The association {TiO2, Al2O3, K2O, Na2O}, or the field [I-1] of Figure 3.2, is characterized by a strong positive linear correlation between the contributing major element oxides (Appendix III-3.5). This association was also observed in the Devonian hydrothermal

cherts of Nandan-Hechi basin, southern China (Zhou, 1987, 1990). There, it is related to potassium-bearing clay minerals, such as illite and chlorite, and was considered as evidence of hydrothermal activity combining with, or alternating with, normal sedimentation. It is likely that such a combining or alternating process existed in the Gusui area, where the elements of this association cluster around the clay-rich sample GS-11.

Positive correlation between Al_2O_3 and TiO_2 is, however, not necessarily caused by clay-rich rocks. Recalculation of correlation coefficients after deleting samples that contain apparently high amounts of clay minerals also shows that there is still a significant positive correlation between Al_2O_3 and TiO_2 [$r(Al_2O_3, TiO_2) = 0.66$; $N = 10$]. Positive correlation between the chemically inert Al and Ti was observed in many other cherts, and was explained as an indication of terrigenous and weathering volcanogenic components (Matsumoto and Iijima, 1983). The Gusui cherts probably represent a different case, Ti and Al are depleted in these cherts, and are strongly repelled by the predominant SiO_2 (negative correlation, c.f. Appendix III-3.5). This suggests that the positive correlation between these two inert elements, Ti and Al, is due to their essential chemical immobility in the leaching process during the ascent of hydrothermal solutions, resulting in their low concentration in the hydrothermal solutions.

The field [I-2], or {Fe_2O_3}, of correspondence analysis reflects the presence of Fe oxide micronodules, which make up the laminated structure of the bedded cherts with microcrystalline quartz phase together. The presence of {Fe_2O_3} and the high Fe_2O_3/FeO ratio implies that the sedimentary environment is non-reducing. Otherwise, Fe^{3+} will be reduced to Fe^{2+}, and the Fe_2O_3/FeO ratio will be low.

The second major oxide factor is <MF-2> = {FeO, MnO, MgO}. The geochemical behavior of MnO and FeO has a dual character, depending on the sedimentary environment. In a study of the Nandan-Hechi cherts, Guangxi, it was demonstrated (Zhou,1990) that a reducing sedimentary environment leads to positive correlation between MnO and FeO. Otherwise MnO will separate from FeO, due to the difference of chemical stability limits of their hydroxides in the Eh - pH phase diagram.

It is interesting to note that correspondence analysis does not support a FeO and MnO combination at Gusui, as indicated by the separation of these two elements in Figure 3.2. Correlation coefficient calculation also shows that MnO and FeO are not significantly

correlated (Appendix III-3.5). Taking into account the fact that the concentration of MnO is low in the Gusui cherts, the factor <MF-2> may be explained in two ways: a) The sedimentary environment was reducing only locally or temporarily; or b) The original FeO-MnO correlation end-member has been masked by later deposition of a ferric nodule phase.

In order to compare the Gusui cherts with known hydrothermal cherts, factor analysis was also performed for the major elements of the cherts from the Franciscan of California, the DSDP Leg 32 of the northern Pacific, the Shimanto of Japan and the northwestern Guangxi of southern China, respectively. The calculated results (Tables 3.3 through to 3.6) demonstrate that the factors of the Gusui chert are comparable to those of known hydrothermal cherts. However, Fe_2O_3 is frequently combined to MnO in these typical hydrothermal cherts.

The third major oxide factor is <MF-3> = {CaO, P_2O_5}. *Its implications are still not clear at present. It can be the product of of fossil sea animals' activity.*

Trace elements appear particularly sensitive to the origin of cherts. The first trace element factor from factor analysis is <TF-1> = {Rb, Cs, Ta, Th, Nb, Th, U, Zr, Hf, W, Sn, Sc; V, Co, Ni, Bi, Sb, Se}. It is characterized by the show up of many trace elements. The presence of many elements in a single factor with a high variance proportion (59.6% of the total; c.f. Appendix III-3.4) indicate that this factor is the most significant of all the factors possible. It may represent the leaching, an indispensable part, of an evolving geothermal system. During circulation, the hydrothermal solution constantly leached and extracted all metal elements possible from the various country rocks that it passed through. Although complicated, this factor is essentially composed of two element associations (Fig. 3.3). The first is {Rb, Cs, Th, Ta, W, Nb, Sn, Hf, Sc...}, which is the characteristic geochemically anomalous element association of southern China basement (Institute of Geochemistry, 1979; Mo and Ye, 1980). This means that the development of the hydrothermal bedded cherts had a consistent geochemical context as the southern China basement at that time. The contribution of {Rb, Cs, Th, Ta, W, Nb, Sn, Hf, Sc...} to the factor <TF-1> suggests a geochemical heredity.

The second association contained in the factor <TF-1> consists of transition elements and thiophile elements, such as Bi, Ni, Zn and Cr, represented by the field [II-1] of Figure 3.3. These elements are commonly depleted in the southern China basement (Institute of Geochemistry, 1979; Mo and Ye, 1980). This element association is in turn further composed

Table 3.3   Factor analysis for major elements of the DSDP Leg32 chert
(<80% SiO2 Excluded)

Oblique Solution Reference Structure-Orotran/Varimax

	Factor 1	Factor 2
SiO2	-0.670	-0.414
TiO2	0.916	-0.047
Al2O3	0.925	-0.090
FeO	-0.237	0.844
Fe2O3	0.816	0.146
MnO	-0.008	0.859
MgO	0.477	0.014
CaO	0.874	-0.002
Na2O	0.269	0.270
K2O	0.348	0.665

Eigenvalues and Proportion of Original Variance

	Magnitude	Variance Prop.
Value 1	5.755	0.576
Value 2	1.733	0.173
Value 3	0.988	0.099
Value 4	0.742	0.074
Value 5	0.355	0.036

Primary intercorrelations-Orthotran/Varimax

	Factor 1	Factor 2
Factor 1	1	.
Factor 2	0.365	. 1

Table 3.4 Factor analysis for major elements of the Shimanto Chert
(<80% SiO2 Excluded)

Oblique Solution Reference Structure-Orotran/Varimax

	Factor 1	Factor 2	Factor 3
SiO2	0.366	-0.878	0.335
TiO2	0.764	0.188	-0.003
Al2O3	0.835	0.006	0.358
FeO	0.692	0.060	-0.275
Fe2O3	0.006	0.882	0.099
MnO	-0.024	0.923	-0.123
MgO	0.239	0.821	0.185
CaO	-0.827	0.107	-0.298
Na2O	0.020	-0.077	0.915
K2O	0.860	-0.426	-0.384

Eigenvalues and Proportion of Original Variance

	Magnitude	Variance Prop.
Value 1	4.144	41.4
Value 2	2.93	29.3
Value 3	1.421	14.2
Value 4	0.609	6.1
Value 5	0.523	5.2

Primary intercorrelations-Orthotran/Varimax

	Factor 1	Factor 2	Factor 3
Factor 1	1		
Factor 2	0.289	1	
Factor 3	0.014	0.03	1

Table 3.5 Factor analysis for major elements of the Franciscan chert
(<88% SiO2 excluded)

Oblique Solution Reference Structure-Orotran/Varimax

	Factor 1	Factor 2	Factor 3
SiO2	-0.935	-1.022	-0.02
TiO2	1.006	0.082	-0.031
Al2O3	0.962	-0.032	0.022
FeO	0.666	-0.238	0.101
Fe2O3	0.026	0.864	-0.068
MnO	0.001	0.725	-0.002
MgO	0.92	-0.014	-0.054
CaO	0.125	-0.065	0.998
Na2O	0.336	-0.276	-0.253
K2O	0.967	0.219	0.079

Eigenvalues and Proportion of Original Variance

	Magnitude	Variance Prop.
Value 1	4.84	0.484
Value 2	1.831	0.183
Value 3	1.01	0.101
Value 4	0.768	0.077
Value 5	0.744	0.074

Table 3.6 Factor analysis for major elements of the northwest Guangxi chert

Oblique Solution Reference Structure-Orotran/Varimax

	Factor 1	Factor 2	Factor 3
SiO2	-1.01	-0.11	-0.15
TiO2	0.88	-0.22	-0.12
Al2O3	0.95	0.03	-0.06
FeO	-0.08	0.94	0.08
Fe2O3	-0.20	-0.13	0.94
MnO	-0.28	0.94	-0.24
MgO	0.98	-0.04	-0.03
CaO	0.67	-0.40	-0.09
Na2O	0.83	0.42	0.09
K2O	0.98	0.04	-0.05

Source: Zhou, 1987

of two factors, <TF-4> and <TF-5>, on factor analysis. On the one hand, these two factors are consistent in the leaching of the country rock by hydrothermal solution, but on the other hand, they have a different sedimentary geochemical behavior. Consider their correlation with Fe_2O_3, which characterizes the ferric oxide micronodules in the Gusui chert. The factor <TF-4> appear to combine preferentially with Fe oxide micronodules, since its components display a significant positive correlation with Fe_2O_3. This is also in accordance with the fact that these elements are negatively correlated to {SiO_2}. In contrast, the elements contained in factor <TF-5> have no such relationship, and do not correlate to elements enriched in the micronodules.

The second trace element factor <TF-2>, corresponding to the field [II-4] of correspondence analysis (Fig. 3.3), is characterized by the enrichment of Au and As and a positive correlation between these two elements. As described earlier, the enrichment of As, Sb and Au is common in modern sea-floor hydrothermal sediments. Therefore the factor <TF-2> may be used as a geochemical index of hydrothermal deposits, and it favors a hydrothermal origin of the Gusui chert. Furthermore, the significant positive linear relationship between As, Au, and FeO implies that the field [II-4] is associated with the field [I-3], or that the deposition of Au and As is controlled by the sedimentary environment.

The field {Ba}, also characterized by <TF-3> and <TF-6> of factor analysis, is especially diagnostic of hydrothermal sediments, since Ba is an element related to hydrothermal activities, and its enrichment is observed in many known hydrothermal deposits.

2.3 Al-Fe-Mn Ternary Diagram

Al-Fe-Mn diagram was first proposed by Boström and Peterson (1969) to differentiate hydrothermal deposits. It has been applied to the study of hydrothermal deposits around the East Pacific Rise (Boström and Peterson, 1969; Piper, 1973), the TAG field of the Mid-Atlantic Ridge (Shearme et al., 1983), the Galapagos Mounds (Moorby and Cronan, 1979), Shimanto Terrain and Franciscan cherts (Yamamoto, 1987), and DSDP Leg 32 (Adachi et al., 1986).

The Gusui cherts fall into the hydrothermal field of the Al-Fe-Mn ternary diagram (Fig. 3.4) with the exception of one sample, and apart from the small Al-rich "hydrothermal-
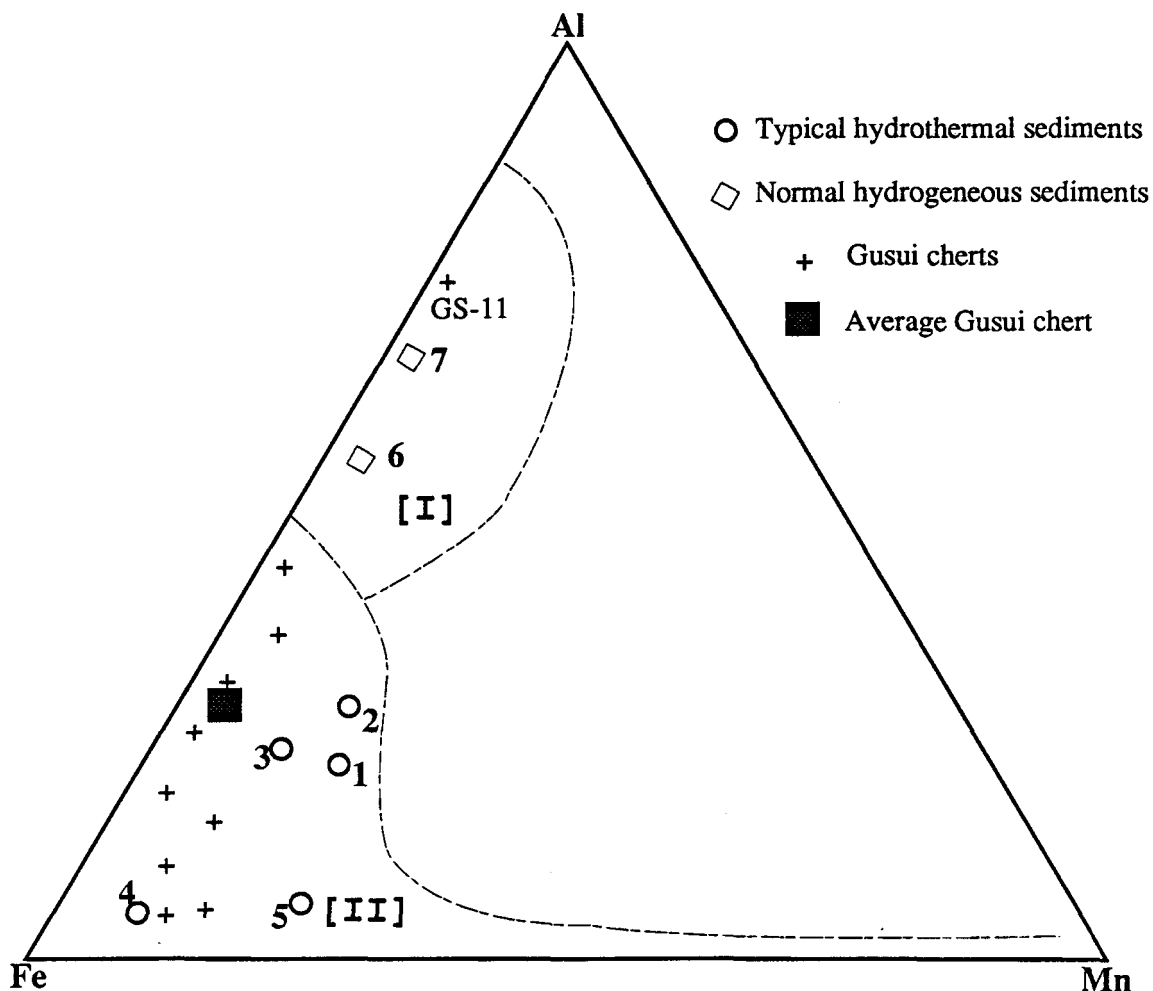
Figure 3.4 Al-Fe-Mn ternary diagram showing the distinguishing between hydrothermal and hydrogeneous sediments

Field II is the hydrothermal field, constrained by the Franciscan chert formation (point 1), Shimanto chert (point 2) (Yamamoto, 1987), DSDP Leg 32 (point 3) (Adachi et al., 1986), East Pacific Rise deposits (point 4 and 5) (Bostrom and Peterson, 1969; Piper, 1973; Laluo, 1983), nontronites in the Galapagos Mound sediment, DSDP Leg 70 (Moorby and Cronan, 1979), sediment from the TAG field, Mid-Atlantic Ridge (Shearme et al., 1983)

Field I is the hydrogeneous field, constrained by the Mino Terrain (point 6) (Yamamoto, 1983, 1987), Yamato Bank of the Japan Sea (Sugisaki, 1979), DSDP Leg 56 & 57, the Japan Trench (Sugisaki, 1980), the northern Central Pacific Basin (Sugisaki, 1981), the central Pacific transect, Wake to Tahiti (Sugisaki and Kinoshita, 1982), and DSDP Leg 62 (point 7) (Yamamoto, 1987)

Gusui cherts fall in the hydrothermal field with the exception of Sample GS-11, which is rich in clay minerals.

free" field, which is constrained by hydrogenous sediments from the Mino Terrain (Yamamoto, 1983; 1987), Japan sea (Sugisaki, 1979), Japan trench (Sugisaki, 1980), northern Central Pacific Basin (Sugisaki, 1981), and DSDP (Yamamoto, 1987).

Hein et al. (1983) subdivided the rhythmically bedded and massive hydrothermal cherts occurring in the Nicoya Complex of Costa Rica into three chemical varieties: a common chert (low Fe and Mn), a high Mn chert (more than 2% element Mn), and a high Fe chert (greater than 2% Fe). The Gusui cherts appear to have lower Mn, and higher Fe, occurring closer to the Fe-apex, which is consistent with the fact that only hematite has been identified in the Gusui chert.

Adachi et al. (1986) concluded that the DSDP Leg 32 chert was a typical hydrothermal chert. As well as those of the Shimanto terrain and the Franciscan formation (Yamamoto, 1987), it has been proposed as a reference for hydrothermal chert. The affinity of geochemical characteristics of the Gusui bedded chert to these typical hydrothermal cherts (c.f. Fig. 3.4) argues in favor of a hydrothermal origin for the Gusui chert.

§3 Rare Earth Elements

3.1 REE Abundance of NASC

Studies of REE distributions in shales and other detrital sedimentary and metasedimentary rocks (Haskin and Gehl, 1962; Balashov et al, 1964; Haskin and Frey, 1966; Haskin et al, 1968; Wildeman and Haskin, 1973; Ronov et al., 1974; Cullers et al., 1974; Nance and Taylor, 1976; 1977; Taylor and McLennan, 1985; McLennan et al., 1984) demonstrated that post-Archean sediment composites as a group have rather uniform REE characteristics, and were distinctly enriched in the lighter REE compared to the REE distribution of chondritic meteorites, although sediments with sources restricted to certain limited environments can deviate considerably from these values (Gromet et al., 1984).

The so-called "North American shale composite (NASC)" is a composite of 40 shales (Gromet et al., 1984). Its relative REE pattern is considered to be representative of the post-Archean upper crust and is used to normalize REE abundances of other sedimentary rocks in a number of geochemical studies (Taylor, 1977). Its original significance stemmed from

Goldschmidt's (1938) proposal that the element abundance of fine grained detrital sediments represents average relative crustal abundance (Gromet et al., 1984).

Several suites of REE concentrations of the NASC have been analyzed by several different methods (Haskin and Frey, 1966; Haskin et al., 1968; Gromet et al., 1984). The recommended values by Gromet et al. (1984), which were prepared by recent high-precision isotope dilution and INAA analyses, seem to provide the best available reference for normalization of REE data, since it improves the constraints on the average REE pattern of NASC, and thus produces a more precise relative REE pattern than the earlier analyses (Gromet et al., 1984).

3.2 Total REE Variability

REE concentrations of the Gusui bedded cherts and geochemical reference data are listed in Table 3.7. This table shows that although the total REE content of the studied cherts varies, two endmembers are recognizable. One is "pure" chert, which contains more than 95% silica and less than 1% Al_2O_3. The other is shaly chert, containing much more Al_2O_3, but less silica. In general, the total REE content is remarkably low, ranging from less than 10 ppm to about 30 ppm, for the pure chert, whereas it varies for impure cherts, depending on the shale contribution to the chert. Even the total REE content of impure cherts may approach that of NASC (e.g. GS-11).

3.3 REE Distribution Patterns

The Masuda-Coryell distribution pattern of the REE of the Gusui cherts is plotted in Figure 3.5 (normalized to NASC) and Figure 3.6 (normalized to chondrite). Figure 3.5 shows that: (1) HREE is enriched in comparison to LREE. The ratio of the average Gusui chert to NASC increases regularly from 0.27 for La to 0.59 for Lu (Table 3.7); (2) δCe may be either more or less than unity.

The distribution and geochemical behavior of the REE of the seawater and ocean bottom sediments were discussed by several authors (Taylor and McLennan, 1988; Piepgras and Jacobsen, 1988; de Baar et al., 1983; 1985; Elderfield and Greaves, 1982; McLennan, 1989; Brookins, 1989; Fleet, 1983). The REE pattern of ocean waters is characterized by a

Table 3.7 REE data and related geochemical reference values of the Gusui cherts

Elements	Chondrite	NASC	GS-01	GS-02	GS-03	GS-04	GS-05	GS-06	GS-07	GS-08	GS-09	GS-10	GS-11	Average	A./NASC
La	0.329	31.1	21.04	2.32	3.99	9.29	4.53	1.18	3.67	0.52	0.21	1.90	43.53	8.38	0.27
Ce	0.865	66.7	56.65	11.29	8.70	27.60	8.36	3.83	6.01	2.21	0.44	7.60	75.88	18.96	0.28
Pr	0.116														
Nd	0.63	27.4	22.26	6.88	4.24	11.83	3.78	1.19	2.71	1.42	0.39	4.65	28.42	7.98	0.29
(Pm)															
Sm	0.203	5.59	6.32	2.07	1.00	3.28	1.05	0.39	0.64	0.40	0.10	1.22	8.30	2.25	0.40
Eu	0.077	1.18	1.58	0.53	0.28	0.74	0.24	0.11	0.12	0.14	0.02	0.31	1.68	0.52	0.44
Gd	0.276														
Tb	0.047	0.85	1.28	0.31	0.13	0.57	0.12	0.07	0.16	0.15	0.03	0.25	1.40	0.41	0.48
Dy	0.325														
Ho	0.073														
Er	0.213														
Tm	0.03														
Yb	0.22	3.06	5.34	1.00	0.58	2.48	0.63	0.31	0.81	0.65	0.15	0.54	4.38	1.53	0.50
Lu	0.0339	0.46	0.98	0.18	0.11	0.44	0.11	0.05	0.15	0.12	0.04	0.10	0.70	0.27	0.59

			GS-01	GS-02	GS-03	GS-04	GS-05	GS-06	GS-07	GS-08	GS-09	GS-10	GS-11	Average	A./NASC
LREE			115.41	24.97	19.50	56.59	19.15	7.16	14.00	5.07	1.25	16.93	167.70	40.70	0.29
HREE			30.12	6.34	3.24	13.87	3.53	1.71	4.51	3.66	0.86	5.15	28.33	9.21	0.49
LREE/HREE			3.83	3.94	6.02	4.08	5.43	4.20	3.10	1.39	1.46	3.29	5.92	3.88	0.31
REE			145.53	31.31	22.74	70.46	22.68	8.86	18.51	8.73	2.10	22.08	196.03	49.91	
Normalized by NASC															
∂Eu			1.04	1.21	1.47	1.02	1.26	1.24	0.75	1.10	0.81	0.97	0.90	1.07	
∂Ce			1.18	1.51	0.96	1.23	0.88	1.45	0.81	1.36	0.76	1.33	0.90	1.12	
Yb/Tb|NASC			1.16	0.90	1.24	1.21	1.43	1.19	1.42	1.20	1.25	0.59	0.87	1.13	
Normalized by Chondrite Average															
∂Eu			0.70	0.81	0.98	0.68	0.84	0.83	0.50	0.74	0.54	0.65	0.60	0.72	
∂Ce			1.25	1.60	1.01	1.29	0.93	1.53	0.86	1.43	0.80	1.40	0.95	1.19	
Yb/Tb|n			0.89	0.69	0.95	0.93	1.10	0.92	1.10	0.93	0.96	0.45	0.67	0.87	
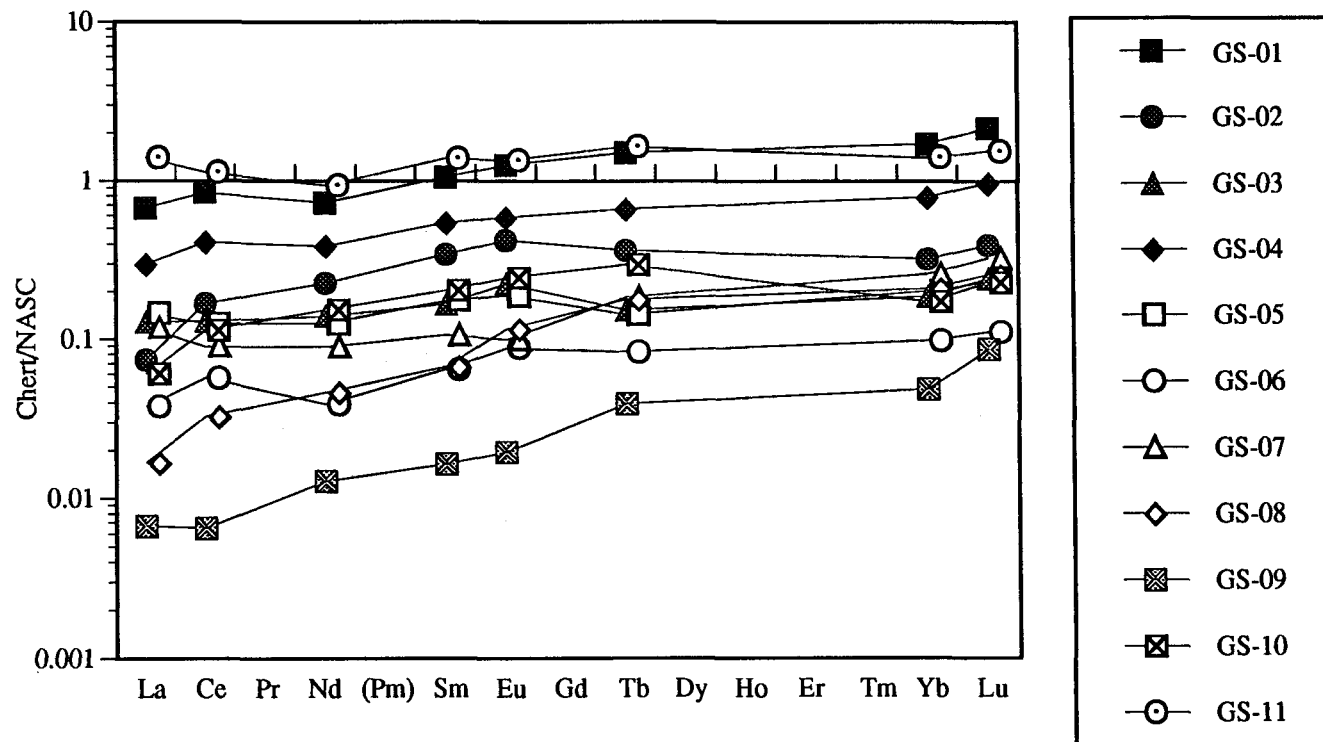
Figure 3.5 REE abundance distribution pattern of the Gusui bedded cherts (normalized to NASC)
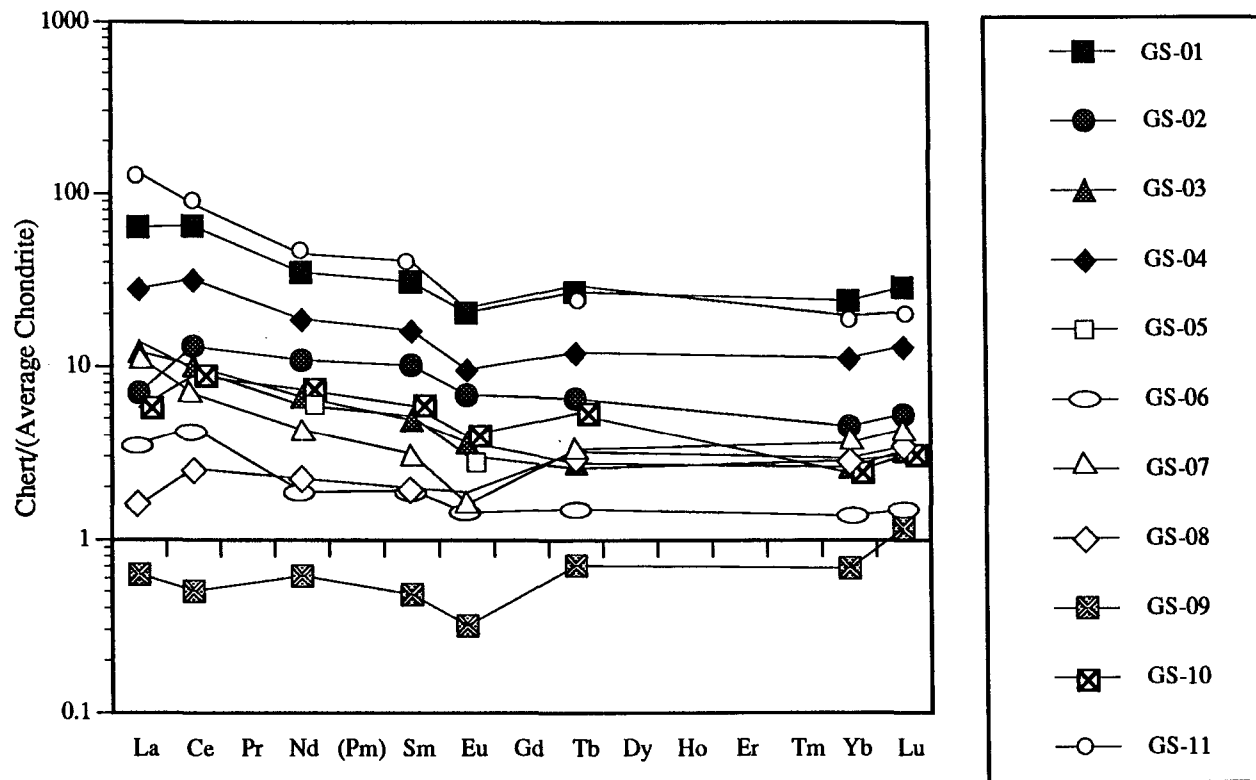
**Figure 3.6   REE abundance distribution pattern of the Gusui bedded cherts
(normalized to the average Chondrite)**

very low overall abundance, ranging over a few parts per billion, the presence of a markedly negative Ce anomaly, slight enrichment in both LREE and HREE relative to the intermediate REE (Table 3.8; Figure 3.7), and a flat HREE pattern with Gd/Ybln rarely outside the range of 1.0-2.0. Usually, the hydrogenous pelagic component has a high REE content, comparable with that of NASC. The marked Ce deficiency is an indication of the fractionation and a short residence time of cerium relative to other REE in ocean waters, and was attributed to the rapid removal of Ce preferential to other lanthanides by the formation of CeO_2, which is often associated with Fe and Mn micronodules (Goldberg, 1961; Elderfield et al., 1981; Fig. 3.8).

It was demonstrated in a study of hydrothermal and hydrogenous ferro-manganese deposits (Fleet, 1983) that deep sea ferro-manganese deposits are not all likely to have formed by either hydrothermal processes or hydrogenous ones, but are often mixtures of materials contributed by both these processes. The hydrogenous and hydrothermal endmembers of this continuum generally have distinct REE contents and distribution patterns. The former tends to be more enriched (normalized to NASC) in cerium relative to other REE, and high in total REE, whereas the hydrothermal endmember is depleted in Ce and is somewhat enriched in HREE relative to LREE (Table 3.9; Fig. 3.9).

Thus, REE abundance and distribution pattern may be used to suggest whether a deposit forms from a hydrothermal or a hydrogenic source or both, by showing that the deposit has received REE from one or both these sources. Generally, hydrothermal deposits accumulate REE without significant fractionation of rare earth elements (Fleet, 1983). They take REE from seawater which has previously lost Ce during its residence time in the oceans but which has undergone no marked change in REE content during hydrothermal circulation. Normalized REE patterns of hydrothermal deposits, therefore, parallel those of seawater. This is demonstrated by the REE distribution pattern of modern ocean-ridge metalliferous sediments and typical fossil hydrothermal deposits, which formed as precipitates from hydrothermal solutions of seawater circulating through the crust (Fig. 3.10; Piper and Graef, 1974; Dymond et al., 1973; Bender et al., 1971; Goldberg et al., 1963; Guichard et al., 1979).

The REE distribution pattern of the Gusui bedded cherts is analogous to that of many known hydrothermal deposits (Fig. 3.10). For the Gusui cherts, the total REE content is characteristically low, and HREE are enriched in comparison to LREE. The regular increase of the ratio of the average REE concentration to NASC (Table 3.7) is indicative of

Table 3.8 REE contents (parts per billion) of selected seawater

Elements	Chondrite (ppm)	NASC (ppm)	Atlantic Ocean		N.W. Pacific Ocean		Average of N. Atlantic
			at 100 m	at 2500 m	at surface	at 2500 m	Deep water
La	0.329	31.1	1.81	4.08	1.2	6.5	3.4
Ce	0.865	66.7	2.35	3.68	1.4	1.3	1.2
Pr	0.116						0.64
Nd	0.63	27.4	1.85	3.61	0.74	4.3	2.8
(Pm)							
Sm	0.203	5.59	0.401	0.714	0.15	0.8	0.45
Eu	0.077	1.18	0.0979	0.136	0.05	0.21	0.13
Gd	0.276		0.536	1.13	0.25	1.3	0.7
Tb	0.047	0.85					0.14
Dy	0.325		0.777	0.991	0.33	1.6	0.91
Ho	0.073						0.22
Er	0.213		0.681	0.851	0.28	1.6	0.87
Tm	0.03						0.17
Yb	0.22	3.06	0.614	0.829	0.19	1.4	0.82
Lu	0.0339	0.46					0.15
Sources			a	b	c	d	e

Sources: a, b, c and d from Taylor and McLennan (1988), also see Brookins (1989);
e from Hogdahl et al. (1968) via Fleet (1983);
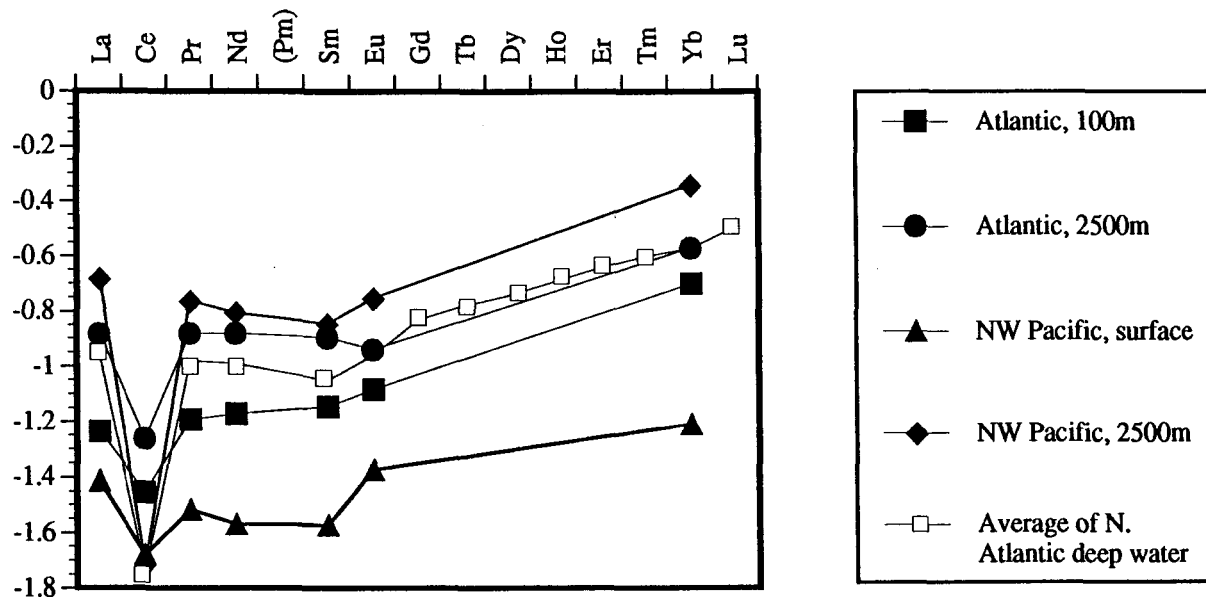
Figure 3.7 REE distribution pattern of selected seawaters (normaized to NASC)

Data of the average Northern Atlantic deep water from Hogdahl et al. (1968);
the others from Taylor and McLennan (1988)
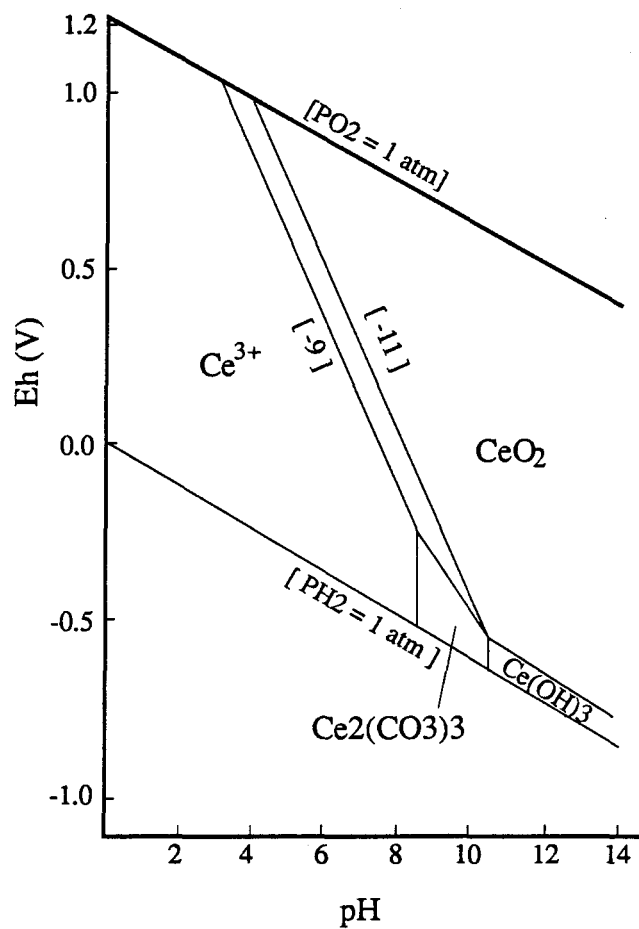
Figure 3.8 Eh - pH diagram for the system Ce-C-O-H

(25 C, 1 atm total pressure; From Brookins, 1989).
Activities: Total dissolved CO2=1.0*E-3, total dissolved
Ce=E-9 and E-11. Fields for aqueous complexes not shown.

Table 3.9 REE contents (ppm) of selected hydrothermal and hydrogenous sediments

Elements	Chondrite	NASC	Average EPR crest	Hydrothermal Deposit "Maximum"*	"Minmum"**	Hydrogenous Deposit Average	"Maximum"$	"Minmum"$$	Average Gusui chert
La	0.329	31.1	100	182.1	4	150	237	5.4	4.86
Ce	0.865	66.7	40	93.7	1.87	1460	2800	60	13.27
Pr	0.116					57			
Nd	0.63	27.4	91	158.9	2.4	200	306	11	5.93
(Pm)									
Sm	0.203	5.59	20	28.3	0.4	55	77.5	1.88	1.65
Eu	0.077	1.18	4.6	6.16	0.105	12	22	0.46	0.41
Gd	0.276	5.5					22		
Tb	0.047	0.85		5.42	0.09	7.5		0.32	0.31
Dy	0.325	5.54				44	10.5		
Ho	0.073					7.3			
Er	0.213	3.28							
Tm	0.03					2.8	3.6	0.16	
Yb	0.22	3.06	16	18.3	1.1	15	23	0.82	1.25
Lu	0.0339	0.46		3.21	0.25	2.7	3.9	0.18	0.23
Sources			Piper and Graef (1974) and Elderfield et al. (1981)			Ehrlich (1968), via Fleet (1983)			

* is Sample A-21 of Piper and Graef (1974); **, Sample 14A FAMOUS of Bonnot-Courtois (1981); via Fleet (1983)
$, Indian Ocean Sample; $$, Pacific Ocean Sample
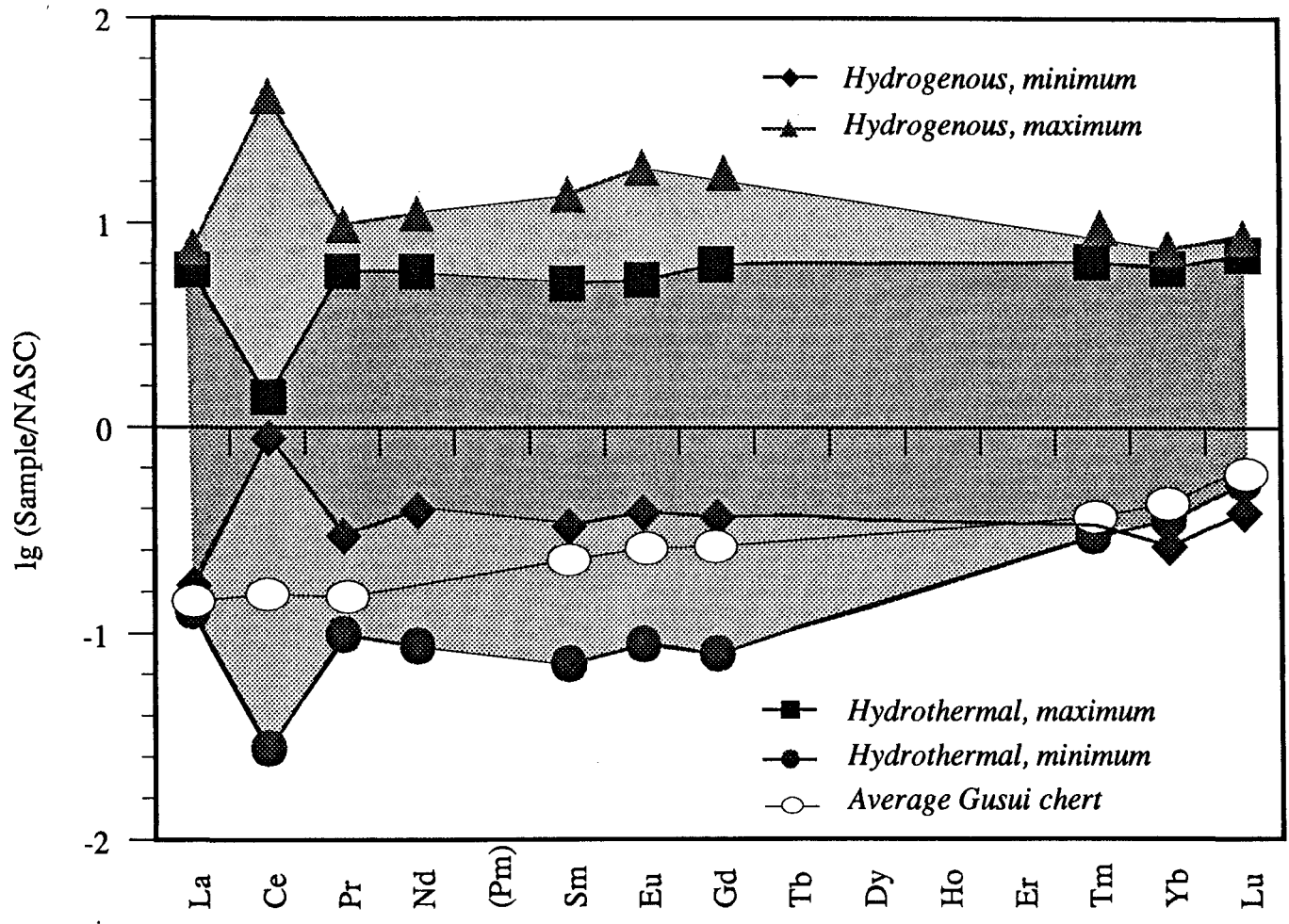
Figure 3.9 REE Abundance Distribution Patterns of Typical Hydrothermal and Hydrogeneous Sediments (Normalized to NASC)

Data from Piper and Graef (1974), Elderfield et al. (1981), Ehrlich (1968).

hydrothermal origin. There is good evidence that HREE are more stable relative to LREE in hydrothermal solutions, because of the stability of HREE complexes is generally greater than those of LREE (Brookins, 1989). Projected onto Figure 3.9, the average Gusui chert falls between the maximum and minimum limits of known hydrothermal deposits, but outside the hydrogenous field.

Despite the predominance of chert of hydrothermal origin, it is also likely that the REE pattern of some Gusui cherts resulted from a combination of a hydrothermal fluid and seawater, or a mixing of hydrothermal and hydrogenous processes. Just as marine ferro-manganese deposits may be formed by either hydrothermal or hydrogenous processes (Fleet, 1983; Bonatti, 1981; Cronan, 1976; Toth, 1980), bedded cherts, especially those rich in clay minerals, may be originally either hydrothermal or hydrogenous deposits, probably most commonly a mixture of them both. The hydrogenous cherts may form by direct precipitation from seawater and by interaction of seawater and surface sediments at the seafloor. The hydrothermal ones are also precipitated from seawater, but from seawater which has circulated through the crust and reacted with the latter at elevated temperatures. Both processes may have contributed to the development of the Gusui chert.

The fact that cerium may be enriched or depleted relative to other REE normalized to NASC in the studied cherts favors a mixing mechanism. The mixing may occur in one of two ways. One is by the periodic alternation of hydrothermal activity and ordinary non-hydrothermal sedimentation, which implies intermittent hydrothermal activity. During a quiescence of hydrothermal activity, ordinary hydrogenous processes prevailed. The alternative mechanism is that both hydrothermal and hydrogenous processes took place at the same time that cherts formed, but contributed at differing rates. The variation of REE content within individual samples is compatible with the variation between different samples.

It should be noted that even a small "hydrogenous REE" content may swamp the "hydrothermal REE", because hydrogenous deposits generally contain higher REE abundances than hydrothermal ones. Therefore only those with predominantly "hydrothermal REE" can be easily recognized. In deep-sea sediments, REE are efficiently attached to clay minerals, which are commonly of hydrogenous origin (Piper, 1974; Fleet, 1984; Brookins, 1989), and ferro-manganese oxyhydroxides (Addy, 1979; Fleet, 1983; Elderfield et al., 1981; de Baar et al., 1983). The presence of any amount of clay minerals will enhance the REE abundance and
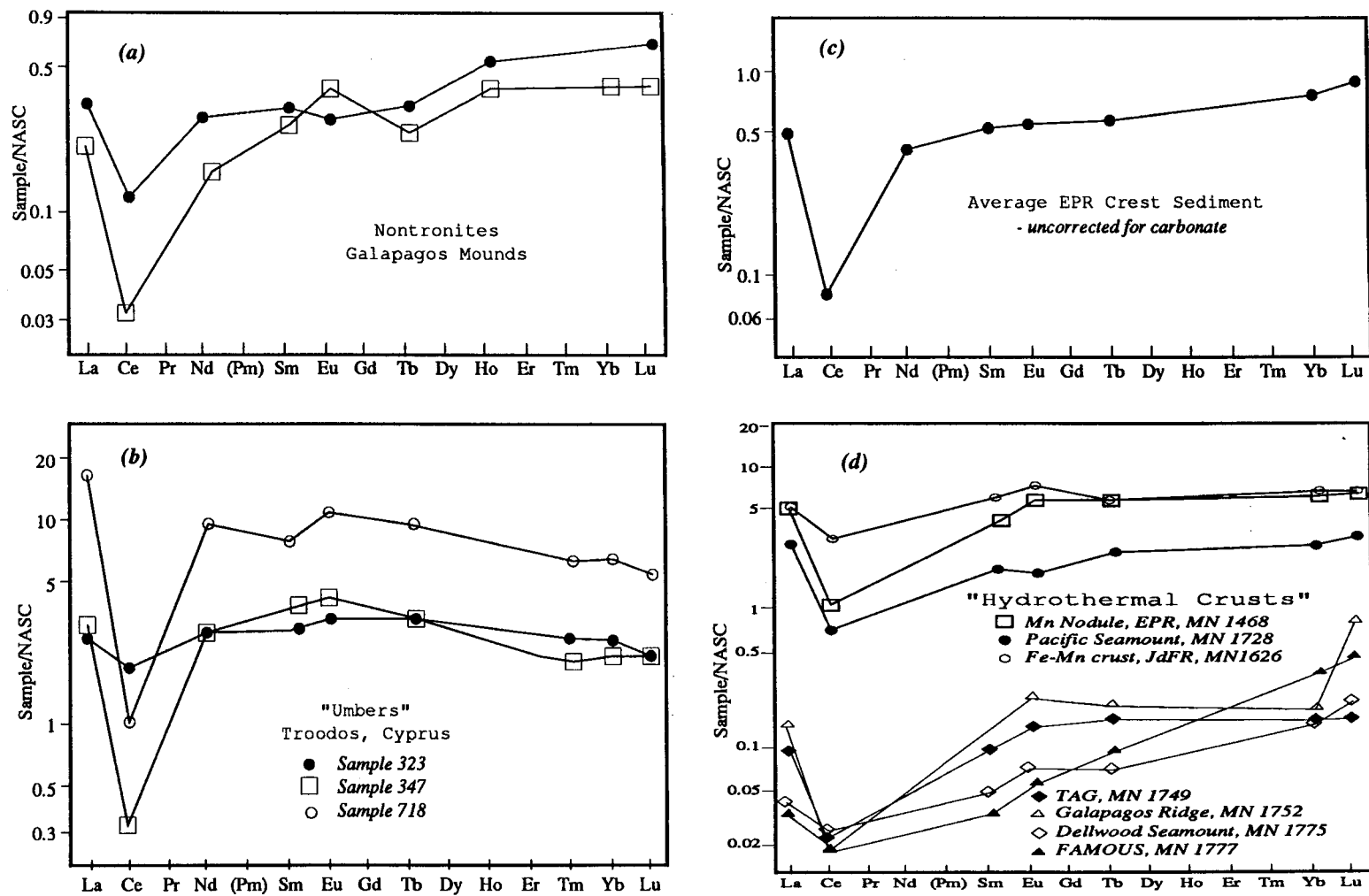
Figure 3.10 REE distribution pattern of some typical hydrothermal deposits compared to NASC

(a) Nontronites from the Galapagos mounds of the eastern Equatorial Pacific (Barret et al., 1984)
(b) "Umbers" (ferro-manganese hydrothermal deposits) from Troodos, Cyprus (Robertson and

Fleet, 1976)
(c) Metalliferous sediments from the crest of the East Pacific Rise (Piper and Graef, 1974)
(d) Ferro-manganese deposits (Toth, 1980)

distort the typical REE distribution pattern of pure hydrothermal cherts. For this reason some mixed cherts in the Gusui chert formation may have a low hydrothermal signature, due to a high proportion of clay minerals.

Regardless of its origin, the Gusui bedded cherts possesses a similar overall REE distribution pattern to the average post-Archean sedimentary rock and the upper continental crust normalized to chondrite, with LREE enrichment relative to HREE and a remarkable ubiquitous Eu depletion (Fig. 3.6). The uniformity of post-Archean sedimentary rocks is the indication of the heritage of a uniform REE upper crust, and has been generally interpreted as resulting from efficient mixing of various provenance components and source lithologies during the extraction, migration and deposit of elements from the upper crust. It may also be caused by an extended sedimentary recycling history (Veizer and Jansen, 1979; 1985) which facilitates mixing and homogenization of REE and other geochemical signatures. Variability may be due to other factors, such as secular trend and variable provenance on a local scale (McLennan, 1989), and secondary mobilization of the REE at the oxidic-anoxic water interface where manganeses and iron oxide micronodules are currently formed (de Baar et al., 1988; Brookins, 1989). The parallelism between the REE patterns of the Gusui bedded chert and the average post-Archean sedimentary rock suggests that the process of the chert formation accomplishes some degree of recycling and homogenization of source rocks by circulating hydrothermal solutions through old country rocks.

§4 Mechanism of Formation

4.1 General Consideration: Conceptional Model for Hydrothermal Activity

The petrological and geochemical characteristics strongly suggests that the Gusui chert formation was the product of a fossil geothermal system taking place during the Sinian period. Various models for the formation of both modern and fossil geothermal systems have been proposed (Rona, 1984; Crerar et al., 1982; Bonatti, 1975; 1981; Boström, 1973). There is a suite of geological conditions that result in the formation of a geothermal system. The essential requirements for a geothermal system are (a) a source of heat, (b) a reservoir to accumulate heat, and (c) a barrier to hold the accumulated heat (Gupta, 1980). The hydrothermal processes involved in the deposition of the Gusui chert formation are outlined

as below (Fig. 3.11):

First, a fault system (down-welling zone) developed in the Precambrian (probably through to Cambrian) sedimentary basin of the Yunkai terrain. Cold and dense seawater penetrated downward through fractures of the fault system into old strata, with variable penetration depths during different stages. The penetrating seawater was gradually heated by an unknown heat engine at depth, and reduced as it reacted with the country rocks. At the same time, the acidity of the solution increased by the incorporation of Mg^{2+} and OH^- from the seawater into Mg-hydroxide, Mg-hydroxy-alumininosilicate, and Mg-hydroxysulfate-hydrate mineral phases, accompanied by the production of hydrogen ions when flow rates replenish seawater faster than the solution could react with the rock surfaces it flowed through (high water-rock mass ratios; seawater-dominated system) (Rona, 1984). The evolving high-temperature, acidic and reducing primary hydrothermal solutions leached the country rocks and extracted from the latter silica and metal elements, such as Li, K, Rb, Nb, Ta and W. After a certain residence time at depth, the silica-enriched primary hydrothermal solutions ascended through gradients of decreasing temperature and pressure, accompanying mixing with low-temperature, alkaline and oxidizing normal seawater in a relatively narrow upwelling zone. Finally, silica and amorphous ferric hydroxide precipitated from these primary or mixed hydrothermal solutions, followed by scavenging of the iron and manganese remaining in the solution, as well as other metals in seawater, by colloidal adsorption on the ferric hydroxides.

The convective model proposed above for the geothermal system that formed the Gusui chert formation is similar to those for the Nandan-Hechi hydrothermal chert, southern China (Zhou, 1987; Chen and Chen, 1990), for the Franciscan chert deposits (Crerar et al., 1982), for the Galapagos geothermal system, and those observed directly at the 21°N EPR vents (Edmond et al., 1979; Edmond, 1980). However, the final exit temperature and composition at the seawater interface are unknown. By analogy with the hydrothermal cherts from the Nadan-Hechi of Guangxi, southern China, where there was no volcanic activity, and the Galapagos Spreading Center at 86°W, the temperature at which the Gusui chert formed could have been lower than 100°C. A temperature range of 29-64°C was obtained for the Nandan-Hechi chert (Chen and Chen, 1990) and 32-42°C for the Galapagos silica deposit (Herzig et al., 1988) by oxygen isotope measurements. These temperatures indicate a "white smokers", and are much lower than that of modern "black smokers" (Cann and Strens, 1982).
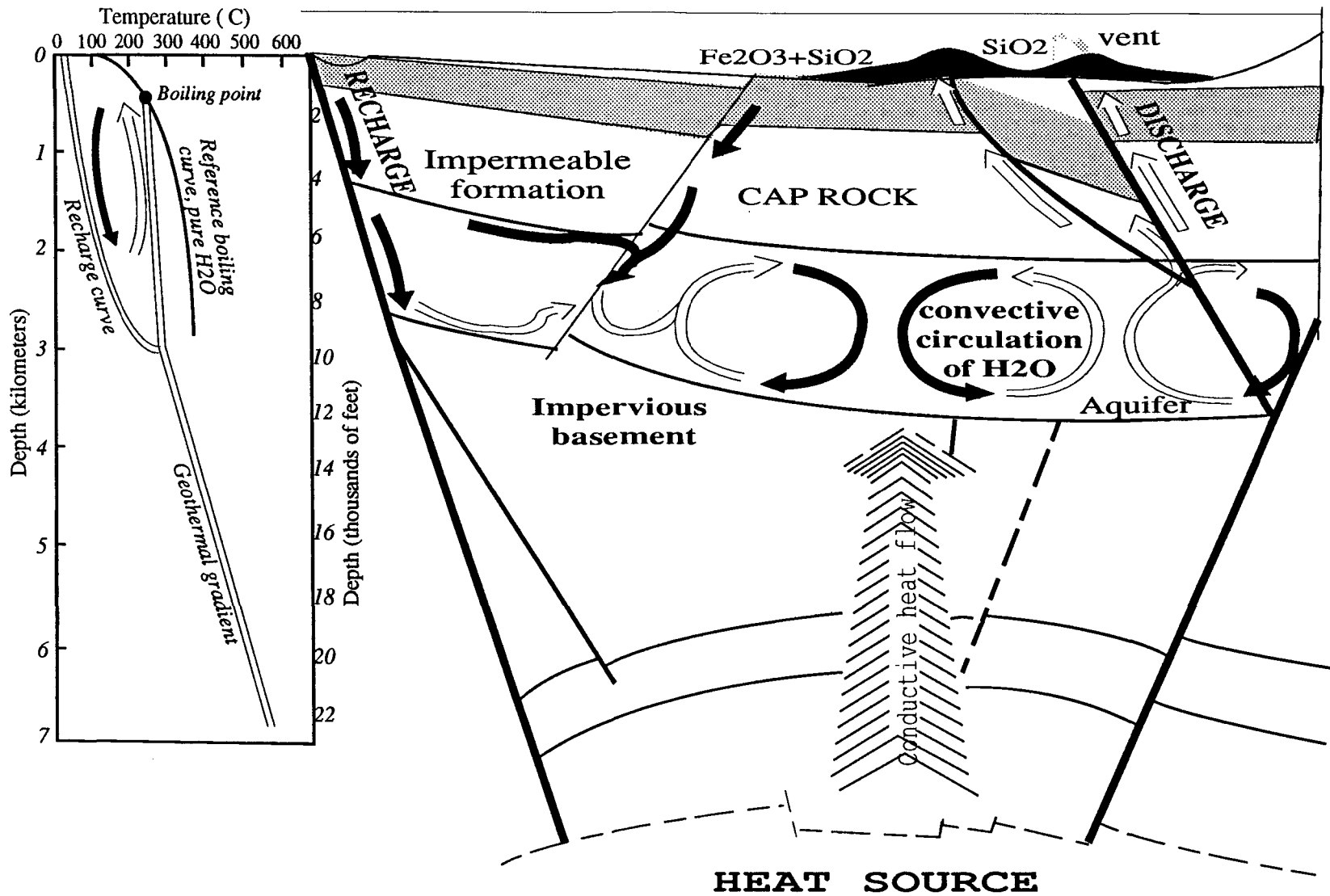
Figure 3.11 Conceptual Model of a Geothermal System Responsible for the Formation of the Gusui Bedded Cherts

4.2 Precipitation of Silica

The initial deposit of silica in the Gusui chert formation was probably amorphous silica and chalcedony, and then transformed to microquartz with geological time. Many factors contributed to the precipitation of silica from hydrothermal solutions, such as natural cooling or cooling by mixing of hydrothermal solution with ambient seawater, and sudden dropping of pressure during fracturing.

The mixing of primary hydrothermal solutions and ambient seawater appears attractive for explaining the precipitation of silica phase of the Gusui chert. Equilibrium path calculations (Janecky and Seyfried, 1984) predicted abundant quartz may precipitate by mixing of hot solutions and ambient seawater. It was suggested (Herzig et al., 1988; Fournier, 1985) that some combination of conductive cooling and mixing account for the deposition of amorphous silica. The deposition of amorphous silica from >350°C solutions, carrying about 500 ppm SiO_2, at the Endeavour Segment, Juan de Fuca Ridge, is due to conductive heat loss during the sluggish percolation of a seawater/hydrothermal fluid mixture through the walls of large sulfide structures (Canadian American Seamount Expedition, 1985). Hekinian (1982) described significant amorphous silica deposits in an off-axis seamount at 13°N, EPR, and suggested that the formation of silica is due to intermixing of seawater with late-stage silica-rich solutions without conductive cooling. Hannington and Scott (1988) shown that mixing of hydrothermal fluids with seawater at Axial Seamount, Juan de Fuca Ridge, was involved in the precipitation of amorphous silica at 185°C, although the high-temperature end-member fluid must have cooled conductively at depth. Alt et al. (1987) suggested that opal at Green Seamount, 21°N, EPR, was deposited as hydrothermal fluids mixed with seawater and were cooled conductively.

The mixing of hot, acid, and reducing hydrothermal solution with cold, alkaline, and oxygenated seawaters could dump rapidly part of the remaining Fe as oxy-hydroxides into the overlying sediments (Crerar et al., 1982), but more Fe, Mn and Si would pass to the sediment-water interface. Some silica is deposited here, but some is lost to local bottom waters and transferred away from the exit opening for later precipitating associated with non-hydrothermal deposits. This is one of the reasons for that non-hydrothermal sediments such as clay are found in the Gusui chert formation. The hydrothermal mound and underlying sediments may have been saturated or supersaturated in silica, resulting in characteristically

low compaction and pseudobrecciation (Crerar et al., 1982), since the silica solubility in the solution decreases from that equilibrated at high temperature at depth to that of low temperature at surface.

4.3 Intermittent Activity

There is good evidence that both the deposition of silica and the activity of the fossil geothermal system were intermittent or periodic. The bedded and laminated structures are a manifestation of intermittent activity. The dark clayey partings in bedded and laminated cherts are characteristic of hydrogenous deposits in a deep sea area, suggesting a temporary weakening of hydrothermal activity.

The microscopic alternation of Fe oxide-rich phase and quartz phase is a result of intermittent hydrothermal activities. Silica is deposited at peak hydrothermal activity, and Fe and Mn oxides, during quiescent times. At depth silica equilibriates with its environment. The solubility of quartz can be as high as 500 ppm at temperature of 300°C depending on pressure. When the hydrothermal solution reaches the exit, its temperature may drop to about 100°C or lower as a "white smoker". At this time, in the case of conductive cooling, the dissolved silica becomes supersaturated with respect to amorphous silica and chalcedony, whose solubility is under 400 ppm. The precipitation of silica, therefore, takes place around the hydrothermal spring openings during hydrothermal activity. In many cases, some silica does not deposit intermediately around the opening, but is transported some distance away from the opening.

Although the initial source of Fe and Mn is not very clear, their short residence time in seawater (Rösler and Lange, 1972) suggests that they may be in part related to the hydrothermal system. The Fe and Mn oxide deposits are commonly formed in a low temperature environment, and represent a quiescent period of hydrothermal activity. Fresh precipitated Fe oxides have extraordinary high surface energies and would readily scavenge and coprecipitate trace metals within the accumulated sediment.

Theoretically, intermittent hydrothermal activity is inevitable. First, it may be caused by periodic tectonic activity, because the site of hydrothermal activity is often within a fracture zone. It may also result from the so-called quartz seal - explosion mechanism.

According to this mechanism (Fournier, 1985), silica and other minerals deposit along the conduit of hydrothermal solution during ascent, even at high temperatures (c.f. Fig. 3.12), resulting in permeability reduction, even a completely impermeable seal. After the establishment of an impermeable quartz seal, eruption takes place with creation of new fractures by tectonic activity or thermal or hydraulic fracturing (Fournier, 1983; Secor, 1965).

4.4 Paleotectonic Setting

Submarine hydrothermal activity occurs in a wide variety of tectonic settings, such as mid-ocean ridges or spreading centers, back-arc marginal basins, intraplate hot spots and oceanic islands, and convergent plate margins and island arcs. The Gusui chert formation appears to be analogous to the Franciscan manganiferous chert deposit, California, for which two alternative environments were suggested (Crerar et al., 1982), either a mid-ocean ridge or back-arc spreading within a marginal basin.

The Gusui area is part of the elongate NE-SW stretching Yunkai terrain, which is classified as a marginal paleogeosyncline. The numerous occurrences of similar bedded chert formation in the terrain align in a nearly linear feature with the Gusui occurrence. The absence of calcite and terrigenous coarse grained clastic rocks in the cherts implies that the Gusui chert formation was deposited below the calcite compensation depth. It is likely that the Gusui bedded chert was formed in a Precambrian rift or extension zone developed within the Yunkai marginal geosyncline, with a fault system linking it to a unknown heat source at depth, which drove convective hydrothermal system.

§5 Summary

The Gusui bedded chert formation (Z^d) occurs at the top of the Sinian strata in the Yunkai terrain. The characteristic structures include bedded structure, laminated structure, massive structure and pseudobrecciated structure. The petrographic characteristics suggest a hydrothermal origin.

Geochemical analysis of elements and element associations favors a hydrothermal origin. The Gusui bedded chert is characterized by its consistently low TiO_2, Al_2O_3 and most trace elements. However, it is enriched in Ba, As, Sb, Hg and Se, which are diagnostic of

hydrothermal sediments. In the Al - Fe -Mn ternary diagrams, nearly all the studied cherts fall into the "hydrothermal field". In short, the Gusui chert has geochemical affinity to cherts attributed to hydrothermal origin.

Elements in the cherts may be grouped into meaningful associations by correspondence analysis and factor analysis. Many elements show up in the factor that represents the leaching of hydrothermal solutions through country rocks. The principal factor of trace elements, {Rb, Cs, Ta, Th, Nb, Ta, Th, U, Zr, Hf, W, Sn}, is the very characteristic element association of the geochemically anomalous south China basement. {As, Au, -Cr}, {Ba, Hg, -Sn} and {Ba, Pb} are diagnostic of hydrothermal deposit. {MnO, FeO, MgO} and {Fe2O3} imply that the Gusui chert formation was developed in an oxiding sedimentary environment, with local and temporary reduction.

Rare earth elements are characterized by a low total content and a gradually increasing NASC-normalized value with increasing atomic number of REE. The REE abundance distribution pattern of the cherts is similar to known hydrothermal sediments, and ranges between the upper and the lower limits of typical hydrothermal deposits. The ambiguous Ce anomaly and higher REE abundance of some samples are due to an admixture of hydrogenous deposits to the hydrothermal chert. There are two possible mixing mechanisms: either by alternation of hydrothermal and hydrogenous processes, or by synchronous activity of both, but with varying contributions.

The Gusui bedded cherts were formed by mixing of discharging hydrothermal solutions with ambient seawaters. The involved geothermal system developed in a Precambrian marginal geosyncline of south China. First, cold and dense seawater recharged along fractures cut through the old tectonic basement and strata. Then the downward penetrating seawater gradually heated and reduced as it reacted with rocks at depth near a unknown heat source. The evolving hydrothermal solution leached the country rock which it passed through, and became enriched in silica and certain metal elements. Finally, the silica-rich hydrothermal solution ascended and discharged. Some silica precipitated as amorphous silica or chalcedony near the exit, and the other was lost in local sea bottom waters and transported away from the exit. The present microquartz is the result of transformation of the initially precipitated amorphous silica phase and chalcedony.

The hydrothermal system has resulted in local enrichment of gold in the bedded

cherts, with an average abundance of 8.7 ppb, about twice that of the crust. The characteristic chondrite-normalized REE pattern of the cherts indicates that the hydrothermal circulating process responsible for the formation of the cherts had accomplished some degree of recycling and homogenization of provenance components (older Sinian strata), and the association of gold with barium in the same factor is an indication that gold has associated with the hydrothermal activity.

Chapter IV

MIGRATION OF TRACE ELEMENTS DURING THERMAL EVENTS

Gold is contained in almost all minerals, either as a principal or significant constituent such as in native gold, electrum, maldonite and sulfides, or as an impurity element such as in many rock-forming minerals (Luan, 1987; Liu et al., 1984). However, it is a minor constituent of rocks as a whole. Although it may be enriched in sulfides and some accessory minerals, a significant proportion of gold of rocks is hosted in rock-forming minerals such as feldspar (Boyle, 1979; Luan et al., 1987; Tu, 1984). This implies that the release of gold from rock-forming minerals, which is necessary for subsequent transport to the site of mineralization, may be important for the formation of economic gold deposits.

This chapter concerns the release or redistribution mechanism of trace elements in rock-forming minerals and source rocks within a thermal field, which is often an integral part of multiple stage mineralization, through reviewing what is known from physical sciences about the migration of elements within minerals, and applying a mathematical treatment to the migration, which is believed to be helpful in exploring the redistribution mechanism of gold during metamorphism. This includes the discussion of possible migration paths and their integration and comparison under various situations, since the redistribution of trace elements is closely tied to migration of matter, which can be achieved in three ways: by diffusion, by infiltration or by flow, with each having its own characteristic movement pattern.

§1 Diffusion

Three types of diffusion are significant in geological environments: diffusion through bulk solids such as single crystals (dry conditions), diffusion along weaknesses such as

intergranular boundaries or fissure films of a bulk solid (either dry or wet condition), and diffusion within bulk fluids (wet condition).

1.1 Atomic Diffusion Mechanism

Consider the diffusion of an atom within a solid. Diffusion is essentially a series of random leaps without memory, and may be treated as a mathematical Random-Walk process with an absorbed wall (Nicolas and Poirier, 1976). Four general types of mechanisms have been recognized (Manning, 1973): exchange, interstitial, vacancy, and interstitialcy (also called indirect interstitial) (Fig. 4.1). Such leaps are generally not oriented. However, when a concentration difference or gradient exists, it may present itself as a macroscopic oriented movement. The rate of diffusion is measured by the diffusion coefficient D, which depends exponentially on the activation energy Q and absolute temperature T according the Arrhenius equation (Manning, 1973),

$$D = D_0 \exp(-Q/RT) \qquad (1)$$

where R is the universal gas constant (1.98 cal/mol/K). The preexponential constant D_0 is temperature independent, and proportional to the number of possible atom migration paths and the average squared jump distance.

Potential barrier is a basic concept related to the activation energy to understand the mechanism of atomic diffusion. An atom tends to rest in a position where it has minimum energy under equilibrium. When it tries to leap from one position to another, it has to overcome a potential barrier keeping it in the present position. The larger the activation energy of an atom and the lower the potential barrier, the more frequently the atom will leap from one position to the next, and therefore the greater its diffusion coefficient.

The total distance that an atom may pass can be obtained on average (the average being taken over many trial runs) by the Random-Walk theory (Nicolas and Poirier, 1976). Einstein showed that the mean square displacement of a particle from the origin after N random steps, each of length L, is given by:

$$<X_N^2> = N L^2$$
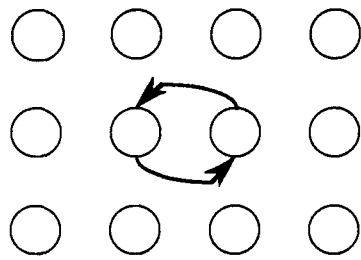
Exchange mechanism
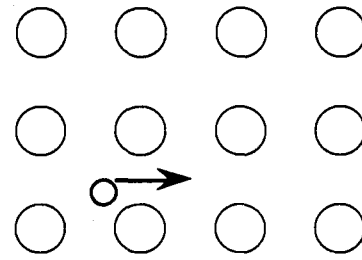
Interstitial mechanism
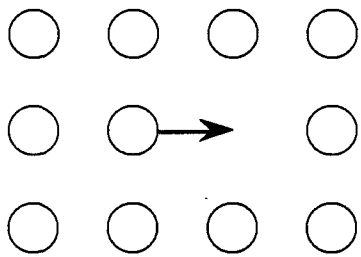
Vacancy mechanism
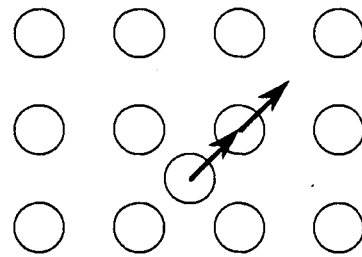
Interstitialcy mechanism

Figure 4.1 Elementary atom jump mechanism within a crystal
Modified from Manning (1973)

(the carets mean average value).

or (Fyfe et al., 1978; Busch and Schade, 1976)

$$< X^2 > = 2 D t \qquad (2)$$

1.2 Types of Diffusion

1. Diffusion within Bulk Solids

Many experimental studies have been carried out on cation diffusion within silicate minerals and sulfides (Fyfe et al., 1978; Birchenall, 1973; Lasaga et al., 1977; Jurewicz and Waston, 1988; Lever and Bradbury, 1985). They were directed towards understanding mass transfer. It was shown that typical values of cation diffusion coefficient in silicates are in the order of 10^{-14} to 10^{-18} cm^{2}sec^{-1} at room temperature, with most around 10^{-15}. For a geological time scale of 10^7 years (about 3×10^{14} seconds), the distance of atomic diffusion in a silicate mineral is about 1 cm. Thus an atom needs to take about 10 Ma on the average to pass from the center to the margin of a crystal 2 cm in diameter. Such a distance is considered by some to be too small for significant transport of ore material. As temperature increases, however, the contribution of volume diffusion increases rapidly until finally it predominates at high temperatures (Manning, 1973). At common metamorphic temperatures, the diffusion coefficient may be multiplied by several orders of magnitude compared to that at room temperature.

2. Diffusion in Bulk Aqueous Solutions

Diffusion coefficients have been obtained for many electrolytes in aqueous solutions at 25°C (Fyfe et al., 1978). Typical diffusion coefficients are about in the order of magnitude 10^{-5} cm^{2}sec^{-1}. These coefficients increase slightly with increasing temperature and reach a maximum at higher concentration.

If the value of 10^{-5} cm^{2}sec^{-1} is taken as representative of the diffusion coefficients of dissolved species in natural aqueous fluids in the earth's crust, and applied to the same time scale of 10^7 years, the approximate diffusion distance is 10^5 cm or 1 km. The actual distance may be enhanced by the transport of fluid flow in fracture systems. The significance of such

a high value should not be underestimated as a means of mass transport.

3. Diffusion along Weaknesses in Bulk Solids

Diffusion along these short-circuit paths may be expected to exceed that within perfect solids. It is common that aqueous solution films are adsorbed on intergranular surfaces and in fissures of various scales. The presence of such solution films will further enhance element migration with respect to dry conditions. It has been shown (Garrels et al., 1949; Fisher and Elliott, 1973; Fyfe et al., 1978) that diffusion along an aqueous solution film as a function of time is dependent on the pore volume (porosity) and the interconnection of the pores (permeability). In a general way, it is apparent that the diffusion coefficient in these thin solution films must range between the limits of bulk fluid and bulk solid, and will approach the latter as the film thickness declines to zero. According to Fisher and Elliott (1973), the diffusion coefficient of many impurity elements in granular boundaries of silicates is about 10^{-5} - 10^{-9} cm^{2}sec^{-1}.

1.3 Equations and their Mathematical Solutions

1. Equations

Chemical diffusion occurs wherever a concentration gradient exists. Phenomenological treatment of diffusion problems are based on Fick's laws (Crank, 1975).

The first law

$$s = - D \operatorname{grad} C$$

together with the continuity equation

$$\operatorname{div} s + \partial C / \partial t = 0$$

yields Fick's second law

$$\partial C / \partial t = \operatorname{div} (D \operatorname{grad} C) \tag{3}$$

where t is time, C(x, y, z) is the concentration of the concerned chemical species, s(x, y, z) is the concentration flux, and D is the diffusion coefficient of the chemical species under

consideration.

Generally, the diffusion coefficient D is a second rank tensor. However, it is often considered, for the sake of simplification, as a scalar quantity which depends on temperature and the continuum medium. Specifically, for only one-dimensional case, equation (3) can be simply reduced to

$$\partial C / \partial t = D \, \partial^2 C / \partial x^2 \tag{4}$$

2. Analytic Solutions

General solutions of Equation (4) with constant D have been obtained for a variety of initial and boundary conditions (Crank, 1975). Such solutions usually comprise of a series of error functions or related integrals.

Consider two groups of initial and boundary conditions and their solutions, the physical implications of which will be discussed later:

(1) The initial distribution occupies a finite region and the initial state is defined by

$$C = \begin{cases} C_0 & x < 0 \\ 0 & x > 0; \end{cases} \qquad t = 0$$

The analytic solution of Equation (4) is

$$C(x, t) = \frac{1}{2} C_0 \, \mathrm{erf}(x / \sqrt{4Dt}) \tag{5}$$

where erf (x) is a standard mathematical function, the error function. The solution is illustrated in Fig. 4.2.

(2) The boundary condition below is referred as a "entrapment path":

Boundary condition:

$$C(x, t)\big|_{x < 0} = 0 \qquad\qquad t > 0 \tag{6}$$
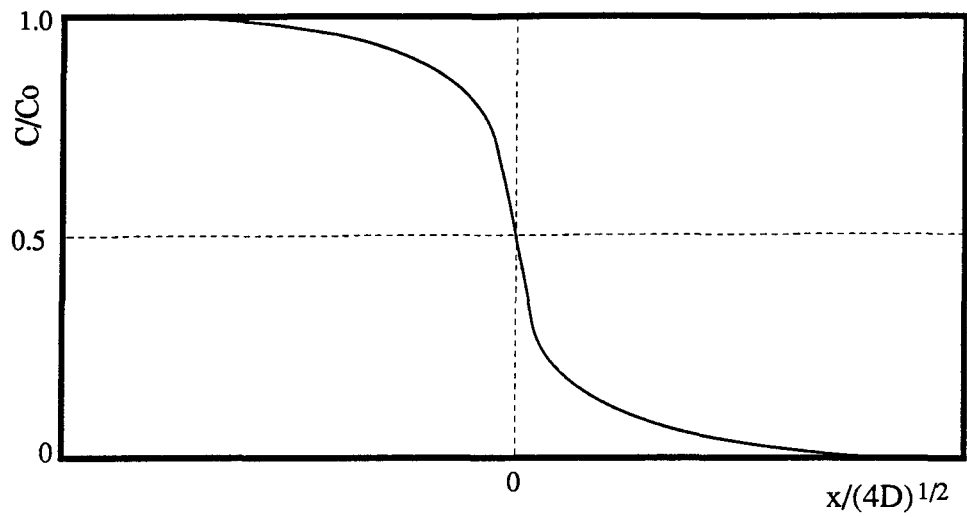
Figure 4.2 Concentration-distance curve for an extended source of infinite extent
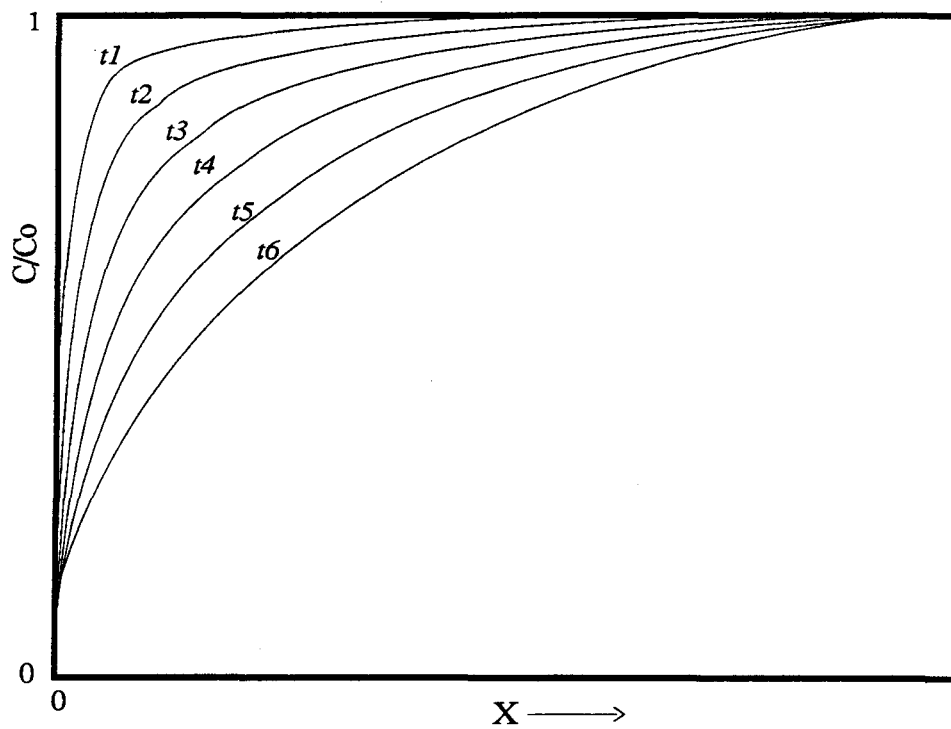
Figure 4.3 Concentration change profile of a migrating substance by diffusion derived from the "entrapment path model"

and initial condition:

$$C(x, t)|_{t=0} = C_0 \qquad x \geq 0 \qquad\qquad (7)$$

$$C(x, t)|_{t=0} = 0 \qquad\qquad \text{else}$$

Equation (4) with initial condition (7) is equal to a type of standard partial differential equation:

$$U_t - a^2 U_{xx} = 0$$

$$U|_{t=0} = \varphi(x)$$

which has a general solution by the method of separation of variables (Fourier integral method):

$$U(x, t) = \int_{-\infty}^{\infty} \varphi(\xi) [1/\sqrt{4a^2 \pi t} \exp(-(x - \xi)/(4a^2\xi))] d\xi$$

Condition (6) belongs to the first type of boundary. The solution for Equation (4), (6) and (7) is

$$C(x, t) = \frac{2C_0}{\sqrt{\pi}} \int_0^{x/(2\sqrt{Dt})} \exp(-z^2) dz$$

or

$$C(x, t) = \frac{C_0}{2} \text{erf}(x/2a\sqrt{Dt}), \qquad x \geq 0 \qquad\qquad (8)$$

since the standard error function (Gaussian distribution) is as follows:

$$\text{erf}(x, t) = \frac{2}{\sqrt{\pi}} \int_0^x \exp(-z^2) dz$$

The distribution curve for the solution (8) is shown in Figure 4.3.

1.4 "Entrapment Paths" and Fractal Structure

1. "Entrapment Paths"

The boundary condition (6) above is an ideal approximation of geological reality. It is clear that the inner part and boundary of a bulk solid cell are two very different phases for diffusion of trace elements. A bulk solid cell here means any form and scale of geological unit (block) occupying a uniform space, such as a mineral grain, a lithon in a deformation zone or a granite body, constrained by boundaries. The boundary phase may be various weaknesses, including intragranular or granular boundaries, cracks and fractures, which may be or not filled with aqueous solution films. The boundary phase has consistently higher diffusion coefficients than the inner part of a solid cell (Manning, 1973; Fyfe et al., 1978). Once they cross the boundary from within a solid cell, the migrating atoms will be trapped by the boundary phase (Fig. 4.4). The boundary phase thus serves as an "entrapment path" for the diffusants out of the inner part of a bulk solid cell. This may be, on the grain scale, exemplified by the textures developed during exsolution growth demonstrated by various workers in the field of physical metallurgy and experimental mineral synthesis. In contrast, diffusion in the opposite sense, from an "entrapment path" toward the inner core of "texturally perfect" solid cells, is negligible because the latter has a diffusion coefficient which is smaller by several orders of magnitude.

Figure 4.5 considers the case of an interstitial (impurity) atom in a crystal. The atom needs high activation energy to overcome the high potential barrier and to leap from one position to the next within the inner part of the host crystal, and even higher from the boundary solution film toward the the inner part of the crystal (Fig. 4.5). The opposite is not true, the potential barrier is much lower for the atom to leap from the margin of a crystal to the aqueous solution film, and along the solution film. Neglect the diffusion from the weaknesses to the inner phase of a neighbor bulk solid cell, or let $C = 0$ or $-\infty$ at these weaknesses, boundary condition (6) can be obtained immediately. As a sequence, impurity trace elements have a tendency to migrate out of the inner part of solid geological units into "entrapment paths".

2. Fractal Structure of "Entrapment Paths"

There are "entrapment paths" of different scales or ranks, corresponding to the transitional series of diffusion coefficient between the limits of bulk solid and bulk fluid. A
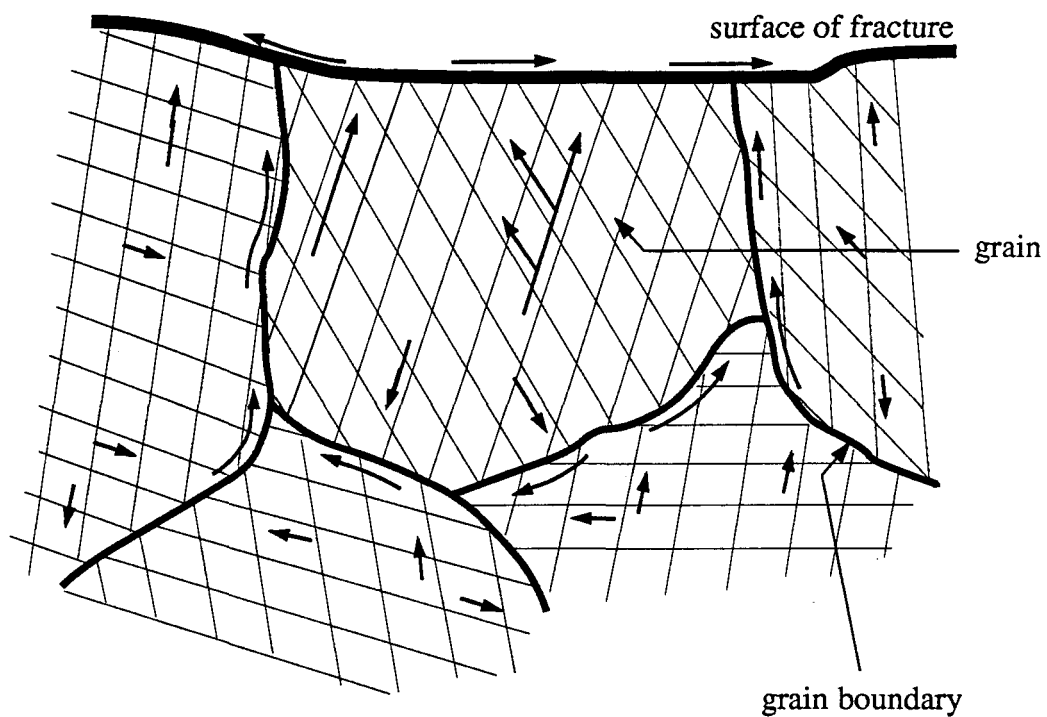
Fingure 4.4 Paths of migration of trace elements in the solid cell and boundary system

Solid cells are exemplified by mineral grains here. The boundary phase consists of granular boundaries and fractures, which serve as "paths" to trap the migrating particles from the inner part of the solid cells. The arrow indicates the migration direction of the particles.

location of the
diffusing particles

lattice locations

Potential energy

bulk solid

*boundary
solution film*
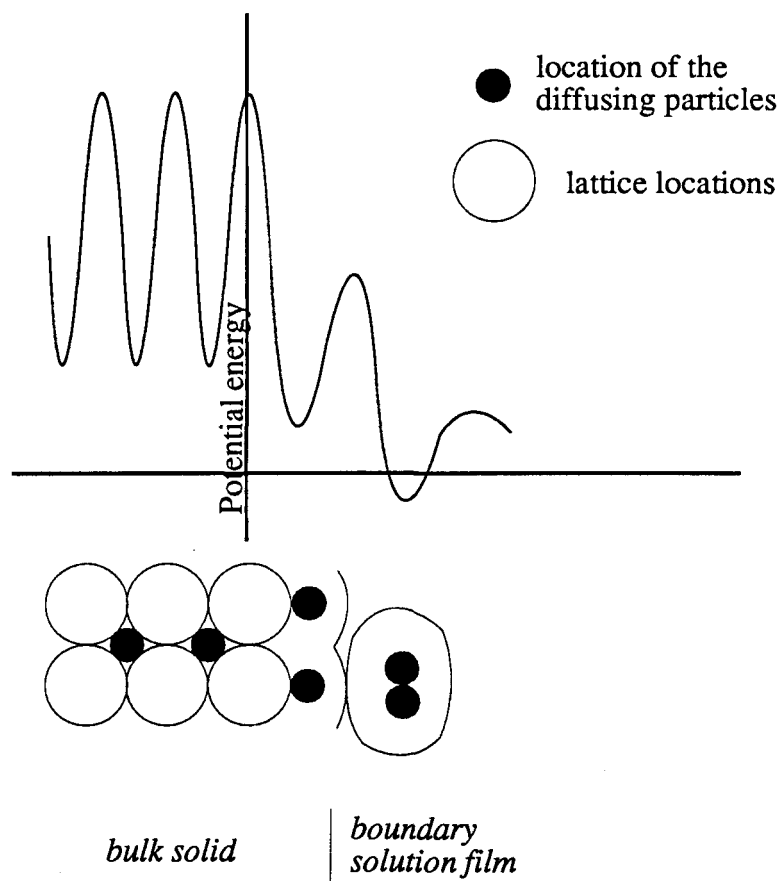
**Figure 4.5 Sketch illustrating the distribution of potential
energy of a diffusing particle within a bulk solid and its
boundary aqueous solution film system**

series of smaller scale (rank) "entrapment paths" may become the inner phase of the cell of a next higher rank geological system. So diffusants in low rank "entrapment paths", now the inner part of the cell of a next higher rank geological system, will migrate toward and finally be trapped within an "entrapment paths" of a higher rank. In nature, the lowest rank end-member is composed of subgrains, and the corresponding rank "entrapment paths" are the linear or planar dislocations. Next come the crystal or grain scale (Fig. 4.6d), the corresponding "entrapment paths" are the granular boundaries. Included among higher ranks are very small scale fissured rocks (Fig. 4.6c), specimen scale fractured rocks (Fig. 4.6b) and geological units constrained by large faults (Fig. 4.6a).

At each rank, the numerous "entrapment paths" and solid cells (bricks) form a mosaic, and many low rank mosaics make up a higher rank mosaic. Such a panorama of "entrapment paths", or mosaic hierarchical array (mosaics are inlaid in a larger scale mosaic), forms a characteristic fractal structure. If a certain layer is magnified or reduced, its mosaic pattern will resemble that of higher or lower order (Fig. 4.6). This is a self-similar structure, which is the very characteristic of mathematical fractals. From the three dimension viewpoint, it is apparent that the fractal structure of "entrapment paths" has a dimension number between 2 and 3.

Since the cells of each layer of mosaic obey the same diffusion equation, i.e., equation (4) with the boundary and initial constraints (6) and (7), there is the same tendency for impurity trace elements to migrate, i.e., from the inner parts of a uniform geological domain outwards to the weaknesses. This is also a self-similarity.

§2 Infiltration and Flow of Aqueous Fluids

2.1 Relationship to diffusion and the implication

The migration of elements may be realized by two completely different mechanisms. In addition to their own migration by diffusion in continuum media, elements can also be transported by infiltration and flow of aqueous fluids, with various flow rates and movement distances.

Infiltration is also called pervasive flow. Instead of movement of individual particles as in the case of diffusion, infiltration and flow are essentially a body movement of the
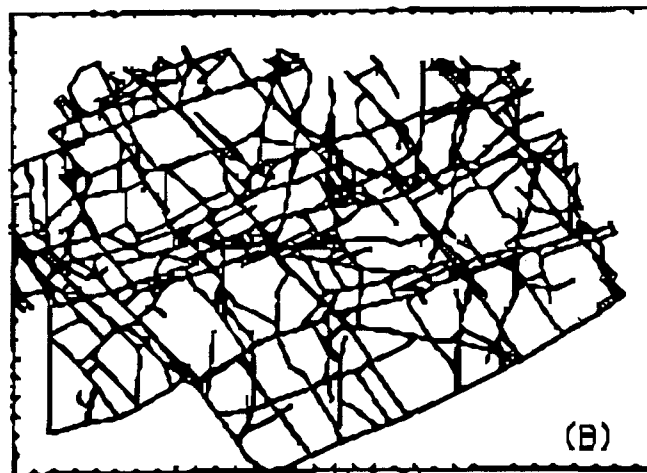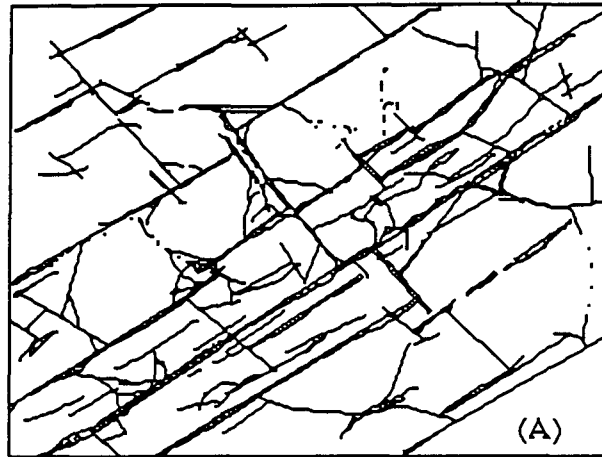
Figure 4.6(1) Similarity of the mosaic structure of different Layers of "entrapment paths"

(A) Fracture network at a mappable geological scale
(B) Fracture network at the hand-sample scale
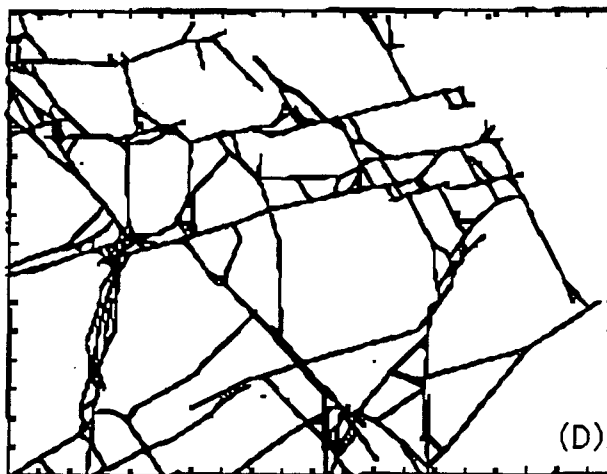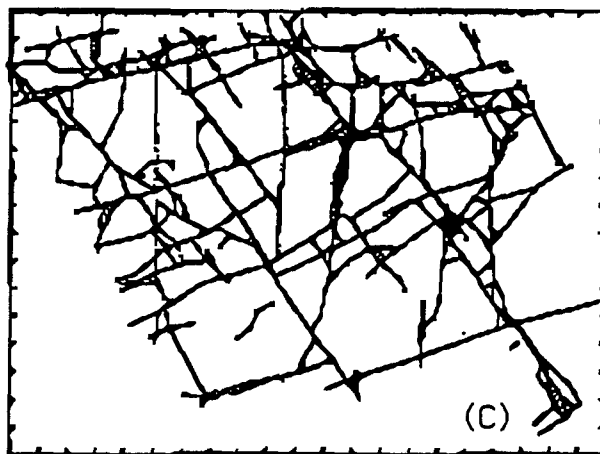
Figure 4.6(2) Similarity of the mosaic structure of different Layers of "entrapment paths"

(C) Microscopic fracture network
(D) Grain-scale mosaic

continuum media (aqueous solutions). They are characterized by a general orientation. The orientation is controlled by physical factors, such as directed pressure gradient and the difference of density, but independent of the chemical concentration gradient of elements.

The relationship of infiltration and flow of fluids to diffusion is not one of replacement, but of superimposition. The result is that infiltration and flow of fluids can increase the effectiveness of migration of trace elements. Usually fluid infiltration and flow, if present, are more effective than diffusion in carrying elements. This is especially true in higher rank "entrapment paths", such as fracturing zones. However, diffusion takes place everywhere, including where fluid infiltration and flow predominate. Migration by diffusion predominates over infiltration and flow in bulk solid cells and low rank "entrapment paths".

It has been shown that the mineralization of gold and many trace elements is often of multi-stage, and requires the migration of the trace elements from the initial positions to favorable ore-hosting locations (Tu, 1984). The discussion above implies that the transport of ore-forming trace elements along visible fractures with flowing fluids is relatively rapid with respect to the migration from the inner part of a rock-forming mineral in source rocks to visible fractures, i.e., the migration from the inner part of a rock-forming mineral to visible fractures is the bottleneck of the entire migration process from the source rock to ore sites. Over this short distance, diffusion prevails.

2.2 Mathematical Treatment

Infiltration and flow of migrating substances are assumed to have a flow rate, u. The combination of such movement with diffusion is called convective diffusion of a substance in a medium (aqueous solution) (Golubev and Garibyants, 1971).

If the substance reacts weakly with the wall rocks and is insignificantly adsorbed by them, the process may be assumed to have no interaction between the substance and the medium. Neglect the adsorption, ion exchange and chemical reaction between the solution and the host rock, the equation of material balance of the migrating substance in a convective diffusion system is obtained (Golubev and Garibyants, 1971) as follows:

$$\partial C / \partial t \quad + \quad (u \text{ grad}) C \quad = \quad D \Delta C \tag{9}$$

Only a one-dimensional problem is examined below for simplicity, in which case the flow of substance is assumed along the x axis at constant rate u. Since exchange of material between the mobile and the fixed phase is absent, then:

$$\partial C / \partial t \; + \; u \, \partial C / \partial x \; - \; D \, \partial^2 C / \partial x^2 \; = \; 0 \qquad\qquad (10)$$

Solve Equation (10) with respect to the filtration and flow of fluids through rock from a semi-infinite bed. For this problem, the initial conditions may be described as below:

$$C(x, 0) \; = \; \begin{cases} Co & x \leq 0 \\ 0 & x > 0 \end{cases} \qquad\qquad (11)$$

The solution may be written in the form (Fig. 4.7):

$$C(x, t) \; = \; \frac{1}{2} \, Co \, \{ \, 1 \, - \, erf \, (\, (x \, - \, ut) \, / \sqrt{4Dt} \,) \, \} \qquad\qquad (12)$$

which may be simplified, to discuss the migration distance of the substance, as:

$$C(x, t) \; = \; \frac{1}{2} \, Co \, \{ \, 1 \, - \, (\, (x \, - \, ut) \, / \sqrt{\pi Dt} \,) \, \}$$

$$\text{or} \qquad\qquad x \; = \; u \, t \; + \; (\, 1 \, - \, C / Co \,) \, \sqrt{\pi Dt} \qquad\qquad (13)$$

Compared to the analytical solution of the pure diffusion equation, the solution of the convective diffusion equation (10) contains an additional term, ut. It follows that during convective diffusion the migration and flow distance is greater than that by pure diffusion by the value, (ut). Equation (13) indicates that the distance of substance migration is predominantly determined by the infiltration and flow of fluid rather than by diffusion, when the rate of infiltration and flow is significantly lager than 0.

2.3 Infiltration Effect

The discussion above applies both to infiltration and to flow of aqueous solutions. Infiltration is to a great extent the same thing as flow. Their differences lie only in the so-called infiltration effect (Korzhinskii, 1970). According to the terminology of Korzhinskii (1970),
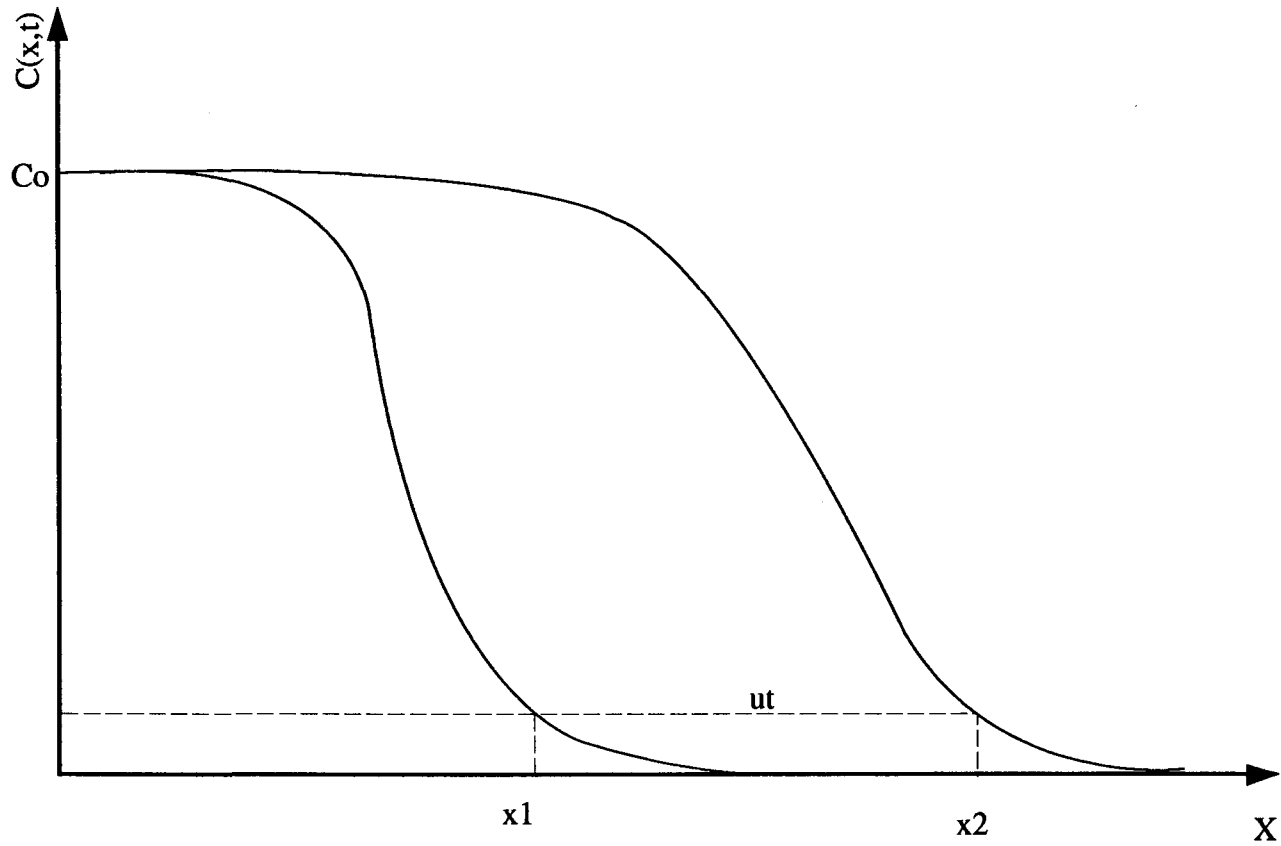
Figure 4.7 Distribution of concentration of the migrating substance during a convective diffusion from a semiinfinite bed

the infiltration effect refers to the lagging behind of dissolved substance in a solvent during movement through porous media, due to the difference of flow rate between cations and anions in a electrolyte solution current. It is characterized by a filtration coefficient φ, which is equal to the ratio of the movement rate of dissolved substance to that of the solvent. Thus, Equation (10) should be revised by substituting u with (φu). Such revision does not change the formula of the analytical solution of Equation (10), so the affect of infiltration and fluid flow on the migration of elements remains the same.

§3 Orientation of Mass Transport

3.1 Effects of Temperature and Temperature Field on Diffusion

1. Temperature

Equation (1) states that diffusion coefficient is positively dependent on temperature. The logarithm of that equation gives:

$$\log D = \log D_0 - Q/RT \tag{14}$$

A number of experimental studies have shown that the diffusion coefficient of many elements increases by orders of magnitude when temperature is elevated to a medium grade metamorphic temperature. Therefore the effects of diffusion under metamorphic conditions must be considered. High temperatures in metamorphic areas favor rapid migration of elements in a solid and the realization of the migration tendency of trace elements from the inner part of a bulk solid cell toward the boundaries and weaknesses, where elements can be further transported by more effective fluid flow and infiltration.

2. Temperature Field

Temperature is not constant over geological space, but is a function of location. The presence of the geothermal gradient, which results in the earth's heat flow, is one of the familiar examples. The temperature increases with increasing depth in the crust. The increasing rate (gradient) varies with tectonic environment, with average around 30°C/km. Another significant example may be found in areas where metamorphism is taking place.

Lateral temperature gradients inevitably occur in these districts.

Again, for the sake of convenience, only one dimension is discussed below. Since the diffusion coefficient depends on T, how does it vary with the temperature gradient (gradient T)? Mathematically, there exits that

$$dD(x, T) /dx = \partial D(x, T) /\partial x + (\partial D(x, T) /\partial T) (\partial T /\partial x)$$

or

$$grad\ D = \partial D(x, T) /\partial T\ grad\ T \tag{15}$$

for diffusion in a homogeneous medium, where the first term on the right side, $\partial D(x, T)/\partial x = 0$.

Take the derivation of Equation (1) in relation to location x, we obtain

$$\partial D(x, T)/\partial T = Do\ Q\ exp\ (- Q/RT) / (RT^2) > 0 \tag{16}$$

The combination of Equation (15) and (16) shows that gradient D and gradient T are positively correlated to each other, and have similar distribution pattern in space. It can be proven mathematically that the temperature gradient is related to the shape of a thermal field, and the abundance of migrating trace elements changes most rapidly in the thermal center, such as in metamorphic centers where higher grade metamorphism is taking place (Demin and Zolotarev, 1980). Ideally this would result in trace elements migrating from high to lower T fields in a nonuniform temperature area; and the higher the temperature, the more rapidly the element changes in abundance.

3.2 Reactivation of Trace Elements by Diffusion

Reactivation of trace elements is of concern in geochemistry and metallogeny. It is known that ore materials may have a relatively high transport rate in aqueous solutions, especially when associated with directed fluid flow, with respect to diffusion in bulk solids. The origin of ore materials and the basic factors that control the initial release of economic elements from source rocks, however, are less clear. There is evidence that reactivation of

trace elements plays a vital role in the release and early stage transport of many trace elements, and so contributes to the formation of an economic deposit.

An atom needs about 5×10^{13} seconds to penetrate an 1 cm thick bulk mineral with a typical diffusion coefficient of $10^{-14} cm^2 sec^{-1}$, under normal conditions. Even with a typical diffusion coefficient of $10^{-7} cm^2 sec^{-1}$, as in the case of an aqueous solution film, it still takes 5×10^6 seconds to cover the same distance. Such calculated results, however, do not mean that diffusion is unimportant in the migration of trace elements. It is diffusion that controls the migration of trace elements from within the host mineral to grain boundaries, and then to various microscopic fractures, which is called the reactivation of elements (early stage migration). By such a reactivation process, trace elements in rock-forming minerals of the source rock may gather into favorable sites (low rank "entrapment path"), where they can be easier to be picked by circulating fluids. This process will be enhanced by elevated temperatures.

The discussion above shows that the reactivation of elements by diffusion is an oriented mass migration on the microscopic scale. It makes trace elements in source rocks more accessible to later transport medium.

§4 Summary

The mineralization of many trace elements requires the migration of the trace elements in the source rock from their initial positions to favorable ore-hosting locations. During the migration process, the transport along visible fractures by circulating fluids is relatively rapid, with respect to the migration from the inner part of rock-forming minerals in the source rock to visible fractures, which is the bottleneck of the entire migration process from the source rock to ore sites. Over this short distance, diffusion prevails.

There are two general tendencies for impurity trace elements to migrate in a geological domain. The first is to migrate from solid cells to the weaknesses ("entrapment paths") of the geological domain. The hierarchical path begins with crystals, through intergranular surfaces and fissures, and finally joins large scale faults filled with aqueous solutions. The other tendency is from a high temperature field toward a lower temperature one. High temperature favors the realization of these two tendencies. Reactivation of trace elements by diffusion is

basically a kind of microscopic oriented mass transport occurring within a source rock.

The rocks of the Hetai area were subjected to a high temperature field during Caledonian period, and the Sinian sequence was metamorphosed. High metamorphic temperatures (550 - 670°C) then must have redistributed the gold and other trace elements in the strata, and even though part of these element may have migrated out of the medium-high grade metamorphic area, metamorphism is important in that it has reactivated much of them to grain boundaries and structural weaknesses, where these elements are more accessible during subsequent events.

Chapter V

DUCTILE SHEAR DEFORMATION AND HYDROTHERMAL ALTERATION RELATED TO ORE FORMATION

Almost all the gold deposits of the Hetai area occur in planar zones of highly altered and deformed rocks. These deformation zones and their associated alteration played a fundamental role in the formation of gold deposits. This is similar to many other epigenetic gold deposits over the world (Colvine et al., 1988; Phillips et al., 1987; Boulter et al., 1987). The following discussion describes the overall pattern of deformation and alteration related to the emplacement of the gold lodes.

§1 Deformation Zones

1.1 Geometry of Deformation Zones

1. Occurrence

The direct ore-controlling deformation system consists of ductile shear zones, striking NE, of varying width and length (c.f. Fig.1.5). In the field, they are observed to cut through various geological units, principally schists and migmatites. Many pre-deformation country rocks may be found as deformed equivalents within a single deformation zone. Typical examples of the deformation zones include the 11# ductile shear zone of the Gaocun ore deposit (Fig. 5.1a, b) and the ductile shear zones of the Dapingding ore deposit (Fig. 5.1c). They strike about N70°E, and dip to the north.
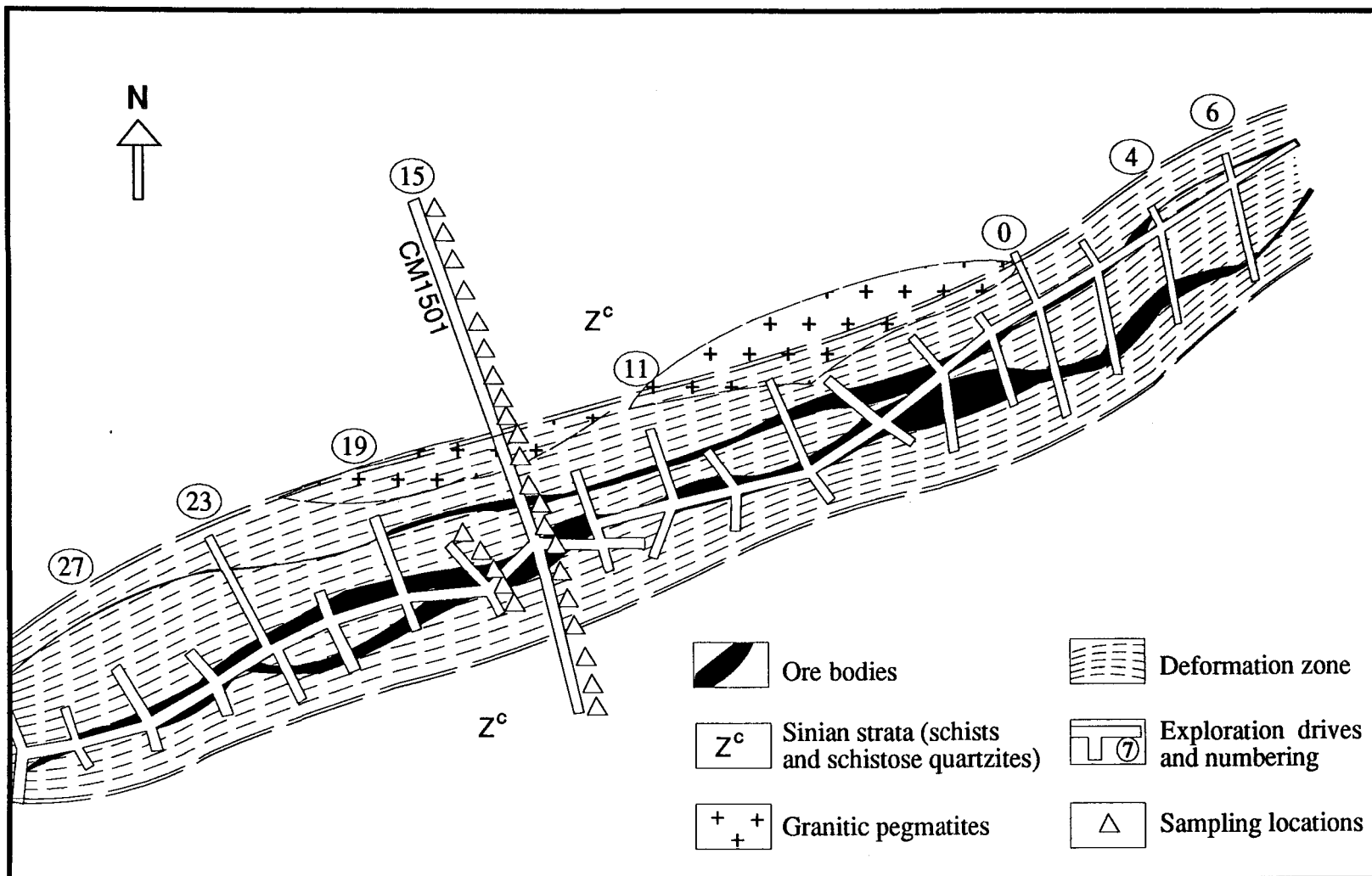
Figure 5.1(a) Geological map at the 240m level of Gaocun ore deposit in the Hetai gold field

The figure legend contains:
- Ore bodies
- Sinian strata (schists and schistose quartzites) — Z^c
- Granitic pegmatites
- Deformation zone
- Exploration drives and numbering
- Sampling locations
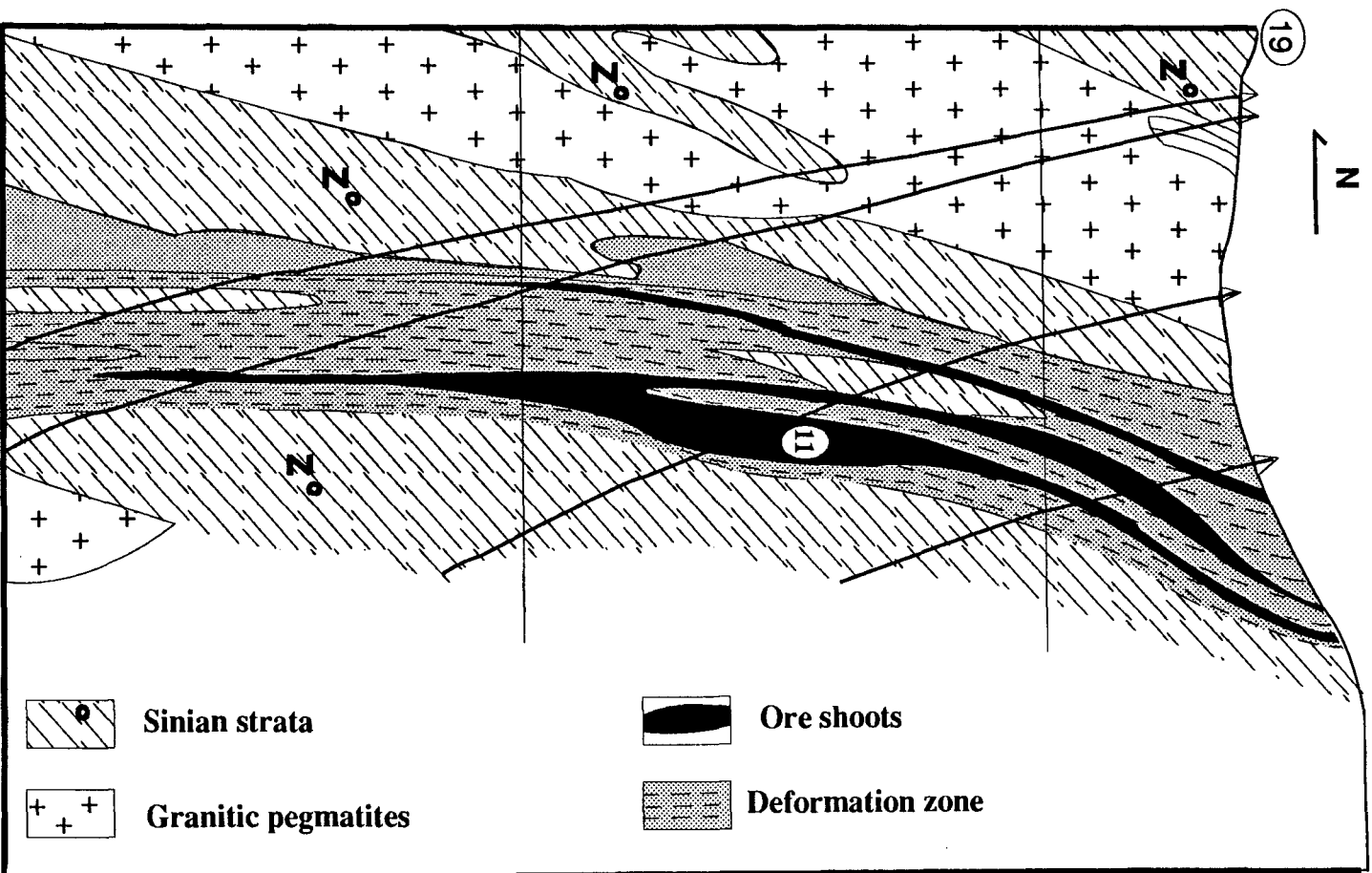
Figure 5.1(b) Vertical aross section (#19) of Gaocun ore deposit occurring in the Hetai gold field (after Ling (1988)

Sinian strata

Granitic pegmatites

Ore shoots

Deformation zone

N

200 m
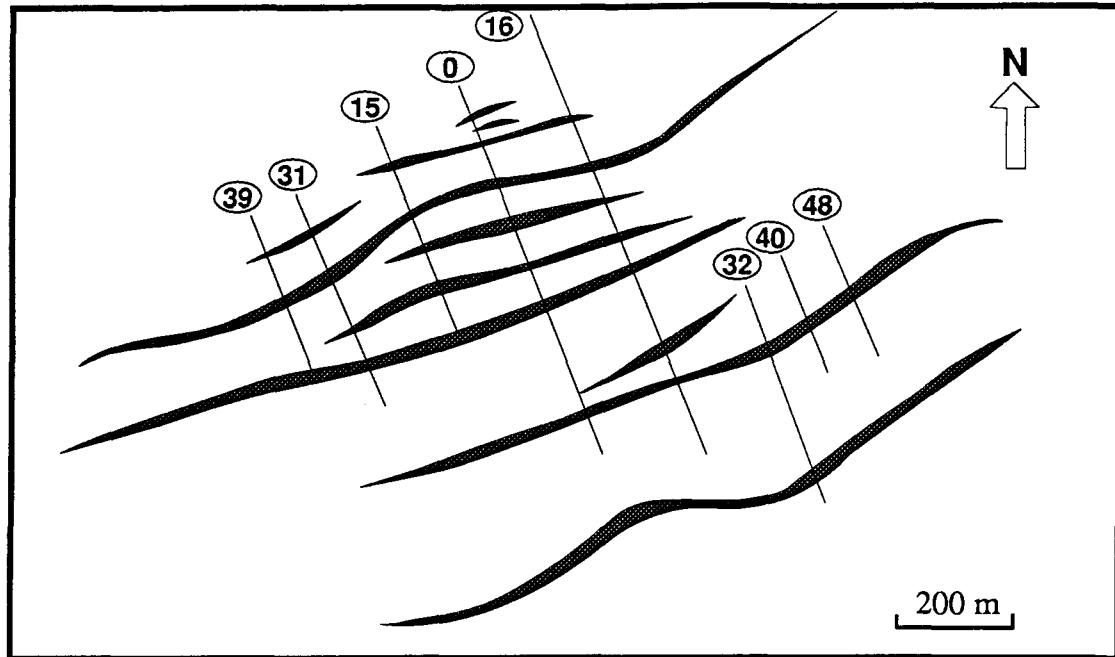
Figure 5.1(c) Occurrence of the ductile shear zones of Dapingding ore deposit of the Hetai gold field

The upper: surface map, and the lower: vertical section.
(after Xiao (1990))

SE

NW

+100m

+200m

+300m

Sinian strata (schists and migmatites)

$+ \gamma p$ granitic pegmatites

ductile shear zones
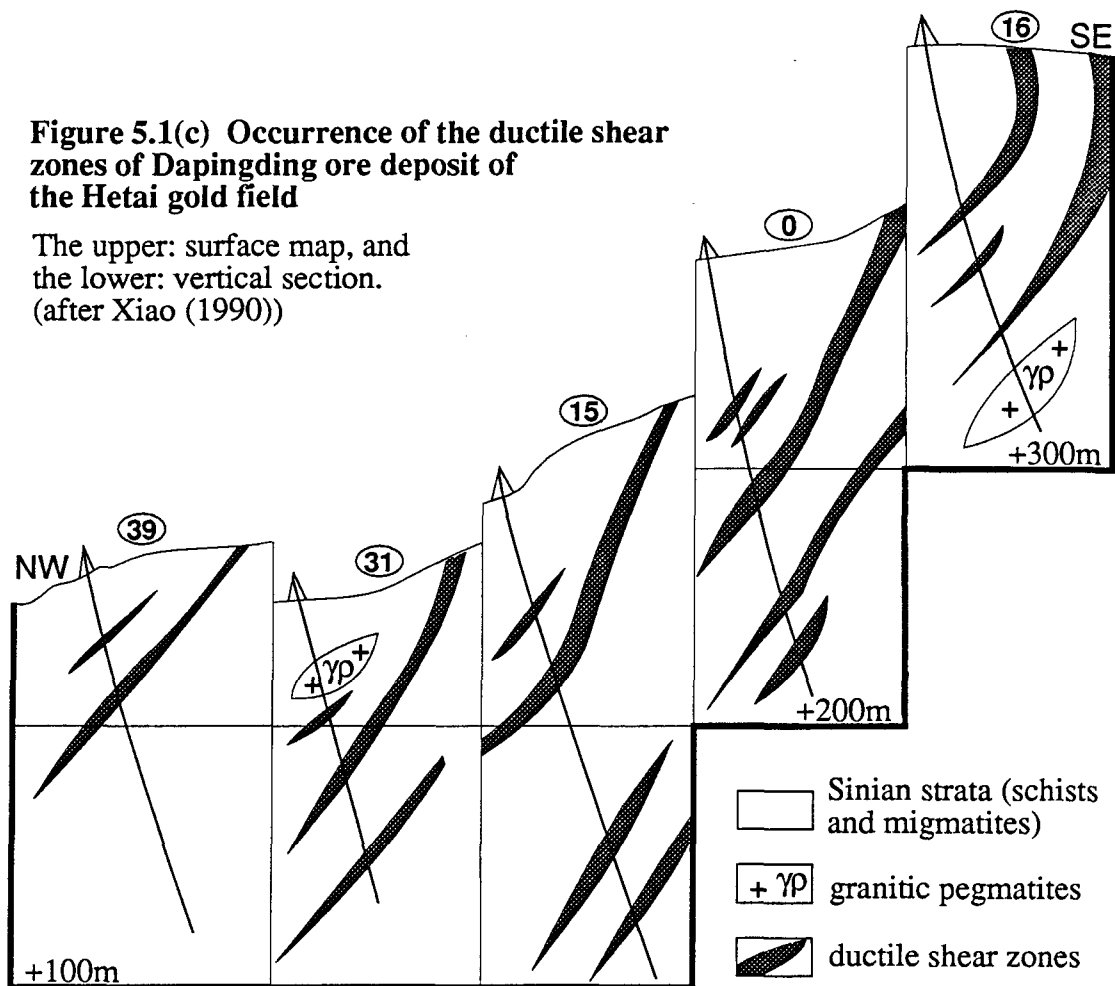
2. Planar Fabrics

Three planar fabrics of different morphology are recognized in the shear zones of the Hetai gold field (Fig. 5.2). According to conventional notation, they are annotated as S, C, and E. At the outcrop or hand specimen scale the S fabric is usually in sigmoidal shape, or subparallel in strike and dip to the ductile shear zone. It is pervasive, spaced on a millimeter scale, and affects most mineral grains. Weakly developed on the margins of the ductile shear zone, the S fabric intensifies toward the centers. There are variable amounts of platy minerals, such as fine-grained muscovite and chlorite, which generally show a strong alignment with the S foliation between the spaced cleavage domains.

The C and E fabrics are distinctively spaced, usually at centimeter intervals. The former is a set of closely spaced fractures whose orientation parallels the walls of the shear zone, while the E fabric is usually characterized by its occurrence in the intervening unstrained lithons in the deformation system, and by filling of thin (millimeter scale) quartz and carbonate veins and thin selvages of pyrite and muscovite. Some researchers (Boulter et al., 1987) considered them to postdate the S-fabric, but in the Hetai lodes, they seem to have formed at the same time as the S or slightly later but still in the same deformation event. Fabrics S, C, and E were derived from a unified stress field. The limited microfolding and kink-band of S is attributed to the formation of C, and develop in response to progressive deformation within the shear zone (Winsor, 1983; Platt, 1984).

3. Zonation

The degree of deformation varies across individual shear zones, becoming more and more intense from the margins toward to the center of the shear zone. Protoliths outside shear zones can often be traced into their mylonitized equivalent within the deformation zone. An ideal zonation of the Hetai shear zones is observed as below:

Zone D: *Protolith*

The protolith is mainly various metamorphic rocks.

Zone C: *Protomylonite*

This zone is composed of lozenge-shaped lithons and porphyroclasts of protolith
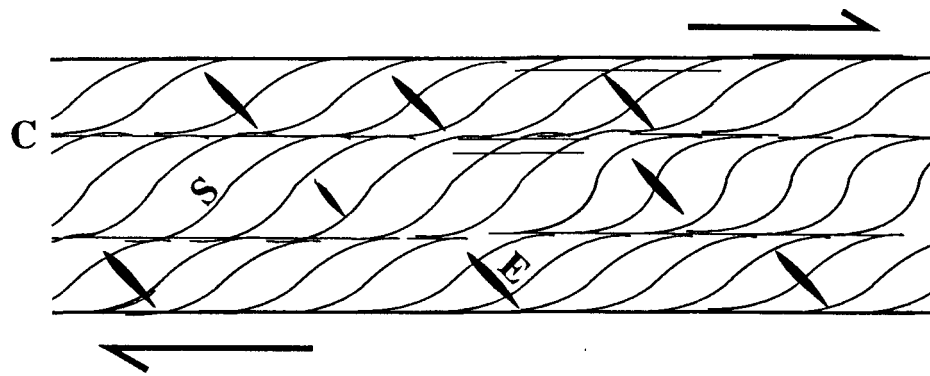
Figure 5.2 Schematic diagram showing the three main fabrics in the shear deformation zone of the Hetai gold field.

Fabrics C, S and E were the product of a unified stress field.
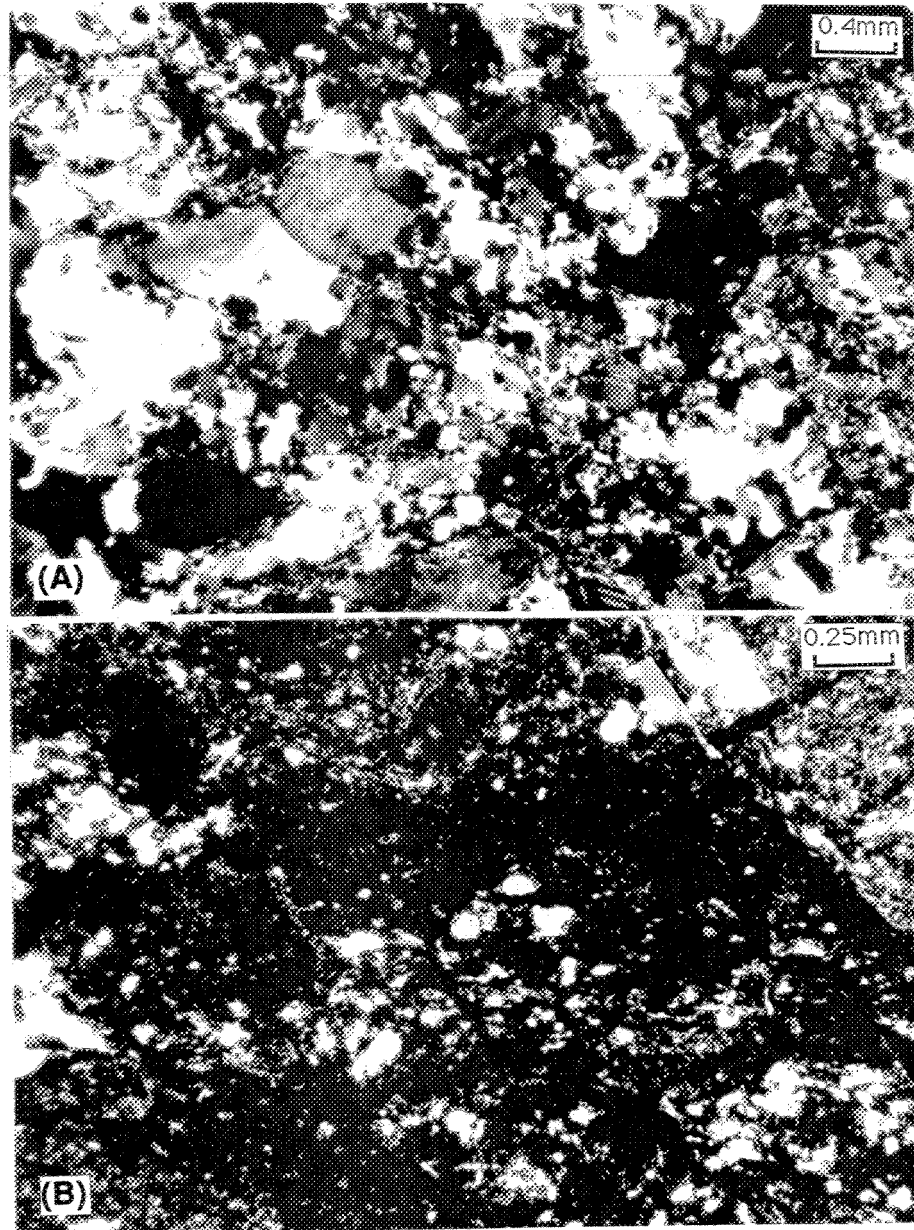
Plate 5.1 Textures of deformed rocks of the ductile shear zone in the Hetai gold field

(A) Protomylonite: Mortar texture, quartz grains are crushed. (B) Ultramylonite: Original competent quartz grains have been transformed into aggregates of small grains. Porphyroclasts and groundmass distribute in the form of bands. All in cross polarized light.
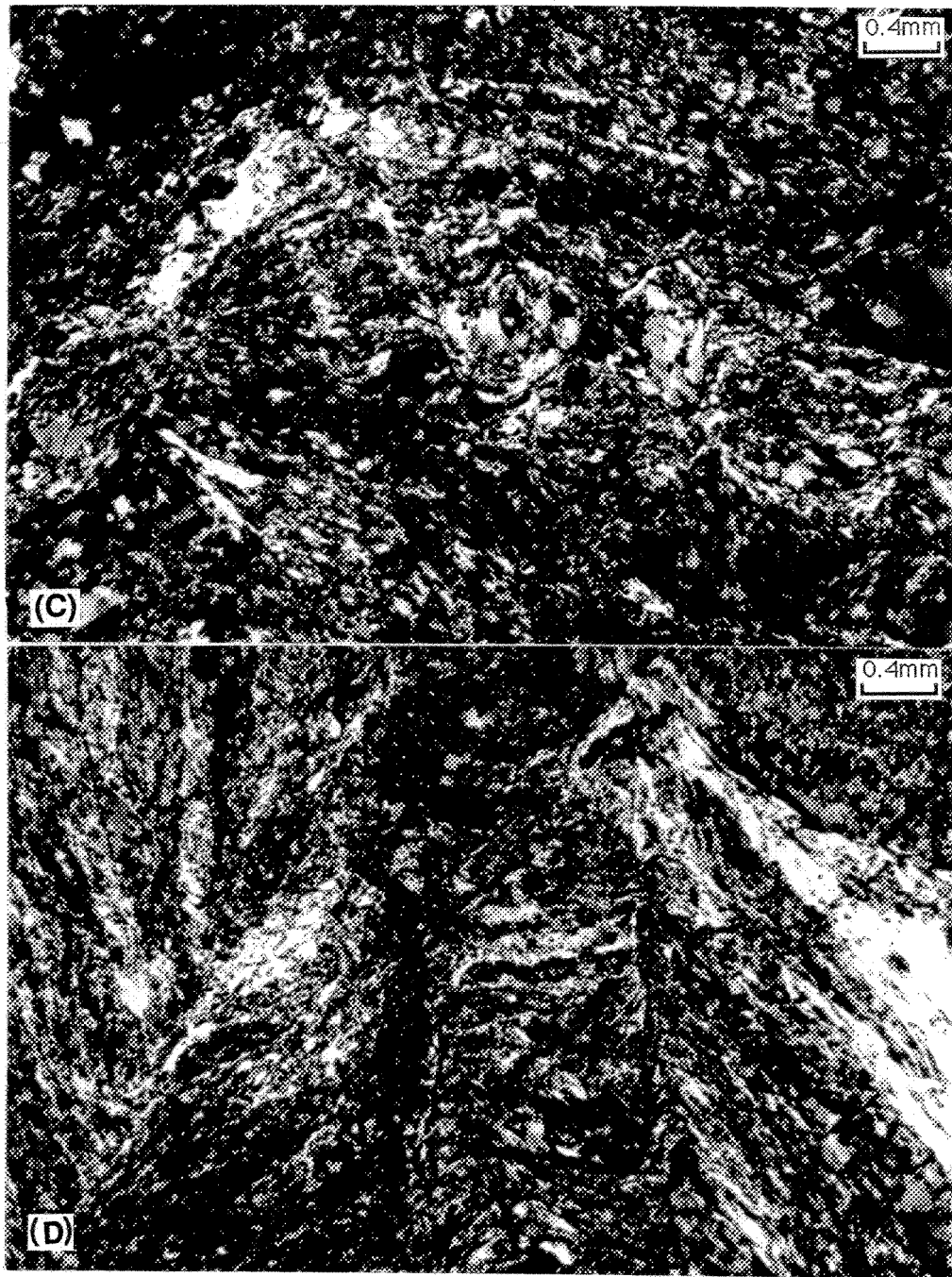
Plate 5.1 Textures of deformed rocks of the ductile shear zone in the Hetai gold field (continued)

(C) Mylonite: Crushed quartz grains and mica flakes are oriented. Certain crushed quartz porphyroclasts have been rotated. (D) Phyllonite: Complete foliation of flaky minerals, deformed by late kink bands. All in cross polarized light.

(Plate 5.1a). The old foliation is rotated progressively from its initial position, and a new schistosity appears and shows a fan from 30° to a few degrees from the shear plane. The new schistosity is weakly outlined by retrometamorphic muscovite and chlorite.

Zone B: Mylonite/phyllonite

This zone is characterized by intensely deformed rocks, characterized by dominant new pervasive cleavage and schistosity (Plate 5.1c, d). The matrix occupies more than 50 percent of the total volume of rock.

Zone A: Ultramylonite

It is localized in or near the center of a ductile shear zone. The schistosity is well developed and parallel to the shear plane. The porphyroclasts are badly crushed (Plate 5.1b).

An example of zoning was observed cross the 11# mylonite zone of the Gaocun deposit (Fig. 5.3).

Although ductile shear deformation is predominant, the deformation zones may locally contain structures indicative of brittle deformation. The brittle and ductile deformations are generally coeval, but are sometimes superimposed on each other, indicating that they may have taken place at different stages of deformation. In brittle deformation zones, non-foliated cataclasites, including breccia and gouges, instead of foliated mylonites, were developed. Between the shear zones, strain may be very weak to nonexistent. The lithons contain weak fabrics and relict wall rock textures.

1.2 Petrography of Deformed Rocks

Grain-scale processes must have operated during the formation of the shear zones. The resultant microtextures are described below.

1. Microscopic Textures

Protomylonite Zone:

Mineral grains show limited internal deformation. Undulose extinction in quartz, bent
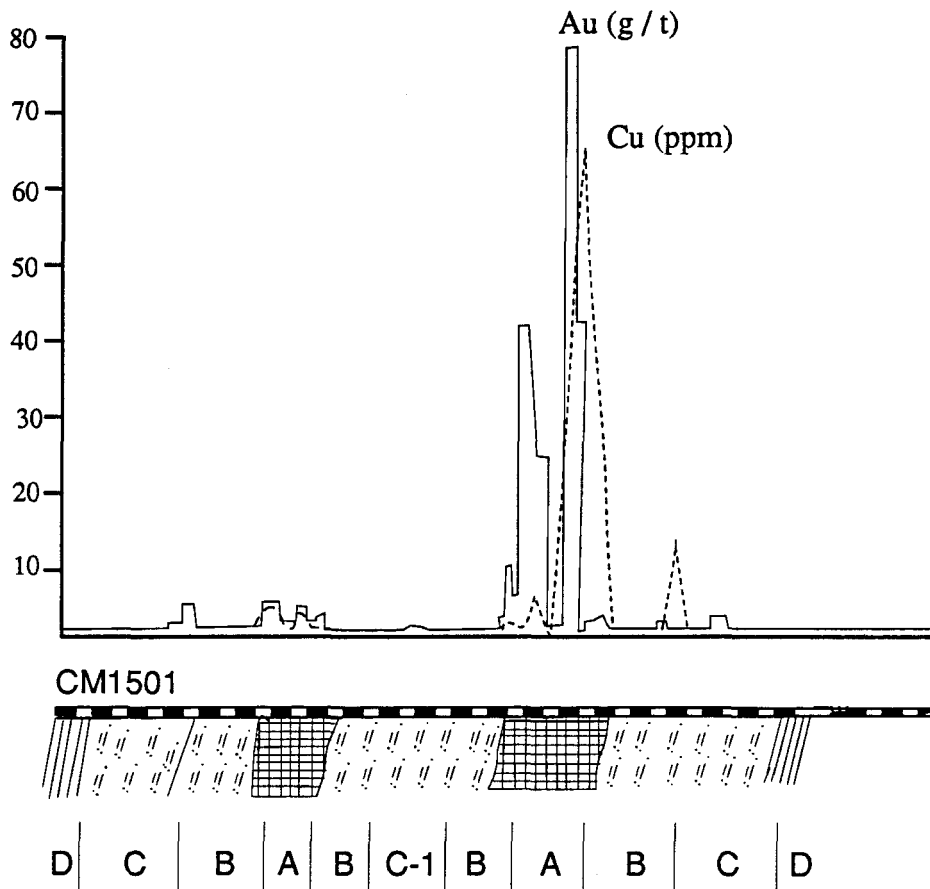
**Figure 5.3 Zonation of ductile shear deformed rocks cross the #11
ductile shear zone (along #15 section at level 240 m)**
(after No.719 Geol. Team, 1987)

(A), ultramylonite; (B), mylonite; (C), protomylonite; D) stands for the
undeformed rock; (C-1), less intensely deformed lithon. The abundance
of gold and copper related to the deformation zone are also shown.

feldspar twin lamellae and mica flakes are common. Mortar texture consists of sub-grains on the boundaries with low to medium disorientation. Recrystallized porphyroclastic mortar texture of plagioclase and quartz grains are also observed. Strings or festoons of zoned polygonal new grains (about 50 μm) occur along the margins of the old grains, which have fewer sub-grains. Sometimes they show a thin rim up to 50 μm thick, which has a continuous variation in extinction angle up to a few degrees.

Mylonite/phyllonite Zone:

A major component of the well developed S fabric is the spaced cleavage. There is nearly perfect alignment of individual mica flakes. Between neighboring flaky mineral cleavage seams (Boulter et al., 1987) are domains of less deformed microlithons. The boundary between these two elements is always discrete and abrupt, but mostly smooth. Within microlithons there is abundant evidence for local scale extension fissures both of a transgranular nature (veinlets) and of an intragranular style within or around individual grains. Minerals may precipitate to fill these fluid-filled extension fissures as veinlets, the width of which varies from a few tens of micrometers to more than 1 mm.

Intense porphyroclastic mortar texture of granular minerals is very common. The festoons of subgrains are often replaced by continuous multiple walls of polygonal new grains of larger size (>100 μm), which may form up to 20% by volume. Some new grains may show undulose extinction and sub-grain texture, suggesting that the deformation may have been periodic.

Ultramylonite Zone:

The porphyroclasts are characteristically small in size (<0.01 mm). Kink banks outlined by foliated minerals and rotation texture are frequently observed.

2. Strained Quartz

The strained quartz grains occurring in the deformed rocks are often characterized by the presence of undulose extinction and mortar texture. Extinction bands are formed by bending of the lattice in response to heterogeneous slip on (0001) (Vernon, 1976). Porphyroclastic mortar texture is the continuation of undulose extinction. The porphyroclasts are often coarse crushed (granulated) quartz grains, surrounded by a groundmass of smaller

grains. The porphyroclasts and groundmass are distributed along bands between the foliated flake mineral seams. A few porphyroclasts are observed to have rotated from their original position due to shear. Many original grains have been transformed into an aggregate of small grains or subgrains. Usually, the edges of grains deform more intensely than the center.

Recrystallization of strained quartz is also observed. The recrystallized grains are small and occur along the boundaries of deformed grains. Unrecrystallized cores of quartz grains have sutured boundaries and show smooth undulose extinction instead of sharp deformation bands. With increasing strain the original grains become flatter and more elongate. Recrystallization may be intergranular or intragranular. The intergranular recrystallization is apparent under the microscope, and the evidence of intragranular recrystallization comes from the observation of the occurrence of fluid inclusions in mineral grains. Under the microscope, secondary fluid inclusions occur along certain particular directions. These oriented trails of fluid inclusions mark original fractures that have been healed.

1.3 Timing

The ductile shear system controlling the emplacement of the Hetai gold deposits may have been developed during the Hercyno-Indosinian period. The shear deformation system is observed in the field to cut the early Hercyno-Indosinian Yunluogan granite, which has an age of 242 ±3.3 Ma (c.f. Ch.2). But the Wucun granite with an age of 210 ±69 Ma (c.f. Ch.2) is not deformed by this shear system.

There are numerous minor felsic pegmatite veins occurring in the mine area, which are genetically related to the Hercyno-Indosinian granites. Some of them are weakly to strongly deformed by the shear zone system, but typically behave more competently than their country rocks. They appear coeval with the deformation. An absolute age of 224 Ma was obtained in an albite pegmatite at the Gaocun ore deposit (zircon U-Pb; Chen et al., 1988), which indicates the middle to late Hercyno-Indosinian period.

The deformation of the Hetai ductile shear zone appears to be episodic over the Hercyno-Indosinian period. The grains of quartz, and euhedral pyrite which are attributed to the early generation of the syndeformational alteration are observed to have been strained,

and fractures in these early pyrite and quartz are filled with, or cemented by pyrite and chalcopyrite of late generations.

The occurrence of dilational sites (veins) in microlithons and mesolithons favors a episodic deformation history. Some dilational veins have been cut obliquely and segmented by late cleavages, suggesting that deformation continued for a long time. Although some fractures have healed, they can still be recognized by the occurrence of oriented fluid inclusions.

§2 Hydrothermal Wall-Rock Alteration

Hydrothermal wall-rock alteration is the product of interaction of the wall rock with hydrothermal fluids, irrespective of the composition and source of the hydrothermal fluids. It results in partial to complete mineral breakdown of the wall rock, often accompanied by an addition or removal of chemical components.

2.1 Types and Characteristics

The alterations developed in the deformation zones and the surrounding wall rocks of the Hetai gold deposits include the following major types, based on the characteristic alteration minerals:

Sericitization:

Sericitization is widely superimposed on the Caledonian regional metamorphic rocks. The principal products are fine-grained muscovite, albite and quartz. Sericitization may have been developed directly by the hydration of silicates. The principal wall rock is the Caledonian schists and migmatites in the Hetai gold field. When the hydrothermal fluid passed through these medium to high grade metamorphic rocks, the original plagioclase, biotite and primary muscovite were attacked. During this process, H_2O and K were introduced, and Fe and Ca removed. The constituents of the newly formed minerals were mainly derived from the decomposition of feldspar. In contrast to many other types of alteration, sericitization may result in leaching of trace elements from wall rocks.

Below are the reactions possible responsible for the formation of the mineral assemblage of sericitization (Piroscho and Hodgson, 1988).

Hydrolysis of alkali feldspar:

$(K,Na)AlSi_3O_8 + H^+ = KAl_3Si_3O_{10}(OH)_2(nH_2O) + NaAlSi_3O_8 + SiO_2 + Na^+$
Alkali feldspar   Muscovite   Albite   Quartz
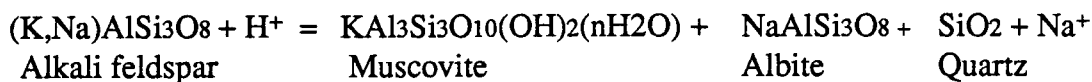
Breakdown of plagioclase:

$(Ca,Na)Al_2Si_2O_8 + CO_2 + H_2O = Ca_2Al_3Si_3O_{12}(OH) + NaAlSi_3O_8 + O_2$
Plagioclase   Epidote   Albite
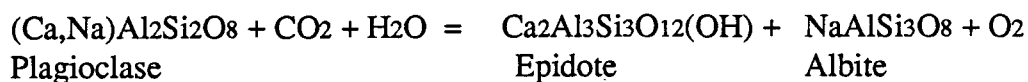
Chloritization:

Chloritization is another common hydrothermal alteration occurring in the Hetai gold field, and is characterized by the formation of chlorite, which developed directly by the hydration of biotite and other mafic silicates. A representative reaction is (Neall and Phillips, 1987):

$KAlFe_3Si_3O_{10}(OH)_2 + H^+ + O_2 = Fe_5Al_2Si_3O_{10}(OH)_8 + SiO_2 + Fe_3O_4 + K^+$
Biotite   Chlorite
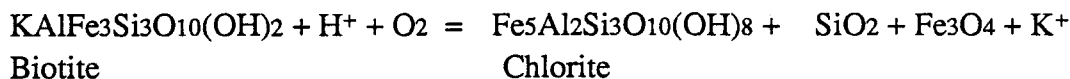
Silicification:

Silicification usually occurs in the inner zone of hydrothermally altered shear zones, with chloritization and sericitization forming the outer envelope (Fig. 5.4). It is spatially associated with intensely deformed rocks and ores, and mainly consists of the development of secondary quartz in the wall rock, either in quartz veining or in flooding, giving rocks a cherty appearance.

Sulfidation:

Similar to silification, sulfidation occurs in the inner zone of altered zones. The principal products are pyrite, chalcopyrite and pyrrhotite, disseminated within the deformed host rocks. Pyrite may be coarse euhedral grains or anhedral fine-grains (<2 mm) along with ankerite, quartz and albite; and is progressively more and more abundant toward the center (<5%) of auriferous shear deformation zones. Chalcopyrite is commonly anhedral fine-
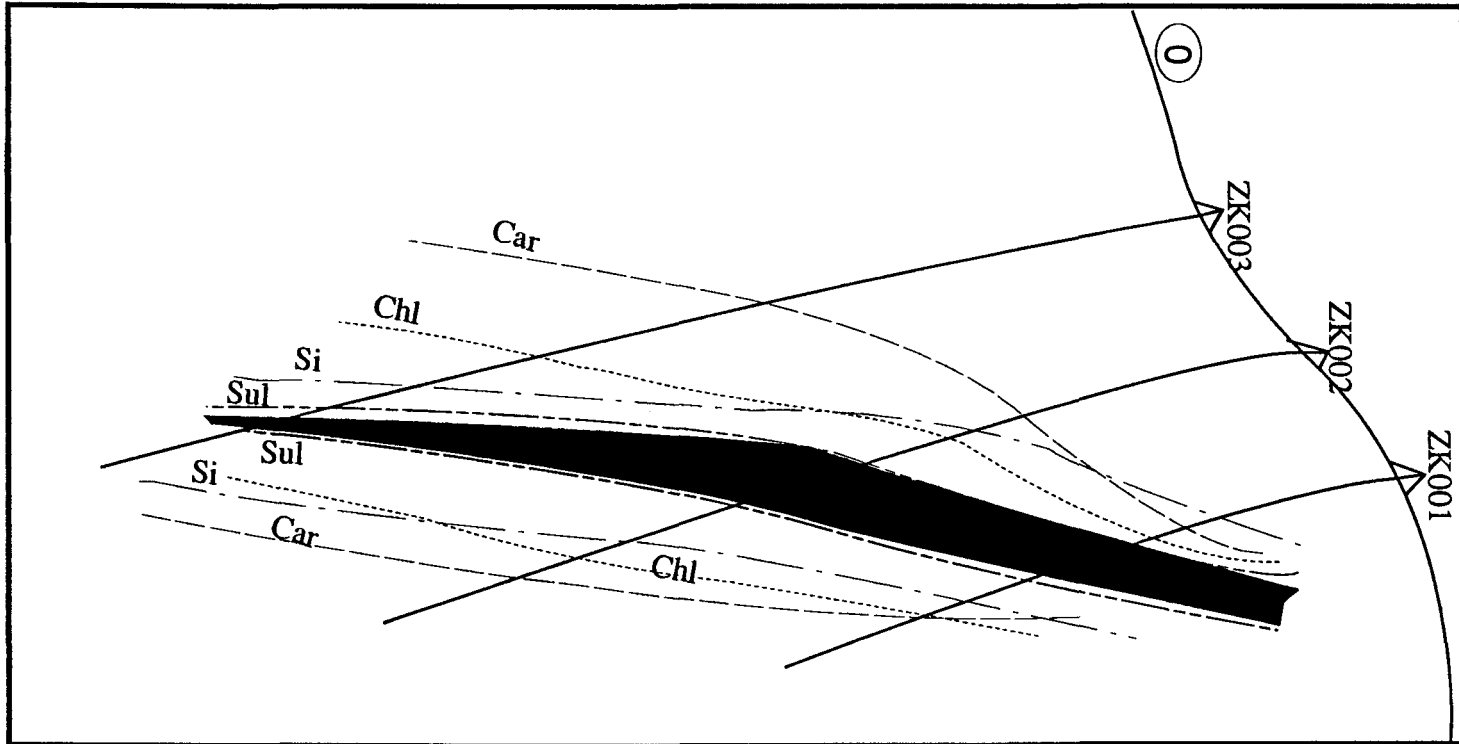
Figure 5.4 Zonation of alteration along the #0 section of the Gaocun ore deposit
(recovered through three exploration drill holes)

Sul — sulfidation line; Si — silicification line; Chl — chloritization line; Car — carbonatization line.
The shadowed area is the ore body (after Dai, 1986; Geol. TEam No.719, 1987)

grained, and is also more abundant in the center of hydrothermal altered shear zones as pyrite. Pyrrhotite forms irregular grain aggregates and rounded grains that are spatially associated with pyrite. Pyrrhotite is sometimes observed to replace pyrite along fractures and grain margins in some samples.

Carbonatization:

Carbonatization is characterized by its extensive distribution on both regional and mine scales in the Hetai area. The main product is ankerite ($CaFe(CO_3)_2$) and calcite. It is difficult to distinguish between ankerite and calcite under the conventional microscope. The carbonates seem to be the result of the introduction of CO_2 with the other constituents, Ca and Fe, coming from the host rock.

2.2 Gold Emplacement as an Integral Part of Alteration

1. Ores

The ores are principally auriferous hydrothermally altered mylonites, with minor auriferous quartz veins. The ores of the auriferous mylonite type are texturally similar to normal mylonites, but they have been overprinted by intense hydrothermal alteration. The intense ubiquitous silicification often gives the ore a cherty appearance. The ores of this type commonly contain disseminated pyrite and chalcopyrite (up to 7%). There is no sharp boundary between the ore and country rock.

The ores of the less abundant auriferous quartz vein type were formed by filling of milky quartz along dilational fractures, with little sulfides. They are observed in the #51 quartz vein of the Hehai ore deposit.

2. Ore Minerals

The main auriferous minerals consist of native gold, chalcopyrite, and pyrite. In some cases, quartz also carries certain amounts of gold.

Native gold, the most important economic mineral, commonly occurs in very small grains, most being smaller than 0.05 mm in diameter, with the shape of droplets or irregular tree branches. It is frequently scattered in the ores as inclusions or interstitial constituents of

quartz and sulfide minerals. The fineness of gold is usually greater than 950 (No.719 Geol. Team, 1987). The gold tenor of ores correlates positively to the amount of contained sulfides.

3. Main Period of Gold Mineralization

As indicated above, the ores of the Hetai gold deposits are essentially hydrothermally altered rocks. The major auriferous minerals were deposited in association with hydrothermal alteration, and are disseminated in altered deformed rocks. This indicates that the final emplacement of gold was closely associated with the hydrothermal alteration system. Therefore, it seems appropriate to refer the gold emplacement associated with the hydrothermal alteration as the main period of gold mineralization in the Hetai gold field.

2.3 Temporal Sequence of Hydrothermal Alteration

1. Quartz

Three distinct groups of quartz are identified in the Hetai ores, corresponding to three evolution stages.

Pre-deformational quartz: This group of quartz is full of small fluid inclusions, and has a dirty appearance under the microscope. It displays undulose extinction, porphyroclastic mortar texture and recrystallization features. Recrystallization appears around the borders of crushed quartz grains.

Early stage hydrothermal quartz: The quartz of this stage usually has a cleaner appearance. It occurs both in veinlets and in granular aggregates. The veinlets and the granular quartz within it are cut by later fractures and sulfide-bearing veinlets. Strain textures are observed, but are not as well developed as those of the pre-deformational quartz. Secondary fluid inclusions are common within the quartz grains, and are distributed along healed fractures. The group of quartz formed during the early stage of ductile shear deformation, representing the prelude to the main period of gold mineralization.

Late stage sulfide-associated hydrothermal quartz: Quartz of this stage is characteristically associated with various sulfides. It may be further subdivided into two substages. The first is linked to coarse-grained euhedral pyrite, and the second to fine-grained
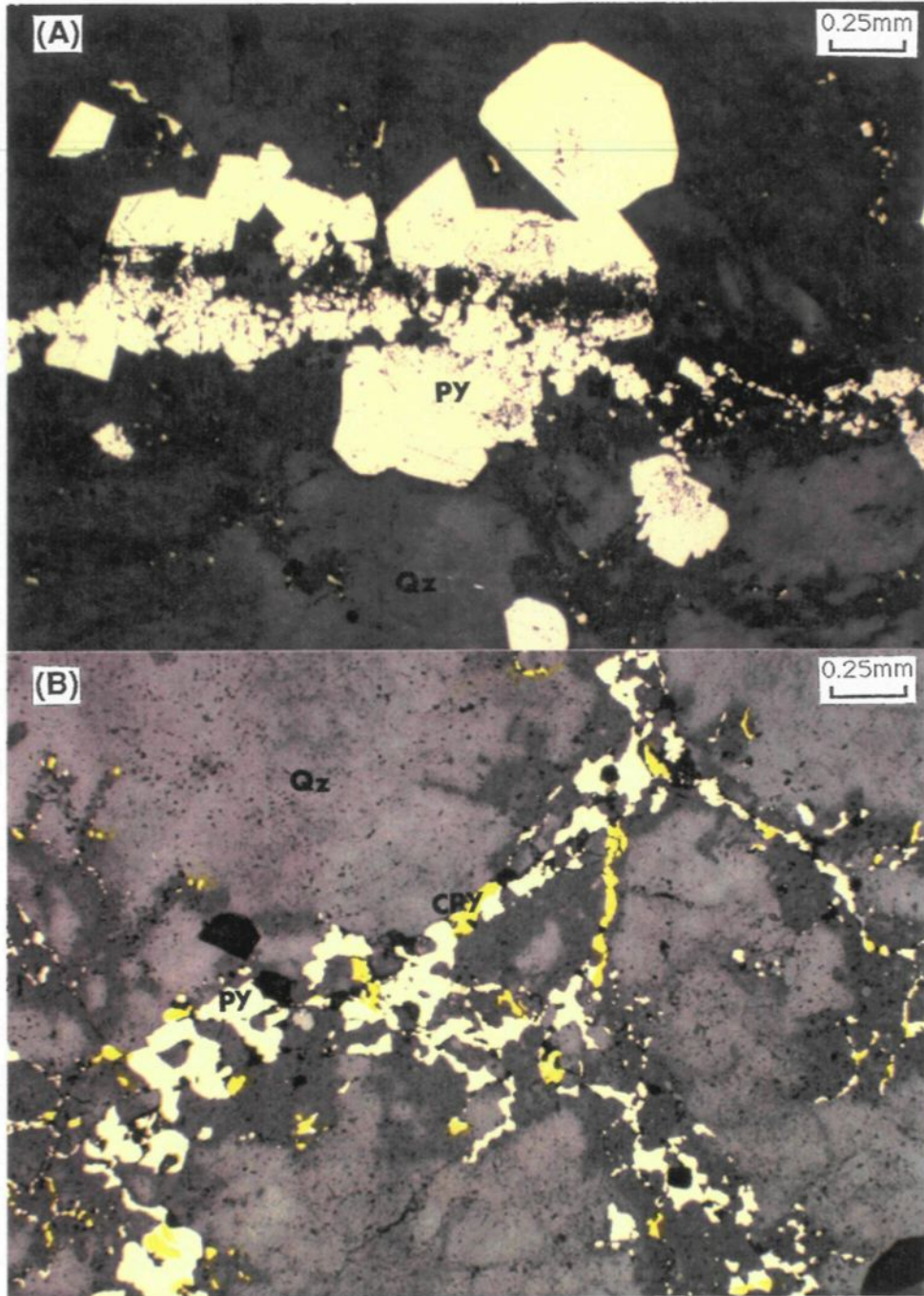
Plate 5.2 Characteristic minerals of alteration in the Hetai gold field

(A) First generation of pyrite (Py) in euhedral coarse grains. Fractured by late deformation. The gray background is quartz (Qz). (B) Second generation of pyrite and chalcopyrite (CPy) in anhedral and fine grained aggregate. Disseminated in the ore rock.

anhedral pyrite as well as chalcopyrite aggregates. Fluid inclusions in this group of quartz may be either primary or secondary.

2. Sulfides

Two generations of sulfide minerals are recognized by their occurrence and the microscopic cross-cutting relationships with each other (Plate 5.2).

The *first generation* consists of pyrite and pyrrhotite. The pyrite of this generation is usually coarse-grained, with the average diameters of about 0.13 mm, and displays good crystal shape. It occurs either as isolated grains or along the fractures and boundaries of the mineral grains of the protolith and the first two stages of quartz just described above. Some of the euhedral pyrite crystals are fractured and brecciated. The fractures which cut through these crystals and the associated breccia fragments are cemented by the second generation of pyrite and chalcopyrite and associated quartz. These indicate that this generation of sulfides was formed relatively early, but after the early stage hydrothermal quartz.

The *second generation* of sulfides is characterized by disseminated fine-grained, anhedral pyrite and chalcopyrite, with no signature of deformation. Chalcopyrite is locally abundant (up to 1%), most intergrown with tiny (<0.1 mm) irregular pyrite grains. The sulfides of this generation probably deposited late in the hydrothermal history. The ores with this generation of sulfides tend to have a high gold tenor.

Pyrite is occasionally observed to be replaced by ankerite at grain edges, and groups of pyrite blebs occur in poikiloblastic ankerite where the latter is abundant. However, convincing replacement textures between pyrite, chlorite and sericite are absent, although pyrite may be surrounded by chlorite and sericite. Such ambiguous relationships between pyrite and other minerals indicate probable fluctuation of the ore-forming physiochemical conditions during gold precipitation.

3. Ankerite and Calcite

Ankerite and calcite are observed to be associated with sulfides in some samples, but more frequently they occur in veinlets and cut through sulfides; and thus appear post-deformational.

4. Position of Gold in Alteration Sequence

There are three stages to the main period of gold mineralization, corresponding to the subdivision of hydrothermal alteration: (1) quartz , (2) quartz + pyrite [I], and (3) quartz + pyrite [II] + chalcopyrite. Although gold was precipitated throughout the entire the hydrothermal wall-rock alteration process, as indicated by the fact that most altered deformed rocks contain higher gold than unaltered ones, the precipitation of gold may have been episodic. The fact that the gold content of the ore correlates directly with the sulfide content, and that the richest ores are those that contain chalcopyrite and fine-grained anhedral pyrite suggest that quartz + pyrite [I] and quartz + pyrite [II] + chalcopyrite represent two pulses of gold emplacement, and the precipitation of gold culminated during the deposition of the second generation of sulfides.

§3 Relations between Deformation and Hydrothermal Alteration

3.1 Spatial and Temporal Relationships

Hydrothermal alteration is spatially associated with the ductile shear system, which can be best shown by the consistency of the zonation of alteration and deformation. There is a general visible pattern, i.e., the inner zone of alteration, which is characterized by the presence of auriferous sulfides, is mainly restricted to the narrow central mylonite zone, while a wider pervasive sericite and chlorite envelope, characterized by only slight chemical modification of the wall-rock, occurs in the protomylonite zone (Figures 5.4 - 5.6). The ore bodies consist mainly of sulfides, and are located in the innermost zone of alteration.

Hydrothermal alteration is also temporally associated with the deformation. Fracturing and infilling of the hydrothermal quartz and pyrite of early generations, and the presence of healed microfractures outlined by the distribution of fluid inclusions argues for an essentially syn-deformational hydrothermal alteration event. The deformation of hydrothermal quartz and pyrite grains occurred in response to late stage deformation.
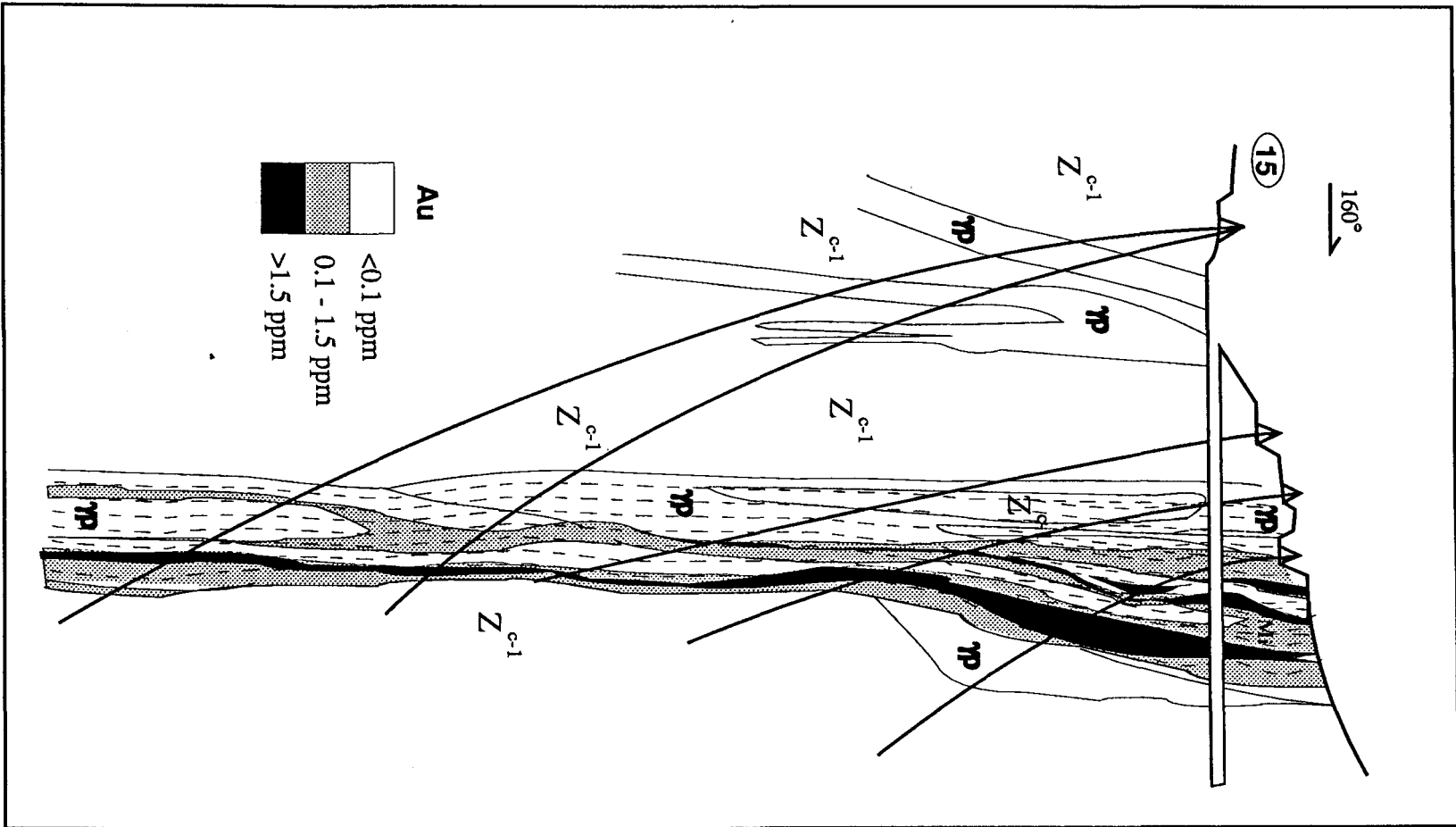
Figure 5.5 Variation of gold grade along the #15 section of the Gaocun deposit
(After No. 719 Geol. Team, 1987)

| Z | Sinian strata | γρ | Felsic pegmatites | ⁻⁻⁻ | Mylonite zone and the foliation direction |
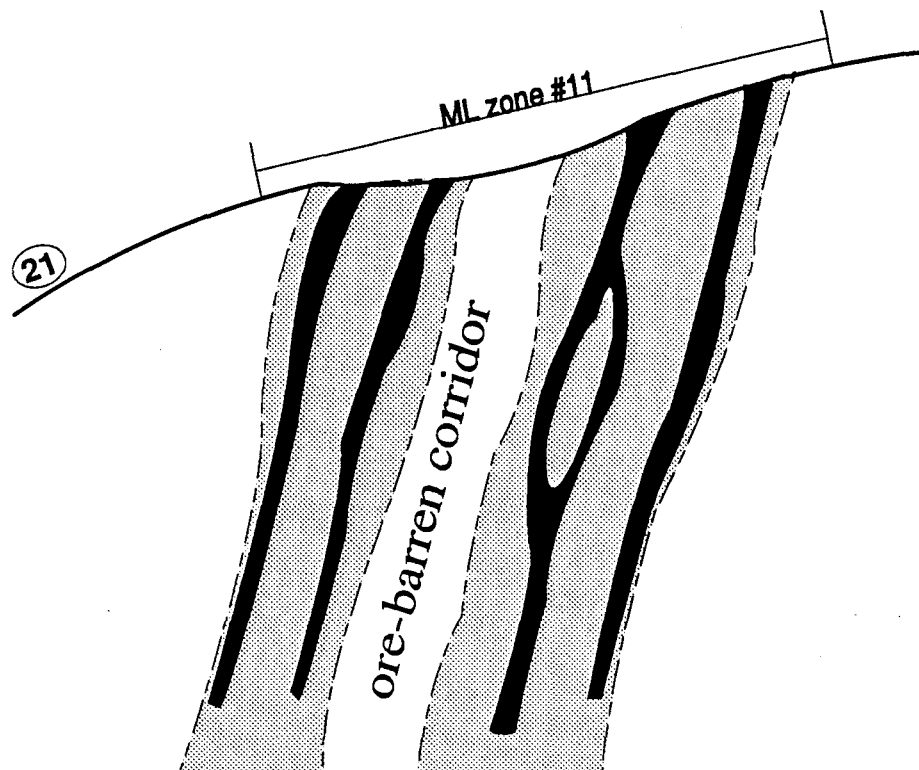
**Figure 5.6 Ore-barren corridor structure showing the basic consistency
between deformation zones and alteration zones**

(Observed at a vertical section across the #11 mylonite zone)

The black shadowed areas are intense sulfidation zones (ore bodies), spatially
associated with intensely deformed rock zones. The gray shadowed areas are
zones of lower sulfidation (very low grade of ores) and less intensely
deformed. A weakly deformed lithon occurs between two intensely deformed
zones. There is basically no sulfides in the lithon. It is a typical ore-barren
corridor.

3.2 Control Mechanism of Alteration by Deformation

Hydrothermal alteration depends on the access of hydrothermal solutions to the wall rock, which is largely controlled by deformation. Deformed zones may provide channelways for hydrothermal solution to reach eventual depositional sites.

Simple flow and infiltration are two most common migration ways of a fluid in geological domains. But in the Hetai gold field, the syn-deformational crack-seal mechanism (Ramsay, 1980; Etheridge et al., 1984) may also have operated, which is suggested by the oriented distribution of secondary fluid inclusions and the presence of abundant healed fractures.

It should be pointed out that although macroscopic to mesoscopic scale dilational quartz veins occur in the Hehai ore deposit, which is a quartz-reef type of lode, discrete macro-to mesoscopic dilational sites are not necessarily a requirement for gold deposition in the Hetai gold field. Deformation within a ductile shear zone can both enhance permeability and provide a driving force for flow of hydrothermal solutions through the deformed rocks.

§4 Geochemical Behavior of elements in Alteration Zones

4.1 Invariant of Mass Change

Element exchange in the process of hydrothermal alteration is problematic, because of the so-called constant sum constraint that no single component is independent of the others (Chayes, 1971; Aitchison; 1981). In any given suite of rocks representing various stages of alteration, the nominal abundance of an element may change in three ways or a combination of the three: by real gains or losses if mobile, by dilution during additions of other components, or by concentration via leaching of other soluble components (Kerrich, 1983).

Various attempts have been made to resolve this problem. Equations involving major oxide data and densities (specific gravities) were formulated by Gresens (1967) to estimate volume and mass changes during alteration. These equations contain two dependent variables (mass change and volume change) with no independent means to determine one of them for general elements.

There are two solutions to Gresens' equations. One is by fixing mass as done by Gresens (1967) and Grant (1986). It was pointed out (Gresens, 1967) that comparison could be made on a quantitative basis with the tacit assumption of constant mass. Gresens' equation may be rearranged to calculate an equal chemical composition line or an "isocon" (Grant, 1986; Kuhns, 1986). Values derived from the chemical analysis of correlated pairs of unaltered and altered rocks are plotted against each other. The isocon line is a line of equal concentration of immobile elements, with slope = 1 assuming constant mass.

The other solution appeals to an isochemical system (MacLean, 1990; Kerrich, 1983). This method is based on the assumption that elements with high degrees of immobility are, since they do not exchange matter with the exterior, conserved in absolute abundance in a hydrothermal alteration system, although they can be nominally diluted by net mass gain of other components, or concentrated in a net mass loss case, due to the constant sum constraint. However, a rigorous calculation of chemical mass balance requires the precursor (unaltered parent rock) to be homogeneous in composition or continuous and predictable, as in an igneous fractionation series. For cases where the altered rocks range widely and irregularly in composition, the problem of measuring mass and chemical changes is considered insolvable (MacLean, 1990).

The assumption that hydrothermal alteration occurs under the condition of constant volume does not hold in the Hetai gold field, since the deposits are essentially a composite of three geological actions — ductile shear deformation, alteration and mineralization, all involved in volume change. Thus it seems necessary to appeal to the isochemical approach. However, the unaltered precursor is so heterogeneous that there is no simple way to determine which individual unaltered rock is responsible for the altered counterpart. Fortunately, the altered zone crosses all possible types of parent rocks, and each type has been sampled and analyzed, so it appears logical to apply the concept of average, i.e., take the ratio of immobile elements of the average of altered rocks to the average of unaltered rocks as a measure to determine the degree of mass change.

For any mass transformation of parent rock to altered product, the mass factor (f_m) may be calculated which corresponds to the isochemical behavior of immobile elements (Kerrich, 1983). According to the notation used by Gresens (1967), $f_m = 1$ signifies constant-mass alteration of reactants to products; $f_m = 1:0.85$ and $f_m = 1:1.5$ correspond to $(1/0.85 - 1)\%$ mass

increase and 50% mass reduction, respectively.

Several criteria have been established to identify whether an element is immobile. One of these criteria is to the constancy of the ratio of non-covarying elements. If immobile, the non-covarying elements will maintain a constant ratio to one another both at the parent rock and at all stages of hydrothermal alteration, irrespective of the change of nominal abundances. It is known that TiO_2, Al_2O_3, Sc, Hf and Zr are usually relatively immobile during alteration (Kuhns, 1986; MacLean, 1990; Kerrich, 1983). This provides a rational basis (reference point) for estimating the volume change of the reaction as a whole.

In the discussion below, TiO_2 is selected as immobile, and so conserved, i.e., the TiO_2-normalized ratio may be used as an indicator of gain or loss of other elements during alteration. The TiO_2-normalized ratio is defined as following:

fm (x) = AA (x) / UA (x)

TiO_2-normalized ratio $=$ fm (x) / fm (TiO_2)

Where x represents an element, while AA (x), UA (x) are the average abundance of element x in altered and unaltered rocks respectively; fm (x), the mass factor of element x.

Elements with TiO_2-normalized ratio less than 1 represent leaching, whereas those with higher than unity represent enrichment or addition. As shown in Table 5.1, the average abundance of TiO_2 is 0.49 and 0.45 for the unaltered and altered rocks, respectively, indicating a AA/UA ratio of 0.92. This suggests that the mass has increased about 8% on the average from the unaltered parent rock to the altered rock in the altered zone of the Hetai gold field as a whole. Such a mass gain is the result of a budget (not including H_2O) of hydrothermal alteration. That is, some components have been introduced; and the others, leached or nearly unchanged.

For the sake of convenience in discussing the evolution of chemical components during alteration, two artificial altered rocks are defined here. The first is referred as the total (average) altered rock, which is the average of all altered rocks, both weakly and intensely altered. The second is referred as the intensely altered rock, only averaging those altered rocks that are characterized by the presence of significant amounts of sulfides and the associated hydrothermal quartz. Thus the ore represents a high intensity (maturation) of alteration, and

the difference between the ore and average altered rock may be used as a measure of the change from general alteration to intense alteration.

4.2 Major Elements

The chemical compositions of altered rocks, and the changes of chemical compositions from the unaltered rock, through the average altered rock, to the intensely altered rock are tabulated in Table 5.1 and illustrated in Figure 5.7. The mass factor of TiO_2 is 1:0.92 for the average altered rock, and reaches its maximum at the intensely altered rock where f_m (TiO_2) = 1:0.84. The important chemical mass transfers are described as follow.

The gain of SiO_2 during the alteration is quite apparent, and the nearer to the ore bodies, the more the gain, as indicated by a higher TiO_2-normalized AA/UA ratio for the intensely altered rock than for the total altered rock (1.38 versus 1.11). Such addition is consistent with that silicification occurred throughout the entire hydrothermal alteration process, and quartz precipitated from the hydrothermal solution during silicification.

K_2O is another component which gains on the total average. Unlike from SiO_2, however, its TiO_2-normalized AA/UA ratio changes from >1 for the average altered rock to <1 for the intensely altered rock, suggesting that K_2O was first added and fixed through the pervasive sericitization of the early stage of alteration, and then removed during late stages of intense alteration, being mainly sulfidation and the associated silicification.

CaO, Na_2O and MgO have a TiO_2-normalized AA/UA ratio less than unity for the average altered rock, and still lower for the intensely altered rock. This indicates that these elements were depleted over the entire range of hydrothermal alteration. It is possible that CaO was leached at first and then reprecipitated during carbonatization, but the budget indicates a loss on the average.

The component Al_2O_3 is approximately at unity for the average altered rock, i.e., it does not exhibit any large departures from the background abundance. However, alumina is severely depleted in the ores, indicating that Al_2O_3 has been diluted or removed during the late intense alteration.

MnO has a similar pattern of K_2O, and therefore probably a similar explanation. It

Table 5.1 Chemical compositons of the altered rocks in the Hetai area

Sample	SiO2	TiO2	Al2O3	Fe2O3	FeO	MnO	MgO	CaO	Na2O	K2O	P2O5
G-10	71.52	0.63	13.66	1.09	3.56	0.06	1.9	0.5	1.62	3.84	0.13
G-11	67.18	0.42	14.98	1.07	2.17	0.03	1.1	0.4	0.59	9.50	0.16
CM17-3	83.17	0.35	8.37	0.93	1.53	0.04	0.8	0.4	1.53	2.10	0.16
GZ-31	64.79	0.49	17.63	1.27	3.42	0.03	2.6	0.6	0.17	4.68	0.14
GZ-31-1	68.75	0.41	13.88	1.27	2.30	0.05	1.7	1.2	0.51	7.10	0.15
GZ-34A	71.67	0.65	13.00	1.16	3.57	0.05	2.2	0.4	0.36	3.48	0.27
GZ-34B	73.95	0.11	14.32	0.51	0.68	0.02	0.6	0.5	2.54	4.08	0.22
SK-s	69.83	0.55	14.28	1.64	2.44	0.07	2.10	0.9	0.54	4.36	0.20
CM1501-5*	69.86	0.60	14.49	0.83	3.42	0.04	2.05	0.37	0.38	4.57	0.07
ZK002-40*	72.19	0.22	13.61	0.68	1.67	0.05	0.80	1.05	1.54	4.97	0.08
CM1701-1*	84.85	0.17	3.32	1.96	2.85	0.08	1.37	0.30	0.02	0.10	0.06
CM1501-9*	67.10	0.48	14.67	1.02	3.37	0.05	1.61	0.41	0.64	8.07	0.06
ZK3201-H4*	75.42	0.05	10.01	4.57	1.29	0.10	0.64	0.36	0.43	3.00	0.00
Zk1603-H20*	69.15	0.13	13.18	2.40	4.48	0.13	0.68	0.95	2.42	3.46	0.00
Pd2401-H75*	71.00	0.10	13.95	2.12	2.19	0.10	0.60	0.41	1.17	4.01	0.00
M15-01**	71.12	0.52	13.12	TFE	4.16	0.11	1.48	0.57	1.38	3.67	0.15
M15-02**	66.90	0.53	13.86	TFE	4.53	0.12	1.50	2.52	2.06	3.29	0.13
M15-03**	65.34	0.84	14.87	TFE	6.35	0.12	2.68	0.48	0.51	4.23	0.28
M15-04**	69.46	0.54	12.77	TFE	4.85	0.13	1.43	0.92	0.26	2.87	0.18
M15-05**	67.94	0.69	14.33	TFE	4.94	0.12	2.07	0.75	0.48	4.71	0.14
M15-06**	66.78	0.46	14.48	TFE	4.51	0.08	1.91	1.12	1.36	4.87	0.13
M15-07**	73.58	0.36	11.85	TFE	3.89	0.11	0.86	0.40	0.68	2.51	0.11
M15-08**	70.50	0.36	13.61	TFE	1.82	0.10	0.74	0.90	2.23	4.88	0.34
M15-09**	76.01	0.30	12.54	TFE	2.29	0.12	0.87	0.93	1.96	2.33	0.15
M15-10**	73.54	0.35	13.27	TFE	3.63	0.10	0.98	0.61	2.35	2.57	0.14
M15-11**	74.46	0.20	13.64	TFE	2.65	0.13	0.49	0.73	2.95	2.61	0.16
M23-01**	70.96	0.65	14.40	1.22	2.86	0.08	1.53	0.57	1.32	2.86	
M23-02**	72.00	0.55	13.95	1.16	2.82	0.10	1.41	0.28	0.13	4.09	
M23-03**	72.96	0.67	13.89	0.95	1.76	1.76	1.01	0.46	0.38	4.23	
M7-01**	68.56	0.58	15.58	1.93	2.80	0.07	1.78	0.32	1.36	3.94	
M7-02**	77.39	0.37	11.92	0.88	1.46	0.07	0.94	0.21	0.49	3.29	

(continued)

Sample	SIO2	TIO2	Al2O3	Fe2O3	FeO	MnO	MgO	CaO	Na2O	K2O	P2O5
M7-03**	66.50	0.80	17.84	2.03	1.28	0.03	0.29	0.16	0.12	5.20	
Zk1503-1**	64.74	0.66	15.59	1.64	2.20	0.13	1.11	2.67	0.83	4.52	
Zk1503-2**	69.97	0.45	11.08	2.38	4.12	0.12	1.18	1.34	0.51	3.03	
Zk1503-3**	67.52	0.58	14.54	1.57	3.00	0.17	1.65	1.08	0.26	4.36	
G-05	65.45	0.04	25.07	0.29	0.30	0.13	0.2	0.8	4.08	1.53	0.16
G-07	74.17	0.04	14.79	0.20	0.28	0.05	0.1	0.8	4.57	3.14	0.22
G-12	74.44	0.06	13.78	0.08	0.34	0.02	0.1	0.6	3.96	5.24	0.17
G-13	80.98	0.33	9.25	1.57	0.59	0.01	0.5	0.2	0.07	3.70	0.14
G-14	81.29	0.35	9.03	1.27	1.32	0.01	0.9	0.2	0.40	2.76	0.16
GZ-32	77.90	0.48	4.41	5.18	1.10	0.02	0.5	0.8	0.03	1.42	0.14
CM17-5	88.12	0.48	0.66	3.84	1.32	0.06	0.1	0.1	0.02	0.14	0.11
AA-O	71.05	0.45	13.44	1.51	2.55	0.13	1.33	0.74	1.03	4.04	0.14
AP	71.35	0.05	17.88	0.19	0.31	0.07	0.13	0.73	4.20	3.30	0.18
AO	82.07	0.41	5.84	2.97	1.08	0.03	0.50	0.33	0.13	2.01	0.14
AA	72.18	0.45	12.66	1.72	2.34	0.12	1.25	0.69	0.94	3.83	0.14
UM	70.32	0.39	14.58	0.44	2.59	0.08	1.17	2.25	3.20	3.48	0.08
US	70.93	0.55	13.87	0.96	3.31	0.05	1.91	0.64	1.18	3.72	0.13
UA	70.69	0.49	14.16	0.75	3.02	0.06	1.61	1.28	1.99	3.62	0.11
AA-O/UA	1.01	0.93	0.95	2.01	0.84	2.18	0.83	0.58	0.52	1.12	1.28
AO/UA	1.16	0.84	0.41	3.94	0.36	0.41	0.31	0.25	0.07	0.55	1.27
AA/UA	1.02	0.92	0.89	2.28	0.78	2.00	0.77	0.54	0.47	1.06	1.28

Normalized by TiO2

Sample	SIO2	TIO2	Al2O3	Fe2O3	FeO	MnO	MgO	CaO	Na2O	K2O	P2O5
IAO/UAI	1.38	1.00	0.49	4.69	0.43	0.49	0.37	0.30	0.08	0.66	1.51
IAA/UAI	1.11	1.00	0.98	2.49	0.85	2.18	0.84	0.59	0.51	1.15	1.40

AA is the total average of all altered rocks including ore rocks but pegmatites excluded;

AP, the average of altered pegmatites; AO, the average of ore rocks;

AA-O, equal to AA but ore rocks excluded;

US is the average of unaltered schists; UM, the average of unaltered migmatites;

UA, the average of all unaltered rocks.

Sources: * comes from No.719 Geol. Team, 1987, p34; ** from Ma, 1989; others from the present study.
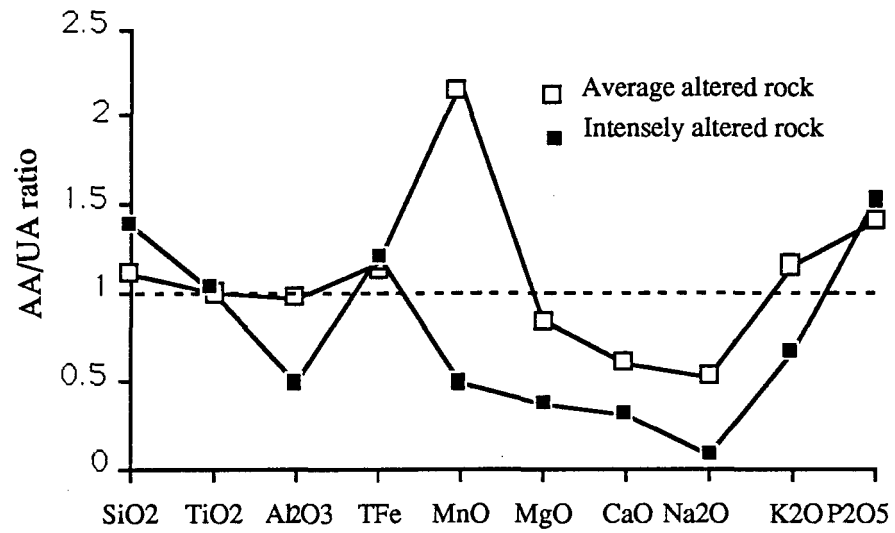
Figure 5.7 TiO2-normalized AA/AU ratio pattern of the major elements of the overall altered rock and the mature altered rock in the Hetai gold field

After TiO2-normalization, the initial unaltered rock is assigned a value of unity

gained mass on the total average, but was depleted in the intense alteration. Total iron (TFe) increases slightly with advanced alteration, but the variations of FeO and Fe_2O_3 in the alteration are not very clear.

4.3 Trace Elements

Trace elements can be classified into groups in the light of the TiO_2-normalized AA/UA ratio and its variation trend from the unaltered protolith, through the average altered rock, to the intensely altered rock (Table 5.2; Fig. 5.8).

The first group consists of the precious metals and most thiophile elements such as Bi, Cu, Hg and Sb. They have a TiO_2-normalized AA/UA ratio significantly higher than 1 for the average altered rock. This TiO_2-normalized AA/UA ratio becomes still higher within the ore bodies. This indicates that they were gradually added to the altered wall rock from the hydrothermal solution with the advance of alteration. Co, Se, Te and Zn are also included in this group, but with a lower enrichment coefficient. Despite depleted in the altered rock, the variation pattern of As abundance is similar to that of this group, increasing from the average altered rock to the average of the ores, so it could be classified into this group.

The second group is represented by Cs, Hf, Zr, Nb, Sc, Th, Ba and REE, being lithophile elements, and characteristic of the southern China basement and granites (Institute of Geochemistry, 1979). In contrast to the first group, this group is characterized by consistently low TiO_2-normalized AA/UA ratio on the overall average of altered rocks. These ratios become further lower within the intense alteration zone. These elements regularly lost mass during the hydrothermal alteration. The major element representative of this group is Na_2O.

Rb, U, W and Ta comprise another group of lithophile elements. They have an overall pattern similar to K_2O. Although they gained mass on the total average, these elements were leached during the late maturation alteration.

Cr, Ni and Pb show little change in the hydrothermal alteration.

The classification above is consistent with the results of factor analysis (Appendix III-5.1), which distinguishes elements into six most significant factors with respect to the

Table 5.2 Trace elements of the altered rocks occurring in the Hetai gold field

Sample	Ag	As	Au	Ba	Bi	Co	Cr	Cs	Cu	Hf	Hg	Nb
G-10	106.6	28.6	9.2	478	10.9	13.5	92	26	71.9	6.9	3.31	14
G-11	183.3	6.4	74	652	20.9	9.8	55	15	281.5	4	8.82	9.1
GZ-31	696.6	38	7.2	705	10.6	12.9	79	12	49.9	2.6	9.74	8
GZ-31-1	120	10.1	138	778	23.1	8.4	57	14	105.8	3.5	2	9.1
GZ-34A	150	26	11	312	11	15	97	9	18	6.5	10.48	17
GZ-34B	120	7.8	14	273	11.2	2.8	11	10.5	16	2.2	9.19	18
CM17-3	53	17	19.5	377	6.7	7.1	57	12	12	11	1.66	7.7
SK-s	120	1.1	118	453	18.2	8.5	73	9.3	67.9	5	20.4	7.7
G-13	1633	0.3	3691	417	20.5	6.7	55	3.4	6209.4	4.9	1.44	4.2
G-14	1213.3	0.3	7061	338	8.3	8	52	4.5	870.6	8.1	11.95	6.8
GZ-32	51960	74	53068	158	41.9	41	56	2.7	20211	2.6	31.8	0.7
CM17-5	5230	1.1	12689	22	13.8	18	48	0.4	15706.1	0.2	0.92	0.5
G-05	120	0.9	20.4	169	7.9	0.5	2.3	4.5	12	1.7	0.04	5.4
G-07	90	0.2	9.5	92	1.9	0.6	18	3.8	4	1.3	0.74	12
G-12	30	1	18	215	22.6	1.1	17	6.1	16	0.7	0.55	5.8
AA-O	193.7	16.9	48.9	503.5	14.1	9.8	65.1	13.5	77.9	5.2	8.2	11.3
AP	80.0	0.7	16.0	158.7	10.8	0.7	12.4	4.8	10.7	1.2	0.4	7.7
AO	15009.1	18.9	19127.3	233.8	21.1	18.4	52.8	2.8	10749.3	4.0	11.5	3.1
AA	5132.2	17.6	6408.3	413.6	16.4	12.6	61.0	9.9	3635.0	4.8	9.3	8.6
UA	93.3	24.3	4.5	522.0	4.9	9.2	64.1	13.7	25.0	6.1	5.1	11.8
AO/UA	160.95	0.78	4287.14	0.45	4.34	2.00	0.82	0.20	430.62	0.65	2.28	0.26
AA/UA	55.03	0.72	1436.35	0.79	3.37	1.38	0.95	0.72	145.62	0.79	1.84	0.73
Normalized by TiO2												
IAO/UAI	191.61	0.93	5103.74	0.53	5.16	2.39	0.98	0.24	512.64	0.77	2.71	0.31
IAA/UAI	60.02	0.79	1566.36	0.86	3.68	1.50	1.04	0.79	158.80	0.86	2.01	0.79

AA is the total average of altered rocks including ore rocks with pegmatites excluded; AP, the average of altered pegmatites; AO, the average of ore rocks (equal to the mature altered rock); AA-O, equal to AA but ore rocks excluded; UA, the average of unaltered rocks.

(Continued)

Sample	Ni	Pb	Rb	Sb	Sc	Se	Sn	Ta	Te	Th	U	V
G-10	50	57.7	206	0.148	13	0.045	3	1.4	0.035	19.9	4.4	29
G-11	66.7	38.5	583	0.174	9.3	0.04	11	1.22	0.03	14.4	5.5	22
GZ-31	75	38	256	1.81	14	0.06	5	1.16	0.05	18	4.9	14
GZ-31-1	66.7	38.5	415	0.2	9.8	0.06	5	1.13	0.055	13.3	6	20
GZ-34A	83.3	38.2	189	0.515	14	0.1	2.5	4.09	0.07	19.3	5.3	38
GZ-34B	33.3	57.5	243	0.13	3.2	0.06	3.5	8.81	0.055	2.9	16	35
CM17-3	33.3	19.2	147	0.032	5.9	0.05	5.5	0.83	0.039	15	3.3	13
SK-s	50	57.7	190	0.206	11	0.06	7	1.03	0.06	15.7	3.6	35
G-13	25	19.2	118	0.148	6.4	0.045	13	0.79	0.029	11	3.3	20
G-14	41.7	19	116	0.12	7	0.042	3	0.82	0.04	14.1	3.9	18
GZ-32	66.7	76.9	57	5.5	3.7	0.08	4	0.37	0.05	5.5	1.7	25
CM17-5	16.7	19	6.4	0.129	0.5	0.085	6	0.04	0.058	0.6	0.1	60
G-05	8.3	57.7	104	0.087	3.2	0.075	12	1.05	0.04	2	31.6	20
G-07	16.7	38.5	207	0.03	1.6	0.035	9	2.55	0.035	1	21.4	32
G-12	25	38.5	212	0.073	1.2	0.04	9	2.17	0.03	0.7	17.6	20
AA-O	57.3	43.2	278.6	0.4	10.0	0.1	5.3	2.5	0.0	14.8	6.1	25.8
AP	16.7	44.9	174.3	0.1	2.0	0.1	10.0	1.9	0.0	1.2	23.5	24.0
AO	37.5	33.5	74.4	1.5	4.4	0.1	6.5	0.5	0.0	7.8	2.3	30.8
AA	50.7	40.0	210.5	0.8	8.2	0.1	5.7	1.8	0.0	12.5	4.8	27.4
UA	48.9	42.8	188.8	0.1	9.5	0.1	7.5	1.1	0.0	19.9	4.1	30.0
AO/UA	0.77	0.78	0.39	15.71	0.47	1.13	0.87	0.44	1.03	0.39	0.55	1.03
AA/UA	1.04	0.93	1.12	8.09	0.86	1.08	0.76	1.59	1.11	0.63	1.18	0.91
Normalized												
IAO/UAI	0.91	0.93	0.47	18.70	0.55	1.34	1.04	0.53	1.23	0.47	0.65	1.22
IAA/UAI	1.13	1.02	1.22	8.82	0.94	1.18	0.83	1.73	1.21	0.68	1.29	1.00

(continued)

Sample	W	Zn	Zr	La	LREE	HREE	REE	HREE/LREE	Nb/Ta	U/Th	Zr/Hf
G-10	0.8	72.5	299	43.2	176.4	19.0	195.4	0.11	10.00	0.22	43.33
G-11	0.8	135	97	33.2	134.1	13.5	147.6	0.10	7.46	0.38	24.25
GZ-31	1.5	195	81	36.9	149.8	16.1	165.9	0.11	6.90	0.27	31.15
GZ-31-1	1.2	67.5	125	30.0	122.3	13.3	135.5	0.11	8.05	0.45	35.71
GZ-34A	0.9	132.5	170	42.3	172.4	21.2	193.6	0.12	4.16	0.27	26.15
GZ-34B	0.8	70	50	6.5	28.2	4.4	32.5	0.16	2.04	5.52	22.73
CM17-3	1	47.5	395	28.1	117.1	13.7	130.8	0.12	9.28	0.22	35.91
SK-s	1.2	95	338	35.4	144.0	16.0	160.0	0.11	7.48	0.23	67.60
G-13	1	145	100	25.3	100.4	11.9	112.3	0.12	5.32	0.30	20.41
G-14	1	42.5	348	27.1	106.3	14.7	121.0	0.14	8.29	0.28	42.96
GZ-32	0.9	225	59	14.0	50.2	5.0	55.1	0.10	1.89	0.31	22.69
CM17-5	0.8	180	16	3.9	16.2	4.6	20.8	0.29	12.50	0.17	80.00
G-05	2	555	96	3.9	14.7	21.4	36.0	1.45	5.14	15.80	56.47
G-07	1.5	42.5	58	2.2	10.1	7.4	17.4	0.73	4.71	21.40	44.62
G-12	1	12.5	45	1.4	6.2	7.7	13.9	1.24	2.67	25.14	64.29
AA-O	1.0	101.9	194.4	35.2	143.7	16.0	159.7	0.11	4.61	0.41	37.29
AP	1.5	203.3	66.3	2.5	10.3	12.1	22.5	1.17	4.02	19.08	53.78
AO	0.9	148.1	130.8	17.5	68.3	9.0	77.3	0.13	6.04	0.29	33.10
AA	1.0	117.3	173.2	27.1	118.6	13.7	132.3	0.12	4.74	0.39	36.14
UA	1.0	101.6	220.9	37.0	151.7	22.0	173.6	0.14	10.35	0.21	36.31
AO/UA	0.96	1.46	0.59	0.47	0.45	0.41	0.45	0.92	0.58	1.40	0.91
AA/UA	1.03	1.15	0.78	0.73	0.78	0.62	0.76	0.80	0.46	1.88	1.00
Normalized											
IAO/UAI	1.14	1.74	0.70	0.56	0.54	0.49	0.53	1.09	0.69	1.66	1.09
IAA/UAI	1.12	1.26	0.85	0.80	0.85	0.68	0.83	0.87	0.50	2.05	1.09
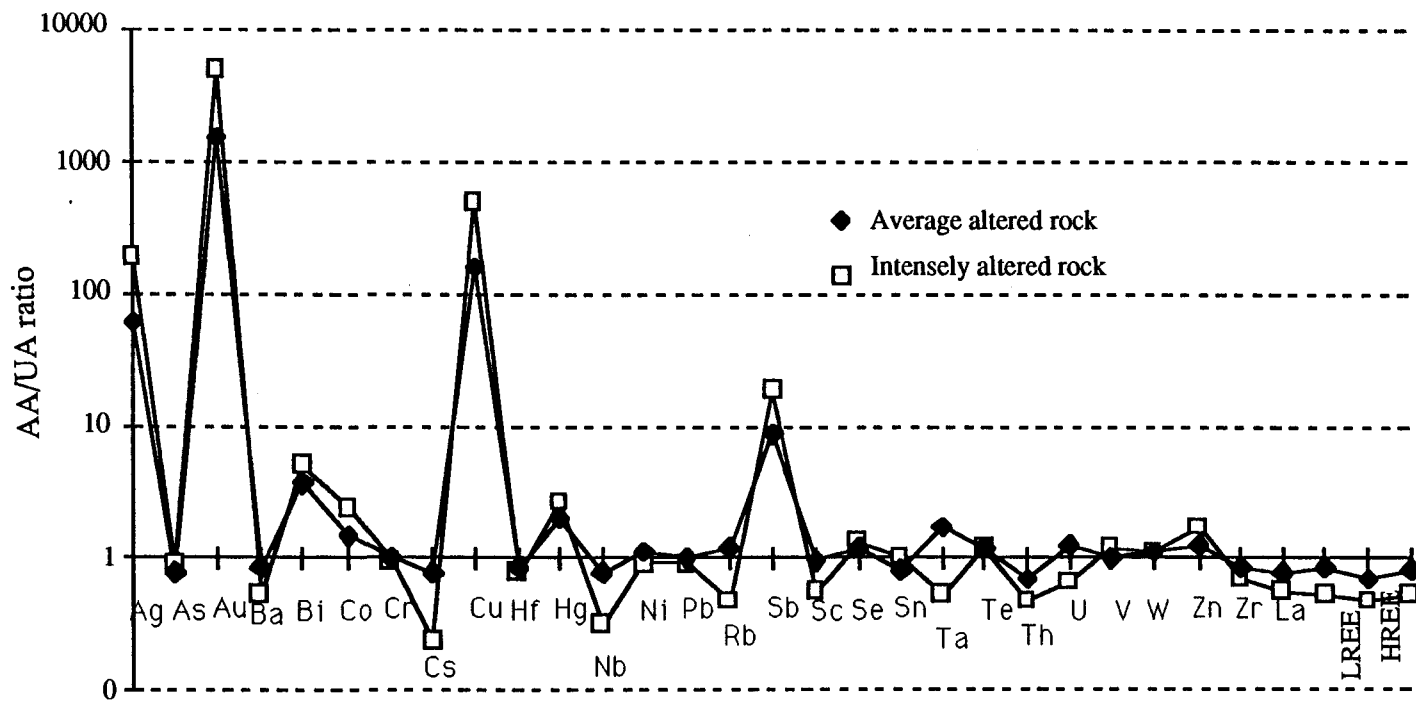
Figure 5.8 TiO₂-normalized AA/AU ratio pattern of the trace elements of the overall altered rock and the mature altered rock in the Hetai gold field

After TiO2-normalization, the initial unaltered rock is assigned a value of unity

hydrothermal alteration. These six factors are as follows:

F-I:	{Ag, Au, As, Bi, Co, Hg, Pb, Sb}
F-II:	{Cs, Rb, Sc, Cr, Ba, Ni, Th}
F-III:	{Nb, Ta, U}
F-IV:	{Se, Te}
F-V:	{Hf, Zr}
F-VI:	{W}

where the factors F-I and F-IV are the mineralized thiophile element associations, while the factors F-II, F-III, F-IV and F-V are characteristic lithophile element associations of the southern China basement and granites (Institute of Geochemistry, 1979). Among them, the factors F-III and F-V demonstrate a significant positive linear correlation (Appendix III-5.2).

One of possible interpretations for the geochemical behavior of the major and trace elements described above is that the hydrothermal solution has contributed part of K_2O and SiO_2 and most ore-forming elements, as implied by the occurrence of pervasive sericitization and silicification, and the elevated precious metal abundances within the altered zone. In the peripheral region of alteration envelopes, most SiO_2 and K_2O may be *in situ* or redistributed from nearby rocks. The depletion of CaO, Na_2O and MgO is related to their removal and the dilution caused by the addition of SiO_2. Within the intense silicification zone and ore bodies, the addition of SiO_2 is marked, so that there is more dilution and higher mass factor in reference to the conserved component TiO_2.

4.4 Rare Earth Elements

The REE abundance distribution patterns of the altered rocks (including ores) and pegmatites occurring within the ore deposit area are illustrated in Figures 5.9 and 5.10. For the sake of comparison, their averages as well as the overall average of the unaltered initial rocks of the Hetai area are drawn separately in Figure 5.11, through which a systematic change of REE distribution pattern can be seen in the series from the unaltered rock, through

Figure 5.9 REE abundance distribution patterns of the altered rocks (including ores, but not pegmatites) occurring in the deformation zones of the Hetai gold field

Figure 5.10 REE abundance distribution patterns of the vein pegmatites occurring in the Hetai gold field
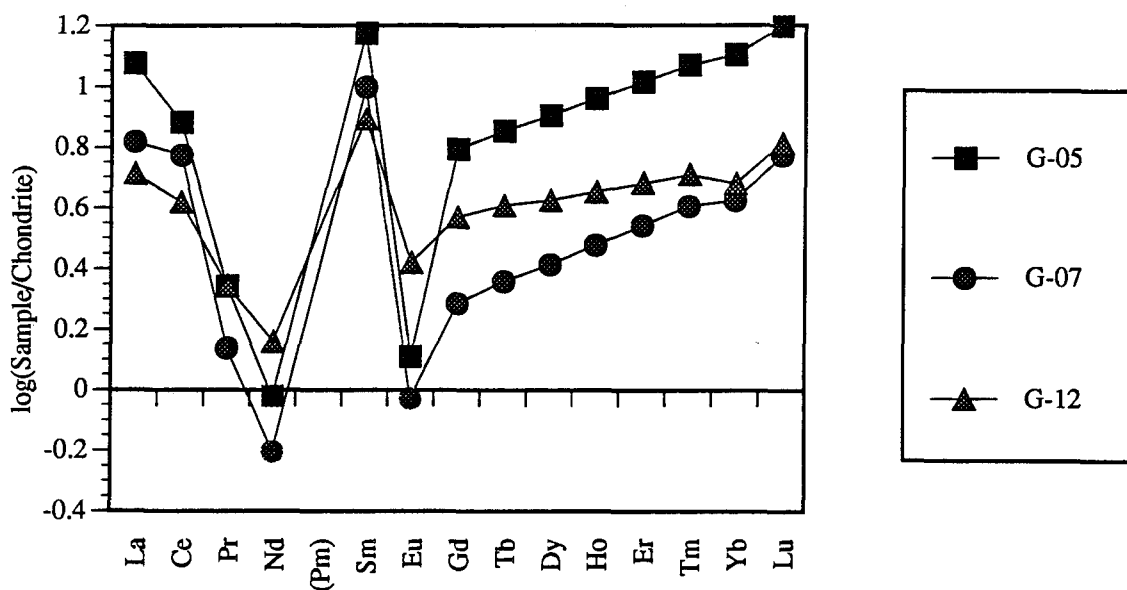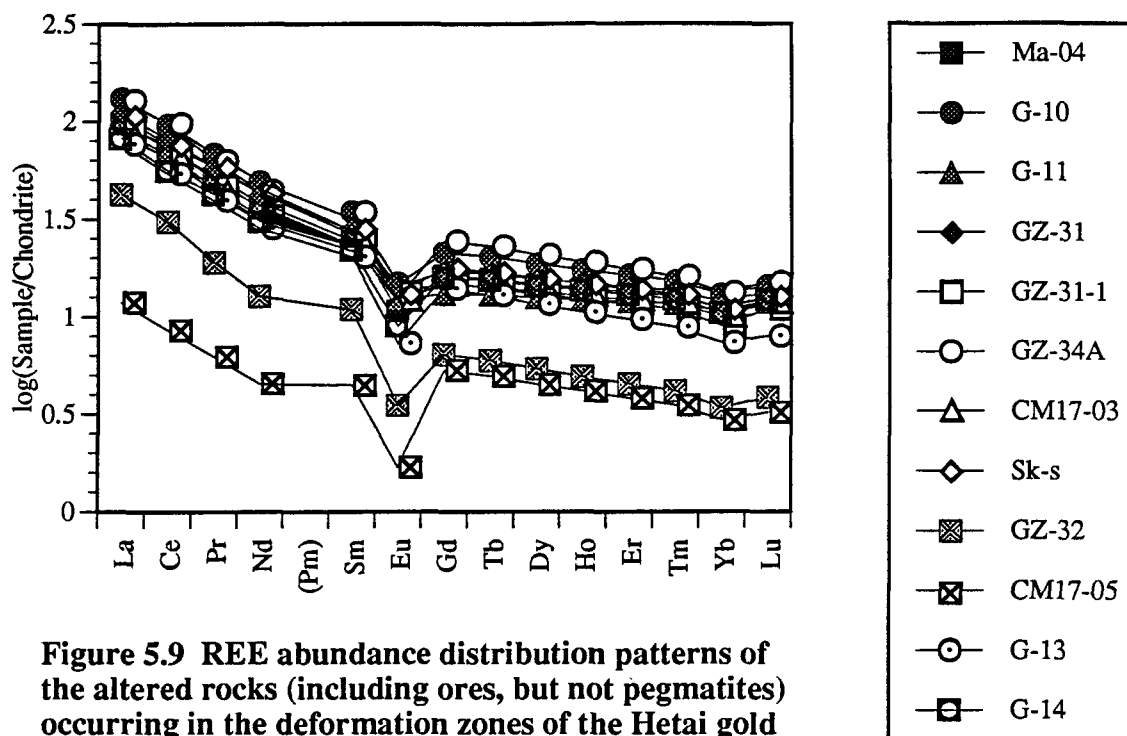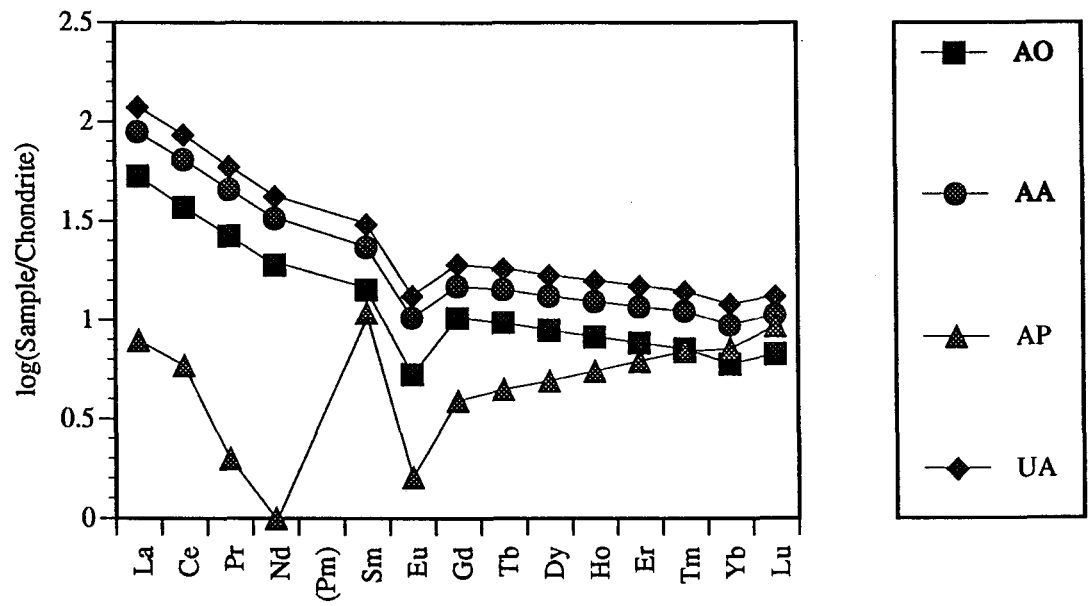
Figure 5.11 Comparison between the REE abundance distribution
patterns of the average unaltered rock (UA), average altered rock
(AA), average ore rock(OA) and average vein pegmatite (AP)

the average altered rock, to the ore. All the original analytic data are listed in Appendix III-5.3. These figure clearly demonstrate that:

(1) The REE pattern of the ore is comparable to that of unaltered rocks. It is characterized by the consistent regular decrease in abundance toward the heavy REE, with an intermediate negative Eu anomaly but no Ce anomaly. The REE are, however, slightly shifted to lower abundance with the original profile of the unaltered rock (Sinian) essentially retained after mineralization. The nearly coherent downward shift is partly due to the removal of REE as other lithophile elements during the hydrothermal alteration, but mostly due to the dilution, caused by the addition of some components, especially hydrothermal quartz, which usually contains negligible amounts of REE.

(2) The granitic pegmatites have a totally different REE distribution pattern to that of the Sinian strata. They have a low total REE content and are highly enriched in heavy REE. The presence of a strongly negative Eu anomaly and a small positive Ce anomaly is characteristic. The overall distribution pattern is in an irregular "W" shape.

(3) Despite their nearly coherent downward shift, the individual REE differentiate slightly in the altered rocks. With increasing atomic number, REE become slightly less depleted. Such a differential is enhanced within the intense alteration zone. The ratio of LREE/HREE decreases on the average from 7.9 for the unaltered rock, through 7.65 for the general altered rock, to 6.68 for the ore. The slight differentiation is attributed to the difference in inherent properties of REE. It was demonstrated (Liu et al., 1984) that LREE are more lithophile than HREE, and HREE are more stable in hydrothermal solutions than LREE. This leads to a little more enrichment of HREE relative to LREE in hydrothermally altered rocks.

§5 Isotopic Characteristics of Ores

5.1 Sulfur Isotopes

The sulfur isotopes of the ores and host Sinian strata are listed in Table 5.3, which shows that sulfur isotopic composition of Fe-sulfides from the ores and host strata are comparable, with $\delta^{34}S$ value ranging from -3 to -1‰ for the ores, and from -3.1 to 0.02‰ for the strata, in relative to the Arizona's Canyon Diablon Troilite (CDT). Lower $\delta^{34}S$ values for

Table 5.3 Sulphur isotope of the ore rocks and host strata of the Hetai gold field

Sample	Location	Mineral	δ 34S(‰)	Source
G29-1	Gaocun	pyrite	-2.53	(d)
G30-7a-1	Gaocun	pyrite	-2.59	(d)
G30-7a-2	Gaocun	pyrite	-2.73	(d)
G30-7a-3	Gaocun	pyrite	-2.73	(d)
G30-7b-2	Gaocun	pyrite	-2.17	(d)
G30-7b-1	Gaocun	pyrrhotite	-2.36	(d)
G35-3	Gaocun	pyrite	-2.5	(d)
G40-34a	Gaocun	pyrite	-2.69	(d)
G40-4a*	Gaocun	pyrite	-2.53	(d)
G74-30*	Gaocun	pyrite	-1.98	(d)
BT5*	Gaocun	pyrite	-2.07	(d)
ZG68*	Gaocun	pyrite	-2.82	(d)
G32-3a*	Gaocun	pyrite	-2.37	(d)
G38-7a*	Gaocun	sphalerite	-4.52	(d)
G38-7b*	Gaocun	galena	-8.13	(d)
G42-16a*	Gaocun	galena	-8.19	(d)
G42-16b*	Gaocun	sphalerite	-4.54	(d)
G42-38a*	Gaocun	galena	-7.3	(d)
G42-34b*	Gaocun	chalcopyrite	-2.32	(d)
G32-3b*	Gaocun	chalcopyrite	-2.28	(d)
G40-4*	Gaocun	chalcopyrite	-2.23	(d)
G33-1a	Shuangbao	pyrite	-1.03	(d)
G33-1b	Shuangbao	pyrite	-1.48	(d)
G33-1c	Shuangbao	pyrite	-1.64	(d)
G33-2	Shuangbao	pyrite	-1.54	(d)
G33-1A-1	Shuangbao	pyrite	0.02	(d)
G33-1A-2	Shuangbao	galena	-2.47	(d)
G28-1	Dapingding	pyrite	-2.93	(d)
H-04	Gaocun	pyrite	-1.48	(c)
H-06	Gaocun	pyrite	-1.53	(c)
HS-2	Gaocun	chalcopyrite	-1.32	(c)
H15-3	Gaocun	galena	-3.2	(c)
H15-4	Gaocun	sphalerite	-3.74	(c)
[1]	Baoyiatang	pyrite	-3	(b)
[2]	Baoyiatang	pyrite	-0.3	(b)
[3]	Yunxi	Pyrrhotite	-2.2	(b)
ZK002-4**	Gaocun	pyrite	-2.3	(a)
ZK002-8**	Gaocun	pyrite	-1.6	(a)
570**	Gaocun	pyrite	-1.8	(a)

Sources: (a) from Lu et al. (1990); (b), Zhang et al. (1989); (c), Chen et al. (1988); (d), Fu (1988)

sphalerite and galena are attributed to be caused by that the heavy isotope ^{34}S varies with the paragenetic sequence of metallic sulfide species in a deposit (Stanton, 1972). At a given temperature the heavy sulfur isotope is generally richest in pyrite, with amount decreasing progressively in sphalerite, (chalcopyrite), and galena.

The initial $\delta^{34}S$ value of the strata is probably about 0 in the Hetai area. However, oxidized fluids or the oxidation of fluid may result in negative $\delta^{34}S$ value of the pyrite. It has been shown (Lambert et al., 1984; Golding and Wilson, 1983; Spooner et al., 1985; Schwarcz and Rees, 1985; Cameron and Hattori, 1987; Colvine et al., 1988) that Fe-sulfide minerals generated from oxidized fluids or by the oxidation of fluids at the precipitation site would have $\delta^{34}S$ values more negative than that of the fluid. The narrow range of distribution approaching zero of the observed $\delta^{34}S$ values may indicate the homogenization of sulfur isotope composition by the Caledonian regional metamorphism and migmatism preceding the ore deposition.

5.2 Lead Isotopes

Lead isotopes were analyzed on the ores, granites and host strata (Sinian). The results are listed in Table 5.4, and displayed in Figure 5.12. The parameters used for plotting the single-stage growth curves and the isochrons of Figure 5.12 include the age of the Earth: T = 4.5 G.a.; primordial lead: $^{206}Pb/^{204}Pb = 9.307$, $^{207}Pb/^{204}Pb = 10.294$, $^{208}Pb/^{204}Pb = 29.497$ (Köppel and Grünenfelder, 1979; Tatsumoto et al., 1973); the decay constants: λ (^{238}U) = 1.55125×10^{-10}/year, λ (^{235}U) = 9.8485×10^{-10}/year, λ (^{232}Th) = 4.9475×10^{-11}/year (Jäger, 1979); and the present atomic ratio, $^{238}U/^{235}U = 137.88$, $\mu = {}^{238}U/^{204}Pb$.

Figure 5.12 shows that the ore lead isotopes do not follow the single-stage growth curve. They scatter to the right of the zero age isochron, and therefore have a negative model age. So do the leads of the Precambrian and Cambrian host strata. This Figure also demonstrated that the leads of the ore, host strata, and granites plot on a linear array, with the Caledonian Shidong (migmatitic) granite — the Hercyno-Indosinian Yunluogan and Wucun granites — the ores — the host strata from left to right.

Table 5.4 Lead isotope compositions of ores, host strata and granites from the Hetai area

Sample	Mineral	Lithology	Location	Pb206/Pb204	Pb207/Pb204	Pb208/Pb204	Model Ages (Ma)	Sources
CM1501-4	galena	ore rock	Gaocun	18.828	15.732	39.178	39	Chen et al. (1988)
574	pyrite	ore rocks	Gaocun	19.014	15.747	39.315	98	Chen et al. (1988)
D161	K-feldspar	granitic pegmatite	Wucun	18.613	15.680	38.726	195	Chen et al. (1988)
HBT-14	K-feldspar	Wucun granite	Wucun	18.532	15.613	38.656	224	Chen et al. (1988)
P3-97-1	K-feldspar	granitic pegmatite	Yunluogan	18.502	15.715	38.822	242	Chen et al. (1988)
P3-91	K-feldspar	Yunluogan granite	Yunluogan	18.554	15.788	38.939	292	Chen et al. (1988)
P3-99	K-feldspar	Shidong granite	Shidong	18.353	15.711	38.472	343	Chen et al. (1988)
CM1501-14	whole rock	Sinian schist	Gaocun	19.395	15.840	38.388	341	Chen et al. (1988)
ZK1501-8	whole rock	Sinian schist	Gaocun	19.455	15.850	38.320	389	Chen et al. (1988)
ZK1502-2	whole rock	Sinian granulite	Gaocun	19.721	15.940	38.518	393	Chen et al. (1988)
G33-1-1	pyrite	ore rock	Shuangbo	18.690	15.760	39.162	163	Fu (1988)
G33-1-2	pyrite	ore rock	Shuangbo	18.664	15.743	39.078	161	Fu (1988)
G33-1A	pyrite	ore rock	Shuangbo	18.674	15.752	39.038	165	Fu (1988)
G28-1	pyrite	ore rock	Dapingding	18.651	15.725	38.945	148	Fu (1988)
G29-2	pyrite	ore rock	Gaocun	18.855	15.743	39.216	24	Fu (1988)
G30-7a	pyrite	ore rock	Gaocun	19.078	15.719	39.502	-170	Fu (1988)
ZK002	pyrite	ore rock	Gaocun	18.635	15.737	39.001	174	Fu (1988)
G38-7	galena	ore rock	Gaocun	18.776	15.728	39.128	62	Fu (1988)
P3-91	K-feldspar	Yunluogan granite	Yunluogan	18.554	15.788	38.939	292	Fu (1988)
P3-97-1	K-feldspar	Yunluogan granite	Yunluogan	18.502	15.715	38.822	242	Fu (1988)
CM1501-14	whole rock	Sinian schist	Gaocun	19.400	15.920	38.390	-141	Fu (1988)
ZK1502-2	whole rock	Sinian schist	Gaocun	19.720	15.950	38.520	-337	Fu (1988)
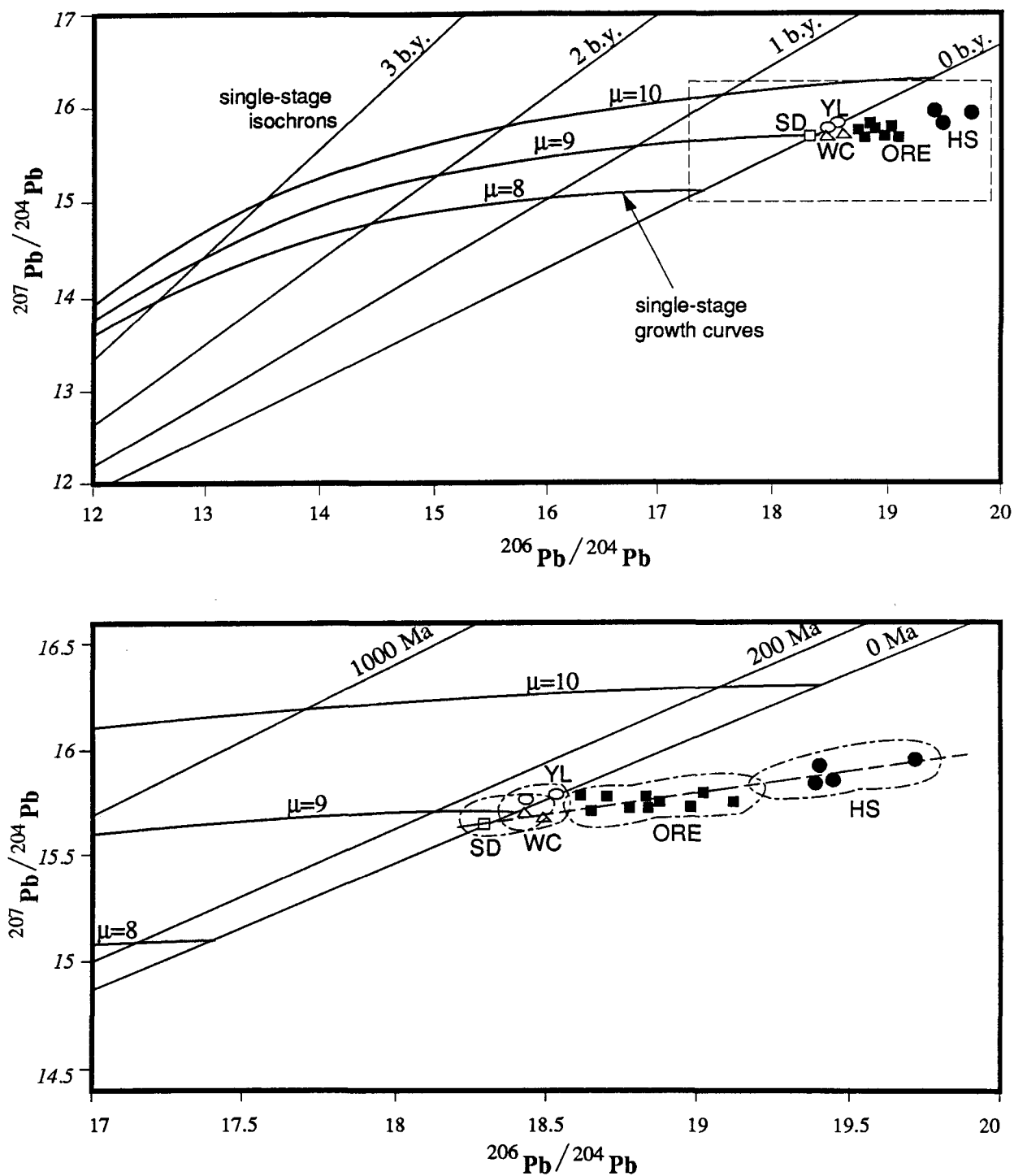
Figure 5.12 Diagram of 207Pb/204Pb versus 206Pb/204Pb showing the relationship of ore rocks, host strata and granites of the Hetai gold field

ORE = ore rock, HS = host strata, SD = Shidong migmatized granite, YL = Yunluogan granite, WC = Wucun granite. Note that they are distributed along a regressive linear curve. Data from Table 5.4

§6 Summary

The gold deposits and ore bodies occurring in the Hetai area are controlled by a Hercyno-Indosinian deformation system and the associated hydrothermal alterations. The deformation system consists of numerous NE-striking ductile shear zones.

Deformation zonation within the ductile shear zones is a common feature. The deformation gradually becomes more intense from the outside toward the deformation center across the shear zones, and the corresponding deformed rock changes from a undeformed primary rock, through protomylonite, to mylonite and locally ultramylonite. Three planar fabrics, S, C and E, and characteristic textures of deformed rocks are observed. At all scales, from the distribution of shear zones in the deformation system, through the internal geometrical features of individual shear zones, to microscopic deformed textures, the characteristic pattern of deformation is anastomosing domains of higher deformation separating rhomboid domains of lower deformation.

Hydrothermal alteration is both spatially and temporally associated with the development of the ductile shear system. The alteration products are principally quartz, sulfides, sericite and ankerite. Silicification occurred throughout the whole alteration process. Three groups of hydrothermal quartz may be distinguished: pre-deformational quartz, early stage hydrothermal quartz, and late stage sulfide-associated hydrothermal quartz. There were two generations of sulfidation, which correlate closely with the precipitation of gold. The sulfides of the first generation are mainly composed of coarse-grained, euhedral pyrite and pyrrhotite, and those of the second generation, of fine-grained, anhedral pyrite and chalcopyrite. The precipitation of gold culminated during the formation of the second generation of sulfides.

The principal ores are essentially auriferous altered mylonites. The main economic minerals disseminated in the ores include native gold, chalcopyrite and pyrite.

Mass equilibrium estimation on the basis of the chemical compositions of altered and unaltered rocks demonstrates that a mass with an average mass factor of 1:0.92 has been added to unaltered initial rocks during hydrothermal alteration. The mass addition reaches its maximum in ore bodies, the intensely altered rocks, with an average mass factor of 1:0.84. Silica, precious metals, and most thiophile elements are regularly introduced into the wall

rocks with the advance of alteration, whereas Na2O and most lithophile elements characteristic of the southern China basement and granites lost mass in the alteration. Some other elements (e.g., K2O, Rb, U, Ta, W) were added in the early stage of alteration, but removed or diluted during late intense alteration.

The ores have a similar chondrite-normalized REE distribution pattern of the unaltered protolith (metamorphosed Sinian strata). But compared to the latter, the REE distribution pattern of altered rocks is shifted slightly downward with little differentiation of individual REE. The granitic pegmatites occurring in the mines is completely different in REE distribution pattern from the ores and the metamorphic Sinian strata. The REE pattern of the pegmatites is characterized by a low total REE content, an irregular "W" shape, with HREE relatively enriched compared to LREE.

Sulfur isotopic compositions of the ores are comparable with the host strata, and the leads of the ores, host strata, and granites plot on a linear array, with the Caledonian Shidong (migmatitic) granite, the Hercyno-Indosinian Yunluogan and Wucun granites, the ores and the host strata from left to right.

Chapter VI

GEOCHEMISTRY OF HYDROTHERMAL FLUID INCLUSIONS

The discussion of the preceding chapter shows that fluids have been actively involved in the emplacement of gold in the Hetai area. It is vitally important to consider the characteristics of the fluids and their linkage with gold mineralization. It was shown (Roedder, 1984) that fluid inclusion study is one of the practical tools to trace mineralization processes and to understand the genesis of ore deposits. The basic geochemical characteristics of fluid inclusions of the Hetai gold field are described in this chapter.

§1 Occurrence of Fluid Inclusions

Selection of the samples used for fluid inclusion analysis was based on the affinity of the host minerals and fluid inclusions to gold mineralization. Only those fluid inclusions that are hosted in hydrothermal quartz, including both the early stage hydrothermal quartz and late stage sulfide-associated hydrothermal quartz, were studied.

The fluid inclusions of the Hetai gold deposits are usually small, with diameter ranging from smaller than 1 to 25 μm, averaging about 3 μm. They may be either primary or secondary in relation to the host quartz, with the secondary being more common. The primary inclusions may be hosted both in the late stage sulfide-associated hydrothermal quartz and in the early stage hydrothermal quartz. The secondary fluid inclusions hosted in the early stage hydrothermal quartz usually occur in three distinct modes: as trails along healed fractures, as irregular spatial clusters, or along grain boundaries of quartz. Healed fractures are indicated by the oriented arrays of many fluid inclusions (Plate 6.1). Although the fluid inclusions occurring along healed fractures are secondary in relation to the early stage hydrothermal quartz (Roedder, 1984; Robert and Kelly, 1987), healed fractures along which the secondary

inclusions are distributed are observed under the microscope to end abruptly at the boundary of the host early stage hydrothermal quartz grains in contact with sulfides or surrounded by sulfides (Plate 6.1c, e), indicating that these secondary fluid inclusions were formed during sulfidation, which was closely associated with gold precipitation.

The irregular clusters of fluid inclusions are characterized by their non-uniform random distribution, generally confined to individual quartz grains. It is proposed (Roedder, 1984; Robert and Kelly, 1987) that such inclusion clusters result from transposition of trails of inclusions, and thus are also secondary in origin. They were probably originally analogous to the fluid inclusions occurring along healed fractures described above.

The healed fractures may be of several different orientations. It is difficult to establish a consistent age relationship among fracture sets of individual samples. Healed fractures are often transgranular, cross-cutting subgrains, and could have been the result of multiple episodes of fracturing, fluid infiltration, and fracture healing.

§2 Classification and Relationships among Different Types

2.1 Classification

Fluid inclusions of different compositions may be distinguished on their appearance at room temperature, combined with the behavior under slight heating (up to 31°C) and cooling (Roedder, 1984). Three major types of fluid inclusions are identified in the host hydrothermal quartz at the Gaocun deposit of the Hetai gold field. In the order of decreasing abundance, these are: CO_2-H_2O inclusions, aqueous inclusions, and CO_2-dominated inclusions.

1. CO_2-H_2O Inclusions

Typically this type of fluid inclusions consists of two phases, liquid water + CO_2 vapor, at room temperature (Plate 6.2). Occasionally, three phases are observed, with a liquid CO_2 between the liquid water and CO_2-rich vapor phases. The inclusions may be rounded or irregular in shape. The CO_2 phase occupies about 5 - 25% of the total volume. Fluid inclusions along the same healed fracture usually have a constant volumetric proportion of CO_2. The relatively constant phase ratio may be the result of the entrapment of a homogeneous fluid.
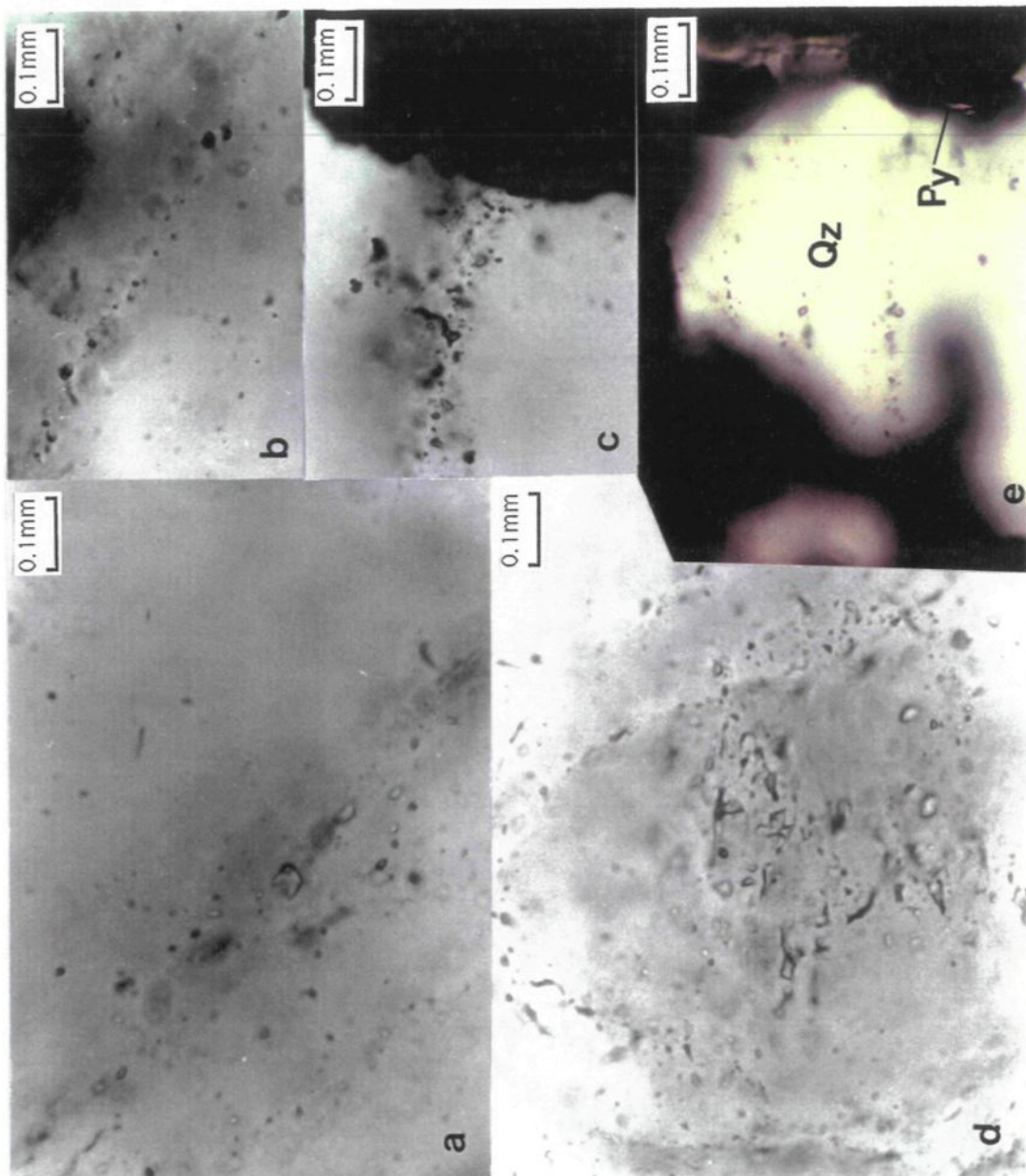
Plate 6.1 Occurrence of fluid inclusions in the host quartz grains
(a) + (b): Oriented distribution of fluid inclusions along healed fractures, indicated by the trail of fluid inclusions. (c) + (e): The trail of fluid inclusions "cuts" through the host quartz, but ends abruptly at the boundary of quartz and sulfides. The host quartz is synchronous with auriferous sulfides, all being the product of the syn-deformational hydrothermal alteration, indicating that the secondary inclusions were trapped during the hydrothermal alteration (mineralization). The opaque is sulfides (Py), and the pale white, quartz (Qz). (d): 3-D cluster of fluid inclusions.
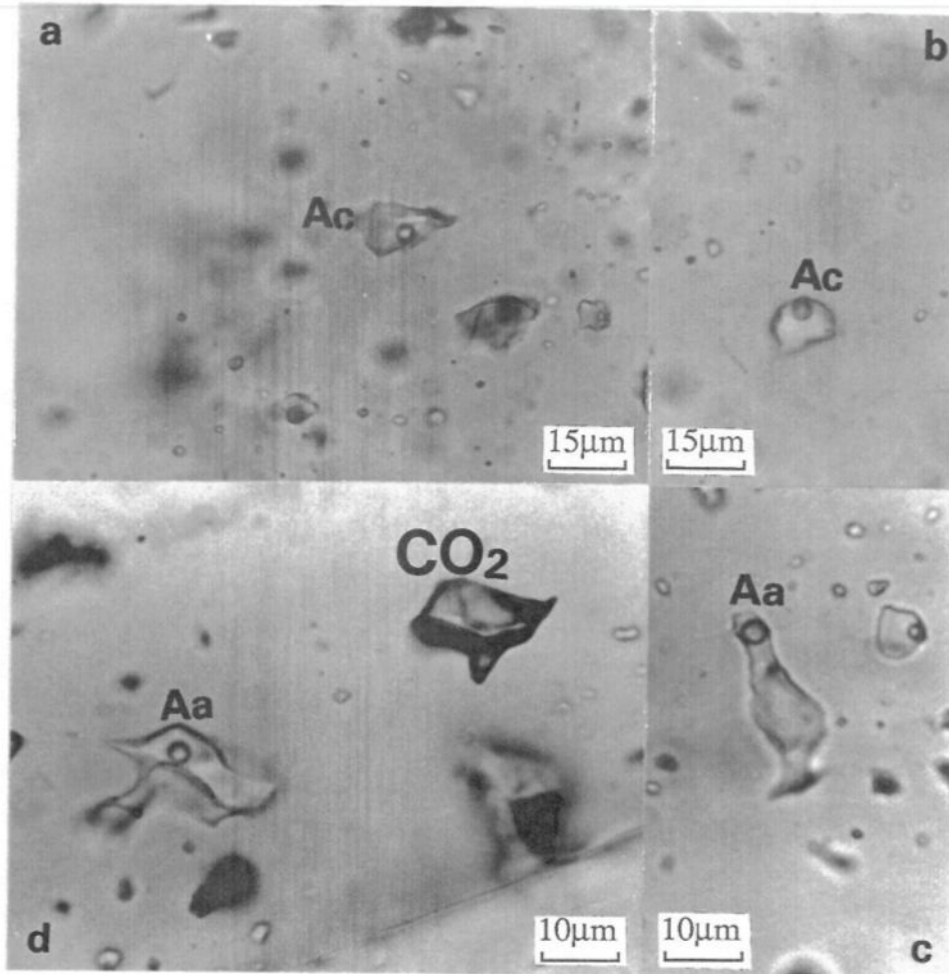
Plate 6.2 Compositional types of fluid inclusions

(a) + (b): Low salinity H2O-CO2 inclusions (Ac); (c): Moderate salinity aqueous inclusions (Aa); (d) non-saline CO2-dominated inclusions (CO2). (d) also show the coexistence of aqueous fluid inclusions (Aa) and CO2-dominated inclusions (CO2) of the same episode.

2. Aqueous Inclusions

This type of fluid inclusions commonly contains two phases at room temperature, a liquid aqueous phase and an aqueous vapor bubble. Daughter minerals were not detected.

3. CO_2-dominated Inclusions

This group of fluid inclusions consist of one or two CO_2 phases (liquid and/or vapor) at room temperature. Negative "crystal" shapes are quite common. On slight heating from room temperature, these inclusions usually homogenize to a vapor phase. Small amounts of H_2O are occasionally observed in some CO_2-dominated inclusions as a thin film rimming the inclusion walls or at the tips of inclusion walls intersecting at acute angles.

2.2 Relationships of Fluid Inclusions and Gold Mineralization

1. Relation between Different Types of Fluid Inclusions

Although they have different abundances of occurrence, all three types of fluid inclusion may occur in the same samples. It is observed that in general, just one type of fluid inclusions is distributed along a given healed fracture or within a cluster, however, there is no priority for which type to associate with a specific set of healed fractures. Within several doubly polished plates, the CO_2-dominated inclusions are found to coexist with the CO_2-H_2O inclusions and aqueous inclusions (Plate 6.2d, e).

2. Relation Between Fluid Inclusions and Gold Mineralization

The fluid inclusions studied include both primary inclusions and secondary inclusions. The secondary ones are hosted in the early stage hydrothermal quartz, and formed during the development of sulfides, which was associated with peak gold precipitation. There is thus a spatial and temporal coincidence between the gold emplacement and the entrapment of these three types of fluid inclusions, implying a close genetic linkage between them. Therefore a knowledge of the characteristics of the hydrothermal solution preserved in the fluid inclusions is helpful to understand the gold mineralization of the Hetai area.

§3 Fluid Inclusion Microthermometry

3.1 Fluid Inclusion Technique

Fluid inclusions were examined in doubly polished thick sections using U.S.G.S gas-flow fluid inclusion microscope and heating-freezing stage system which has been calibrated with commercially available chemical standards.

Heating and freezing determinations on fluid inclusions permit the observation of phase changes. The measured temperatures at which a phase change of a fluid inclusion system takes place include the following:

Tfm (Te): first melting temperature (eutectic melting temperature)

Tm_{CO_2}: melting temperature of solid CO_2

Tm: last melting temperature of ice

Th: final homogenization temperature

It should be pointed out that the eutectic melting temperature may not always be determined for all examined samples, mainly due to the the small size of the fluid inclusions. Occasionally, a clathrate melting temperature (Tcm) can also be obtained.

In addition to the minimum temperature of trapping and confining pressure, the salinity, chemical system, density of the fluids can be estimated by comparison of the measurements with experimentally derived phase equilibrium diagrams. Such information is particularly useful for defining the characters of the hydrothermal fluid active during hydrothermal alteration.

3.2 Homogenization Temperature

The observed homogenization temperatures of the fluid inclusions hosted in the hydrothermal quartz of the Hetai gold field are listed in Table 6.1 and displayed in Figure 6.1. They range from 130 to 310°C (uncorrected for pressure). There is no distinct difference in
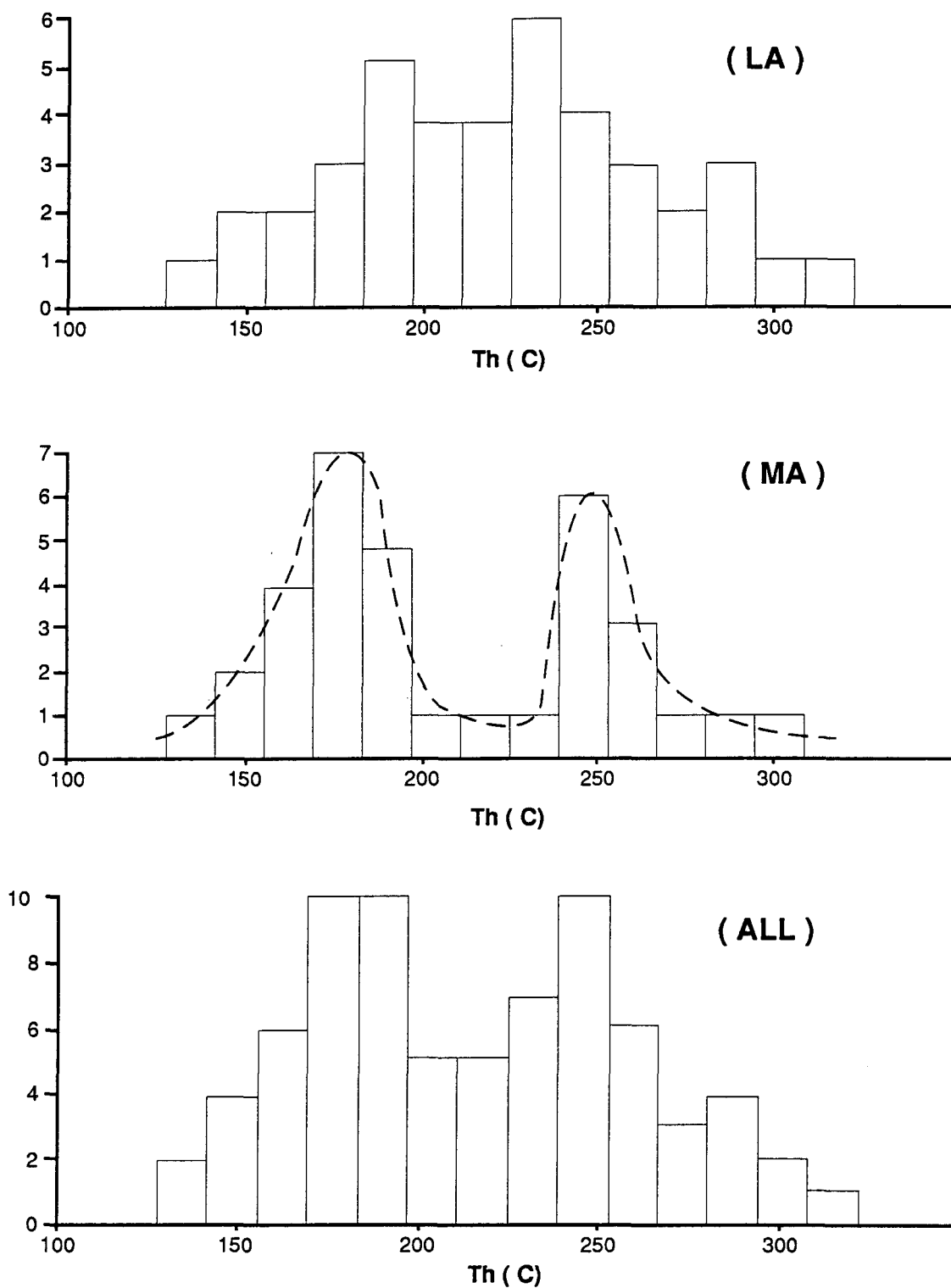
Figure 6.1 Observed homogenization temperatures of the fluid inclusions of the Hetai gold deposits

LA = low salinity H2O-CO2 fluid inclusions;   ALL = LA + MA
MA = moderate salinity aqueous fluid inclusions;

Table 6.1 Microthermal measurements of the fluid inclusions in the Hetai gold deposits, southern China

Inclusion Number	Sample Number	Location and level	Type	Host Mineral	V% at 25°C	Tfm °C	Tm(CO2) °C	Tm °C	Th(CO2) °C	Th °C	Tcm °C	Salinity wt% NaCl equi.	Bulk dens. g/cm3	Pressure MPa
A1	Bai-160-1	Gaocun, 160	LA	quartz	10	-21.3		-1.6		168.2		2.7	0.922	81
A2	Bai-160-1	Gaocun, 160	LA	quartz	10	-19.9		-1.7		141.8		2.9	0.947	91
A3	Bai-160-1	Gaocun, 160	LA	quartz	10	.	-57.1	-1.6		188.3		2.7	0.900	90
A4	Bai-160-1	Gaocun, 160	LA	quartz	15			-2.4		309.4		4.0	0.730	50
B1	Bai-160-2	Gaocun, 160	LA	quartz	10	-35.0		-1.5		220.7		2.5	0.861	105
B2	Bai-160-2	Gaocun, 160	LA	quartz	10					250.6				
B3	Bai-160-2	Gaocun, 160	C	quartz	84		-64.3		30.1					
C1	Liang-160-1	Gaocun, 160	LA	quartz	10			-2.6		233.3		4.3	0.861	76
C2	Liang-160-1	Gaocun, 160	LA	quartz	15	-20.6		-0.9		305.7	5.0	1.6	0.698	50
C3	Liang-160-1	Gaocun, 160	LA	quartz	15	-22.0		-0.9		239.6		1.6	0.822	86
C4	Liang-160-1	Gaocun, 160	LA	quartz	10		-56.7	-1.9		134.3		3.2	0.956	117
C5	Liang-160-1	Gaocun, 160	LA	quartz	10	-66.9		-2.4		177.1		4.0	0.921	127
C6	Liang-160-1	Gaocun, 160	MA	quartz	10	-61.2		-7.5		250.6		11.1	0.903	71
D1	Liang-160-2	Gaocun, 160	MA	quartz	10	-22.1		-7.7		173.3		11.4	0.979	62
D2	Liang-160-2	Gaocun, 160	LA	quartz	10	-20.6				177.8				
D3	Liang-160-2	Gaocun, 160	MA	quartz	10	-47.1		-8.5		294.0		12.3	0.864	50
D4	Liang-160-2	Gaocun, 160	MA	quartz	10	-58.9		-6.0		289.3		9.3	0.836	50
D5	Liang-160-2	Gaocun, 160	C	quartz	45		-56.3		158.3					
E1	CM17-5	Gaocun, 240	C	quartz	90		-57.4		17.6					
E2	CM17-5	Gaocun, 240	LA	quartz	13			-2.1		268.3		3.6	0.800	55
E3	CM17-5	Gaocun, 240	LA	quartz	10			-2.3		283.1		3.8	0.778	56
E4	CM17-5	Gaocun, 240	MA	quartz	10	-37.9		-9.2		277.4		13.1	0.892	63
E5	CM17-5	Gaocun, 240	MA	quartz	10	-22.1		-7.7		239.2		11.4	0.917	60
E6	CM17-5	Gaocun, 240	MA	quartz	10	-20.3		-6.1		241.6		9.4	0.898	57
E7	CM17-5	Gaocun, 240	LA	quartz	10			-0.9		250.3		1.6	0.806	70
F1	Liang-240	Gaocun, 240	C	quartz	45		-57.3		30.2					
F2	Liang-240	Gaocun, 240	C	quartz	85		-56.0		19.7					
F3	Liang-240	Gaocun, 240	C	quartz	70		-69.3		25.7					

F4	Liang-240	Gaocun, 240	MA	quartz	12	-59.3		-9.9		170.5		13.9	1.000	72
G1	CM17-3	Gaocun, 240	LA	quartz	10	-63.1		-1.0		175.2		1.7	0.908	83
G2	CM17-3	Gaocun, 240	LA	quartz	20		-57.0	-2.3		240.9		3.8	0.845	58
G3	CM17-3	Gaocun, 240	LA	quartz	10	-22.1		-1.9		135.7		3.2	0.955	74
G4	CM17-3	Gaocun, 240	MA	quartz	10	-44.2				137.6				
H1	G-14	Gaocun, 240	C	quartz	80		-58.1		29.4					
H2	G-14	Gaocun, 240	C	quartz	50		-79.3		153.9					
H3	G-14	Gaocun, 240	LA	quartz	10	-59.9		-2.4		231.5		4.0	0.860	98
I1	G-13	Gaocun, 240	LA	quartz	15	-20.1		-0.9		244.4		1.6	0.816	53
I2	G-13	Gaocun, 240	LA	quartz	15	-66.3		-1.7		279.4		2.9	0.772	51
I3	G-13	Gaocun, 240	MA	quartz	10	-21.3		-7.6		147.3		11.2	1.001	95
J1	G-12	Gaocun, 240	MA	quartz	17	-56.0		-8.4		181.8		12.2	0.977	117
J2	G-12	Gaocun, 240	MA	quartz	10	-59.3		-6.4		179.5		9.5	0.961	123
J3	G-12	Gaocun, 240	MA	quartz	10	-22.0		-9.8		144.9		13.8	1.021	171
J4	G-12	Gaocun, 240	LA	quartz	10		-57.3	-1.5		167.2	5.5	2.5	0.922	144
J5	G-12	Gaocun, 240	LA	quartz	10		-56.3	-1.5		179.1		2.5	0.909	123
J6	G-12	Gaocun, 240	C	quartz	100		-57.1		13.7					
K1	GZ-32	Gaocun, 240	LA	quartz	15					184.6				
K2	GZ-32	Gaocun, 240	LA	quartz	15	-21.3				207.3				
K3	GZ-32	Gaocun, 240	LA	quartz	15			-2.3		250.9		3.8	0.830	57
K4	GZ-32	Gaocun, 160	MA	quartz	15			-7.7		191.6		11.4	0.961	56
K5	GZ-32	Gaocun, 160	LA	quartz	20		-56.6	-1.4		200.2		2.3	0.885	83
K6	GZ-32	Gaocun, 160	LA	quartz	10	-20.3		-2.4		224.5		4.0	0.870	71
K7	GZ-32	Gaocun, 160	LA	quartz	10	-57.1		-3.0		235.3		4.9	0.864	50
K8	GZ-32	Gaocun, 160	LA	quartz	10		-56.6	-1.5		208.0		2.6	0.877	69
L1	Bai-160-3	Gaocun, 160	LA	quartz	10	-20.6		-1.5		203.7		2.5	0.883	87
L2	Bai-160-3	Gaocun, 160	LA	quartz	15	-20.7		-2.4		182.5		3.9	0.915	117
L3	Bai-160-3	Gaocun, 160	LA	quartz	10	-21.0		-2.8		227.1		4.6	0.872	103
L4	Bai-160-3	Gaocun, 160	LA	quartz	15	-20.1		-3.4		216.8		5.5	0.892	98
L5	Bai-160-3	Gaocun, 160	LA	quartz	20	-20.6		-1.5		277.6		2.6	0.771	50
L6	Bai-160-3	Gaocun, 160	LA	quartz	15	-22.1		-0.9		281.3		1.6	0.750	50

M1	Bai-160-3	Gaocun, 160	MA	quartz	10	-60.6	-9.2	173.5	13.1	0.992	103
M2	Bai-160-3	Gaocun, 160	MA	quartz	10	-20.1		158.4			
M3	Bai-160-3	Gaocun, 160	MA	quartz	15	-20.9		164.2			
M4	Bai-160-3	Gaocun, 160	MA	quartz	10	-20.6	-6.4	149.2	9.5	0.988	170
M5	Bai-160-3	Gaocun, 160	MA	quartz	10	-20.3	-7.2	154.0	10.7	0.992	133
M6	Bai-160-3	Gaocun, 160	MA	quartz	15	-20.4	-4.2	170.1	6.7	0.948	140
M7	Bai-160-3	Gaocun, 160	MA	quartz	10	-59.7		167.3			
M8	Bai-160-3	Gaocun, 160	MA	quartz	10	-56.1		169.5			
M9	Bai-160-3	Gaocun, 160	MA	quartz	15	-22.1		182.4			
M10	Bai-160-3	Gaocun, 160	MA	quartz	10	-21.5		201.4			
N1	Bai-160-4	Gaocun, 160	MA	quartz	10	-21.3		245.1			
N2	Bai-160-4	Gaocun, 160	MA	quartz	10	-60.0	-5.4	241.9	8.4	0.890	50
N3	Bai-160-4	Gaocun, 160	MA	quartz	10	-60.2	-5.8	237.8	9.0	0.898	57
N4	Bai-160-4	Gaocun, 160	MA	quartz	10			267.1			
N5	Bai-160-4	Gaocun, 160	MA	quartz	15		-6.8	245.6	10.3	0.902	60
N6	Bai-160-4	Gaocun, 160	MA	quartz	15		-5.3	170.4	8.3	0.959	96
O1	Bai-240-1	Gaocun, 240	MA	quartz	10			226.3			
O2	Bai-240-1	Gaocun, 240	MA	quartz	15			230.8			
O3	Bai-240-1	Gaocun, 240	MA	quartz	10			238.4			
O4	Bai-240-1	Gaocun, 240	MA	quartz	15			166.8			
O5	Bai-240-1	Gaocun, 240	MA	quartz	15			206.9			
O6	Bai-240-1	Gaocun, 240	MA	quartz	10			194.1			
O7	Bai-240-1	Gaocun, 240	MA	quartz	15		-6.2	234.4	9.5	0.907	78
P1	Bai-240-6	Gaocun, 240	MA	quartz	10			266.7			
P2	Bai-240-6	Gaocun, 240	MA	quartz	10		-7.2	278.2	10.8	0.868	50
P3	Bai-240-6	Gaocun, 240	MA	quartz	10		-7.2	245.9	10.7	0.906	51
P4	Bai-240-6	Gaocun, 240	MA	quartz	10			170.3			
P5	Bai-240-6	Gaocun, 240	MA	quartz	10			176.8			
P6	Bai-240-6	Gaocun, 240	MA	quartz	10			169.3			
P7	Bai-240-6	Gaocun, 240	MA	quartz	10		-8.3	130.4	12.1	1.021	60
P8	Bai-240-6	Gaocun, 240	MA	quartz	10			223.8			

ID	Sample	Location	Type	Mineral	V%	Tfm	TmCO2	Tm	Tcm	Th		wt%NaCl	density	P
R1	Bai-240-9	Gaocun, 240	LA	quartz	10			-1.5		246.0		2.6	0.824	64
R2	Bai-240-9	Gaocun, 240	LA	quartz	15			-1.7		252.1		2.8	0.818	71
R3	Bai-240-9	Gaocun, 240	LA	quartz	10			-1.5		260.0		2.6	0.801	57
R4	Bai-240-9	Gaocun, 240	LA	quartz	10					274.0				
R5	Bai-240-9	Gaocun, 240	LA	quartz	10					259.7				
R6	Bai-240-9	Gaocun, 240	LA	quartz	15					243.7				
R7	Bai-240-9	Gaocun, 240	LA	quartz	15			-1.5		130.0		2.5	0.955	88
S1	Bai-240-10	Gaocun, 240	LA	quartz	10					156.3				
S2	Bai-240-10	Gaocun, 240	LA	quartz	10					175.0				
S3	Bai-240-10	Gaocun, 240	LA	quartz	10					200.6				
S4	Bai-240-10	Gaocun, 240	LA	quartz	10					253.0				
S5	Bai-240-10	Gaocun, 240	LA	quartz	10					278.0				
T1	Bai-240-10	Gaocun, 240	MA	quartz	10			-6.4		172.3		9.8	0.968	84
T2	Bai-240-10	Gaocun, 240	MA	quartz	10			-7.1		223.0		10.6	0.927	51
T3	Bai-240-10	Gaocun, 240	MA	quartz	10					193.5				
T4	Bai-240-10	Gaocun, 240	LA	quartz	15					265.0				
T5	Bai-240-10	Gaocun, 240	MA	quartz	15			-6.9		197.8		10.4	0.948	90
T6	Bai-240-10	Gaocun, 240	MA	quartz	15			-7.4		225.6		11.0	0.927	52
T7	Bai-240-10	Gaocun, 240	MA	quartz	10			-8.6		207.8		12.4	0.950	70
U1	Bai-240-11	Gaocun, 240	LA	quartz	10	-20.1		-1.7		269.6		2.9	0.790	56
U2	Bai-240-11	Gaocun, 240	LA	quartz	15	-21.3		-2.0		307.4		3.3	0.724	53
U3	Bai-240-11	Gaocun, 240	LA	quartz	15			-2.1		256.1		3.5	0.819	62
U4	Bai-240-11	Gaocun, 240	LA	quartz	10			-3.4		310.9		5.6	0.752	50
U5	Bai-240-11	Gaocun, 240	LA	quartz	10					154.0				
U6	Bai-240-11	Gaocun, 240	LA	quartz	20					281.9				
U7	Bai-240-11	Gaocun, 240	LA	quartz	10					263.4				
V1	Bai-240-13	Gaocun, 240	LA	quartz	10					240.6				
V2	Bai-240-13	Gaocun, 240	LA	quartz	10					289.4				
V3	Bai-240-13	Gaocun, 240	LA	quartz	10					219.7				
V4	Bai-240-13	Gaocun, 240	LA	quartz	10					290.4				

LA = low-salinity H2O-CO2 fluid inclusions, MA = moderate-salinity aqueous fluid inclusions, C = non-saline CO2-rich fluid inclusions;

Tfm = first melting temperature, TmCO2=melting temperature of solid CO2, Tm = last melting temperature of ice, Th = homogenization temperature,

Tcm = melt temperature of clathrate; V% at 25° = ratio of vapor phase at room temperature, wt% NaCl equi. = weight percent salt equivalent;

Bulk density, mole fraction and pressure were calculated using the FORTRAN program FLINCOR (Brown, 1989).

the range of homogenization temperature between the CO_2-H_2O inclusion and the aqueous inclusion. This is also true between the fluid inclusions hosted by different healed fractures. However, homogenization temperature appears to differ between the fluid inclusions of various generations of host mineral. The early generations of quartz may host inclusions with both high and low homogenization temperature, and the CO_2-H_2O inclusions seem slightly more likely to be trapped by early generations of quartz. In contrast, late generations of hydrothermal quartz usually host fewer CO_2-H_2O inclusions.

Statistically, the frequency distribution of homogenization temperature shows maxima at 245° and 170°C, which is especially characteristic of the aqueous inclusions (Fig. 6.1). In the homogenization temperature vs salinity plot (Fig. 6.2), it may be seen that there is a greater proportion of CO_2-H_2O inclusions with a high Th than the aqueous inclusions, which are preferentially of low Th.

3.3 Last Melting Temperature of Ice and Salinity

1. CO_2-H_2O Inclusions

For this type of fluid inclusions, the last melting temperature of ice ranges from about -0.9 to -3.7°C (Fig. 6.3), indicating a low salinity. The corresponding equivalent NaCl content is about 1.5 to 6 wt.%. The few observed clathrate (CO_2 hydrate) melting temperatures also argue for a low salinity. In a few inclusions, CO_2 hydrate which formed upon heating frozen inclusions was recorded to melt at temperatures around 5.2°C, corresponding to a salinity of about 2.1 equiv weight percent NaCl (Collins, 1979).

2. Aqueous Inclusions

The observed last melting temperatures of ice ranges from -3.7 to -10°C, and the calculated salinity varies from about 6 to 14 equivalent weight percent NaCl (Fig. 6.3). This indicate that this type of inclusions is moderately saline, compared to 1.5 to 6% equivalent weight percent NaCl for the low-salinity CO_2-H_2O inclusions.

3. CO_2-dominated Inclusions

CO_2-dominated fluid inclusions are nearly non-saline.
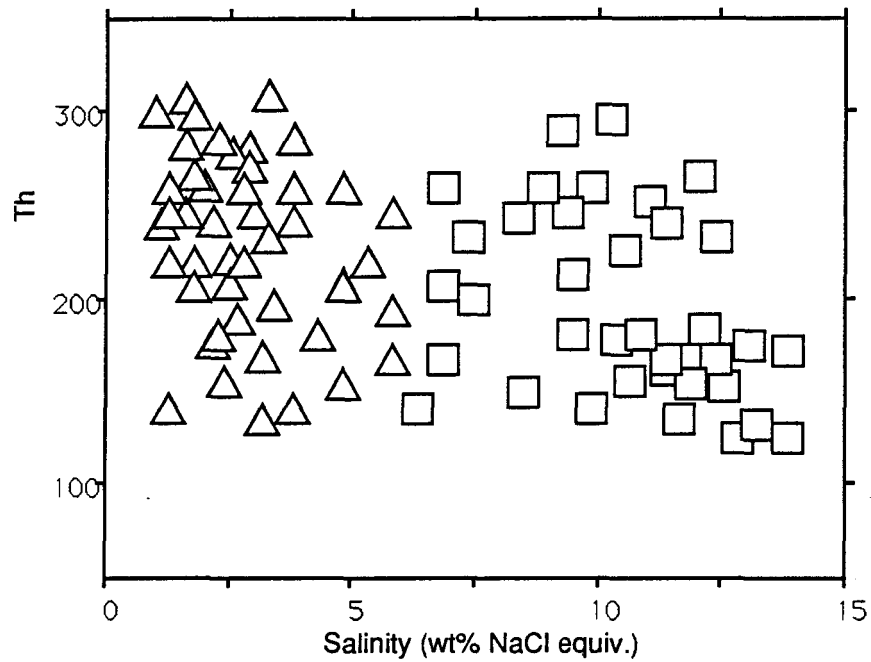
**Figure 6.2 Plot of homogenization temperature vs salinity of the fluid
inclusions of the Hetai gold field**

N.B.: Two fields are clearly distinguished: one moderate salinity (MA)
and one low salinity (LA). There is little difference in homogenization
temperature range between these two groups of fluid inclusions, but in a
general sense, LA contains greater proportion of inclusions with relative
higher Th than MA.
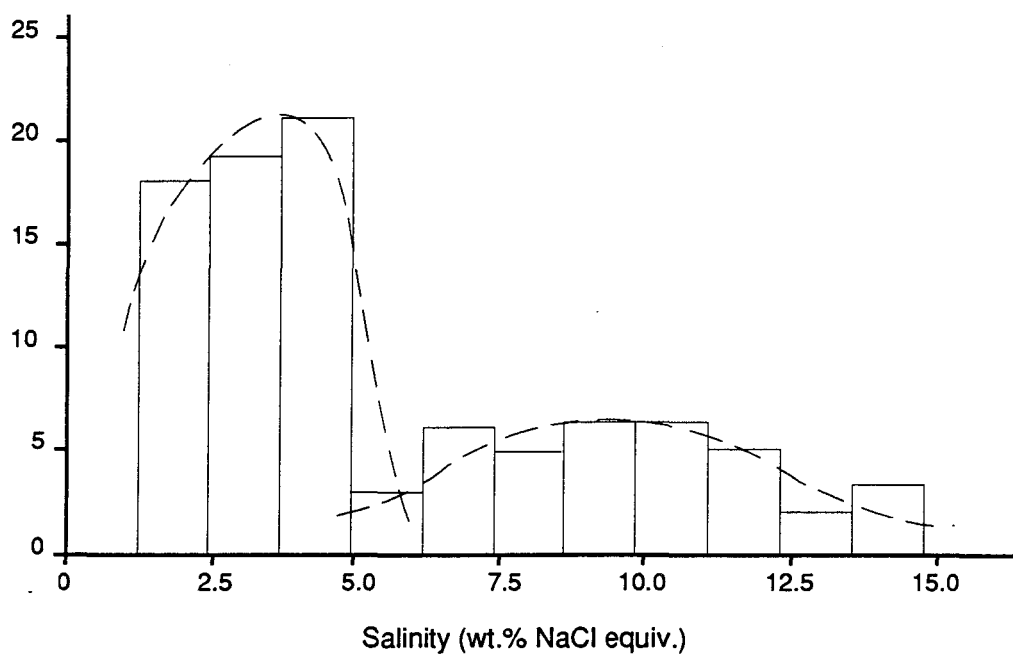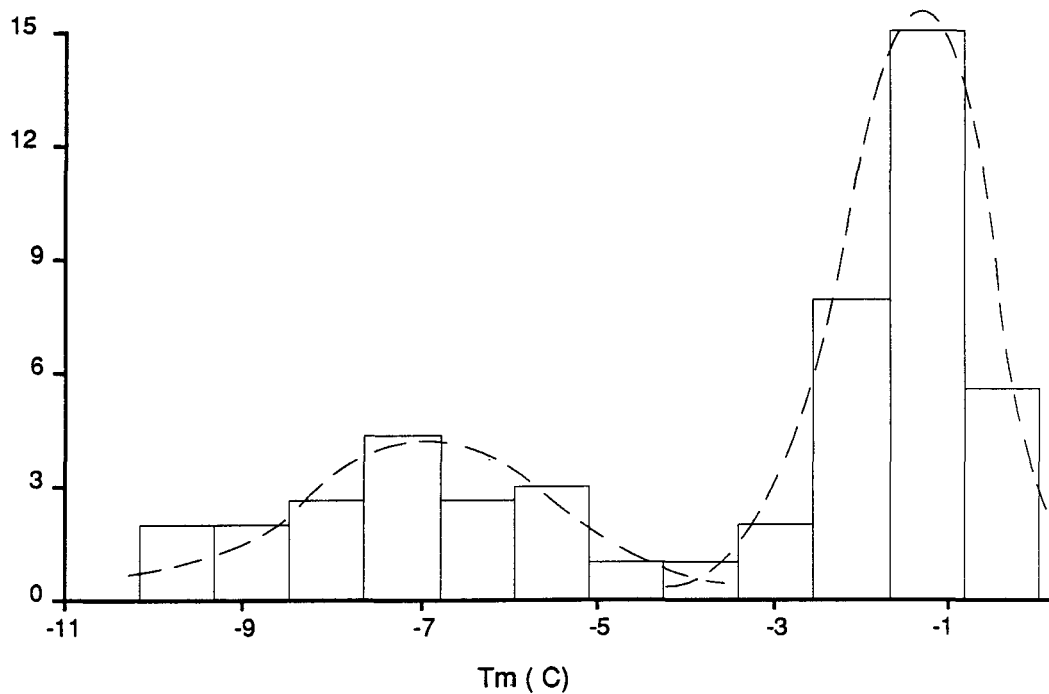
Figure 6.3 Distribution of the observed final melting temperatures (upper) and the corresponding salinities (lower) of the fluid inclusions of the Hetai gold field
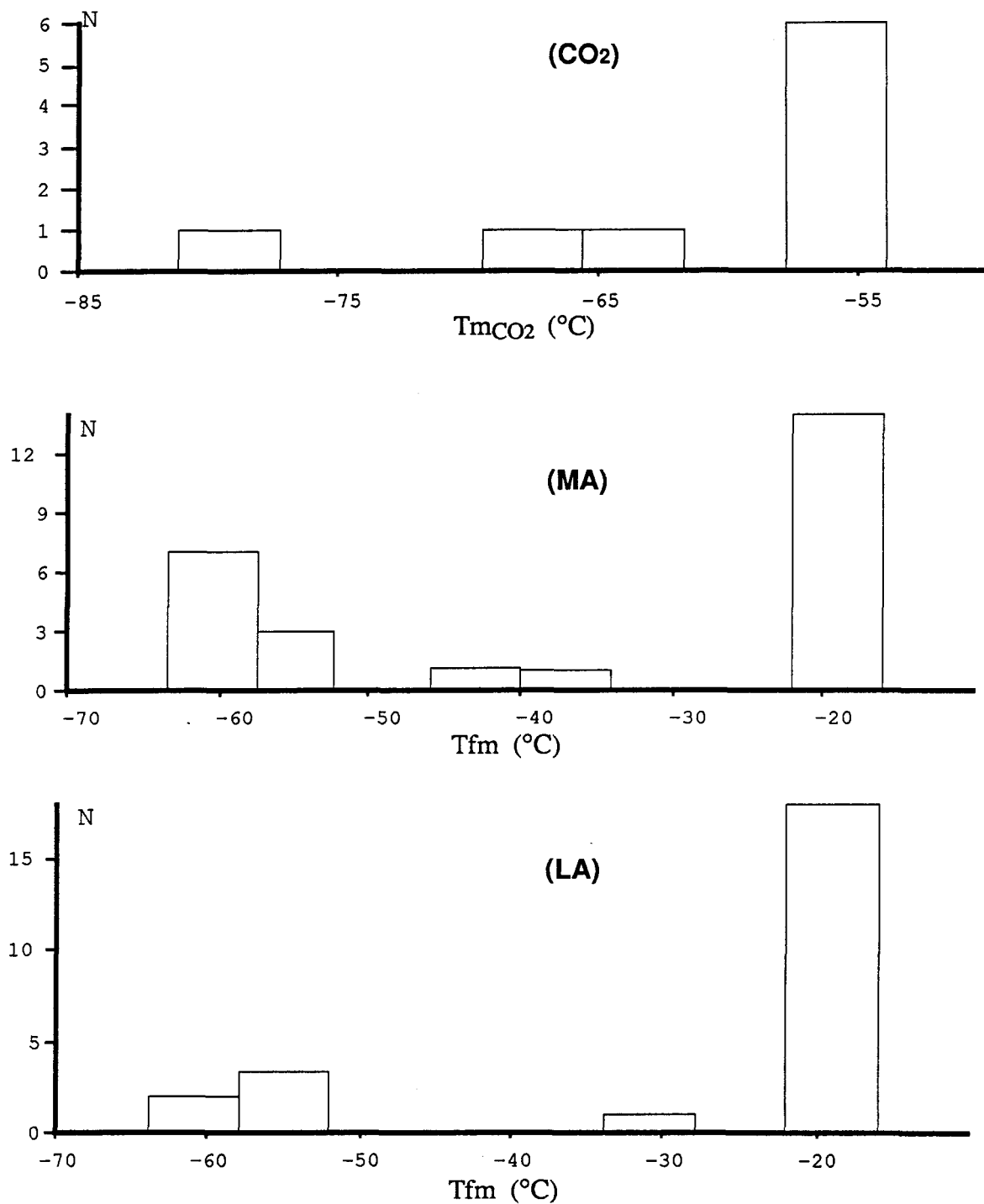
Figure 6.4 Histogram of observed first melting temperatures of the crystalline solids formed after complete freezing of the fluid inclusions of the Hetai gold deposits, southern China.

N.B.: For CO2-dominated inclusions, TmCO2, instead of Tfm, is given out.
LA = low salinity fluid inclusions; MA = moderate salinity fliud inclusions; CO2 = CO2–dominated fluid inclusions

3.4 Eutectic Melting Temperature and Chemical System

1. Aqueous Inclusions

The fluid solution contained in the inclusions completely changes into solid phases after being frozen to about -120°C. The first melting temperature of the crystalline solids of the aqueous inclusions ranges from -62°C to -20°C, with a major frequency mode at about -21°C and another minor one around -60°C (Fig. 6.4). Such observations suggests that these inclusions are a multicomponent system, with H_2O-NaCl dominated (Roedder, 1984) and possible presence of Ca^{2+} (Crawford, 1981). The wide range of first melting temperature ranges (from -62°C to -20°C) is attributed to the variable ratios (e.g. $CaCl_2$/NaCl) of dissolved salts in the multicomponent system. Previous results using inclusion leachate analysis (Dai, 1986) show that the fluid contained in the fluid inclusions of the Gaocun deposit of the Hetai gold field is characterized by $Na^+ > K^+$, $Ca^{2+} > Mg^{2+}$, and $Cl^- > SO_4^{2-}$.

2. CO_2 - H_2O Inclusions

Upon warming after complete freezing, the first melting temperature of crystalline solids usually ranges between about -67°C and -20°C (Table 6.1), with a statistical mode at about -20.8°C (Fig. 6.4). A number of H_2O - CO_2 inclusions are not detected to have a low first melting temperature, because the small size of the inclusions limits reliable observation. The eutectic temperature of around -20.8°C is an indication of NaCl. In addition, a melting temperature (Tm_{CO_2}) of around -56.6°C is observed in the central vapor bubble, indicating that the vapor bubble consists of CO_2. Therefore, these low-salinity inclusions may approximate to a H_2O - NaCl - CO_2 system. The occasional record of a first melting temperature lower than -56.6°C suggests the presence of other unknown minor components in addition to the dominant H_2O + NaCl + CO_2 components.

3. CO_2-dominated Inclusions

The first melting temperature of this group of fluid inclusions ranges between -80° and -56°C (Fig. 6.4), with a frequency maximum around -56.6°C, the eutectic temperature of the CO_2 system, and therefore suggests a CO_2-dominated system. A few inclusions record a melting temperature of lower than -56.6°C, indicating the presence of small concentrations of other gases such as CH_4 in the inclusions, in addition to the predominant CO_2.

3.5 Ambient Pressure

The pressure at which hydrothermal fluids were trapped may be estimated using the method described by Holloway (1981), Roedder (1984), and Nicholls and Crawford (1985). The principle is that the behavior of a gas under changing pressure and temperature can be approximated by the equation of gas state (de Santis et al., 1974), which depends on the effective pressure (P), temperature (T), and volume (V) of the fluid inclusion, and if the volume change of fluid inclusions is negligible, assigning a value for T will allow a solution for P. The pressure at the formation time of the fluid inclusions of the Hetai gold deposit is calculated using FLINCOR, a computer program specialized for treating fluid inclusion data by Brown (1989), and the modified Redlich Kwong equation of state (MRK). The result ranges from about 80 - 170 MPa (Table 6.1).

Estimates of the pressure at which mineralization took place can also be made using the method of intersecting isochores of CO_2-rich and H_2O-predominating immiscibility pairs (Roedder, 1984, p.279). Isochores were calculated using the program FLINCOR (1989). Two systems, H_2O-CO_2 and H_2O-NaCl, were examined. The Lam's and Brown's equations of state (Brown, 1989) were used. In several samples, H_2O-CO_2 and H_2O-NaCl types of inclusions coexist, which are attributed to the unmixing of the initial hydrothermal solution (see below) and separate entrapment in the same healed fracture system, so the pressure of entrapment may be presented by the intersection of the isochores of H_2O-CO_2 system and H_2O-NaCl system. The results indicates that the entrapment pressure of fluid inclusions at homogenization temperature is from about 50 - 150 MPa. The resultant values of pressure is nearly consistent with the pressure obtained by the first method.

§4 Oxygen and Hydrogen Isotopic Characteristics

Oxygen and hydrogen isotopes were measured for the fluid inclusions that are related to the gold episode of the Hetai gold deposits (Fu, 1988; Chen et al., 1988). Table 6.2 lists the δD and $\delta^{18}O$ values of the hydrothermal solutions contained in the fluid inclusions. δD is determined by direct analysis of the fluid inclusions hosted in the hydrothermal quartz, whereas $\delta^{18}O$ is derived from the observed $\delta^{18}O$ values using the fractionation equation of water and quartz.

Table 6.2 Oxygen and hydrogen isotopic compositions of the hydrothermal fluid related to the formation of the Hetai gold deposits

	Mineral	Homogenization temperature (°C)	∂D(fluid) (per mil)	$\partial^{18}O$ (per mil) Observed(quartz)	$\partial^{18}O$ (per mil) Calculated(fluid)	Sources
CM1501-8	quartz	150	-56.9	8.6	-0.4	(a)
ZK002-6	quartz	150	-81.5	11.5	-2.0	(a)
CM1701-1	quartz	220	-59.5	14.5	1.1	(a)
CM2301-1	quartz	255	-54.0	7.0	-0.4	(a)
G33-1A	quartz			9.2		(b)
G28-1	quartz	273-424		10.9	2.96 to 7.34	(b)
G29-2B	quartz			11.14		(b)
G30-7a	quartz	165-413	-80.2	9.7	-4.52 to 5.92	(b)
G32-3	quartz	429 (?)		11.5	8.04	(b)
G35-3	quartz	145-207		10.73	-5.21 to -0.5	(b)
G35-4	quartz	169-310		11.29	-2.62 to 4.71	(b)
574(M1701-1)	quartz	250	-59.5	11.5	2.54	(b)
CM1501-8	quartz	300	-56.9	14.5	7.61	(b)
CM2301-1	quartz	250	-54	8.6	-0.36	(b)
ZK002-6	quartz	250	-81.5	7	-1.96	(b)
G201	quartz	169-397	-71.4	10.7	-3.2 to 6.57	(b)

∂D of fluid determined by direct analysis of the fluid enclosed in the fluid inclusions of hydrothermal alteration quartz;

$\partial^{18}O$ of fluid derived from the observed $\partial^{18}O$ values of quartz using the fractionation equation of water and quartz;

Sources: (a) from Chen et al. (1988); (b) from Fu (1988)
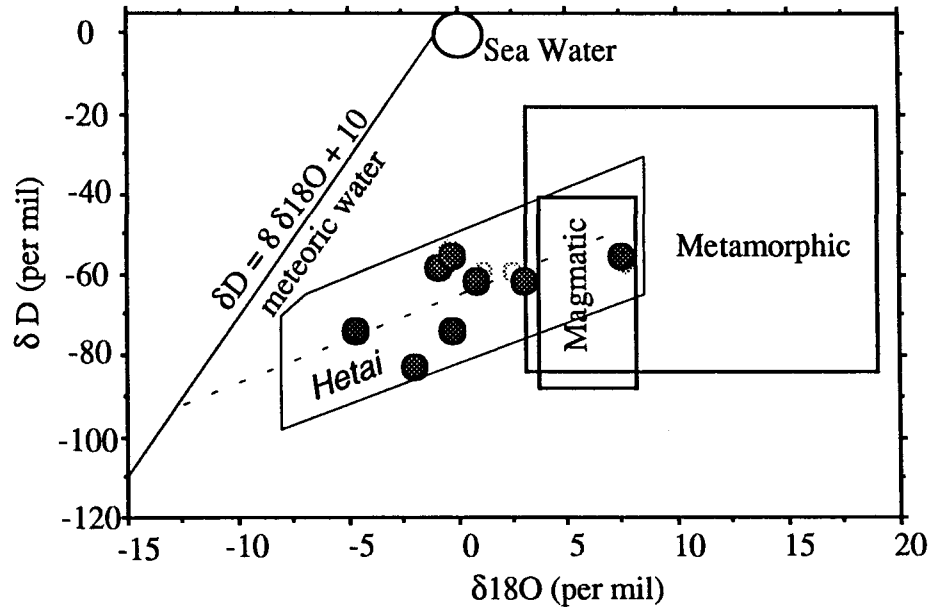
Figure 6.5   Oxygen and hydrogen isotopic diagram showing the relationship of the ore-forming fluid of the Hetai gold deposits to known fluid reservoirs

The oxygen and hydrogen isotopic data for the water component of the Hetai fluid inclusions are projected in Figure 6.5, with isotopically constrained by characterized fluid reservoirs. This figure illustrates that the Hetai hydrothermal fluid falls into the transitional zone between the meteoric line and metamorphic water field, and far from the oceanic water field.

§5 Geological and Geochemical Interpretations

5.1 Fluid Contemporaneity and Immiscibility

As shown earlier, there are sets of healed fractures of different orientation that host the secondary fluid inclusions. They cut early generations of hydrothermal quartz but end abruptly at the boundary of the last generation of sulfides and quartz, indicating that these fractures and the hosted fluid inclusions were formed during the ore-related deformation and hydrothermal alteration period. Despite the difference in abundance, the low salinity H_2O-CO_2 inclusion, moderate-salinity aqueous inclusion and CO_2-rich inclusion have no priority as to which type is associated to a specific set of healed fractures. They occasionally occur in the same host grains (Plate 6.2), suggesting a penecontemporaneity of the three fluid inclusions.

Three types of fluid inclusions imply that there were three different fluids present in the ore-forming hydrothermal system: a low-salinity H_2O-CO_2 fluid, a moderate-salinity aqueous fluid, and a non-saline CO_2-dominated fluid. In the terms of chemical composition, the first type of fluid can be produced by combining the other two. The compositional continuum of these three fluids may be the indication of the close genetic linkage among them.

It was shown by experimental data and thermodynamic calculations (Roedder, 1984) that a two-phase immiscibility domain for the H_2O-CO_2 system exists at low temperatures (Figure 6.6). The addition of NaCl to this system only extends the two-phase domain to higher temperatures (Bowers and Helgeson, 1983). A higher salinity aqueous fluid can be produced by unmixing of a relatively low-salinity H_2O-CO_2 fluid (Bowers and Helgeson, 1983). The coexistence of a moderately saline aqueous fluid with the non-saline CO_2-dominated fluid in the Hetai area can be analogous to the situation of unmixing of a low salinity H_2O-CO_2 fluid,

as found at the Sigma mine (Robert and Kelly, 1987). Unmixing may be produced by progressive cooling of the fluid or by a sudden pressure decrease.

In fact, the characteristics of the fluid inclusions occurring in the Hetai gold field may be explained if the low salinity H_2O-CO_2 fluid inclusion is assumed to represent the primary hydrothermal solution. The gradual CO_2 effervescence and sudden unmixing of a low-salinity H_2O-CO_2 fluid may result in immiscible moderate-salinity aqueous fluid and non-saline CO_2-dominated fluid, which are separately trapped in different fractures. Based on the observation of the low salinity H_2O-CO_2 fluid inclusions (c.f. Fig. 6.3), the parent homogeneous hydrothermal fluid in Hetai had a salinity of 1.5 to 6 equiv. weight percent NaCl and a CO_2 content of about 5 to 25 volume percent.

5.2 Temperature and Pressure Conditions at Fluid Entrapments

The homogenization temperature of fluid inclusions can be considered to be the minimum temperature of a primary hydrothermal fluid (Roedder, 1984). The homogenization temperature of the fluid inclusions of the Hetai gold field is not high in comparison to other replacement type of gold deposits (Colvine et al., 1988). Low homogenization temperatures was attributed (Robert and Kelly, 1987) to CO_2 effervescence from the initial aqueous fluid as a result of pressure fluctuation at the time of fluid entrapment. Such an explanation relies on the assumption that after unmixing, the aqueous and CO_2-rich fluids are trapped separately along different fractures. Once isolated in individual fractures, the two fluids are no longer in equilibrium. As a consequence, the homogenization temperature does not represent the temperature of entrapment, but is lower.

Prior to isolation of the unmixed fluids in separate fractures, the immiscible aqueous fluid phase coexisting and in equilibrium with the CO_2-rich phase must be saturated with respect to CO_2. It was shown (Robert and Kelly, 1987) that as an aqueous fluid saturated in CO_2 ascends through the ore-formation system, the lithostatic pressure decreases and CO_2 escapes from the fluid due to its decreased solubility with decreasing pressure.

Because the ore-forming system is spatially related to a ductile shear deformation zone, the confining pressure of the hydrothermal fluid system is likely to vary as a result of dynamic deformation. The actual fluid pressure could vary from lithostatic to hydrostatic,

depending on the leakage of the system (Roedder and Bodnar, 1980). In such an environment, CO_2 effervescence from the primary aqueous fluid becomes possible, and the released CO_2 would likely migrate into different fractures, separating from the parent aqueous fluid.

As demonstrated above, the estimation of confining pressure by the method of the equation of gas state of a vapor system and the method of isochore intersection of H_2O-CO_2 and H_2O-$NaCl$ systems shows that the entrapment pressure of the fluid inclusions at homogenization temperature varies from about 50 to 170 MPa. It should be pointed out that both H_2O-CO_2 and H_2O-$NaCl$ is a highly simplified system, so deviation of the calculated pressures from the real one seems inevitable. However, the estimated pressures provide a first approximation of the actual pressure.

5.3 Implications and Mechanism

Fluid inclusion data obtained from the Hetai gold field are analogous to those from many other gold deposits. It was shown that low salinity, CO_2-bearing hydrothermal fluids are characteristic of many gold deposits throughout the world, such as at the Yilgarn block, Western Australia (Ho et al., 1985), where primary H_2O-CO_2 inclusions with salinity of <2 equiv wt% NaCl were reported. Similar examples are also found at the O'Brien mine of Cadillac, Québec (Krupka et al., 1977), the McIntyre-Hollinger mine of Timmins, Ontario (Wood et al., 1986; Smith et al., 1984), the Yellowknife area, Northwestern Territory (English, 1981), and the Pamour mine, Porcupine, Ontario (Walsh et al., 1984). Two coexisting immiscible fluids, one moderately saline aqueous and the other CO_2-rich, existed in all these gold deposits.

There are indications (Krupka et al., 1977; Wood et al., 1986; Robert and Kelly, 1987; Ho et al., 1985) that the timing of peak gold precipitation in ore rocks coincides with the fluid unmixing taking place in these gold deposits. Fluid unmixing process, alternating with CO_2 effervescence, may have operated during the formation of the Hetai gold deposits (Fig. 6.6). The moderate-salinity aqueous inclusions and the CO_2-dominated inclusions are the result of unmixing of the low salinity CO_2-bearing primary ore-forming hydrothermal fluid.
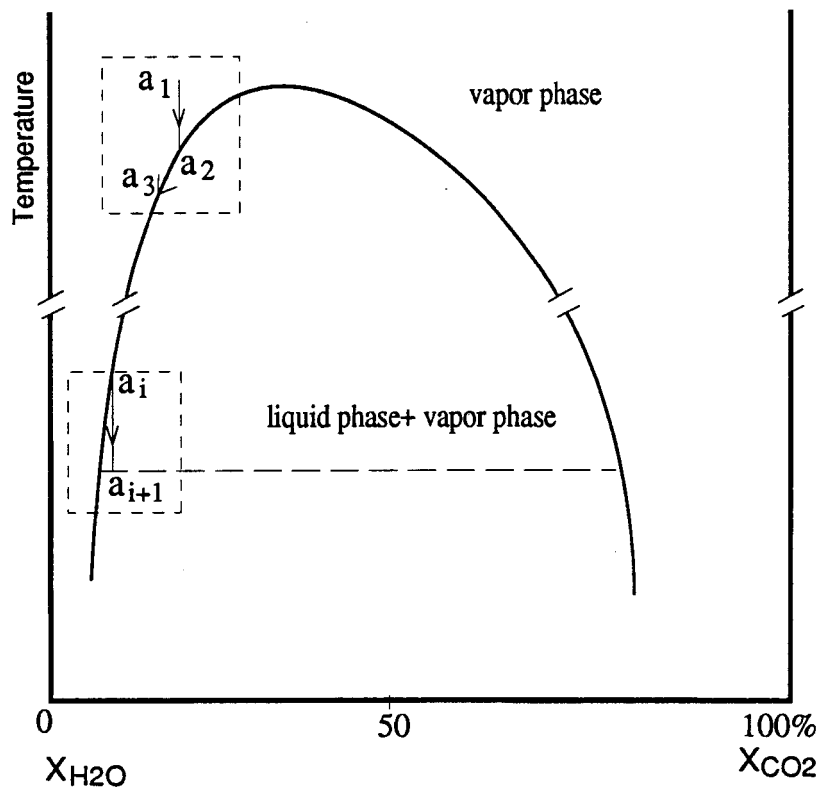
Figure 6.8 Topological composition-temperature phase diagram for the system H2O-CO2-NaCl and the evolution path of the hydrothermal solution of the Hetai gold field during gold emplacement

The evolution of the hydrothermal solution from a(2) to a(3) is characterized by CO2 effervescenCe and the entrapment of low salinity H2O-CO2 fluid inclusions; while unmixing occurs from a(i) to a(i+1), accompanied by the formation of moderate salinity aqueous inclusions and CO2 inclusions.

§6 Summary

Many fluid inclusions occur along healed fractures, and thus are secondary in origin in relation to their host mineral. However, they were formed no later than the last episode of hydrothermal alteration, and gold precipitation was closely associated both in time and in space with the entrapment of these fluid inclusions.

There are three compositional types of fluid inclusions in the Hetai gold deposits: a low-salinity (about 1.5 - 6 equivalent weight percent NaCl) H_2O-CO_2 one, a moderate-salinity (about 6 - 14 equiv. wt. % NaCl) aqueous one, and a CO_2-dominated one. Their homogenization temperature ranges from 130° to 310°C with two statistical modes around 245° and 170°C. The confining pressure of the fluid inclusions at homogenization temperature approximately ranges from 50 - 170 MPa. The studied fluid inclusions fall in the transitional zone between the meteoric line and metamorphic water field, and far from the oceanic water field in the oxygen and hydrogen isotopic diagram.

The low-salinity H_2O-CO_2 inclusions represents the primary ore-forming hydrothermal fluid. It is a H_2O-NaCl-CO_2-dominated system, with probable presence of other components such as Ca^{2+} and CH_4. During the ascent of the primary hydrothermal fluid, CO_2 effervescence and unmixing took place, with almost all the ore material remaining in the resulting aqueous phase. The unmixing of the primary hydrothermal fluid into a moderately saline aqueous phase and a non-saline CO_2-dominated phase was caused by sudden release of pressure.

Chapter VII

METALLOGENETIC MECHANISM

§1 Structural Controls

1.1 Regional Faults — Controlling the Distribution of Ore Deposits

Regional fault systems play a key role in confining the distribution of gold deposits. On a regional scale, the Yunkai gold province is limited by the Wuchuan - Sihui major fault zone on the southeast and the Bobai - Wuzhou major fault zone on the northwest (c.f. Fig. 1.2). On the district scale, all ore deposits of the Hetai gold field occur in the northwest block of the Luoding - Guangning fault zone and stretches parallel to this fault zone. From southwest to northeast occur in order the Dapingding, the Yunxi, the Shangtai, the Gaocun, the Taozishan, the Kangwei, the Huojing, and the Hehai gold deposits (c.f. Fig.1.5).

1.2 Ductile Shear Zones — Localizing Gold Mineralization

A critical aspect of the gold metallogenetic process in the Hetai area is that the main period of gold mineralization is synchronous with the shear deformation system, and the NE striking ductile shear zones control the geometry, extent, and modes of occurrence of gold orebodies. Gold abundance increases anomalously to a peak wherever a deformation zone is encountered, regardless of the original lithology of the host rock, and decreases sharply away from the deformation zone. Such a phenomenon was also observed in many gold deposits in the Archean, where gold ore bodies commonly occur in ductile deformation systems (Colvine et al., 1988; Phillips et al., 1987). This indicates that the ductile shear deformation zones are one of critical parameters for gold emplacement. Theoretically, it is natural for deformation

zones to be the preferred site of gold mineralization, as they provide focussing of ore-forming fluids and multiple channelways of efficient fluid extraction through the host rocks, a requirement to ensure efficient formation of the ores.

§2 Ore-forming Hydrothermal Fluids

2.1 Source of Fluid

The ore-forming fluid preserved in the fluid inclusions of the Hetai gold deposits is characterized by low salinity, low homogenization temperature and the presence of CO_2. This type of information, used in combination with geological, petrological and stable isotope data, can provide useful constraints on the possible sources of the ore-forming fluid.

It is unlikely that such fluid is of sedimentary origin. It is shown (Zimmerman and Kesler, 1981; Colvine et al., 1988) that diagenetic, saline fluids in sedimentary basins are usually characterized by low temperature (80° to 150°C) and moderate to high salinities, but negligible CO_2 contents. Magmatic reservoirs cannot either be the major contributor, since magmatic fluids related with high level granitic and granodioritic intrusive rocks are commonly saline aqueous brines and are trapped at high temperature (400-700°) (Nash, 1976; Kelly and Rye, 1979). That $K+>Na^+$ and $Cl^->F^-$ obtained through inclusion leachate analysis (Dai, 1986) also does not favor juvenile granitic magmas as the major source of the ore-forming fluid. Fluids derived from granitic magmas are generally characterized by $Na^+/K^+ < 1$ and $F^-/Cl^- < 1$ (Lu et al., 1990; Roedder, 1984).

Two possible sources remain, either metamorphic or meteoric. It was demonstrated (Crawford, 1981; Touret and Dietvorst, 1983; Colvine et al., 1988) that CO_2-rich fluids are typical of high grade metamorphic terrain regardless of host-rock composition. Another important characteristic of metamorphic fluids is a generally low salinity in calc-silicate rock area (Crawford, 1981). These characteristics is comparable with those of the hydrothermal fluid of the the Hetai gold field. In a study of the Archean Golden Mile gold deposit, Kalgoorlie, Phillips et al. (1987) described a sample that CO_2 and H_2O and some other elements can be extracted during metamorphism.

Hydrothermal solution evolved from meteoric water may also have the characteristics

of the fluid inclusions observed in the Hetai gold deposits. Meteoric fluids of many epithermal precious metal deposits usually have low salinity and low CO_2. When meteoric water is heated and circulated through the host rocks along deformation zones, it may obtain salts and CO_2 (Nesbitt et al., 1986; Colvine et al., 1988).

The oxygen and hydrogen isotopes of the fluid inclusions related to the gold episode of the Hetai gold deposits (c.f. Fig. 6.5) favor that the auriferous hydrothermal fluid is a mixture of metamorphic and meteoric waters. The Hetai hydrothermal fluid falls in the transitional zone between the meteoric line and metamorphic water field, and far from the oceanic water field in the δD vs $\delta^{18}O$ diagram, suggesting meteoric water may have undergone oxygen and hydrogen isotopic exchange with the metamorphic country rocks, and encountered with metamorphic fluids during its circulation. Their mixture evolved into the principal auriferous hydrothermal fluid, and finally moved up the deformation zone.

2.2 Physiochemical Conditions

The chemical system, temperature and pressure has been outlined out by the fluid inclusion study. The primary hydrothermal fluid was a H_2O-$NaCl$-CO_2-dominated system, with the presence of minor amounts of Ca^{2+}, methane and other unidentified components.

The temperature range of the hydrothermal fluid should approximate or be slightly higher than that of homogenization temperature of fluid inclusions (Roedder, 1984), which ranges from 130° to 310°C, with two peaks around 245° and 170°C respectively in the Hetai gold deposits. The confining pressure of the hydrothermal fluid was about 50 - 170 MPa during the entrapment of fluid inclusions.

§3 Possible Sources of Gold

There are various viewpoints on the identification and role of potential gold source. Phillips et al. (1987) considered that neither special Au-riched source rocks nor unreasonable large volumes of source strata are required to produce a giant gold deposit. However, Groves et al. (1989) suggested that lamprophyres represent a potential gold donor to the metamorphic-hydrothermal system of the gold mineralization in the Yilgarn Block, Western Australia, which is controlled by faults. Many strata-bound gold deposits in China have an evident

source strata (Tu, 1984). It is implicit that all rocks and strata are not of equal importance for the formation of gold deposits. A potential source may play an important role in the formation of ore deposits, and therefore the evaluation of potential gold sources appears to be helpful in understanding the entire process of gold mineralization.

Sources of gold have been addressed by numerous authors (Rock et al., 1989; Colvine et al., 1988; Macdonald, 1984; Tu, 1984; Boyle, 1979). Three points are important in the study of gold source. The first is the gold content in various types of rock. Boyle (1979) discussed the capacity of various country rocks to supply gold. It was shown (Boyle, 1979; Luan, 1987) that the abundance of gold in the crust and in many rock types is about 4 ppb. The second point is the so-called gold-enrichers and carriers. It is demonstrated (Luan, 1987) that mica and accessory minerals are generally rich in gold in comparison with other rock-forming minerals, however, the main gold-carriers may be feldspar and, sometimes, quartz, due to their high volume percentage in rocks. The last point is the ability of minerals to release gold contained in them under the influence of tectonic or thermal events. Gold contained in minerals may be redistributed and released during regional metamorphism (Luan, 1987).

3.1 Potential Source Rock

There are two different viewpoints of the gold source of the Hetai gold field. One attributes the Sinian strata to be the principal donor of gold, because of its high gold content (Chen et al., 1988; No. 719 Geol. Team, 1987). The other notes the close spatial proximity of the gold deposits and the Hercyno-Indosinian Yunluogan and Wucun granite bodies and associated granitic pegmatite veins, and considers these granitic rocks as the possible gold source (Fu, 1989). Besides these two candidates, there are other possibilities, such as a mantle source.

3.2 Geochemical Constraints

1. Trace Elements

The low gold abundance of the granites, less than 4 ppb (c.f. Ch. 2), in comparison to 10 to 15 ppb of the Sinian - Cambrian strata, does not favor the granites as the principal gold

donor. The overall low concentration of thiophile elements in granites and granitic pegmatites are also incompatible with the enrichment trend of thiophile elements in the intensely altered zones. Thiophile elements and precious elements regularly increase in abundance with incresing hydrothermal alteration in the ore zones, as shown in the preceding chapters. Therefore granitic rocks contributed, if any, at most a minor amount of gold to the gold mineralization. The fact that gold ore bodies were so far found to be hosted only within the strata instead of within the granites also seems to favor this viewpoint.

2. Rare Earth Elements

The geochemical features of rare earth elements appear to favor that the materials of the Hetai gold field were principally derived from the Sinian strata, instead of the granitic rocks. As illustrated in the Figure 5.11, the REE distribution pattern of the ore is highly analogous to that of the unaltered Sinian strata. In contrast, the altered granitic pegmatite has a completely different REE pattern, characterized by a low total content, high ratio of HREE/ LREE, and irregular "W" shape of distribution pattern. The parallelism of REE pattern of the ores and host strata suggests that the REE of the ore may has been derived from the host strata.

3. Sulfur Isotopes

The sulfur isotopes also indicate that the ore material may have originated from the host Sinian strata. As shown in Table 5.3, the sulfur isotopic composition of Fe-sulfides from the ores and host strata are comparable, with $\delta^{34}S$ value ranging from -3 to -1‰ for the ores, and from -3.1 to 0.02‰ for the strata, in relative to the Arizona's Canyon Diablon Troilite (CDT). The similarity of sulfur isotopes between the ore and the strata suggests the consistency of their initial source.

4. Lead Isotopes

Lead isotopes (c.f. Figure 5.12) demonstrate that the leads of the ores, host strata, and granites plot on a linear.array, with the Caledonian Shidong (migmatitic) granite — the Hercyno-Indosinian Yunluogan and Wucun granites — the ores — the host strata from left to right. This can be interpreted if the ore leads was derived from the Sinian strata. That the data points of the strata plot further to the right of the ore in the $^{207}Pb/^{204}Pb$ vs $^{206}Pb/^{204}Pb$ diagram means an excess of the ^{206}Pb and ^{207}Pb of the host strata over the ore. Such an excess

was derived from the radiogenic lead accumulation in the strata from the mineralization event time up to the present due to the decay of ^{238}U and ^{235}U, since the material analyzed from the host strata is the whole rock, which contains certain amounts of uranium.

In contrast, galena and pyrite were analyzed for the ores. Uranium is usually infinitesimal in galena and pyrite, and so lead isotope evolution practically ceased at the time of isolation, and the present isotope ratio presents that of the "lock in" time (Guilbert and Park, 1986). The isotope evolution equation is as following:

$$(^{20X}Pb/^{204}Pb)_{present} = (^{20X}Pb/^{204}Pb)_0 + (^{23Y}U/^{204}Pb)_{present}\,(e^{\lambda t}-1)$$

This equation may be used to deduct the radiogenic lead of the host strata accumulated since the mineralization event, and examine the consistency of the calibrated lead isotopes between the ore and the host strata, if the present $^{235}U/^{204}Pb$ and $^{238}U/^{204}Pb$ ratios are observed.

Although it was suggested (Köppel and Grünenfelder, 1979) that the linear array in lead-lead diagrams could imply incomplete mixing of two different common leads, granites alone cannot explain the anomalous lead isotope composition of the Hetai gold ores. As indicated in Table 5.4, the mineral examined in granites is K-feldspar. Similar to galena and pyrite of the ores, K-feldspar usually contains so little uranium that the presently observed $^{20X}Pb/^{204}Pb$ values approximate that of the "lock in" time. It has been shown that both the gold emplacement and the Yunluogan and Wucun granite are nearly synchronous, which means that they should have a consistent lead isotope composition if the lead of the ore came from the granites. However, the ores have evidently higher $^{20X}Pb/^{204}Pb$ ratios than the granites (Figure 5.12) where the ores plot to the right of the granites. Such isotope compositions cannot be derived just from the granites. The linearity of the granites, ore and host strata simply indicates the consistency of their initial sources: the Shidong Caledonian migmatitic granite formed the earliest, so has lowest "lock in" $^{20X}Pb/^{204}Pb$ values, next came the Hercyno-Indosinian granites and ores. Unlike galena and pyrite of the ores and K-feldspar of the Hercyno-Indosinian granite, the host strata was never isolated from a radioactive uranium source, and so have the highest $^{20X}Pb/^{204}Pb$ ratios.

Lead isotopic characteristics of the ore also shows that the mantle cannot be a major direct contributor, since the leads of the ore do not follow the single-stage growth curve. The ore scatters to the right of the zero age isochron, and has a negative model age, implying a

crustal origin, which develops in two or several stages (Köppel and Grünenfelder, 1979). Thus both sulfur and lead in the ores appear to be derived from a crustal source.

3.3 Significance of Hydrothermal Sedimentation

It is worth noting that bedded cherts, the product of a fossil geothermal system, are present in the Sinian sequence, the capable potential source strata of gold. There is evidence that the Sinian hydrothermal activity may have participated in the initial preconcentration of gold, and bedded cherts are a particular type of source rock: (1) The gold abundance of the bedded cherts are 8.7 ppb, about twice that of the crust; (2) Au is significantly associated with As in the diagnostic factor of hydrothermal sediments; (3) Most elements that are concentrated in the cherts with respect to the crust, such as Ag, As, Au, Bi, Hg, Sb and Se (Table 3.1), are also the elements that are introduced into the intensely altered zone (ore body), while most lithophile elements, such as Cs, Hf, Nb, Rb, Sc, (Ta), Th, U, Zr and REE, are consistently depleted both in the cherts and the intensely altered zone.

In addition, the relative enrichment of gold in the bedded chert formation (Z^d, top of the Sinian) also indirectly supports that the lower Sinian strata may have been an important initial gold source. As concluded in Chapter 3, the hydrothermal process, which resulted in the formation of the cherts, had accomplished some degree of recycling and homogenization of provenance components. It is likely that the gold in the cherts came from the older strata through the circulation of the early hydrothermal fluid, since that the gold abundance in the unmetamorphosed fine grained clastic rock is 20 ppb (No. 719 Geol. Team, 1987), high enough to provide the 8.7 ppb Au to the cherts, that most metal trace elements show up in the first principal factor of factor analysis representing the leaching of hydrothermal solutions, and that Au is associated with As, a diagnostic element of hydrothermal sediments.

§4 Role of Metamorphism

4.1 Spatial Correlation between Metamorphic Rock and Gold Deposit

Many gold deposits occurring in the Yunkai Terrain have a close spatial relationship with the metamorphic rocks. The metasedimentary gneiss type of gold deposit is an extreme

example. In the Jinniu ore deposit situated at Silun of Luoding county, ore bodies are concordant with the host metamorphic strata. Fine-grained native gold is finely scattered along the gneissosity planes of the metamorphic rocks, which have no signature of late deformation and hydrothermal alteration. The auriferous gneiss facies series was formed during the Caledonian period, and the strata involved is Sinian. The metamorphic series consists of fine-grained biotite-plagioclase gneiss, interbedded with hornblende-rich quartziferous beds. As in many gold deposits, there is no absolute boundary between the ore and country rocks. The ore possesses typical metamorphic textures and structures. It was attributed to be the direct result of regional metamorphism (No.719 Geological Team, 1987).

Although the metasedimentary gneiss type of gold deposits are commonly composed of low grade of ores, they may be of large scale when they are associated to late hydrothermally altered deformation zones.

4.2 Metamorphism and Redistribution of Gold

The significance of regional metamorphism lies on its basic role to redistribute gold in the potential source rocks. This may be performed in two ways: (1) Gold is released, accompanying the breakdown of the host minerals during prograde metamorphism, which is usually characterized by successive mineral reactions. Gold may leave with fluids from dehydration reactions. (2) Diffusion and transport by fluid flow and infiltration prevail when chemical reactions do not occur.

According to the discussion in Chapter 4, gold, as an impurity trace element in the souce rock, tends to migrate from high temperature fields toward lower temperature ones, or from domains with a high metamorphic grade toward domains with lower metamorphic grades, since a metamorphic district may be abstracted as a relict thermal field, and the sequence from migmatites to low grade metasediments represents an ideal profile from high to low temperature, with the migmatitic zone representing the highest part of the thermal field. This is exemplified by the Hetai area, where the abundance of gold in the Sinian strata regularly decreases with increasing metamorphic grade (Table 7.1 and Fig. 7.1). Gold is depleted in the migmatites by a factor of about one with respect to the low metamorphic grade equivalents or the inferred protolith.

Table 7.1 Gold abundances of the rocks in the Hetai area

Lithology	Average concentration (ppb)	
	(1)	(2)
Fine grained clastic rock	20	
low-grade fine grained metasediment	11.9	
low grade schist	7.8	
schist	5.8	5.2
migmatite	4.7	2.0
granite	3.0	2.5
mylonite	68.4	48.9
ore rock	>300	>1000

Sources: (1) from No.719 Geol. Team (1987); (2) from the present study
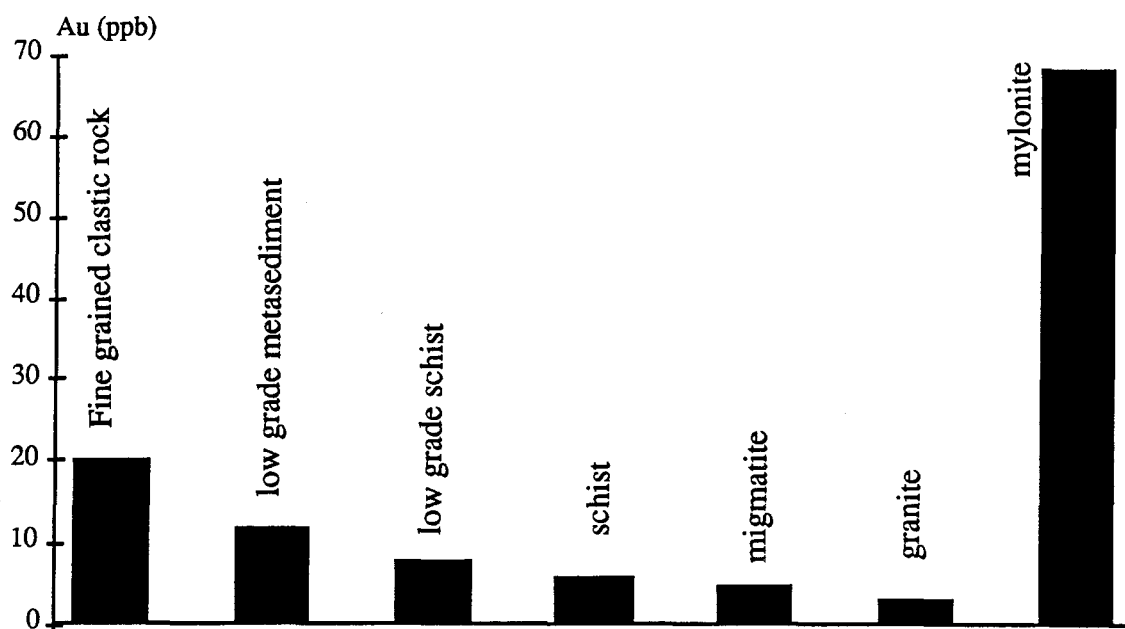
Figure 7.1 Gold abundance of various rocks in the Hetai area

Even though metamorphism causes part of gold in the source rocks to migrate out of a medium - high grade metamorphic belt, it still plays a positive role for the later gold mineralization in medium and high grade metamorphic areas. As shown in Chapter 4, rock-forming minerals such as feldspars and probably quartz may be the important gold carrier, in spite of their low gold concentration. This implies that the release and migration of gold in these big carriers to the ore sites is fundamental for the formation of a gold deposit. Although fluid flow and infiltration are effective in transport of materials when fluids are present, they are not able to directly contact the gold within the minerals. Therefore the migration of gold from the inner part of the rock-forming minerals to the weaknesses of rocks, where fluids can be more easily accessed, will become the bottleneck in the entire migration process of gold from the initial positions to the ore-forming sites. The fractal structure of entrapment paths shows that gold has another tendency of migration, from the inner part of the solid cell toward various rank sinks, including all weaknesses of rocks. This is important for the ore deposits that have their ore materials from a source rock.

The discussion above indicates that gold may be redistributed in response to elevated temperature during metamorphism. The Caledonian regional metamorphism must have played a role in the redistribution of gold in the Hetai gold field. The high temperature at which the Hetai metamorphic rock developed must have helped to establish the redistribution pattern of gold in the source strata. Such a role of metamorphism should be acknowledged in discussing the actual history of the Hetai gold deposits. The fractal structure of entrapment paths can help to explore the mechanism of the redistribution of gold during metamorphism.

§5 Role of Granites

5.1 Spatial and Temporal Relationship of Granites with Gold Deposits

No altered mylonite type of gold deposits are found within granite bodies, however, spatial relationship between granites and gold deposits is apparent. Gold deposits of the Yunkai Terrain frequently occur near a granitic intrusion (No.719 Geological Team, 1987). In addition, minor felsic vein pegmatites, which are believed to be related to the coeval granites, may occur next to the gold ore body.

There is also a temporal coincidence between the granitic magmatism and the main period of gold mineralization. In the Hetai gold field, the Yunluogan and Wucun granites and associated granitic pegmatite veins are nearly synchronous with the ore-controlled deformation and hydrothermal wall-rock alteration.

5.2 Magmatic Heat Source

Although granitic magmas are unlikely to be the principal gold source for the gold mineralization, their role in the main period of gold mineralization of the Hetai gold field should not be discounted. Granitic magmatism can have provided an external heat source necessary for initiating and driving the circulation of the ore-forming hydrothermal system, which is an integral part of the Hetai gold metallogenetic system. This is favored by the close relationships between the granites, deformation, alteration and gold deposits.

§6 Alteration and Precipitation of Gold

Hydrothermal wall-rock alteration, especially silicification and sulfidation, is characteristic of the Hetai gold deposits, and the precipitation of gold was an integral part of the hydrothermal alteration system. There is a marked increase in the abundance of gold concomitant with the appearance of sulfides in the ores, indicating that sulfidation was accompanied by the culmination of gold precipitation during the main period of gold mineralization.

Many local factors may have affected the stability of gold and led to the precipitation of gold from the hydrothermal fluid. Among them, the key factors include temperature drop, sudden release of confining pressure, and the unmixing of the hydrothermal fluid into a gas phase and a saline aqueous phase.

§7 Model of Gold Emplacement

7.1 Composite Relationship

The gold metallogenesis of the Hetai gold field is the result of many geological and geochemical processes, and a practicable genetic model must acknowledge the possible role of each of them. A possible relationship between the gold emplacement and each of the contributing factors is thus proposed in Figure 7.2. Sedimentation, regional metamorphism, granitic magmatism, deformation and hydrothermal activity, have all contributed to the formation of the Hetai gold deposits.

7.2 History of Gold: Temporal Sequence

The Hetai gold field is a consequence of many stages of evolution.

During the Precambrian to Cambrian period, a thick source strata of gold was developed. During that period gold underwent a preliminary enrichment. Hydrothermal activity of a fossil geothermal system participated in the preliminary enrichment of gold.

Regional metamorphism during the Caledonian orogeny redistributed gold in the source strata. There were two general tendencies for the redistribution of gold. One is that gold migrated from the inner part of minerals to various weaknesses in the source rocks, where gold is more accessible in subsequent events. The other is from a high temperature domain toward lower temperature ones.

The Yunluogan and Wucun granites formed, and the ductile deformation system and associated hydrothermal alteration developed during the Hercyno-Indosinian period. Gold emplacement was controlled by the deformation system. The auriferous hydrothermal fluid evolved principally from metamorphic water and meteoric water, and its circulation may have been initiated and driven by the heat source tied to the magmatism.

The deposition of gold was tied with sulfidation, and culminated in the formation of the second generation of sulfides, consisting characteristically of fine-grained anhedral pyrite
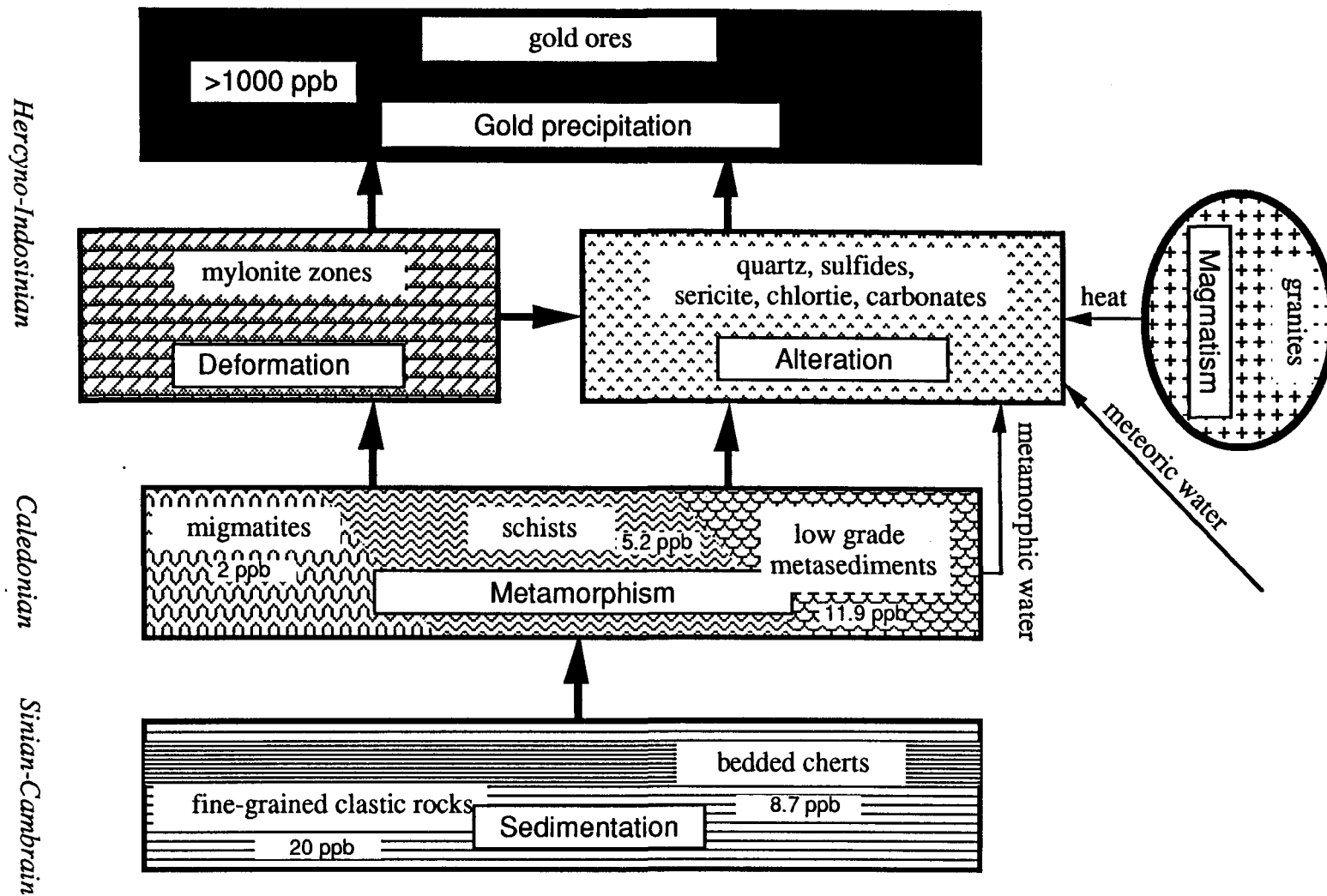
Figure 7.2 Sketch showing the metallogenetic model of the Hetai gold field

and chalcopyrite. Temperature drop, sudden release of pressure, the unmixing of the primary hydrothermal fluid were key factors leading to the deposition of gold from the ore-forming hydrothermal solution.

Chapter VIII

CONCLUSIONS

1. Regional Metamorphic Rocks and Granites

The metamorphic Sinian sequence, which is the predominant country rocks of the Hetai gold deposits, consists mainly of schists, schistose quartzite and migmatites. The characteristic mineral paragenesis is quartz + muscovite + biotite ± staurolite ± sillimanite ± almandine garnet. The metamorphic rocks developed in a medium or medium-low pressure metamorphic facies series during the Caledonian period. The temperature and pressure at which the dominant schists formed range from about 550° to 670°C and from 230 to 600 MPa, respectively. The protolith are mainly pelitic or semi-pelitic, with intercalated chert.

The migmatite is an integral part of the Hetai metamorphic series, and defines the upper end of the latter. Its formation is characterized by a gradual introduction of SiO_2, K_2O and probably Na_2O. Most metallic elements, especially sulfophile ones, are depleted with respect to the average Hetai schist. Only a few incompatible elements, such as Rb, Ta, Nb, Hf, Zr and Sc, remain unchanged or are enriched. The concentration of trace elements is controlled and balanced by two different processes: the natural tendency of trace element migration from high temperature toward lower temperature domains, and the introduction of incompatible elements accompanying the injection of the resultant melt derived from the protolith by partial melting. The REE of the migmatite inherited the REE abundance distribution pattern of the schist, with HREE slightly more preferred in migmatite than LREE.

The Shidong, Yunluogan and Wucun granites represent a complete evolution sequence from autochthonous, through parautochthonous, to intrusive magmas in the studied area. The Shidong granite developed during the Caledonian period, and has a similar origin to the coeval migmatites. The Yunluogan and Wucun granites formed during the Hercyno-

Indosinian period. Sr and O stable isotopic evidence suggests that these granites were derived from the upper crust, with the Wucun granite probably containing certain materials from a deeper source.

2. Bedded Cherts and their Origin

Bedded cherts occur within the Sinian strata. Microcrystalline quartz is the principal mineral component. Minor minerals include clay, hematite, barite and occasionally pyrite. Bedded, laminated and massive structures, as well as pseudobrecciated one, are identified. The petrographic characteristics suggest a hydrothermal origin for the cherts. The well preserved pseudobrecciated structure and low compaction degree result from rapid precipitation and transformation of opaline silica to microcrystalline quartz.

Geochemical evidence favors the viewpoint of a hydrothermal origin. The bedded cherts are characterized by consistently low TiO_2, Al_2O_3, K_2O, and most metallic elements. However, they are enriched in Ba, As, Sb, Hg and Se, which are typical of known hydrothermal deposits. In the Al - Fe -Mn ternary diagram, they fall into the "hydrothermal field".

Characteristic element associations recognized by correspondence analysis and factor analysis include {As, Au, -Cr}, {Ba, Hg, -Sn} and {Ba, Pb}, which are considered to diagnostic of hydrothermal deposits. Most trace elements show up on the leaching factor of the hydrothermal solution. Take into account the low MnO, the factors {MnO, FeO, MgO} and {Fe_2O_3} imply that the cherts formed in an oxiding-dominated sedimentary environment, with local reduction.

The rare earth elements are characterized by a generally low total content and a NASC-normalized distribution pattern ranging between the upper and the lower limits of typical hydrothermal deposits. The Ce anomaly may be either positive or negative. The ambiguous Ce anomaly and higher REE abundance of some samples are attributed to the contamination of hydrogenous deposit to hydrothermal deposit. Two manners of contamination are most possible: either by the hydrothermal processes and the hydrogenous processes alternating, or by their common presence at the same time and space domain with varying contribution rates.

A formation mechanism is proposed. The process began with the recharge of cold and dense seawater along fractures cutting through the old strata and tectonic basement of the marginal geosyncline of south China, and then the downward penetrating seawater gradually heated and reduced as it reacted with rocks at depth near an unknown heat source. The ever-evolving hydrothermal solution leached the country rocks which they passed through, and finally the silica-rich hydrothermal solutions rose and discharged, mixing with seawater and accompanied by the deposition of silica.

3. Migration Pattern of Trace Elements during Thermal Events

The relationship of infiltration and flow of fluids to diffusion is not one of replacement, but of superimposition. Despite the high effectiveness of infiltration and flow of fluids in transporting elements, diffusion is vitally important to the migration of an impurity trace element in source rocks.

The concept of "entrapment path" is a mathematical abstraction of the imperfection of bulk solids and the different diffusion behavior of trace elements in bulk solids and the contained weaknesses. In geological reality, weaknesses occur in all bulk rocks and geological domains. They are often filled with a solution film, and are much more effective for trace elements to diffuse than the "structurally perfect" cells of the host bulk solids. The mosaic of "entrapment paths" is a typical fractal structure.

There are two general tendencies for trace elements to migrate. One is that trace elements tend to migrate out of solid cells and enriched in the weaknesses. Through various rank entrapment paths, trace elements will finally joins a bulk aqueous solution filling in significantly large scale faults. The other tendency is from high temperature fields toward lower ones. High temperature and temperature gradient favor the establishment of these tendencies.

Reactivation of trace elements by diffusion is essentially a kind of short-range oriented mass transport within bulk solids and lower ranks entrapment paths. The path is the same as the migration tendency of a trace element in the fractal structure of entrapment path.

4. Ductile Shear Deformation and Alteration Related to Ore Formation

The ores of the Hetai gold field are principally auriferous altered mylonites. The Hercyno-Indosinian ductile shear zones and the associated hydrothermal alterations control the formation and occurrence of the Hetai gold deposits.

The geometrical patterns of internal features of shear zones, and the patterns of shear zones in a shear zone system are commonly similar. At all scales, the characteristic pattern is anastomosing domains of higher deformation separating rhomboid domains of lower deformation.

Zonation is a common characteristic of the ductile shear zones. Across a single ductile shear zone, the deformation gradually becomes more intense, and the corresponding deformed rock changes from undeformed primary rocks, through protomylonites, to mylonites and locally to ultramylonites, from the outside toward the deformation center.

Hydrothermal alteration is both spatially and temporally associated with the development of the ductile shear zones. The alteration products are mainly quartz, sulfides, sericite, and ankerite. The quartz of altered rocks may be distinguished into three groups: a pre-mylonite quartz, an early stage hydrothermal quartz, and a sulfide-associated quartz in the order of time. The gold precipitation is an integral part of the hydrothermal alteration system. Native gold, chalcopyrite and pyrite are the most important economic minerals. They are disseminated in the ore.

Mass equilibrium calculation shows an addition of mass with an average mass factor 1:0.92 to the unaltered initial rock during alteration. The mass addition reaches its maximum in ore bodies (intensely altered rocks characterized by the presence of sulfides), where the average mass factor is 1:0.84. Silica, precious metals, and most of thiophile elements such as Bi, Cu, Hg, Sb, Se, Te, Zn, Co, and probably As are included among the added components, whereas Na_2O, and most of lithophile elements, such as Cs, Hf, Zr, Nb, Sc, Th, Ba and REE, lost mass in alteration and mineralization. Some others (e.g., K_2O, Rb, U, Ta, W) were first added, but depleted in the intense late stage mineralization.

The ore has a similar chondrite-normalized REE distribution pattern of the unaltered Sinian strata, which is completely different to that of granitic pegmatites. The latter are

characterized by low total REE content, an irregular "W" shape, with HREE relatively enriched compared to LREE.

5. Geochemistry of Fluid Inclusions

Most fluid inclusions are secondary in origin in relation to the early stage hydrothermal quartz, and occur along healed fractures. However, petrographic evidence indicates that they were formed no later than the last episode of gold mineralization. The gold precipitation was closely associated both in time and in space with entrapment of these inclusions.

Three compositional types of fluid inclusion may be distinguished: a low-salinity (about 1.5 - 6 wt % NaCl equivalent) H_2O-CO_2 one, a moderate-salinity (about 6 - 14 wt % NaCl equivalent) aqueous one, and a CO_2-dominated one. All of these three types of fluid inclusions were contemporaneous. Their homogenization temperature ranges from 130° to 310°C with two statistical modes around 245° and 170°C, and the calculated ambient pressures are between 50 - 170 MPa. The low-salinity H_2O-CO_2 fluid inclusions is considered as the primary hydrothermal solution. It is basically a H_2O-$NaCl$-CO_2-dominated hydrothermal system, with the probable presence of small amounts of Ca^{2+}, CH_4 and other components.

CO_2 effervescence and unmixing the have alternatively taken place during the evolution of the primary hydrothermal solution. In both cases, CO_2 escaped from the hydrothermal solution, with almost all ore materials remaining in the resulting aqueous phase. Two large scale unmixing events are postulated to have taken place at 245° and 170°C.

6. Metallogenetic Mechanism

The Hetai gold deposits are a cumulative product of the integration of many stages and many geological and geochemical processes. Sedimentation, regional metamorphism, granitic magmatism, deformation and hydrothermal activities have made their contributions to the formation of the gold deposits under study.

The Sinian strata are the main gold source, as indicated by trace element, rare earth element and isotopic evidence. The presence of a fossil geothermal system in the Sinian sequence, as indicated by the study of the Z^d bedded cherts, implying the possibility that

hydrothermal activities may have taken a part in the preliminary concentration of gold during the formation of the source rock.

The Caledonian regional metamorphism played a basic role in the redistribution of gold from the host minerals to the weaknesses of the source rock, where gold is easier to to be picked up by later circulating fluids.

The Hercyno-Indosinian period is the main stage of gold mineralization. Gold emplacement was constrained by deformation zones and the associated hydrothermal alteration. The drop of temperature, sudden release of pressure, and the unmixing of the primary low salinity hydrothermal solution into a CO_2-dominated vapor phase and a moderate salinity aqueous phase, as well as the fluid interaction with Fe-bearing country rock are key factors for gold precipitation out of the hydrothermal solution. Based on petrographic and mineralogical observation, the deposition of gold culminated during the second generation of sulfidation.

The Yunluogan and Wucun granites are not the main source of gold, but provided the necessary heat source for the circulation of the ore-forming hydrothermal fluid, which is a mixture of meteoric water and metamorphic water evidenced from the fluid inclusion study.

REFERENCE

Adachi, M., Yamamoto, K. and Sugisaki, R., 1986, Hydrothermal cherts and associated siliceous rocks from the northern Pacific: their geological significance as indication of ocean ridge activity, Sedimentary Geology, **47**, 125-148

Addy, S. K., 1979, Rare earth element patterns in the manganese nodules and micronodules from northwest Atlantic, Geochimica et Cosmochimica Acta, **43**, 1105-1115

Ahrhand, S., Chatt, J. and Davies, N. R., 1958, The relative affinities of ligand atoms for acceptor molecules and ions: Chemistry Society Quartery Review, **12**, 265-276

Aitchison, J., 1981, A new approach to null correlation of proportions, Journal of Mathematical Geology, **13**, 175-189

Allègre, C. J. and Minster, J. F., 1978, Quantitative models of trace element behavior in the magmatic processes, Earth and Planetary Science Letters, **38**, 1-25

Alt, J. C., Lonsdale, P., Haymon, R. and Muehlenbachs, K., 1987, Hydrothermal sulfide and oxide deposits on seamounts near 21°N, East Pacific Rise, Geological Society America Bulletin, **98**, 157-168

Anderson, R. N., Hobart, M. A. and Langseth, M. G., 1979, Geothermal convection through oceanic crust and sediments of the Indian Ocean, Science, **204**, 828-832

Andrews, A. J., Hugon, H., Durocher, M., Corfu, F. and Lavigne, M. J., 1986, The anatomy of a gold-bearing greenstone belt: Red Lake, northwestern Ontario, Canada, *In:* Proceedings of Gold'86, an International Symposium on the Geology of Gold, Toronto, *edited by* A. J. Macdonald, 3-22

Atherton, M. P., 1968, The variation in garnet, biotite and chlorite composition in medium grade pelitic rocks from the Dalradian, Scotland, with particular reference to the zonation in garnet, Contributions to Mineralogy and Petrology, **18**, 347-371

Babcock, R. S., 1973, Computational models of metasomatic processes, Lithos, **6**, 279-290

Balashov, Y. A., Ronov, A. B., Migdisov, D. D. and Turanskaya, N. V., 1964, The effect of climate and facies environment on the fractionation of the rare earths during sedimentation, Geochemistry International, **5**, 951-969

Barber, G. A., 1985, Review on Gold '82: Proceedings of the Symposium Gold '82, Zimbabwe, Economic Geology, **80**, 780

Barbey, P. and Cuney, M., 1982, K, Rb, Ba, U and Th geochemistry of the Lapland granulites (Fennoscandia): LILE fractionation controlling factors, Contributions to Mineralogy and Petrology, **81**, 304-316

Barnes, H. L., 1979, Solubility of ore minerals, *In:* Geochemistry of Hydrothermal Ore Deposits, *edited by* H. L. Barnes, Wiley-Interscience, New York, 405-461

Barrett, T. J., 1982, Stratigraphy and sedimentology of Jurassic bedded chert overlying ophiolites in the north Apennines, Italy, Sedimentology, **29**, 353-373

Barrett, T. J., Fleet, A. J. and Friedrichsen, H., 1984, Major element, rare earth element, and O- and H- isotopic composition of metalliferous and pelagic sediments from the Galapagos mounds area, Leg 70, Initial Reports of the Deep Sea Drilling Project, Volume 70, US Government Printing Office, Wasthing, D.C.

Bender, M. L., Broecker, W., Garnitz, V., Middel, V., Kay, R., Sun, S. S. and Biscaye, P., 1971, Geochemstry of three cores from the East Pacific Rise, Earth and Planetary Science Letters, 12, 425-433

Berger, B. R. and Silbeman, M. L., 1985, Relationships of trace-element patterns to geology in hot-spring-type precious-metal deposits, *In:* Geology and Geochemistry of Epithermal Systems, *edited by* B. R. Berger and P. M. Bethke, Reviews in Economic Geology, Volume 2, Society of Economic Geologists, 233-248

Bernard-Griffiths, J., Peucat, J.-J., Iglesias Ponce de Leon, M. and Gil Ibarguchi, J. I., 1985, U-Pb, Nd isotope and REE geochemistry in eclogites from the Cabo Ortegal Complex, Galicia, Spain: an example of REE immobility conserving MORB-like patterns during high-grade metamorphism, Chemical Geology, 52, 217-225

Bertine, K. K. and Keene, M. J., 1975, Submarine barite-opal rocks of hydrothermal origin, Science, 188, 155-152

Best, M. G., 1982, Igneous and Metamorphic Petrology, W. H. Freeman and Company, San Francisco, 630p.

Beswick, A. E. and Soucie, G., 1978, A correction procedure for metasomatism in Archean greenstone belt, Precambrian Research, 6, 235-248

Bhatia, M. R., 1985, Rare earth element geochemistry of Australian Paleozoic graywackes and mud rocks: Provenance and tectonic control, Sedimentary Geology, 45, 97-114

Bickle, M. J. and McKenzie, D., 1987, The transport of heat and matter by fluids during metamorphism, Contributions to Mineralogy and Petrology, 95, 384-392

Binns, R. Boyd, T. and Scott, S., 1991, Precious metal barite spires from the Western Woodlark Basin, Papua New Guinea, Program with Abstracts, Volume 16, Geological Association of Canada, Mineralogical Association of Canada, and Society of Economic Geologists, A12

Bischoff, J. L. et al., 1981, Hydrothermal alteration of graywacke by brine and seawater: Role of alteration and chlorides complexing on metal solubilization, Economic Geology, 76, 659-676

Bischoff, J. L., 1979, Geochemistry of deep-sea sediments from the Pacific manganese nodule province: Dome Site A, B and C, *In:* Marine Geology and Oceanography of the Pacific Manganese Nodule Province, *edited by* J. L. Bischoff, Plenum Press, New York, 397-436

Bonatti, E., 1975, Metallogenesis at oceanic spreading centers, Annual Review of Earth and Planetary Science Letters, 3, 401-431

Bonatti, E., 1981, Metal deposits in the oceanic lithosphere, *In:* The Sea, *edited by* C. Emiliani, Volume 8, Wiley Interscience

Bonatti, E., Honnorez, J., Joensuu, O. and Rydell H. S., 1972, Submarine iron deposits in the Mediterranean Sea, *In:* The Mediterranean Sea, *edited by* D. J. Stanley, Ros Strondsberg Pennsylvania, 701-710

Boström, K. and Peterson, M. N. A., 1969, The origin of aluminum-poor ferromanganoan sediments in areas of high heat-flow on the East Pacific Rise, Marine Geology, 7, 427-447

Boström, K., 1975, The origin and fate of ferromanganoan active ridge sediments, Stockholm Contributions to Geology, 27, 149-243

Boulter, C. A., Fotios, M. G. and Phillips, G. N., 1987, The Golden Mile, Kalgoorlie: A giant gold deposit localized in ductile shear zones by structurally induced infiltration of an auriferous metamorphic fluid, Economic Geology, 82, 1661-1678

Bower, T. S., von Damm, K. L. and Edmond, J. M., 1985, Chemical evolution of mid-ocean ridge hot springs, Geochimica et Cosmochimica Acta, 49, 2239-2252

Bowers, T. S. and Helgeson, H. C., 1983, Calculations of the thermodynamic consequences of nonideal mixing in the system H_2O-CO_2-NaCl on phase relations in geologic systems: Metamorphic equilibria at high pressures and temperatures, American Mineralogist, 68, 1059-1075

Bowers, T. S., et al, 1985, Chemical evolution of mid-ocean ridge hot springs, Geochimica et Cosmochimica Acta, **49**, 2239-2252

Boyle, R. W., 1979, The Geochemistry of Gold and its Deposits, Geological Survey of Canada Bulletin 280, 584p.

Boyle, R. W., 1987, Gold: History and Genesis of Deposits, Society of Economic Geologists, 676p.

Brookins, D. G., 1989, Aqueous geochemistry of rare earth elements, *In:* Geochemistry and Mineralogy of Rare Earth Elements, *edited by* B. R. Lipin and G. A. McKay, Reviews in Mineralogy, Volume 21, 201-226

Brown, P. E., 1989, FLINCOR: A microcomputer program for the reduction and investigation of fluid-inclusion data, The American Mineralogist. **74**, 1390-1393

Bursnall, J. T., 1989, Mineralization and Shear Zones, Short Course Notes Volume 6, Geological Association of Canada, 299p.

Busch, G. and Schade, H., 1976, Lectures on Solid State Physics, International Series in Natural Philosophy, Volume 79, Pergamon Press, 538p.

Cameron, E. M. and Hattori, K., 1985, The Hemlo gold deposit, Ontario: A geochemical and isotopic study, Geochimica et Cosmochimica Acta, **49**, 2041-2050

Cameron, E. M. and Hattori, K., 1987, Archean gold mineralization and oxidized hydrothermal fluids, Economic Geology, **82**, 1177-1191

Canadian American Seamount Expedition, 1985, Hydrothermal vents on an axis seamount of the Juan de Fuca ridge, Nature (London), **313**, 212-214

Cann, J. R. and Strens, M. R., 1982, Black smokers fuelled by freezing magma, Nature, **298**, 147-149

Cerny, P., Fryer, B. J., Longsstaffe, F. J. and Tammemagi, H. Y., 1987, The Archean Lac du Bonnet batholith, Manitoba: igneous history, metamorphic effects, and fluid overprinting, Geochimica et Cosmochimica Acta, **51**, 421-438

Chayes, F., 1971, Ratio Correlation, University of Chicago Press

Chen, C. T., Ji, M. J. and Hu, X. T., 1988, Preliminary analysis on the ore-forming conditions of the Hetai gold deposit, Guangdong, (in Chinese), Geology of Guangdong, No.1, 1-16

Chen, X. P. and Chen, D. F, 1990, Geochemistry of upper Devonian hydrothermal mammilated chert, Guangxi, southwest China, Chinese Journal of Geochemistry, **9**, 46-53

Chi, G. X., 1992, Polygenetic Control of the Location of Proximal vs Distal Deposits in the Xinlu Tin-polymetallic Ores Field, Guangxi, Southern China, Ph. D. Thesis, Université du Québec à Chicoutimi

Choukroune, P., Francheteau, J. and Le Pichon, X., 1978, In situ observations along transform fault "P" in the FAMOUS area, Mid-Atlantic Ridge, Geological Society of America Bulletin, **89**, 1013-1029

Church, W. R., 1987, REE mobility due to alteration of Indian Ocean basalt: discussion, Canadian Journal of Earth Sciences, **24**, 192

Collins, P. L. F., 1979, Gas hydrates in CO2-bearing fluid inclusions and the use of freezing data for estimation of salinity, Economic Geology, **74**, 1435-1444

Colvine, A. C., Andrews, A. J., Cherry, M. E., Durocher, M. E., Fyon, A. J., Lavigne, M. J., Macdonald, A. J., Marmont, S., Poulsen, K. H., Springer, J. S. and Troop, D. G, 1984, An integrated model for the origin of Archean lode gold deposits, Open File Report 5524, Ontario Geological Survey, 98p.

Colvine, A. C., Fyon, J. A., Heather, K. B., Marmont, S., Smith, P. M. and Troop, D. G., 1988, Archean Lode Gold Deposits in Ontario, Miscellaneous Paper 139, Ontario Geological Survey, 136p.

Coniglio, M., 1987, Biogenic chert in the Cow Head Group (Cambro-Ordovician), western Newfoundland, Sedimentology, **34**, 813-823

Corliss, J. B., Dymond, J., Gordon, L. I., Edmond, J. M., von Herzen, R. P., Ballard, R. D., Green, K., Williams, D., Bainbridge, A., Crane, K. and van Andel, T. H., 1979, Submarine thermal springs on the Galapagos Rift, Science, 203, 1073-1083

Cox, S. F., Etheridge, M. A. and Wall, V. J., 1986, The role of fluid in syntectonic mass transport, and the localization of metamorphic vein-type ore deposits, Ore Geology Reviews, 2, 65-86

Craigie, E. R., 1986, Foreword, In: Proceedings of Gold '86, An International Symposium on the Geology of Gold: Toronto, 1986, edited by A. J. Macdonald, A. J. Macdonald

Crank, J., 1975, The Mathematics of Diffusion, Oxford University Press, London, 414p.

Crawford, M. L., 1981, Phase equilibria in aqueous fluid inclusions, Mineralogy Association of Canada Short Course Handbook, 6, 75-100

Crerar, D. A., Namson, J, Chyi, M. S., Willians, L. and Feigenson, M. D., 1982, Manganiferious chert of the Franciscan assemblage: I) General geology ancient and modern analogues and implications for hydrothermal conversion at oceanic spreading centres, Economic Geology, 77, 519-540

Crocket, J. H., 1990, Distribution of gold in the Earth's crust. Gold Metallogeny and Exploration. Glasgow, Blackie and Son.

Crocket, J. H., 1990, Noble metals in seafloor hydrothermal mineralization from the Juan de Fuca and Mid-Alantic Ridges: A Fractionation of gold from platinum metals in hydrothermal fluids, Canadian Mineralogist, 28, 639-648

Cronan, D. S., 1976, Manganese nodules and other ferro-manganese oxide deposits, In: Chemical Oceanography (2nd edition), Volume 5, edited by J. P. Riley and R. Chester, Academic Press, 217-263

Cullers, R. L., Yeh, Long-Tsu, Chaudhuri, S. and Guidotti, C. V., 1974, Rare earth elements in Silurian pelitic schists from N. W. Maine, Geochimica et Cosmochimica Acta, 38, 389-400

Dai, 1986, Investigations on Metallogenetic Geochemistry of Hetai Gold Deposit, Western Guangdong Province, unpublished M.Sc Thesis, Nanjing University, 195p.

Davies, J. F., Whitehead, R. E. S., Cameron, R.A., and Duff, D., 1982, Regional and local pattern of CO2-K-Rb-As alteration: A guide to gold in the Timmins area, In: Geology of Canadian Gold Deposits, edited by R. W. Hodder and W. Petruk, Special Volume 24, Canadian Institute of Mining and Metallurgy, 130-143

De Baar, H. J. W., Bacon, M. P. and Brewer, P. G. and Bruland, K. W., 1985, Rare earth elements in the Pacific and Atlantic Oceans, Geochimica et Cosmochimica Acta, 49, 1943-1959

De Baar, H. J. W., Bacon, M. P. and Brewer, P. G., 1983, Rare-earth distributions with a positive Ce anomaly in the Western North Atlantic Ocean, Nature, 301, 324-327

de Baar, H. J. K., German, C. R., Eldergield, H. and Van Gaans, P., 1988, Rare earth element distributions in anoxic waters of the Cariaco Trench, Geochimica et Cosmochimica Acta, 52, 1203-1220

de Santis, R., Breedveld, G. J. F. and Prausnitz, J. M., 1974, Thermodynamic properties of aqueous gas mixtures at advanced pressures, Industrial and Engineering Chemical Processes, Designs and Devices., 13., 374-377

Deer, W. A., Howie, R. A. and Zussman, J, 1982, Orthosilicates, Longman House, London and New York, 919p.

Demin, U. I. and Zolotarev, V. G., 1980, Isothermal stabilization and gradient zones in granitoid fields and the possibilities of finding mineral deposits, Geochemistry, No.5, 3-17

Dickin, A. P., 1988, Evidence for limited REE leaching from the Roffna gneiss, Switzerland — a discussion of the paper by Vocke et al. (1987), Contributions to Mineralogy and Petrology, 99, 273-275

Dickson, F. W. and Potter, J. M., 1982, Rock-brine chemical interactions: Final report, Electric Power Research Institute Project 653-2, AP-2258, 89p.

Doe, B. R. and Zartman, R. E., 1979, Plumbotectonics, The Phanerozoic Geochemistry of Hydrothermal Ore Deposits (2nd ed), John Wiley & Sons

Dymond, J., Corliss, J. B., Heath, G. R., Field, C. W., Dasch, E. J. and Veeh, H. H., 1973, Origin of metalliferous sediments from the Pacific Ocean, Bulletin of the Geology Society of America, **84**, 3355-3372

Edmond, J. M., 1980, Ridge crest hot springs: the story so far, EOS (American Geophysical Union Transaction), **61**, No.12, 129-131

Edmond, J. M., 1980, The chemistry of the 350°C hot spring at 21°N on the East Pacific Rise, EOS **61**, 992

Edmond, J. M., 1983, Hot springs at the sea-floor, American Journal of Science, **248**, No.4, 37-50

Edmond, J. M., Measures, C., Mangum, B., Grant, B., Sclater, F. R., Collier, R., Hudson, A., Gordon, L. I. and Corliss, J. B., 1979, On the formation of metal-rich deposits at ridge crests, Earth and Planetary Science Letters, **46**, 19-30

Edmond, J. M., Measures, C., McDuff, R., Chan, L. H., Collier, R., Grant, B., Gordon, L. I. and Corliss, J. B., 1979, Ridge-crest hydrothermal activity and the balances of the major and minor elements in the ocean: The Galapagos data, Earth and Planetary Science Letters, **46**, 1-18

Ehlers, E. G. and Blatt, H., 1982, Petrology — Igneous, Sedimentary and metamorphic, W. H. Freeman and Company, San Francisco, 732p.

Elderfield, H. and Greaves, M. J., 1982, The rare earth elements in seawater, Nature, **296**, 214-219

Elderfield, H., Hawkesworth, C. J., Greaves, M. J. and Calvert, S. E., 1981, Rare earth element geochemistry of oceanic ferromanganese nodules and associated sediments, Geochimica et Cosmochimica Acta, **45**, 513-528

Ellis, A. J., 1979, Explored geothermal systems, *In:* Geochemistry of Hydrothermal Ore Deposits (2nd edition), *edited by* H. L. Barnes, John Wiley and Sons, New York, 632-683

England, P. C. and Thompson, A. B., 1984, Pressure-temperature-time paths of regional metamorphism: 1) Heat transfer during the evolution of regions of thickened continental crust, Journal of Pectrology, **25**, 894-928

English, P. J., 1981, Gold-quartz veins in metasediments of the Yellowknife Supergroup, Northwest Territories: A fluid inclusion study, Unpubl. M.Sc Thesis, Edmonton, Canada, Univ. Alberta, 108p.

Etheridge, M. A., Wall, V. J., Cox, S.F. and Vernon, R. H., 1984, High fluid pressures during regional metamorphism and deformation — implications of mass transport and deformation mechanism, Journal of Geophysical Research, **89**, 4344-4358

Evans, B. W. and Guidotti, C. V., 1966, The sillimanite-potash feldspar isograd in western Maine, U.S.A., Contributions to Mineralogy anf Petrology, **12**, 25-62

Evans, B. W., 1965, Application of a reaction-rate method to the breakdown equilibria of muscovite ans muscovite plus quartz, American Journal of Science, **263**, 647-667

Faure, G., 1977, Isotope Geology, New York, John Wiley & Son, 464p.

Fediukova, E., 1977, Chemistry of garnets from granulites of the Holubor bore hole (South Bohemian Moldanubicum), J. Geol. Sci., Econ. Geol. Min. (Prague), **19**, 169-198

Fehn, U., 1986, The evolution of low-temperature convection cells near spreading centers: A mechanism for the formation of the Galapagos mounds and similar manganese deposits, Economic Geology, **81**, 1396-1407

Ferry, J. M., 1986, Infiltration of aqueous fluid and high fluid:rock ratios during greenschist facies metamorphism: A reply, Journal of Petrology, **27**, 695-714

Ferry, J. M., 1987, Metamorphic hydrology at 13 km depth and 400-500°C, The American Mineralogist, **72**, 39-58

Finlay, C. A. and Kerr, A., 1979, Garnet growth in a metapelite from the Moinian rocks of northern Sutherland, Scotland, Contributions to Mineralogy and Petrology, 71, 185-191

Finlow-Bates, T. and Stumpfl, E. F., 1981, The behavior of the so-called immobile elements in hydrothermally altered rocks associated with volcanogenic submarine-exhalative ore deposits, Mineralium Deposita, 16, 319-328

Fisher, G. W. and Elliott, D., 1973, Criteria for quasi-steady diffusion and local equilibrium in metamorphism, *In:* Geochemical Transport and Kinetics, *edited by* A. W. Hofmann, B. J. Giletti, H. S. Yoder, Jr. and R. A. Yund, Carnegie Institution of Washington, 231-242

Fleet, A. J., 1983, Hydrothermal hydrogenous ferro-manganese deposits: Do they form a continuum? The rare earth element evidence, *In:* Hydrothermal Processes at Seafloor Spreading Centers, *edited by* P. A. Rona, K. Boström, K. Laubier and K. L. Smith, Plenum Press, New York, 535-556

Fleiss, J. L., 1981, Statistical Methods for Rates and Proportions (2nd edition), John Wiley & Sons, Now York, 321p.

Fleming, B. A. and Crerar, D. A., 1982, Silicic and ionization and calculation of silica solubility at elevated temperature and pH — Application to geothermal fluid processing and reinjection, Geothermics, 11, 15-29

Folk, R. L. and McBride, E. F., 1978, Radiolarites and their relation to subjacent "oceanic crust" in Liguria, Italy, Journal of Sedimentary Petrology, 48, 1069-1102

Foster, R. P. (ed.), 1984, Proceedings of Gold'82: the Geology, Geochemistry and Genesis of Gold Deposits, Special publication 1, Geological Society of Zimbabwe,

Foster, R. P., 1989, Archean gold mineralization in Zimbabwe: Implications for metallogenesis and exploration, The Geology of Gold Deposits: The Perspective in 1988, Economic Geology Monograph 6, 54-70

Fournier, R. O. and Marshall, W. L., 1983, Calculation of amorphous silica solubilities at 25° to 300°C and apparent hydration numbers in aqueous salt solutions using the concept of effective density of water, Geochimica et Cosmochimica Acta, 47, 587-596

Fournier, R. O. and Potter, R. W. II, 1982, An equation correlating the solubility of quartz in water from 25° to 900°C at pressures up to 10,000 bars, Geochemica et Cosmochimica Acta, 46, 1969-1973

Fournier, R. O. and Truesdell, A. H., 1970, Chemical indicators of subsurface temperature applied to hot-spring waters of Yellowstone National Park, Wyoming, in Proceedings from the United Nations Symposium on the Development and Utilization of Geothermal Resources: Geothermics (Special Issue 2), Volume 2, Part 1, 529-535

Fournier, R. O., 1973, Silica in thermal waters: Laboratory and field investigations, *In:* Proceedings of International Symposium on Hydrogeochemistry and Biogeochemistry, Japan 1970, Volume 1, Hydrogeochemistry, Washington, D. C., 122-139

Fournier, R. O., 1983, A method of calculating quartz solubilities in aqueous sodium chloride solutions, Geochemica et Cosmochimica Acta, 47, 579-586

Fournier, R. O., 1985, The behavior of silica in hydrothermal solution, *In:* Geology and Geochemistry of Epithermal Systems, *edited by* B. R. Berger and P. M. Bethke, Reviews in Economic Geology, Volume 2, Society of Economic Geologists, 45-62

Franklin, J. M., Lydon, J. W. and Sangster, D. F., 1981, Volcanic-associated massive sulfide deposits, Economic Geology, 75th Anniversary Volume, 484-627

Frondel, C., 1978, Characters of quartz fibers, The American Mineralogist, 63, 17-27

Frost, B. R. and Frost, C. D., 1987, CO2, melts and granulite metamorphism, Nature, 327, 503-506

Fu, L. F., 1985, Division of metamorphic-tectonic units and the metamorphic characteristics of Guangdong Province *(in Chinese)*, Guangdong Institute of Geology, 1-46

Fu, L. F., 1988, Some considerations on the relationship between the metamorphism of fractures and gold mineralization, Geology of Guangdong, No.1, 31-44

Fu, L. F., 1989, Discussion on the genesis of Hetai gold deposit, Geology of Guangdong, 4, No.4, 35-43

Fyfe, W. S. and Kerrich, R., 1984, Gold: Natural concentration processes, *In:* Proceedings of Gold'82: the Geology, Geochemistry and Genesis of Gold Deposits, *edited by* R. P. Foster, Special Publication 1, Geological Society of Zimbabwe, 99-127

Fyfe, W. S., Price, N. J. and Thompson, A. B., 1978, Fluids in the Earth's Crust, Elsevier, New York, 383p.

Fyon, J. A. and O'Donnell, L., 1986, Regional strain state and alteration patterns related to gold mineralization in the Uchi - Confederation - Woman Lakes area, *In:* Summary of Field Work and Other Activities, *edited by* P. C. Thurston, O. L. White, R. B. Barlow, M. E. Cherry and A. C. Colvine, Miscellaneous Paper 132, Ontario Geological Survey, 266-275

Garrels, R. M., 1987, A model for the deposition of microbanded Precambrian iron formation, American Journal of Science, 287, 81-106

Garrels, R. M., Dreyer, R. M. and Howland, A. L., 1949, Diffusion of ions through intergranular spaces in water-saturatedrocks, Geological Society of America Bulletin, 60, 1809

Garrison, R. E., Rowland, S. M. and Horan, L. J., 1975, Petrology of siliceous rocks recovered from marginal seas of the western Pacific, Leg 31, Deep Sea Drilling Project, *In:* Initial Reports of Deep Sea Drilling Project, *edited by* J. C. Karig, Jr., et al., Washington, D. C., U.S. Govt. Print. Office, 31, 519-529

Geeslin, J. H. and Chafetz, H. S., 1982, Ordovician Aleman ribbon cherts: an example of silicification prior to carbonate lithification, Journal Sedimentary Petrology, 52, 1283-1293

Gibson, H. L., Watkinson, D. H. and Comba, C. D. A., 1983, Silicification: Hydrothermal alteration in an Archean geothermal system within the Amulet "Rhyolite" Formation, Noranda, Québec, Economic Geology, 78, 954-971

Gladney, E. S., Buens, C. E. and Roelandts, I., 1983, 1982 compilation of elemental concentrations in the eleven United States Geological Survey rock standards, Geostandard Newsletters, No.7, 3-226

Goldberg, E. D., 1961, Chemistry in the oceans, *In:* Oceanography, Am. Assoc. Adv. Sci. Publ. 67, 583-597

Goldberg, E. D., Koide, M., Schmitt, R. A. and Smith, R. H., 1963, Rare element distribution in the marine environment, Journal of Geophysical Research, 68, 4209-4217

Golding, S. D. and Wilson, A. F., 1983, Geochemical and stable isotope studies of the No.4 lode, Kalgoorlie, Western Australia, Economic Geology, 78, 438-450

Goldstein, S. J. and Jacbsen, S. B, 1988, Rare earth elements in river waters, Earth and Planetary Science Letters, 89, 35-47

Golubev, V. S. and Garibyants, A. A., 1971, Heterogeneous Processes of Geochemical Migration, Consults Bureau, New York, 150p.

Grant, J. A., 1985, Phase equilibria in partial melting of pelitic rocks, *In:* Migmatites, *edited by* J. R. Ashworth, Blcakie, New York, 86-144

Grant, J. A., 1986, The isocon diagram — A simple solution to Gresens' equation for metasomatic alteration, Economic Geology, 81, 1976-1982

Grauch, 1989, Rare earth elements in metamorphic rocks, *In:* Geochemistry and Mineralogy of Rare Earth Elements, *edited by* B. R. Lipin and G. A. McKay, Reviews in Mineralogy, Volume 21, 147-168

Gresens, R. L., 1967, Composition-volume relationships of metasomatism, Chemical Geology, 2, 47-55

Grinenko, V. A. and Grinenko, L. N., 1967, Fractionation of sulphur isotopes in high temperature decomposition of sulphides by water vapour, Geochemistry International. 4, 843-848

Gromet, L. P., Dymek, R. F., Haskin, L. A. and Korotev, R. L., 1984, The "North American shale composite": its compilation, major and trace element characteristics, Geochimica et Cosmochimica Acta, 48, 2469-2482

Groves, D. I. and Phillips, G. N., 1987, The genesis and tectonic control on Archean gold deposits of the western Australian shield — a metamorphic replacement model, Ore Geology Reviews, 2, 287-322

Guangdong Bureau of Geology, 1977 (unpublished), 1:200000 Geological Map of Guangdong Province (with attached description)

Guangxi Bureau of Geology and Resources, 1985, Annals of Regional Geology of Guangxi Zhang Autonomous Region, Geology Press, Beijing

Guha, J., Lu, H. Z., Robert, F. and Gagnon, M., 1991, Fluid characteristics of vein and altered wall rock in Archean mesothermal gold deposits, Economic Geology, 86, 667-684

Guha, J., Lu, H. Z. and Gagnon, M., 1990, Gas composition of fluid inclusions using solid probe mass spectrometry and its application to study of mineralizing processes, Geochimica et Cosmochimica Acta, 54, 553-558

Guichard, F., Church, T. M., Treuil, M. and Jaffrezic, H., 1979, Rare earths in barites: distribution and effects on aqueous partitioning, Geochimica et Cosmochimica Acta, 43, 983-997

Guilbert, J. M. and Park, C. F., Jr., 1986, The Geology of Ore Deposits, W. H. Freeman and Company, New York, 985p.

Gupta, H. K., 1980, Geothermal Resources: An Energy Alternative, Amsterdam, Elsevier Scientific Publishing Company, 227p.

Hajash, A., Jr., 1984, Rare earth element abundances and distribution patterns in hydrothermally altered basalts: experimental results, Contributions to Mineralogy and Petrology, 85, 409-412

Hannington, M. D. and Scott, S. D., 1988, Mineralogy and geochemistry of a silica-sulfide-sulfate deposit in the caldera of Axial Seamount, N.E. Pacific Ocean, Canadian Mineralogist, 26, 603-626

Hanson, G. N., 1978, The application of trace elements to the petrogenesis of igneous rocks of granitic composition, Earth and Planetary Science Letters, 38, 26-43

Harris, D. C, 1986, Mineralogy and geochemistry of the main Hemlo Gold Deposit, Hemlo, Ontario, Canada, In: Proceedings of Gold'86, an International Symposium on the Geology of Gold, Toronto, edited by A. J. Macdonald, 297-310

Harte, B. and Johnson, M. R. W., 1969, Metamorphic history of Dalradian rocks in Glens Clova, Esk and Lethnot, Angus, Scotland, Scottish Journal of Geology, 54-80

Haskin, L. A. and Frey, F. A., 1966, Dispersed and not-so-rare earths, Sciences, 152, 299-314

Haskin, L. A. and Gehl, M. A., 1962, The rare-earth distribution in sediments, Journal of Geophysical Research, 67, 2537-2541

Haskin, L. A., Haskin, M. A., Frey, F. A. and Wilderman, T. R., 1968, Relative and absolute terrestrial abundance of the rare-earths, In: Origin and Distribution of the Elements, edited by L. H. Ahrens, Pergamon, New York, 889-912

Haymon, R. M. and Kastner, M., 1981, Hot spring deposits on the East Pacific Rise at 21°N: preliminary description of mineralogy and genesis, Earth and Planetary Science Letters, 53, 363-381

Hein, J. R. and Scholl, D. W., 1978, Diagenesis and distribution of Late Cenozoic sediment in the southern Bering Sea, Geological Society America Bulletin, 89, 197-210

Hein, J. R., Kuijpers, E. P., Denyer, P. and Sliney, R. E., 1983, Petrology and geochemistry of cretaceous and paleogene cherts from Western Costa Rica, In: Siliceous Deposits in the Pacific Region, edited by A. Iijima, J. R. Hein and R. Seiver, Elsevier, Amsterdam, 143-174

Hein, J. R., Vallier, T., L. and Allan, M. A., 1982, Chert petrology and geochemistry, mid-Pacific mountains and Hess Rise, DSDP Leg 62, in Initial Reports of Deep Sea Drilling Project, Washington, D. C., U.S. Govt. Print. Office, 62, 711-748

Hekinian, R. and Fouquet, Y., 1985, Volcanism and metallogenesis of axial and off-axial structures on the East Pacific Rose near 13°N, Economic Geology, 80, 221-249

Helgeson, H. C and Lichtner, P. C., 1987, Fluid flow and mineral reactions at high temperatures and pressures, Journal of the Geological Society of London, 144, 313-326

Helvaci, C. and Griffin, W. L., 1983, Metamorphic feldspathization of metavolcanics and granitoids, Avnik area, Turky, Contributions to Mineralogy and Petrology, 83, 309-319

Henderson, J. H., Jackson, M. L., Syers, J. K, Clayton, R. N. and Rex, R. W., 1971, Cristobalite of authigenic origin in relation to montmorillonite and quartz origin in bentonites, Clays and Clay Minerals, 19, 229-1238

Henley, R. W. and Ellis, A. J., 1983, Geothermal systems ancient and modern: A geochemical review, Earth Science Reviews, 19, 1-50

Henley, R. W. and McNabb, A., 1978, Magmatic vapor plumes and ground-water interaction in porphyry copper emplacement, Economic Geology, 73, 1-19

Henley, R. W., Truesdell, A. H., Barton, Jr, P.B. and Whitney, J. A. (ed), 1984, Fluid-Mineral Equilibria in Hydrothermal System, Reviews in Economic Geology, Volume 1, 267p.

Herzig, P. M., Becker, K. P., Stoffers, P., Backer, H. and Blum, N., 1988, Hydrothermal silica chimney fields in the Galapagos Spring Center at 86°W, Earth and Planetary Science Letters, 89, 261-272

Hesse, R., 1988, Origin of chert, I. Diagenesis of biogenic siliceous sediment, Geoscience Canada, 15, 171-192

Hesse, R., 1989, Silica diagenesis: Original of inorganic and replacement cherts, Earth Science Reviews, 26, 253-284

Hékinian, R., 1982, Petrology of the Ocean Floor, Elsevier, Amsterdam, 393p.

Hékinian, R., Francheteau, J., Renard, V., Ballard, R. D., Choukroune, P., Cheminée, J. L., Albarède, F., Minster, J. F., Charlou, J. L., Marty, J. C. and Boulègue, J., 1983, Intense hydrothermal activity at the rise axis of the East Pacific Rise near 13°N: Submersible witnesses the growth of sulfide chimney, Marine Geology Research, 6, 1-14

Ho, S. E., Groves, D. I. and Phillips, G. N., 1986, Fluid inclusions as indicators of the nature and source of the ore fluids and ore depositional conditions for Archaean gold deposits of the Yilgarn block, Western Australia, Geological Association of South Africa Transaction, 88, 149-158

Holloway, J. R., 1981, Compositions and volumes of supercritical fluids in the earth's crust, In: Fluid Inclusions: Applications to Petrology, edited by L. S. Hollister and M. L. Crawford, Mineralogy Association Canada Short Course, 6, 13-38

Hoschek, G., 1969, The stability of staurolite and chloritoid and their significance in metamorphism of pelititc rocks, Contributions to Mineralogy anf Petrology, 22, 208-232

Hounslow, A. W. and Moore, J. M. (Jr.), 1967, Chemical petrology of Grenville Schists near Fernleigh, Ontario, Journal of Petrology, 8, 1-28

Huang, L. F., 1988, Characteristics and genesis of the granitic rocks in the Hetai area, (in Chinese), Geology of Guangdong, No.1, 45-54

Hughes, C. J., 1976, Volcanogenic cherts in the Late Precambrian Conception Group, Avalon Peninsula, Newfoundland, Canadian Journal of Geosciences, 13, 512-519

Hugon, H. and Schwerdtner, W. M., 1988, Structural signature and tectonic history of deformed gold-bearing rocks in northwestern Ontario, Open File Report 5666, Ontario Geological Survey,113p.

Hugon, H., 1986, Role of shearing in gold deposition (extended abstract), *In:* Gold'86 Poster Volume, *edited by* A. M. Charter, Konsult International Inc., Toronto, 379-387

Hugon, H., 1986, The Hemlo Gold Deposit, Ontario, Canada: A central portion of a large scale, wide zone of heterogeneous ductile shear, *In:* Proceedings of Gold '86: An International Symposium on the Geology of Gold: Toronto (1986), *edited by* A. J. Macdonald, 379-387

Hutchinson, R. W., 1982, Syn-depositional hydrothermal processes and Precambrian sulfide deposits, *In:* Precambrian Sulfide Deposits, *edited by* R. W. Hutchinson, C. D. Spence and J. M. Franklin, Special Papers, Volume 25, Geological Association of Canada, 761-791

Hutchinson, R. W., 1987, Metallogeny of Precambrian gold deposits: Space and time relationships, Economic Geology, **82**, 1993-2007

Iijima, A., Hein, J. R. and Seiver, R., 1983, Siliceous Deposits of the Pacific Region, Elsevier, N. Y., 472p.

Il'in, V. A., 1986, Active geothermal processes and crustal energetics, International Geology Review, **28**, 1262-1268

Institute of Geochemistry, Academia Sinica, 1979, Geochemistry of Granites of Southern China, Science Press, Beijing, 421p.

Janecky, D. R. and Seyfried, W. E., Jr., 1984, Formation of massive sulfide deposits on oceanic ridge crests: Incremental reaction models for mixing between hydrothermal solutions and seawater, Geochimica et Cosmochimica Acta, **48**, 2723-2738

Jäger, E., 1979, Introduction to Geochronology, *In:* Lectures in Isotope Geology, *edited by* E. Jäger and J. C. Hunziker, Springer-Verlag, Berlin, 1-12

Jones, J. B. and Segnit, F. R., 1971, The nature of opal. 1. Nomenclature and consistent phases, Journal of Geological Society of Australia, **18**, 57-68

Jurewicz, A. J. G. and Waston, E. B., 1988, Cation in olivine, Part 2: Diffusion in olivine xenocrysts, with applications to petrology and mineral physics, Contributions to Mineralogy and Petrology, **99**, p.186-201

Kano, K. and Taguchi, K., 1982, Experimental study on the ordering of opal-CT, Geothermal Journal, **16**, 33-41

Keays, R. R. and Skinner, B J., 1989, Introduction, *In:* The Geology of Gold Deposits: The Perspective in 1988, *edited by* R. R. Keays, W. R. H. Ramsay and D. I. Groves, Economic Geology Monograph 6, 1-8

Keays, R. R., Ramsay, W. R. H. and Groves, D. I. (ed.), 1989, The Geology of Gold Deposits: The Perspective in 1988, Economic Geology Monograph 6, 667p.

Keene, J. B. and Kastner, M., 1977, Clays and the formation of deep sea cherts, Nature, **249**, 754-755

Keene, J. B., 1983, Chalcedonic quartz and occurrence of quartzine (length-slow chalcedony) in pelagic sediments, Sedimentology, **30**, 449-454

Keith, T. E. C. and Muffler, L. J. P., 1978, Minerals produced during cooling and hydrothermal alteration of ash flow tuff from Yellowstone drill hole Y-5, Journal of Volcanology and Geothermal Research, **3**, 373-402

Keith, T. E. C., White, D. E. and Beeson, M. H., 1978, Hydrothermal alteration and self-sealing in Y-7 and Y-8 drill holes in northern part of Upper Geyser Basin, Yellowstone National Park Wyoming, U.S. Geological Survey Professional Paper, Volume 1054-A, 26

Kelly, W. C. and Rye, R. O., 1979, Geologic, fluid inclusion, and stable isotope study of the tin-tungsten deposits of Panasquiera, Portugal, Economic Geology, **74**, 1721-1822

Kerrich, R. and Fyfe, W. S., 1981, The gold-carbonate association: Source of CO_2 and CO_2 fixation reactions in Archaean lode deposits, Chemical Geology, **33**, 265-294

Kerrich, R. and Hodder, R. W., 1982, Achean lode gold and base metal deposits: Evidence for metal separation into separate hydrothermal systems, *In:* Geology of Canadian Gold Deposits, *edited*

by R. W. Hodder and W. Petruk, Special volume 24, Canadian Institute of Mining and Metallurgy, 144-160

Kerrich, R., 1983, Geochemistry of Gold Deposits in the Abitibi Greenstone Belt, The Canadian Institute of Mining anf Metallurgy Special Volume 27, 75p.

Kerrich, R., 1989, Archean gold: Relation to granulite formation or felsic intrusions? Geology, 17, 1011-1015

Kerrich, R., Fryer, B. J., King, R. W., Willmore, L. M. and van Hees, E., 1987, Crustal outgassing and LILE enrichment in major lithosphere structures, Archean Abitibi greenstone belt: evidence on the source reservoir from strontium and carbon isotope tracers, Contributions to Mineralogy and Petrology, 97, 156-168

Kerrich, R., Fyfe, W. S., Gorman, B. E. and Allison, I., 1977, Local modification of rock chemistry by deformation, Contributions to Mineralogy and Petrology, 65, 183-190

Klinkhammer, G., Elderfield, H. and Huson, A., 1983, Rare earth elements in seawater near hydrothermal vent, Nature, 305, 185-188

Knauth, L. P. and Epstein, S., 1975, Hydrogen and oxygen isotope ratios in silica from the JOIDES Deep Sea Drilling Project, Earth and Planetary Science Letters, 25, 1-10

Knauth, L. P. and Epstein, S., 1976, Hydrogen and oxygen isotope ratios in nodular and bedded cherts, Geochimica et Cosmochimica Acta, 40, 1095-1108

Korzhinskii, D. S, 1970 (translated by J. Agrell), Theory of Metasomatic Zoning, Clearndon Press, Oxford, 162p.

Köppel, V. and Grünenfelder, 1979, Isotope geochemistry of lead, *In:* Lectures in Isotope Geology, *edited by* E. Jäger and J. C. Hunziker, Springer-Verlag, Berlin, 134-153

Krupka, K. M., Ohmoto, H. and Wickman, F. E., 1977, A new technique in neutron activation analysis of Na/K ratios of fluid inclusions and its application to the gold-quartz veins at the O'Brien mine, Quebec, Canada, Canadian Journal of Earth Sciences, 14, 2760-2770

Kuhns, R. J., 1986, Alteration styles and trace element dispersion associated with the Golden Giant deposit, *In:* Proceeding of Gold'86, An International Symposium on the Geology of Gold, *edited by* A. J. Macdonald, Konsult International Inc., Toronto, 340-354

Kuijper, E. P. and Denyer, P., 1979, Volocanic exhalative manganese deposits of the Nicoya Ophiolite Complex, Costa Rica, Economic Geology, 74, 672-678

Laluo, C. and Brichet, E., 1982, Ages and implications of East Pacific Rise sulfide deposits at 21°N, Nature, 300, 169-171

Laluo, C., 1983, Genesis of ferromanganese deposits: hydrothermal origin, *In:* Hydrothermal Processes at Seafloor Spreading Centers, *edited by* P. A. Rona, K. Boström, K. Laubier and K. L. Smith, NATO Conference Series 4, Plenum Press, New York, 503-534

Lambert, I. B., Phillops, G. N. and Groves, D. L., 1984, Sulphur isotope compositions and genesis of Archean gold mineralization, Australia and Zimbabwe, *In:* Proceedings of Gold '82: the Geology, Geochemistry, and Genesis of Gold Deposits, *edited by* R. P. Foster, Geological Society of Zimbabwe, Special Publication 1, 373-387

Lasaga, A. C., 1981, The atomistic basis of kinetics: defects in mineral, *In:* Kinetics of Geochemical Processes, *edited by* A. C. Lasaga and R. J. Kirkpatrick, Review in Mineralogy, Volume 8, Mineralogical Society of America, 261-317

Lasaga, A. C., Richardson, S. W. and Holland, H. D., 1977, The mathematics of cation diffusion and exchange under metamorphic conditions, *In:* Energetics of Geological Processes, *edited by* Saxena and Bhattacharji, Springer-Verlag, New York, 353-388

Laschet, C., 1984, On the origin of cherts, Facies 10, 257-290

Laznicka, P., 1985, Empirical Metallogeny: Depositional Environment, Lithologic Associations and Metallic Ores, Part A, Elsevier, Amsterdam, 1002p.

Leone, M., Alaimo, R. and Calderone, S., 1975, Genesis of chlorite pellets from Mesozoic bedded cherts of Sicily, Journal of Sedimentary Petrology, 45, 618-628

Leroy, J. L. and Turpin, L., 1988, REE, Th and U behaviour during hydrothermal and supergene processes in a granitic environment, Chemical Geology, 68, 239-251

Lever, D. A. and Bradbury, M. H., 1985, Rock-matrix diffusion and its implications for radionuclide migration, Mineralogical Magazine, 49, 245-254

Lide, D. R. (ed.), 1990, Handbook of Chemistry and Physics, CRC Press, Inc., F-49, E-16

Ling, J. S., 1988, The ductile shear zones and their mineralizing characteristics in the Gaocun gold deposits, (in Chinese), Geology of Guangdong, 1, No.1, 17-24

Lister, G. S. and Snoke, A. W., 1984, S - C mylonites, Journal of Structural Geology, 6, 617-638

Liu, G. M., 1989, Outline of metamorphic rocks in Guangdong Province, Geology of Guangdong, 4, No.4, 1-19

Liu, Y. Z., Chao, L. M., Li, C. L., Wang, H. N., Chu, T. Q. and Zhang, J. R., 1984, Geochemistry of Elements, Beijing, Science Press, 548p.

Long, D. T. and Angino E. E., 1982, The mobilization of selected trace metals from shales by aqueous solutions: effects of temperature and ionic strength, Economic Geology, 77, 646-652

Lovering, T. G., 1972, Jasperoid in the United States: Its characteristics, origin, and economic significance, U.S. Geological Survey Professional Paper 710, 164p.

Lu, J. J., Wang, H. N., Shen, W. Z. and Dai, A. H., 1990, The isotopic study of the Hetai gold deposits, On Geological Exploration, 5, No.1, 84-91

Lu., H. Z., Li., B. L., Shen, K., Zhao, X. J., Yi, T. J. and Wei, J. X., 1990, Geochemistry of Fluid Inclusions, Geology Press, Beijing, 242p.

Luan, S. W. (ed.), 1987, The Geology and Prospecting of Gold Deposits, Sichuan Publishing House of Science and Technology, 435p.

Lyle, M. Heath, G. R. and Robbins, J. S., 1984, Transport and release of transition elements during early diagenesis: sequential leaching of sediments from MANOP Sites M and H, Part I. pH 5 acetic acid leach, Geochimica et Cosmochimica Acta, 48, 1705-1715

Ma, J. L., 1989, Structural Geochemistry and Metallogenesis of Ductile Shear Zones, Unpublished M.Sc Thesis, Institute of Geochemistry, Academia Sinica, 92p.

Macdonald, A. J. (ed.), 1986, Proceedings Volume of Gold '86, An International Symposium on the Geology of Gold: Toronto, 1986, 504p.

Macdonald, A. J., 1984, Gold mineralization in Ontario, I: the role of banded iron formation, In: Chibougamau - Stratigraphy and Mineralization, edited by J. Guha and E. H. Chown, Special Volume 34, Canadian Institute of Mining and Metallurgy, 412-430

MacGeehan, P. J. and MacLean, W. H., 1980, An Archean sub-seafloor geothermal system, "calc-alkali" trends, and massive sulfide genesis, Nature, 286, 767-771

MacLean, W. H. and Kranidiotis, P., 1987, Immobile elements as monitors of mass transfer in hydrothermal alteration: Phelps Dodge massive sulfide deposit, Matagami, Québec, Economic Geology, 82, 951-962

MacLean, W. H., 1988, Rare earth element mobility at constant inter-REE ratios in the alteration zone at the Phelps Dodge massive sulphide deposit, Matagami, Québec, Mineralium Deposita, 23, 231-238

MacLean, W. H., 1990, Mass change calculations in altered rock series, Mineralium Deposita, 25, 44-49

Mahon, W. A. J., Klyen, L. E. and Rhode, M., 1980, Neutral sodium/bicarbonate/sulphate hot waters in geothermal systems, Chinetsu (Journal Japanese Geothermal Energy Association), 17, 11-24

Malahoff, A., McMurthy, G. M., Wilshire, J. C. and Yeh, H. W., 1982, Geology and chemistry of hydrothermal deposits from active submarine volcano Loihi, Hawaii, Nature, 298, 234-239

Manna, S. S. and Sen, S. K., 1974, Origin of garnet in the basic granulites around Saltora, W. Bengal, Contributions to Mineralogy and Petrology, **44**. 195-218

Manning, J. R., 1973, Diffusion kinetics and mechanisms in simple crystals, *In:* Geochemical Transport and Kinetics, *edited by* A. W. Hofmann, B. J. Giletti, H. S. Yoder, Jr. and R. A. Yund, Carnegie Institution of Washington, 3-14

Marshall, W. L. and Chen, C. T. A., 1982, Amorphous silica solubilities, V. Predictions of solubility behavior in aqueous mixed electrolyte solutions to 300°C, Geochemica et Cosmochimica Acta, **46**, 289-291

Marshall, W. L., 1980, Amorphous silica solubilities, II. Activity coefficient relations and predictions of solubility behavior in salt solutions, 0-300°C, Geochemica et Cosmochimica Acta, **44**, 925-931

Matsumoto, R. and Iijima, A., 1983, Chemical sedimentology of Permo-Jurassic and Tertiary bedded cherts in central Honshu, Japan, *In:* Siliceous Deposits in the Pacific Region, *edited by* A. Iijima, J. R. Hein and R. Seiver, Elsevier, Amsterdam, 175-192

Maxchiy, V., et al., 1982, Some geochemical indicators for discrimination between diagenetic and hydrothermal metalliferous sediments, Marine Geology, **50**, 241-256

McBride, E. F. and Folk, R. L., 1979, Features and origin of Italian Jurassic radiolarites deposited on continental crust, Journal of Sedimentary Petrology, **49**, 837-869

McInnes, B. I., Crocket, J. H. and Ploeger, F. R., 1986, Wallrock alteration and fluid evolution in an Archean lode gold deposit, Lake Shore Mine, Kirkland Lake, Ontario (extended abstract), *In:* Gold'86 Poster Volume, *edited by* A. M. Chater, Konsult International Inc., Toronto, 102-104

McLennan, S. M., 1989, Rare earth elements in sedimentary rocks: Influence of provenance and sedimentary processes, *In:* Geochemistry and Mineralogy of Rare Earth Elements, *edited by* B. R. Lipin and G. A. McKay, Reviews in Mineralogy, Volume 21, 169-200

McLennan, S. M., Taylor, S. R. and McGregor, V. R., 1984, Geochemistry of Archean metasedimentary rocks from West Greenland, Geochimica et Cosmochimica Acta, **48**, 1-13

Meliers, F., Deroo, G. and Herbin, J. P., 1982, Organic-matter-rich and hypersiliceous Aptian sediments from western mid-Pacific mountains, DSDP Leg 32, in Initial Reports of Deep Sea Drilling Project, Washington, D. C., U.S. Govt. Print. Office, Volume 62, 903-921

Meyer, W. J., 1977, Chertification in the Mississippian Lake Valley Formation, Sacramento Moutains, New Mexico, Sedimentology, **24**, 75-105

Michard, A. and Albarède, F., 1986, The REE content of some hydrothermal fluids, Chemical Geology, **55**, 51-60

Michard, A., Albarede, F., Michard, G., Minster, J. F., and Charlou, J. L., 1983, Rare earth elements and uranium in high temperature solutions from East Pacific Rise hydrothermal vent field (13°N), Nature, **303**, 795-797

Mironov, A. G., Zhmodik, S. M. and Maksomova, E. A, 1981, An experimental investigation of the sorption of gold by pyrites with different thermoelectric properties, Geochemistry International, **18**, No.2, 153-160

Miyashiro, A., 1973, Metamorphism and Metamorphic Belts, Halsted Press, New York, 492p.

Mo, Z. S. and Ye, B. D., 1980, Geology of Nanling Granites, Geology Press, Beijing, 363p.

Moorby, S. A. and Cronan, D. S., 1979, Chemical composition of sediments from Sites 506, 507, 508 and 509, DSDP Leg 70, in Initial Reports of Deep Sea Drilling Project, Washington, D. C., U.S. Govt. Print. Office, **70**, 269-275

Morrow, C. A., Shi, L. Q. and Byerlee, J. D., 1984, Permeability of fault gouge under confining pressure and shear stress, Journal of Geophysical Research, **89**, 3193-3200

Mottl, M. J., 1983, Metabasalts, axial hot springs, and the structure of hydrothermal systems at mid-ocean ridges, Geological Society America Bulletin, **94**, 161-180

Murata, K. J. and Randall, R. C., 1975, Silica mineralogy and structure of the Monterey Shale, Temblor Range, California, U.S. Geological Survey, Journal of Research, 30, 567-572

Nan, Y., 1989, Outline of stratigraphy of Guangdong Province, Geology of Guangdong, 4, No.2, 1-22

Nance, W. B. and Taylor, S. R., 1976, Rare earth element patterns and crustal evolution I: Australia post-Archean sedimentary rocks, Geochimica et Cosmochimica Acta, 40, 1539-1551

Nance, W. B. and Taylor, S. R., 1977, Rare earth element patterns and crustal evolution II: Archean sedimentary rocks from Kalgoorlie, Australia, Geochimica et Cosmochimica Acta, 41, 225-231

Nash, J. T., 1976, Fluid inclusion petrology-data from porphyry copper deposits and applications to exploration, United States Geological Survey Professional Paper 907-D, 16

Neall, F. B. and Phillips, G. N., 1987, Fluid - wall rock interaction in an Archean hydrothermal gold deposit: A thermodynamic model for the Hunt Mine, Kambalda, Economic Geology, 82, 1679-1694

Nesbitt, B. E., 1986, Oxide-sulfide-silicate equilibria associated with metamorphosed ore deposits. Part I, Theoretical considerations, Economic Geology, 81, 831-840

Nicholls, J. and Crawford, M. L., 1985, Fortran programs for calculation of fluid properties from microthermometric data on fluid inclusions, Computer and Geosciences, 11, 619-645

Nicholls, J., 1988, The statistics of Pearce element diagrams and the Chayes closure problem, Contributions to Mineralogy and Petrology, 99, 11-24

Nicolas, A. and Poirier, J. P., 1976, Crystalline Plasticity and Solid State Flow in Metamorphic Rocks, John Wiley & Sons, 444p.

Nicolas, A., 1988, Principles de Tectonique (2e édition), Masson, Paris, 223p.

No.719 and 704 Geological Teams, 1983 (unpublished), Proposal on the perspective investigations (1/200,000) for gold of the western Guangdong area

No.719 Geological Team, 1987 (unpublished), Report of Geological Prospecting for the Gaocun Ore Deposit in the Hetai Gold Field, 85p.

Norton, D. L., 1978, Source lines, source regions, and path lines for fluid in hydrothermal systems related to cooling plutons, Economic Geology, 73, 21-28

Norton, D. L., 1984, Theory of hydrothermal systems, Annual Review of Earth and Planetary Sciences, 12, 155-177

Oehler, J. H., 1976, Hydrothermal crystallization of silica gel, Geological Society of American Bulletin, 87, 1143-1152

Ohashi, M., 1985, Depositional environments and chemical compositions of manganese micronodules, Journal of the Geological Society of Japan, 91, 787-803

Olesen, N. O., 1987, Plagioclase fabric development in a high-grade shear zone, Jotunheimen, Norway, Tectonophysics, 142, 291-308

Olsen, S. N, 1983, A quantitative approach to local mass balance in migmatites, In: Migmatites, Melting and Metamorphism, edited by M. P. Atherton and C. D. Gribble, Shiva Publishing Limited, UK, 201-233

Parnell, J., 1986, Devonian Magadi-type cherts in the Orcadian Basin, Journal of Sedimentary Petrology, 56, 495-500

Pearce, T. H., 1987, The identification and assessment of spurious trends in Pearce-type ratio variation diagrams: A discuss of some statistical arguments, Contributions to Mineralogy and Petrology, 97, 529-534

Pearson, R. G. (ed.), 1973, Hard and Soft Acids and Bases, Stroudsburg, Pennsyvania, 480p.

Peterson, M. N. A. and von der Borch, C. C., 1965, Chert - modern inorganic deposition in a carbonate precipitating locality, Science, 149, 1501-1503

Phillips, G. N. and DeNooy, D., 1988, High-grade metamorphic processes which influence Archean gold deposits, with particular reference to Big Bell, Australia, Journal of Metamorphic Geology, **6**, 95-114

Phillips, G. N., Groves, D. I. and Clark, M. E., 1983, The importance of host-rock mineralogy in the location of Archean epigenetic gold deposits, in Special Publication 7, Geological Society of South Africa, 79-86

Phillips, G. N., Groves, D. I.. and Brown, I. J., 1987, Source requirements for the Golden Mile, Kalgoorlie: significance to the metamorphic replacement model for Archean gold deposits, Canadian Journal of Earth Sciences, **24**, 1643-1651

Phillips, W. J., 1973, Mechanical effects of retrograde boiling and its probable importance in the formation of some porphyry ore deposits, Institute Mining Metallurgy Transcripts, Sec. B, **82**, B90-98

Phinney, W. C., 1963, Phase equilibria in the metamorphic rocks of St, Paul Island and Cape North, Nova Scotia, Journal of Petrology, **4**, 90-130

Piper, D. Z. and Graef, P. A., 1974, Gold and rare-earth elements in sediments from the East Pacific Rise, Marine Geology, **17**, 287-297

Piper, D. Z., 1974, Rare earth elements in the sedimentary cycle: a summary, Chemical Geology, **14**, 285-304

Platt, J. P., 1984, Secondary cleavages in ductile shear zones, Journal of Structural Geology, **6**, 439-442

Poirier, J. P., 1985, Creep of Crystals: High Temperature Deformation Processes in Metals, Ceramics and Minerals, Cambridge University Press, Cambridge, 260p.

Pollock, S. G., 1987, Chert formation in an Ordovician volcanic arc, Journal of Sedimentary Petrology, **57**, 75-87

Pottorf, R. J. and Barnes, H. L., 1983, Mineralogy, geochemistry and ore genesis of hydrothermal sediments from the Atlantis II Deep, Red Sea, Economic Geology Monograph Issue 5, 198-223

Ramsay, J. G., 1980, Crack-seal mechanism of rock deformation, Nature, **284**, 135-139

Ramsay, J. G., 1980, Shear zone geometry: a review, Journal of Structural Geology, **2**, 83-99

Rimstidt, J. D. and Barnes, H. L., 1980, The kinetics of silica-water reactions, Geochimica et Cosmochimica Acta, **44**, 1683-1699

Rimstidt, J. D. and Cole, D. R., 1983, Geothermal mineralization, I. The mechanism of formation of the Beowawe, Nevada, siliceous sinter deposit. American Journal of Science, **283**, 861-875

Robert, F. and Kelly, W. C., 1987, Ore-forming fluid in Archean gold-bearing quartz vein at the Sigma Mine, Abitibi greenstone belt, Québec, Canada, Economic Geology, **82**, 1464-1468

Roberts, R. G., 1987, Archean lode gold deposits, In: Ore Deposit Model, edited by R. G. Roberts and P. A. Sheahan, Geoscience Canada Reprint Series 3, 1-15

Roberts, R. G., 1987, Ore deposit model, Number 11: Archean lodge gold deposits, Geoscience Canada, **14**, 37-52

Robertson, A. H. F. and Fleet, A. J., 1976, The origin of rare earths in metalliferous sediments of the Troodos Massif, Cyprus, Earth and Planetary Science Letters, **28**, 285-394

Rock, N. M. S., 1987, The need for standardization of normalized multi-element diagrams in geochemistry: a comment, Geochemical Journal, **21**, 75-84

Rock, N. M. S., Groves, D. I, Perring, C. S. and Golding, S. D., 1989, Gold, lamprophyres and porphyries: What does their association mean? The Geology of Gold Deposits: The Perspective in 1988, Economic Geology Monograph 6, 609-625

Roedder, E. and Bodnar, R. J., 1980, Geologic pressure determinations from fluid inclusions studies: Annual Review of Earth and Planetary Sciences, **8**, 263-301

Roedder, E., 1984, Fluid inclusion evidence on the environments of gold deposition, *In:* Proceedings of Gold'82: the Geology, Geochemistry and Genesis of Gold Deposits, *edited by* R. P. Foster, Special Publication 1, Geological Society of Zimbabwe, 129-163

Roedder, E., 1984, Fluid Inclusions: Reviews of Mineralogy, **12**, 644p.

Rogers, D. S., 1979, Archean precious-metal hydrothermal systems, Dome Mine, Abitibi greenstone belt: I) Pattern of alteration and metal distribution, Canadian Journal of Earth Sciences, **16**, 421-439

Rollinson, H. R. and Robert, C. R., 1986, Ratio correlations and major element mobility in altered basalts and komatiites, Contributions to Mineralogy and Petrology, **93**, 89-97

Romberger, S. B., 1986, The solution chemistry of gold applied to the origin of hydrothermal deposits, *In:* Gold in the Western Shield, *edited by* Lloyd A. Clark, Special Volume38, Canadian Institute of Mining and Metallurgy, 168-186

Romberger, S. B., 1987, Disseminated gold deposits, *In:* Ore Deposit Model, *edited by* R. G. Roberts and P. A. Sheahan, Geoscience Canada Reprint Series 3, 21-30

Rona, P. A., 1984, Hydrothermal mineralization at seafloor spreading centers, Earth Science Reviews, **20**, 1-104

Rona, P. A., Boström, K., Laubier, K. and Smith, K. L. (ed.), 1983, Hydrothermal Processes at Seafloor Spreading Centers, Plenum Press, New York, 796p.

Ronov, A. B., Balashov, Y. A., Girin, Y. P., Bratishki, R. K. and Kazakov, G. A., 1974, Regularities of rare-earth element distribution in the sedimentary shell and in the crust of the earth, Sedimentology, **21**, 171-193

Rosenbauer, R. J. and Bischoff, J. L., 1983, Uptake and transport of heavy metal by heated seawater: a summary of the experimental results, *In:* Hydrothermal Processes at Seafloor Spreading Centers, *edited by* P. A. Rona, K. Boström, K. Laubier and K. L. Smith, NATO Conference Series 4, Plenum Press, New York, 177-197

Rosenbauer, R. J., 1983, Hydrothermal alteration of graywacke and basalts by 4 mol. NaCl, Economic Geology, 1701-1710

Ross, G. M. and Chiarenzelli, J. R., 1985, Paleoclimatic significance of widespread Proterozoic silcretes in the Bear and Churchill Provinces of the northwestern Canadian Shield, Journal of Sedimentary Petrology, **55**, 196-204

Rothbaum, H. P., Anderton, B. H., Harrison, R. F., Rhode, A. G. and Slatter, A., 1979, Effect of silica polymerization and pH on geothermal scaling, Geothermics, **8**, 1-20

Rösler, H. J. and Lange, H., 1972, Geochemical Tables, Edition Leipzig, 393p.

Rubin, D. M. and Friedman, G. M., 1981, Origin of chert grains and a halite-silcrete bed in the Cambrian and Ordovician Whitehall Formation of Eastern New York State, Journal of Sedimentary Petrology, **51**, 69-72

Rumble, D. III, 1982, The role of perfectly mobile components in metamorphism, Annual Review of Earth and Planetary Sciences, **10**, 221-233

Rybach, L., et al. (ed.), 1981, Geothermal Systems: Principles and Case Histories, John Wiley &Son, New York,

Sahu, K. N., 1973, Garnets from khondalites of Tapang, Orissa, Journal of Geology and Mining Metallurgy Society of India, **45**, 211-214

Sawyer, E. W., 1987, The role of partial melting and fractional crystallization in determining discordant migmatite leucosome compositions, Journal of Petrology, **28**, 445-473

Schidlowski, M., Eichmann, R. and Junge, C. E., 1975, Precambrian sedimentary carbonates: C and O isotope geochemistry and implications for the terrestrial oxygen budget, Precambrian Research, **2**, 1-69

Schwarcz, H. P. and Ress, C. E., 1985, Sulphur isotope studies of Archean gold deposits, Grant 202, *In:* Geoscience Research Grant Program, Summary of Research 1984-1985, *edited by* V. G. Milne, Ontario Geological Survey Miscellaneous Paper 127, 151-156

Scott, S. D., Hannington and Herzig, P. M.,1989, Gold-rich massive sulfide deposits of the modern ocean floor and their ancient analogues, Terra Abstracts, 1, 7

Secor, D. T., Jr., 1965, Role of fluid pressure in jointing, American Journal of Science, 263, 633-646

Seward, T. M., 1973, Thio complexes of gold in hydrothermal ore solutions, Geochimica et Cosmochimica Acta, 37, 379-399

Seward, T. M., 1984, The transport and deposition of gold in hydrothermal systems, *In:* Proceedings of Gold'82: the Geology, Geochemistry and genesis of Gold Deposits, *edited by* R. P. Foster, Special Volume 1, Geological Society of Zimbabwe, 165-182

Shearme, S., Cronan, D. S. and Rona, P. A., 1983, Geochemistry of sediments from TAG hydrothermal field, M. A. R. at latitude 26°N , Marine Geology, 51, 269-291

Shimizu, H., et al, 1977, Cerium in cherts as indicator of marine environment of its formation, Nature, 266, No.24, 346-348

Sibson, R. H., 1987, Earthquake rupturing as a mineralizing agent in hydrothermal systems, Geology, 15, 701-704

Silberschmidt, V. V. and Silberschmidt, V. G., 1990, Fractal models in rock fracture analysis, Terra Nova, 2, 484-188

Simonson, B. M., 1987, Early silica cementation and subsequent diagenesis in areites from four Early Proterozoic Iron Formations of North America, Journal of Sedimentary Petrology, 57, 494-511

Skibsted, L. H. and Bjerrum, J., 1974, Studies on gold complexes, II: The equilibrium between gold(I) and gold(III) in the ammonia system and the standard potentials of the couples involving gold diamminegold(I) and tetramminegold(III), Acta Chimia Scandinavia, 28, 764-770

Smith, T. J., Cloke, P. L. and Kesler, S. E., 1984, Geochemistry of fluid inclusions from the McIntyre-Hollinger gold deposit, Timmins, Ontario, Canada, Economic Geology, 79, 1265-1285

Spear, F. S. and Cheny, J. T., 1989, A petrogenetic grid for pelitic schists in the system SiO2-Al2O3-FeO-MgO-K2O-H2O, Contributions to Mineralogy and Petrology, 101, 149-164

Spooner, E. T. C., Burrows, D. R., Callan, N. J., De Ronde, C. E. J. and Wood, P. C., 1987, High hydrothermal fluid pressures, hydraulic fracturing and fluid pressure dilation of shear zones in Archean Au-quartz vein systems (abstract), in Program with Abstracts, Summer Field Meeting, Geological Association of Canada, Yellowknife

Spooner, E. T. C., Wood, P. C., Burrows, D. R., Thomas, A. V., and Noble, S. R.,1985, Geological, fluid inclusion, and isotopic(carbon and sulphur) studies of Au-quartz-carbonate-pyrite-scheelite vein mineralization and intrusion-hosted Cu-(Au-Mo) mineralization in the Hollinger-Mcintyre system, Timmins, Ontario, Grant 236, *In:* Geoscience Research Grant Program, Summary of Research 1984-1985, *edited by* V. G. Milne, Ontario Geological Survey, Miscellaneous Paper 127, 229-246

Stahle, H. J., Raith, M., Hoernes, S. and Delfs, A., 1987, Element mobility during incipient granulite formation at Kabbaldurga, southern India, Journal of Petrology, 28, No.5, 803-834

Staudigel, H. and Hart, S. R., 1983, Alteration of basaltic glass: Mechanisms and significance for the oceanic crust-seawater budget, Geochimica et Cosmochimica Acta, 47, 337-350

Stauffer, R. E. and Thompson, J. M., 1984, Arsenic and antimony in geothermal waters of Yellowstone National Park, Wyoming, USA, Geochimica et Cosmochimica Acta, 48, 2547-2561

Stein, C. L., 1982, Silica recrystallization in petrified wood, Journal of Sedimentary Petrology, 52, 1277-1282

Stordal, M. C. and Wasserburg, G. J., 1986, Neodymium isotopic study of Baffin Bay water: sources of REE from very old terrains, Earth and Planetary Science Letters, 77, 259-272

Sugisaki, R., 1979, Chemical composition of argillaceous sediments around the Yamato Bank in the Japan sea, Geological Survey of Japan Cruise Report, No.13, 75-88

Sugisaki, R., 1980, Major element chemistry of the Japan Trench sediments, Legs 56 and 57, Deep Sea Drilling Project, *In:* Initial Reports of the Deep Sea Drilling Project, US Government Printing Office, Wasthing, D.C., *edited by* M. Langseth, H. Okada et al., 1233-1249

Sugisaki, R., 1981, Major-element chemistry of bottom sediments from the GH 79-1 area, the northern Central Pacific Basin, Geological Survey of Japan Cruise Report 15, 236-244

Sugisaki, R., 1984, Relation between chemical composition and sedimentation rate of Pacific ocean-floor sediments deposited since the middle Cretaceous: Basin evidence for chemical constraints on depositional environments of ancient sediments, Journal of Geology, **92**, 235-259

Tatsumoto, G. R., Knignt, R. J. and Allegre, C. J., 1973, Time difference in the formation of meteorites as dertermined from the ratio of lead-207 to lead-206, Science, **180**, 1279-1283

Taylor, S. R. and McLennan, S. M., 1985, The Continental Crust: Its Composition and Evolution, Blackwell, Oxford, 312p.

Taylor, S. R. and McLennan, S. M., 1988, The significance of the rare earths in geochemistry and cosmochemistry, *In:* Handbook on the Physics and Chemistry of Rare Earths, Volume 11, *edited by* K. A. Gschneider and L. Eyring, Elsevier, Amsterdam, 485-580

Thompson, A. B., 1987, Some aspects of fluid motion during metamorphism, Journal of the Geological Society of London, **144**, 309-312

Thomson, J., Carpenter, M. S. N., Colley, S., Wilson, T. R. S., Elderfield, H. and Kennedy, H., 1984, Metal accumulation rates in northwest Atlantic pelagic sediments, Geochimica et Cosmochimica Acta, **48**, 1935-1948

Tivey, M. K. and Delaney, J. R., 1986, Growth of large sulfide structures on the Endeavour Segment of the Juan de Fuca Ridge, Earth and Planetary Science Letters, **77**, 303-317

Toth, J. R., 1980, Deposition of submarine crusts rich in manganese and iron, Bulletin of the Geology Society of America, **91**, 44-54

Touret, J. and Dietvorst, P., 1983, Fluid inclusions in high-grade anatectic metamorphites, Journal of the Geological Society of London, **140**, 635-649

Trocine, R. P. and Trefry, J. H., 1988, Distribution and chemistry of suspended particles from an active hydrothermal vent site on the Mid-Atlantic Ridge at 26°N, Earth and Planetary Science Letters, **88**, 1-15

Trommsdorff, V. and Skippen, G., 1986, Vapour loss ("boiling") as a mechanism for fluid evolution in metamorphic rocks, Contributions to Mineralogy and Petrology, **94**, 317-322

Tu, G. Z. et al., 1984, Geochemistry of the Strata-bound Ore Deposits of China (Volume 1), Science Press, Beijing

Van Weering, T. C. E. and Klaver, G. Th., 1985, Trace element fractionation and distribution in turbidites, homogeneous and pelagic deposits, the Zaire Fan, Southeast Atlantic Ocean, Geo-Mar. Lett., **5**, p165-170

Varenstov, I. M., Timofeev, P. P. and Rateev, M. A., 1982, Geochemical history of post Jurassic sedimentation in the central northwestern Pacific, western mid-Pacific mountains, DSDP Site 463, in Initial Reports of Deep Sea Drilling Project, Washington, D. C., U.S. Govt. Print. Office, **62**, 785-804

Veizer, J. and Jansen, S. L., 1979, Basement and sedimentary recycling and continental evolution, Journal of Geology, **87**, 341-370

Veizer, J. and Jansen, S. L., 1985, Basement and sedimentary recycling -2: time dimension to global tectonics, Journal of Geology, **93**, 625-643

Vernon, R. H., 1976, Metamorphic Processes: Reactions and Microstructure Development, George Allen & Unwin Ltd, London, 243p.

Vocke, R. D., Jr., Hanson, G. N. and Grunenfelder, M., 1987, Rare earth element mobility in the Roffna Gneiss, Switzerland, Contributions to Mineralogy and Petrology, 95, 145-154

Walsh, J. F., Cloke, P. L. and Kesler, S. E., 1984, Fluid (H2O-CO2) immiscibility and fO_2 as factors in gold deposition: Parmour No. 1 mine, Timmins, Ontario [abs.], Geological Society of America Abstracts with Programs, 16, 686

Walther, J. V. and Orille, P. M., 1982, Volatile production and transport in regional metamorphism, Contributions to Mineralogy and Petrology, 79, 252-257

Weissberg, B., G., 1969, Gold-silver ore-grade precipitates from New Zealand thermal waters, Economic Geology, 64, 54-108

Welder, G., 1976, Chemisorption: An Experimental Approach, (Translated by D. F. Klemperer), Butterworths, London, 250p.

Weres, O., Yee, A. and Tsao, L., 1982, Equations and type curves for predicting the polymerization of amorphous silica in geothermal brines, Society of Petrological Engineering Journal (Feb. 1982), 9-16

White, D. E., 1981, Active geothermal systems and hydrothermal ore deposits, Economic Geology, 75th Anniversary Volume, 392-423

White, J. F. and Corwin, J. F., 1961, Synthesis and origin of chalcedony, American Mineralogist, 46, 112-119

White, S. H., Burrows, S. E., Carreras, L., Shaw, N. D. and Humfreys, F. J., 1980, On mylonites in ductile shear zones, Journal of Structural Geology, 2, 175-187

Wildeman, T. R. and Haskin, L. A., 1973, Rare earths in Precambrian sediments, Geochimica et Cosmochimica Acta, 37, 419-438

Wilks, M. E., 1988, the Himalayas - a modern analogue for Archean crustal evolution, Earth and Planetary Science Letters, 87, 127-136

Williams, L. A. and Crerar, D. A., 1985, Silica diagenesis, II: General mechanisms, Journal of Sedimentary Petrology, 55, 312-321

Winkler, H. G. F., 1979, Petrogenesis of Metamorphic Rocks (Fifth Edition), Springer-Verlag, New York, 320p.

Winsor, C. N., 1983, Vein and syntectonic fibre growth associated with multiple slaty cleavage development in the lake Moondarra area, Tectonophysics, 92, 195-210

Wit, M. T. D. et al., 1982, Archean abiogenic and probable biogenic structures associated with mineralized hydrothermal vent systems and regional metasomatism, with implications for greenstone belt studies, Economic Geology, 77, 1783-1802

Wood, B. J. and Graham, C. M., 1986, Infiltration of aqueous fluid and high fluid:rock ratios during greenschist facies metamorphism: a discussion, Journal of Petrology, 27, 751-761

Wood, B. J., 1974, The solubility of alumina in orthopyroxene coexisting with garnet, Contributions to Mineralogy and Petrology, 46, 1-15

Wood, D. A., Gibson, I. L., and Thompson, R. N., 1976, Element mobility during zeolite facies metamorphism of the Tertiary basalts of eastern Iceland, Contributions to Mineralogy and Petrology, 55, 241-254

Woodall, R., 1979, Gold — Australia and the world, University of Western Australia, Geological Department Publications No.3, 1-34

Wyman, D. A., Kerrich, R. and Fryer, B. J., 1986, Gold mineralization overprinting Iron Formation at the Agnico-Eagle deposit, Québec, Canada: Mineralogical, microstructural and geochemical evidence, In: Proceedings of Gold'86, an International Symposium on the Geology of Gold, Toronto, edited by A. J. Macdonald, 108-123

Xiao, H. Q., 1990, Geological characteristics of Taipingding deposit of Hetai gold ore field, Geology of Guangdong, 5, No.3, 83-87

Xu, J. W., Zhu, G., Tong W. X., Cui, K. R. and Lui, Q., 1987, Formation and evolution of the Tangcheng- Lujiang wrench fault system: a major shear system to the northwest of the Pacific Ocean, Tectonophysics, **134**, 273-310

Yamamoto, K., 1987, Geochemical characteristics and depositional environments of cherts and associated rocks in the Franciscan and Shimanto terranes, Sedimentary Geology, **52**, 65-108

Yamamoto, S., 1986, Correlation between iron and manganese and its significance of the distribution of heavy metals in deep-sea cherts, Sedimentary Geology, **49**, 261-280

Yamamoto, S.,1978, Metallic trace elements in some chert nodules of Pacific Seamounts: a comparative study, in Initial Reports of the Deep Drilling Project, **62**,

Yang, S. F., 1981, Metamorphism-migmatitism and their relationship to tectonics of the Luoding district of the Yunkai Mountainous Area, M.Sc Thesis

Ye, B. D., 1989, Isotopic age data from Yunkai area of Guangdong and Guangxi Provinces and their geological implications, Geology of Guangdong, **4**, No.3, 39-55

Ye, S., 1988, Structure and its Relationship to Rock and Ore Formation of the Hetai Gold Field, Unpublished Ph.D Thesis, Institute of Geomechanics, Chinese Academy of Geology

Yin, J. H. Kajiwara, Y. and Fulii, T., 1989, Distribution of transition elements in the surface sediments of the southwestern margin of Japan Sea, Geochemical Journal, **23**, 161-180

Yuan, Z. X. and Huang, F. Q., 1990, New view on structural control and minerogenetic features of Gaocun gold deposit in the Hetai ore field, western Guangdong, Geology of Guangdong, **5**, No.2, 72-82

Zhou, Y. Z., 1987, Study of Sedimentary Geochemistry and Geomathematical Characteristics of Intra-platform Facies Strata —— Anatomy of the Upper Devonian Nandan-Hechi Basin, M.Sc Thesis, Institute of Geochemistry, Chinese Academy of Sciences, 202p.

Zhou, Y. Z., 1990, Geochemical characteristics of siliceous rocks originated from a fossil hydrothermal system in the upper Devonian strata, Guangxi, southern China, Acta Sedimentologia, **8**, No.3, 75-83

Zhou, Y. Z., 1990, Robust abundance analysis and trace element abundance of Nadan-Hechi basin, sothern China, GEOCHEMISTRY, No.2, p.159-165

Zhou, Y. Z., 1991, Element reactivation by diffusion: an embedded mosaic sink model, Program with Abstracts, Volome 16, Geological Association of Canada, Mineralogical Association of Canada, and Society of Economic Geologists, Toronto, A137

Zhou, Y. Z., Chown, E. H., Guha, J., Lu, H. Z. and Tu, G. Z., 1991, Cherts: Evidence of a fossil geothermal system, A case study, Program with Abstracts, Volome 16, Geological Association of Canada, Mineralogical Association of Canada, and Society of Economic Geologists, Toronto, A138

Zhou, Y. Z., Guha, J., Tu, G. Z., Lu, H. Z. and Chown, E. H., 1990, On the geological and geochemical features of the Hetai gold deposit, Guangdong Province, Southern China, Program with Abstracts, 8th IAGOD Symposium, Ottawa, A291

Zierenberg, R. A. and Shanks, W. C., Mineralogy and geochemistry of epigenetic features in metalliferous sediments, Atlantis II Deep, Red Sea, Economic Geology, **78**, 57-72

Zimmerman, R. K. and Kesler, S E., 1981, Fluid inclusion evidence for solution mixing, Sweetwater (Mississppi Valley-type) district, Tennessee, Economic Geology, **76**, 134-142

Appendix I

SAMPLE DESCRIPTION

[1] Schists occurring in the Hetai area (c.f. Tables 2.1, 2.7, 2.9(1))

G-01: quartz two-mica schist; quartz (60%) + muscovite (15%) + biotite (20%); schistose structure, cyclopean granular blastic texture and granular lepidoblastic texture. Sampled at an exploration channel near Gaocun.

G-02: staurolite two-mica schist; quartz (40%) + muscovite (25%) + biotite (30%) + staurolite; schistose and plication structure, lepidoblastic texture; staurolite occurring as idioblast and porphyroblast, containing quartz inclusions (sieve texture). Sampled at an exploration channel near Gaocun.

G-03: quartz two-mica schist; quartz (75%) + muscovite (10%) + biotite (10%); gneissic structure, flaky granoclastic texture. Sampled from a drilling core near Gaocun.

G-3-2: sillimanite two-mica schist; muscovite (25%) + biotite (40%) + quartz (30%) + sillimanite; schistose structure, lepidoblastic texture and fibroblastic texture (sillimanite). Sampled at an exploration channel near Gaocun.

G-06: almandine quartz two-mica schist; quartz (50%) + muscovite (25%) + biotite (20%) + almandine; schistose structure, grano-lepidoblastic texture and porphyroblastic texture (almandine). Sampled near Gaocun ore deposit.

G-08: sillimanite two-mica schist; muscovite (30%) + biotite (30%) + quartz (35%) + sillimanite; schistose structure, lepidonematoblastic texture. Sampled at an exploration channel near Gaocun.

G-09: two-mica schist; quartz (40%) + muscovite (15%) + biotite (40%) + staurolite; schistose structure, granular lepidoblastic texture. Sampled at an exploration channel near Gaocun.

GZ-23: schistose quartzite; quartz (80%) + biotite (5%) + muscovite (10%); massive and striped structure, granoblastic texture. Sampled near Gaocun.

GZ-28: staurolite two-mica schist; muscovite (40%) + biotite (30%) + quartz (25%) + staurolite; schistose structure, lepidoblastic texture and porphyroblastic texture. Sampled near Gaocun.

GZ-30: two-mica schist; muscovite (25%) + biotite (25%) + quartz (45%); schistose structure, lepidoblastic texture. Sampled at an exploration channel near Gaocun.

P1-15: quartz two-mica schist; quartz + muscovite + biotite. Sampled at Gaocun. From No. 719 Geol. Team (1987).

P1-16: two-mica schist; muscovite + biotite + quartz. Sampled at Gaocun. From No. 719 Geol. Team (1987).

CM1501-1: biotite granoblastite. Sampled at Channel 15 of the 240 m. level of Gaocun. From No. 719 Geol. Team (1987).

CM1501-12: biotite quartz granoblastite. Sampled at Channel 15 of 240 m. level of Gaocun. From No. 719 Geol. Team (1987).

Zk001-H137: schistose quartzite. Sampled at Dapinding. From No. 719 Geol. Team (1987).

[2] Migmatites occurring in the Hetai area (c.f. Tables 2.4, 2.7 and 2.9(2))

S-02: biotite gneissic migmatite; gneissic structure, consisting of biotite-rich schlieren and quartz-feldspar leucosomes. The dark-colored schlierens parallel to the main foliation, and the leucosomes are sugary textured. Sampled at a road-cut near Songbo.

S-03: biotite layered migmatite; quartz-feldspar layer, about 1 cm thick, occurring in weakly veined biotite quartz-feldspar gneiss (paleosome). The paleosome have typical metasomatic textures, whereas most leucosomes are straight and parallel sided, with local pinch-and-swell structure. Sampled at a road-cut near Songbo.

S-06: biotite nebulitic migmatite; shady or nebulitic structure. The dark-colored minerals occur as shady spots. The leucocratic portion have a granitic texture. Sampled at a road-cut near Songbo.

[3] Granites occurring in the Hetai area (c.f. Tables 2.12 and 2.13)

WC-01: Wucun porphyritic granite; massive structure, porphyrous granitic texture. The major minerals are quartz (30%), microcline (35%), oligoclase (20%) and biotite (10%). Sampled near the town of Hetai.

WC-02: Wucun porphyrous granite; massive structure, porphyrous granitic texture. The major minerals include quartz (25%), microcline (40%), oligoclase (20%) and biotite (10%). Sampled near the town of Hetai.

W35: Wucun granite. From Huang (1988).

W36: Wucun granite. From Huang (1988).

W88: Wucun granite. From Huang (1988).

W100-1: Wucun granite. From Huang (1988).

G70-3: Wucun granite. From Huang (1988).

253: Wucun granite. From No.719 Geol. Team (1987).

YL-01: Yunluogan medium-grained biotite granodiorite. The major mineral constituents include andesine (45%), K-feldspar (15%), quartz (25%) and biotite (10%).

G49: Yunluogan granodiorite. From Huang (1988).

G96-6: Yunluogan granodiorite. From Huang (1988).

P3-88: Yunluogan granodiorite. From Huang (1988).

P3-90: Yunluogan granodiorite. From Huang (1988).

P3-91-1: Yunluogan granodiorite. From Huang (1988).

P3-95: Yunluogan granodiorite. From Huang (1988).

P3-96: Yunluogan granodiorite. From Huang (1988).

P3-97: Yunluogan granodiorite. From Huang (1988).

15162: Yunluogan granodiorite. From No.719 Geol. Team (1987).

15169: Yunluogan granodiorite. From No.719 Geol. Team (1987).

11153: Yunluogan granodiorite. From No.719 Geol. Team (1987).

[4] Bedded cherts occurring in the Gusui section (c.f. Table 3.1)

GS-01: laminated chert; bright green to pale white color; laminated structure. Sampled at Z^d formation of Gusui section.

GS-02: bedded chert; pale green to pale white color; bedded structure. Sampled at Z^d formation of Gusui section.

GS-03: laminated chert; greenish, white and brown color; laminated structure, with thin quartz veins. Sampled at Z^d formation of Gusui section.

GS-04: bedded chert; greenish pale white color; bedded structure, the bedding plane being indicated by shaly partings. Sampled at Z^d formation of Gusui section.

GS-05: massive chert; pale white color; massive structure. Sampled at Z^d formation of Gusui section.

GS-06: massive chert; greasy white color; massive structure. Sampled at Z^d formation of Gusui section.

GS-07: bedded chert; reddish pale white color; bedded structure. Sampled at Z^d formation of Gusui section.

GS-08: massive chert; pale white color; massive structure. Sampled at Z^d formation of Gusui section.

GS-09: jasperoid chert; bright green to pale white color; massive structure. Sampled at Z^d formation of Gusui section.

GS-10: jasperoid chert; bright green to reddish and pale white color; pseudobreccia structure: centerimeter-sized chunk of reddish to white chert suspended in a white and green matrix. Sampled at Z^d formation of Gusui section.

GS-11: mudstone, intercalated within bedded chert; black color; containing carbonaceous materials. Sampled at Z^d formation of Gusui section.

[5] Altered and deformed rocks occurring in the Hetai gold field (c.f. Tables 5.1, 5.2 and 5.5)

G-10: chloritized and silicified mylonite; mortar texture, oriented distribution of mica flakes. The main altered minerals include chlorite and quartz, with little pyrite. The protolith is two-mica schist. Sampled at 240 m. level of the 11# mylonite zone of Gaocun ore deposit.

G-11: chloritized and sericitized phyllonite; mortar texture, perfect alignment of flaky mica. The main altered minerals include chlorite and sericite. The protolith is two-mica schist. Sampled at 240 m. level of the 11# mylonite zone of Gaocun ore deposit.

CM17-3: chloritized, sericitized and silicified mylonite; mylonitic texture. The protolith is two-mica schist. Sampled at 240 m. level of the 11# mylonite zone of Gaocun ore deposit.

GZ-31: mylonitic schist; weak mylonitic texture; chloritized. Sampled at 160 m. level of the 11# mylonite zone of Gaocun ore deposit.

GZ-31-1: mylonite; intense mortar texture, the porphyroclast is small. Chloritized and

silicified. Sampled at 160 m. level of the 11# mylonite zone of Gaocun ore deposit.

GZ-34: silicified mylonite; mylonitic texture. The protolith is quartz two-biotite schist. Sampled at 160 m. level of the 11# mylonite zone of Gaocun ore deposit.

SK-s: chloritized phyllonite; intense phyllonitic texture and kink band texture. Sampled at a exploration drilling hole near Gaocun.

CM1501-5: sericitized and silicified phyllonite. Sampled at Gaocun. From No.719 Geol. Team (1987).

ZK002-40: altered phyllonite. Sampled at Gaocun. From No.719 Geol. Team (1987).

CM1701-1: silicified cataclasite. Sampled at Gaocun. From No.719 Geol. Team (1987).

CM1501-9: altered ultramylonite. Sampled at Gaocun. From No.719 Geol. Team (1987).

ZK3201-H4: sericitized, silicified phyllonite. Sampled at Gaocun. From No.719 Geol. Team (1987).

Zk1603-H20: pyritized, silicified phyllonite. The protolith is migmatitic schist. Sampled at Dapingding. From No.719 Geol. Team (1987).

Pd2401-H75: silicified phyllonite. The protolith is migmatitic schist. Sampled at Dapingding. From No.719 Geol. Team (1987).

M15-01: altered protomylonite. Sampled at Gaocun ductile shear zone. From Ma (1989).

M15-02: altered mylonite. Sampled at Gaocun ductile shear zone. From Ma (1989).

M15-03: altered mylonite. Sampled at Gaocun ductile shear zone. From Ma (1989).

M15-04: altered ultramylonite. Sampled at Gaocun ductile shear zone. From Ma (1989).

M15-05: altered mylonite. Sampled at Gaocun ductile shear zone. From Ma (1989).

M15-06: altered mylonite. Sampled at Gaocun ductile shear zone. From Ma (1989).

M15-07: altered ultramylonite. Sampled at Gaocun ductile shear zone. From Ma (1989).

M15-08: altered mylonite. Sampled at Gaocun ductile shear zone. From Ma (1989).

M15-09: altered mylonite. Sampled at Gaocun ductile shear zone. From Ma (1989).

M15-10: altered protomylonite. Sampled at Gaocun ductile shear zone. From Ma (1989).

M23-01: altered mylonite. Sampled at Gaocun ductile shear zone. From Ma (1989).

M23-02: altered ultramylonite. Sampled at Gaocun ductile shear zone. From Ma (1989).

M23-03: altered mylonite. Sampled at Gaocun ductile shear zone. From Ma (1989).

M7-01: altered mylonite. Sampled at Gaocun ductile shear zone. From Ma (1989).

M7-02: altered ultramylonite. Sampled at Gaocun ductile shear zone. From Ma (1989).

M7-03: altered mylonite. Sampled at Gaocun ductile shear zone. From Ma (1989).

Zk1503-1: altered mylonite. Sampled at Gaocun ductile shear zone. From Ma (1989).

Zk1503-2: altered ultramylonite. Sampled at Gaocun ductile shear zone. From Ma (1989).

Zk1503-3: altered mylonite. Sampled at Gaocun ductile shear zone. From Ma (1989).

G-05: mylonitic felsic pegmatite. Sampled near Gaocun main ore body.

G-07: mylonitic felsic pegmatite. Sampled near Gaocun main ore body.

G-12: mylonitic felsic pegmatite. Sampled near Gaocun main ore body.

G-13: intensely silicified rock (ore), occurring near the center of deformation zone; containing high content of pyrite and chalcopyrite. Sampled at the exploration channel CM1501 of the Gaocun main ore body.

G-14: intensely silicified rock (ore), occurring near the center of deformation zone; containing high content of pyrite and chalcopyrite. Sampled at the exploration channel CM1501 of the Gaocun main ore body.

GZ-32: intensely silicified rock (ore), occurring near the center of deformation zone; containing high content of pyrite and chalcopyrite. Sampled at 160 m. level exploration channel of the Gaocun ore deposit.

CM17-5: intensely silicified rock (ore); containing high content of pyrite and chalcopyrite. Sampled at the exploration channel CM1701 of the Gaocun main ore body.

[6] Ores of the Gaocun gold deposit used for microthermal measurements of fluid inclusions (c.f. Table 6.1)

Liang-160-1: ore rock. Chalcopyrite and pyrite are main auriferous minerals. They are disseminated in the ore rock. There are two generations of hydrothermal quartz. One is paragenetic with chalcopyrite and pyrite. The other is older, and containing secondary fluid inclusions along healed fractures. Sampled from the main ore body at 160 m level.

Liang-160-2: the same as above, but sampled at the margin of the main ore body.

Liang-240: ore rock. The hydrothermal minerals include sericite, chlorite, quartz, pyrite and chalcopyrite. The fluid inclusions may be either primary or secondary. The secondary ones occur along healed fractures which cut the first hydrothermal quartz. Sampled from the main ore body at the exploration channel CM701 of 240 m level.

Bai-160-1: ore rock. The hydrothermal minerals mainly include quartz, pyrite and chalcopyrite. The fluid inclusions may be either primary or secondary. The secondary ones occur along healed fractures of the first hydrothermal quartz. Sampled from the main ore body at 160 m level.

Bai-160-2: the same as above.

Bai-160-3: the same as above.

Bai-160-4: the same as above.

Bai-240-1: ore rock. The hydrothermal minerals mainly include sericite, chlorite and quartz, with little pyrite and chalcopyrite. Most fluid inclusions are secondary in relation to

the hydrothermal quartz. Sampled along the exploration channel CM2301 at 240 level, about 5 meters from the main ore body.

Bai-240-2: ore rock. The hydrothermal minerals mainly include sericite, chlorite and quartz. Pyrite and chalcopyrite are little. Most fluid inclusions are secondary in relation to the hydrothermal quartz. Sampled along the exploration channel CM2301 at 240 level, about 3 meters from the main ore body.

Bai-240-6: ore rock. The hydrothermal minerals mainly include quartz, with a little of pyrite and chalcopyrite. Most fluid inclusions are secondary in relation to the hydrothermal quartz. Sampled along the exploration channel CM2301 at 240 level, about 1.5 meters from the main ore body.

Bai-240-9: low grade ore. The hydrothermal minerals mainly include quartz, as well as pyrite and chalcopyrite. Fluid inclusions may are primary or secondary in relation to the hydrothermal quartz. Sampled along the exploration channel CM2301 at 240 level, near the main ore body.

Bai-240-10: ore rock. Chalcopyrite and pyrite are main auriferous minerals. There are two generations of hydrothermal quartz. One is paragenetic with chalcopyrite and pyrite. The other is older, and containing secondary fluid inclusions along healed fractures. Sampled at the main ore body of the exploration channel CM2301 at 240 m level.

Bai-240-11: ore rock. Chalcopyrite and pyrite are main auriferous minerals. There are two generations of hydrothermal quartz. One is paragenetic with chalcopyrite and pyrite. The other is older, and containing secondary fluid inclusions along healed fractures. Sampled at the main ore body of the exploration channel CM2301 at 240 m level.

Bai-240-13: ore rock. Chalcopyrite and pyrite are main auriferous minerals. There are two generations of hydrothermal quartz. One is paragenetic with chalcopyrite and pyrite. The other is older, and containing secondary fluid inclusions along healed fractures. Sampled at the main ore body of the exploration channel CM2301 at 240 m level.

CM17-3: very low grade ore. Hydrothermal quartz developed, but with little pyrite and chalcopyrite. Sampled at the margin of the main ore body along the exploration channel CM1701 of 240 m level.

CM17-5: ore rock, consisting mainly of hydrothermal quartz, pyrite and chalcopyrite. Sampled at the exploration channel CM1701 of the 240 m level.

G-13: ore rock, consisting mainly of hydrothermal quartz, pyrite and chalcopyrite. Sampled at the exploration channel CM1501.

G-13-2: the same as above.

G-14: ore rock, consisting mainly of hydrothermal quartz, pyrite and chalcopyrite. Sampled at the exploration channel CM1501.

GZ-32: ore rock, consisting mainly of hydrothermal quartz, pyrite and chalcopyrite. Sampled at 160 m. level exploration channel.

Appendix II

DESCRIPTION OF ELEMENT ANALYSIS METHODS

Sample preparation

All samples except those that are cited from a reference were prepared according routine procedure in the present study. They were first crushed in a steel jaw crusher, then milled in an alumina shatter-box to minimize W, Co and contamination. The resulting pulverized rock powders were sent to the involved laboratories for analysis.

Analyzed elements

All samples in the present study were systematically analyzed for the following items: (a) conventional major element oxides, including SiO_2, TiO_2, Al_2O_3, Fe_2O_3, FeO, MnO, MgO, CaO, Na_2O, K_2O, P_2O_5 and LOI (loss on ignition) (12 items); (2) trace elements, including Ag, As, Au, Ba, Bi, Co, Cr, Cs, Cu, Hf, Hg, Nb, Ni, Pb, Rb, Sb, Sc, Se, Sn, Ta, Te, Th, U, V, W, Zn, Zr (27 items); (3) rare earth elements, including La, Ce, Nd, Sm, Eu, Tb, Yb, Lu (8 items).

Laboratories and methods

Major element oxides were determined at the central analysis laboratory of the Institute of Geochemistry, Academia Sinica (IGCAS). The methods include the gravimetry for SiO_2, titrimetry involving EDTA for CaO and FeO, colorimetry for TiO_2, Al_2O_2, Fe_2O_3 and P_2O_5, and atomic absorption spectrometry for Na_2O, K_2O and MgO.

Table A-1 Comparison between the analyzed values obtained in the present analysis and the in-house standard.

Elements	Analyzed		Recommended	Elements	Analyzed		Recommended
	Run 1	Run 2			Run 1	Run 2	
As	24.5	22.6	19	La	32.4	31.9	33
Ba	714	728	685	Ce	62.7	59.4	65
Co	29.2	27.8	28	Nd	24.1	23.8	33
Cr	112	117.6	119	Sm	5.94	5.7	5.28
Cs	3.4	3.3	3.3	Eu	1.17	1.09	1.19
Hf	4.0	3.4	4	Tb	0.87	0.85	0.74
Rb	129.8	132.8	127	Yb	2.96	2.79	2.8
Sb	1.44	1.46	1.47	Lu	0.52	0.57	0.41
Sc	19.8	19.5	21				
Ta	1.19	1.5	1.3				
Th	9.0	8.9	9				
U	4.8	5.0	4.8				
Zr	100.6	141.4	149				

All elements are presented in ppm

Table A-2 Comparison between the analyzed values of duplicate samples

Elements	1	2	Elements	1	2
SiO2	87.14	87.18	Ag	90	87
TiO2	0.06	0.06	Au	3	4
Al2O3	0.75	0.89	Bi	5.5	5.1
Fe2O3	0.31	0.21	Cu	30	27
FeO	0.76	0.87	Hg	0.73	0.68
MnO	0.10	0.11	Nb	9.1	10.0
MgO	1.30	1.24	Pb	38.5	36.1
CaO	4.13	4.29	Se	0.052	0.042
Na2O	0.06	0.10	Sn	4	3.5
K2O	0.37	0.38	Te	0.043	0.052
P2O5	0.01	0.02	V	29	32
LOI	5.03	5.01	W	1	1
			Zn	112.5	115.7

Major element oxides are presented in wt %; trace elements, in ppm, with the exception of Au and Ag (in ppb)

Among trace elements, Ag, Au, Bi, Cu, Hg, Nb, Ni, Pb, Se, Sn, Te, V, W and Zn, were determined at IGCAS, using the X-ray fluorescence, (non-flame) atomic absorption spectrometry, inductively coupled plasma-atomic emission spectrometry, ion-selective electrodes, depending on different elements. All analysis completed at IGCAS is calibrated by commercial or scientific standards.

REE, as well as As, Ba, Co, Cr, Cs, Hf, Rb, Sb, Sc, Ta, Th, U and Zr, were determined at Université du Québec à Chicoutimi cooperating with l'École Polytechique (Montréal) using the instrumental neutron activation analysis method (INAA). According to the reporter [1], the values obtained at UQAC are within 5% of the accepted values for Sc, within 10% for As, Ba, Hf, La, Rb, Sb, Sm, Ta, Tb, Th and Yb, within 15% for Ce, Co, Cr, Cs, Eu, Nd, Ni, U, Zn and Zr, and 20% for Lu.

Precision

In order to monitor the precision, an in-house standard (shale: SH-19) is included in every run at UQAC. This standard was adopted and provided by UQAC. At IGCAS, duplicate sample method are used. The results are listed in the enclosed tables.

.

---

[1] Bedard, L. P. and Barnes, S.-J., 1990, Instrumental neutron activation analysis by collecting only one spectrum: results for international geochemical reference samples, Geostandards Newsletter, v.14, p.479-484.

Appendix III

Appendix III-2.1 Chemical compositons of the schists occurring in the Hetai area

Sample	SiO2	TiO2	Al2O3	Fe2O3	FeO	MnO	MgO	CaO	Na2O	K2O	P2O5	K2O/Na2O	LOI	Total
GZ-28	60.42	0.86	17.63	1.26	5.22	0.07	3.4	1.2	0.34	5.30	0.13	15.59	3.35	99.18
P1-16*	62.34	0.70	17.73	2.59	4.13	0.04	2.67	0.3	0.78	4.46	0.05	5.72	3.44	99.23
G-3-2	62.62	0.77	18.51	1.05	4.48	0.07	2.6	0.4	0.85	5.53	0.15	6.51	2.30	99.33
G-09	66.42	0.77	15.86	0.78	4.20	0.07	2.2	0.5	1.51	4.61	0.14	3.05	2.07	99.13
G-08	67.99	0.61	14.98	1.42	3.77	0.05	2.3	0.5	1.09	3.67	0.14	3.37	2.59	99.11
CM1501-12*	68.98	0.50	14.81	0.25	5.00	0.06	2.31	0.3	1.46	3.80	0.09	2.60	1.61	99.21
GZ-30	69.92	0.40	14.32	0.65	1.83	0.03	1.2	1.2	2.40	5.31	0.25	2.21	1.66	99.17
G-02	69.97	0.67	14.32	0.81	3.82	0.05	2.1	0.4	0.76	4.02	0.13	5.29	1.99	99.04
CM1501-1*	70.13	0.48	14.26	1.32	3.15	0.06	1.91	0.3	1.09	3.91	0.16	3.59	2.46	99.25
P1-15*	70.88	0.51	14.35	1.29	3.75	0.04	1.85	0.4	0.94	3.36	0.05	3.57	2.57	99.99
G-06	71.92	0.37	14.54	0.58	2.32	0.03	1.5	0.5	1.40	3.54	0.19	2.53	2.16	99.05
G-01	75.14	0.46	12.56	0.46	2.69	0.03	1.4	0.5	1.04	3.37	0.17	3.24	1.62	99.44
Zk001-H137*	78.01	0.48	10.10	1.04	2.26	0.10	1.45	1.1	1.39	2.54	0.00	1.83	2.18	100.62
G-03	84.36	0.35	7.49	0.29	1.73	0.03	0.8	0.7	1.78	1.28	0.15	0.72	0.78	99.74
GZ-23	84.90	0.35	6.61	0.65	1.27	0.03	0.9	1.2	0.83	1.06	0.13	1.28	1.10	99.03
Average	70.93	0.55	13.87	0.96	3.31	0.05	1.91	0.64	1.18	3.72	0.13			
NASC	64.80	0.78	16.90	ΣFeO	5.70	0.06	2.85	3.56	1.15	3.99	0.11			
A.W. Shale	58.11	0.65	15.40	ΣFe2O3	6.70	-	2.44	3.10	1.30	3.24	0.17			

Sources: * from No.719 Geol. Team (1987), p21; Others from the present work

NASC is the "North American Shale Composite" (Gromet et al., 1984)

A.W. Shale is the average abundance of shales over the world (Rösler and Lange, 1972)

Appendix III-2.2 Results of factor analysis for the schists in the Hetai region

Eigenvalues and Proportion of Original Variance

	Magnitude	Variance Prop.
Value 1	6.086	.553
Value 2	1.839	.167
Value 3	1.138	.103
Value 4	.831	.076
Value 5	.654	.059
Value 6	.219	.02

Oblique Solution Primary Pattern Matrix-Orthotran/Varimax

	Factor 1	Factor 2	Factor 3
SiO2	-.982	-4.23E-4	.043
TiO2	.822	-.256	.178
Al2O3	.958	.037	-.139
Fe2O3	.232	-.607	-.261
FeO	.766	-.314	-.041
MnO	.417	-.291	.698
MgO	.832	-.312	.045
CaO	-.068	.363	.794
Na2O	-.08	.765	.193
K2O	1.056	.355	.105
P2O5	.304	.942	-.092

(to be continued)

Oblique Solution Reference Structure-Orthotran/Varimax

	Factor 1	Factor 2	Factor 3
SiO2	-.893	-3.85E-4	.041
TiO2	.747	-.233	.167
Al2O3	.871	.034	-.131
Fe2O3	.211	-.552	-.246
FeO	.697	-.285	-.039
MnO	.379	-.265	.658
MgO	.757	-.283	.043
CaO	-.062	.33	.749
Na2O	-.073	.695	.182
K2O	.96	.322	.099
P2O5	.276	.857	-.086

Primary Intercorrelations-Orthotran/Varimax

	Factor 1	Factor 2	Factor 3
Factor 1	1		
Factor 2	-.324	1	
Factor 3	-.192	-.195	1

Variable Complexity-Orthotran/Varimax

	Orthogonal	Oblique
SiO2	1.061	1.004
TiO2	1.491	1.294
Al2O3	1.102	1.045
Fe2O3	2.052	1.678
FeO	1.481	1.333
MnO	2.334	2.025
MgO	1.457	1.281
CaO	1.462	1.417
Na2O	1.314	1.15
K2O	1.071	1.245
P2O5	1.131	1.226
Average	1.451	1.336

Appendix III-2.3 Correlation coefficients between major elements of the migmatites occurring in the Hetai area (N= 10)

	SiO2	TiO2	Al2O3	Fe2O3	FeO	MnO	MgO	CaO	Na2O	K2O	P2O5
SiO2	1.00	-0.97	-0.93	-0.57	-0.79	-0.47	-0.83	-0.93	-0.39	0.87	-0.33
TiO2	-0.97	1.00	0.81	0.49	0.84	0.45	0.82	0.86	0.17	-0.83	0.23
Al2O3	-0.93	0.81	1.00	0.65	0.63	0.47	0.71	0.89	0.67	-0.85	0.38
Fe2O3	-0.57	0.49	0.65	1.00	0.02	0.13	0.05	0.66	0.51	-0.31	0.59
FeO	-0.79	0.84	0.63	0.02	1.00	0.44	0.92	0.64	0.03	-0.88	0.02
MnO	-0.47	0.45	0.47	0.13	0.44	1.00	0.65	0.18	0.43	-0.55	-0.46
MgO	-0.83	0.82	0.71	0.05	0.92	0.65	1.00	0.63	0.25	-0.87	-0.10
CaO	-0.93	0.86	0.89	0.66	0.64	0.18	0.63	1.00	0.41	-0.74	0.60
Na2O	-0.39	0.17	0.67	0.51	0.03	0.43	0.25	0.41	1.00	-0.45	0.24
K2O	0.87	-0.83	-0.85	-0.31	-0.88	-0.55	-0.87	-0.74	-0.45	1.00	-0.08
P2O5	-0.33	0.23	0.38	0.59	0.02	-0.46	-0.10	0.60	0.24	-0.08	1.00

Appendix III-2.4 Results of Factor Analysis for the Migmatites in the Hetai Region

Eigenvalues and Proportion of Original Variance

	Magnitude	Variance Prop.
Value 1	6.688	.608
Value 2	2.205	.2
Value 3	1.287	.117
Value 4	.501	.046
Value 5	.159	.014
Value 6	.106	.01

Orthogonal Transformation Solution-Varimax

	Factor 1	Factor 2	Factor 3
SiO2	-.893	-.28	-.332
TiO2	.927	.222	.147
Al2O3	.726	.308	.59
Fe2O3	.171	.647	.611
FeO	.974	-.071	-.103
MnO	.484	-.586	.563
MgO	.943	-.217	.147
CaO	.747	.573	.29
Na2O	.097	.098	.927
K2O	-.891	.007	-.331
P2O5	.06	.945	.089

(to be continued)

Oblique Solution Primary Pattern Matrix-Orthotran/Varimax

	Factor 1	Factor 2	Factor 3
SiO2	-.853	-.231	-.189
TiO2	.931	.19	-.009
Al2O3	.623	.237	.488
Fe2O3	.029	.592	.564
FeO	1.042	-.084	-.255
MnO	.402	-.664	.583
MgO	.96	-.257	.031
CaO	.702	.537	.139
Na2O	-.1	.002	.967
K2O	-.86	.061	-.216
P2O5	.017	.95	-.006

Oblique Solution Reference Structure-Orthotran/Varimax

	Factor 1	Factor 2	Factor 3
SiO2	-.8	-.226	-.174
TiO2	.873	.186	-.008
Al2O3	.585	.232	.45
Fe2O3	.027	.579	.52
FeO	.977	-.082	-.235
MnO	.377	-.649	.538
MgO	.9	-.251	.029
CaO	.658	.525	.128
Na2O	-.093	.002	.891
K2O	-.806	.059	-.199
P2O5	.016	.929	-.005

Primary Intercorrelations-Orthotran/Varimax

	Factor 1	Factor 2	Factor 3
Factor 1	1		
Factor 2	.097	1	
Factor 3	.347	.205	1

Appendix III-2.5 Correspondence analysis for the trace elements of the migmatites and schists in the Hetai area (N=13, Np=31)

Elements	Masses	Distances	Coordinates						Absolute	
			F1	F2	F3	F4	F5	F6	F1	F2
Ag	0.09	0.17	-0.22	-0.27	0.15	-0.03	-0.12	0.01	3.60	10.90
As	0.02	4.38	-1.97	0.70	0.01	0.08	0.09	0.03	74.50	18.90
Au	0.00	4.25	0.15	-0.65	1.17	0.29	1.53	-0.15	0.10	3.00
Ba	0.00	1.00	0.00	0.00	0.00	0.00	0.00	0.00	0.00	0.00
Bi	0.00	0.57	-0.42	-0.19	0.20	0.37	-0.11	0.06	0.70	0.30
Co	0.01	0.17	-0.23	-0.22	0.20	0.00	-0.11	0.03	0.40	0.80
Cr	0.00	1.00	0.00	0.00	0.00	0.00	0.00	0.00	0.00	0.00
Cs	0.01	0.19	-0.23	-0.18	0.14	-0.08	-0.15	-0.07	0.60	0.70
Cu	0.02	0.50	0.04	-0.45	0.23	0.29	-0.05	0.38	0.00	8.10
Hf	0.01	0.35	0.27	0.49	0.15	-0.05	0.04	0.08	0.30	2.30
Hg	0.01	1.54	0.12	0.03	-0.89	-0.33	0.36	0.56	0.10	0.00
Nb	0.01	0.04	0.03	-0.11	-0.01	-0.02	-0.02	-0.10	0.00	0.20
Ni	0.05	0.08	-0.07	-0.09	0.08	0.15	-0.12	-0.06	0.20	0.80
Pb	0.04	0.34	0.14	-0.03	-0.37	0.40	0.06	-0.08	0.70	0.10
Rb	0.00	1.00	0.00	0.00	0.00	0.00	0.00	0.00	0.00	0.00
Sb	0.00	0.50	-0.47	0.38	-0.12	0.22	0.13	-0.01	0.00	0.00
Sc	0.01	0.10	-0.12	-0.19	0.12	0.01	-0.11	-0.02	0.10	0.60
Se	0.00	0.12	0.10	0.13	-0.07	0.18	-0.01	0.04	0.00	0.00
Sn	0.01	0.20	-0.04	0.11	-0.13	0.30	-0.08	-0.03	0.00	0.10
Ta	0.00	0.06	-0.02	-0.12	-0.08	-0.09	0.03	0.06	0.00	0.00
Te	0.00	0.07	0.10	0.08	-0.13	0.14	0.03	0.04	0.00	0.00
Th	0.02	0.06	0.06	-0.01	-0.18	-0.10	0.10	-0.02	0.10	0.00
U	0.00	0.08	0.08	-0.04	-0.17	-0.08	0.09	0.01	0.00	0.00
V	0.02	0.13	0.11	-0.04	-0.20	0.21	0.03	0.03	0.20	0.10
W	0.00	0.19	0.18	0.13	-0.07	0.31	-0.06	0.02	0.00	0.00
Zn	0.10	0.06	-0.04	-0.19	0.01	-0.04	-0.01	-0.10	0.20	6.30
Zr	0.20	0.24	0.32	0.36	0.11	0.01	-0.02	0.01	18.20	44.60
La	0.04	0.03	0.01	-0.06	-0.09	-0.09	0.04	0.00	0.00	0.30
LREE	0.14	0.02	0.00	-0.06	-0.07	-0.10	0.04	0.01	0.00	0.90
HREE	0.02	0.02	0.01	-0.02	-0.10	0.00	0.03	-0.02	0.00	0.00
REE	0.16	0.02	0.00	-0.06	-0.07	-0.09	0.04	0.01	0.00	0.90

Samples	Masses	Distances	Coordinates						Absolute	
			F1	F2	F3	F4	F5	F6	F1	F2
G-01	0.07	0.05	0.08	-0.07	0.07	0.09	-0.11	-0.02	0.40	0.50
G-02	0.09	0.24	0.03	-0.27	0.29	0.05	0.28	0.00	0.10	11.60
G-03	0.07	0.31	0.36	0.40	0.06	0.03	0.00	0.05	7.20	18.10
G-3-2	0.09	0.06	0.00	-0.18	0.04	-0.06	-0.12	-0.01	0.00	5.00
G-06	0.06	0.14	-0.01	-0.13	-0.08	0.30	-0.10	0.08	0.00	1.70
G-08	0.08	0.09	-0.02	-0.21	0.02	0.05	-0.10	0.15	0.00	6.20
G-09	0.11	0.90	-0.91	0.26	0.00	0.00	0.03	-0.01	75.60	12.90
GZ-23	0.08	0.48	0.41	0.52	0.18	-0.08	-0.02	0.03	10.80	34.70
GZ-28	0.11	0.09	-0.02	-0.19	0.05	-0.16	-0.11	-0.10	0.10	6.80
GZ-30	0.08	0.11	0.09	-0.07	-0.23	-0.12	0.07	0.08	0.50	0.60
S-02	0.07	0.20	0.16	-0.04	-0.35	-0.12	0.17	0.04	1.40	0.20
S-03	0.07	0.05	0.15	-0.02	-0.05	-0.03	0.00	-0.10	1.40	0.00
S-06	0.04	0.29	0.26	0.15	-0.24	0.31	0.05	-0.21	2.60	1.80

(continued)

Elements	Contributions				Squared Correlations					
	F3	F4	F5	F6	F1	F2	F3	F4	F5	F6
Ag	7.20	0.60	9.30	0.20	0.28	0.42	0.12	0.01	0.09	0.00
As	0.00	0.80	1.30	0.30	0.88	0.11	0.00	0.00	0.00	0.00
Au	21.80	2.00	67.70	1.30	0.01	0.10	0.32	0.02	0.55	0.00
Ba	0.00	0.00	0.00	0.00	0.00	0.00	0.00	0.00	0.00	0.00
Bi	0.70	3.80	0.40	0.30	0.31	0.07	0.07	0.25	0.02	0.01
Co	1.40	0.00	0.80	0.10	0.31	0.29	0.23	0.00	0.07	0.00
Cr	0.00	0.00	0.00	0.00	0.00	0.00	0.00	0.00	0.00	0.00
Cs	0.90	0.50	2.00	1.00	0.28	0.17	0.10	0.03	0.12	0.03
Cu	4.70	11.30	0.40	48.10	0.00	0.41	0.11	0.17	0.01	0.29
Hf	0.50	0.10	0.10	0.60	0.20	0.69	0.07	0.01	0.00	0.02
Hg	14.30	3.00	4.20	21.70	0.01	0.00	0.51	0.07	0.08	0.21
Nb	0.00	0.00	0.00	1.60	0.01	0.30	0.00	0.01	0.01	0.24
Ni	1.40	6.70	5.70	2.60	0.06	0.12	0.09	0.28	0.20	0.05
Pb	22.70	40.40	1.10	4.20	0.06	0.00	0.41	0.46	0.01	0.02
Rb	0.00	0.00	0.00	0.00	0.00	0.00	0.00	0.00	0.00	0.00
Sb	0.00	0.00	0.00	0.00	0.44	0.29	0.03	0.10	0.03	0.00
Sc	0.50	0.00	0.80	0.00	0.14	0.38	0.13	0.00	0.13	0.00
Se	0.00	0.00	0.00	0.00	0.09	0.13	0.04	0.27	0.00	0.01
Sn	0.40	3.20	0.30	0.10	0.01	0.06	0.08	0.44	0.03	0.01
Ta	0.00	0.00	0.00	0.10	0.01	0.24	0.12	0.13	0.02	0.07
Te	0.00	0.00 ·	0.00	0.00	0.15	0.09	0.25	0.29	0.02	0.03
Th	2.20	1.10	1.20	0.10	0.05	0.00	0.51	0.17	0.15	0.01
U	0.40	0.10	0.20	0.00	0.07	0.02	0.33	0.07	0.09	0.00
V	3.80	6.10	0.10	0.40	0.09	0.01	0.33	0.33	0.01	0.01
W	0.00	0.60	0.00	0.00	0.17	0.09	0.03	0.50	0.02	0.00
Zn	0.00	0.90	0.10	16.30	0.03	0.60	0.00	0.02	0.00	0.18
Zr	9.30	0.10	0.70	0.30	0.43	0.52	0.05	0.00	0.00	0.00
La	1.10	2.00	0.30	0.00	0.00	0.16	0.31	0.35	0.05	0.00
LREE	2.70	8.70	1.50	0.40	0.00	0.17	0.23	0.47	0.07	0.01
HREE	0.70	0.00	0.10	0.10	0.01	0.02	0.57	0.00	0.06	0.01
REE	3.30	7.90	1.60	0.30	0.00	0.17	0.28	0.42	0.07	0.01

Samples	Contributions				Squared Correlations					
	F3	F4	F5	F6	F1	F2	F3	F4	F5	F6
G-01	1.50	3.20	6.00	0.50	0.13	0.09	0.12	0.16	0.26	0.01
G-02	28.80	1.50	48.60	0.00	0.00	0.31	0.35	0.01	0.32	0.00
G-03	0.90	0.30	0.00	2.70	0.42	0.52	0.01	0.00	0.00	0.01
G-3-2	0.50	1.80	8.60	0.10	0.00	0.52	0.02	0.05	0.22	0.00
G-06	1.30	33.50	4.20	5.90	0.00	0.11	0.04	0.64	0.07	0.05
G-08	0.10	1.00	5.60	26.60	0.00	0.50	0.00	0.02	0.11	0.25
G-09	0.00	0.00	0.70	0.00	0.92	0.08	0.00	0.00	0.00	0.00
GZ-23	9.20	3.30	0.20	1.10	0.35	0.56	0.07	0.02	0.00	0.00
GZ-28	1.30	17.00	9.90	16.90	0.01	0.38	0.03	0.27	0.14	0.11
GZ-30	15.50	6.60	2.40	6.40	0.07	0.04	0.48	0.13	0.04	0.05
S-02	30.80	5.70	13.00	1.20	0.12	0.01	0.60	0.07	0.14	0.01
S-03	0.60	0.30	0.00	10.30	0.42	0.01	0.04	0.01	0.00	0.19
S-06	9.70	25.70	0.80	28.10	0.23	0.08	0.19	0.32	0.01	0.15

Appendix III-2.6 REE data of the schists occurring in the Hetai area

Elements	Chondrite	GZ-23	GZ-28	GZ-30	G-01	G-02	G-03	G-04	G-06	G-08	G-09	Average schist
La	0.329	31.47	61.03	43.42	29.55	42.97	28.47	48.41	24.54	43.47	50.69	40.40
Ce	0.865	61.76	120.40	86.81	55.11	82.96	53.76	93.17	47.43	80.61	97.05	77.91
Pr	0.116											
Nd	0.63	21.84	40.42	29.93	19.23	33.68	20.98	31.24	16.80	29.10	36.89	28.01
(Pm)												
Sm	0.203	5.23	9.52	8.07	4.87	6.90	4.75	7.71	4.41	7.03	8.39	6.69
Eu	0.077	0.68	1.49	1.04	0.92	0.88	0.90	1.26	1.10	1.13	1.52	1.09
Gd	0.276											
Tb	0.047	0.60	1.31	0.95	0.68	0.93	0.83	1.01	0.67	0.90	1.18	0.91
Dy	0.325											
Ho	0.073											
Er	0.213											
Tm	0.03											
Yb	0.22	2.15	3.51	2.26	2.11	2.83	2.40	3.37	2.10	2.80	3.32	2.68
Lu	0.0339	0.38	0.59	0.37	0.35	0.49	0.41	0.57	0.34	0.48	0.58	0.46

LREE		126.62	243.47	177.02	114.75	175.75	114.18	190.05	98.64	168.94	203.92	161.34
HREE		14.23	28.52	20.01	15.42	20.97	18.44	23.50	15.23	20.39	26.03	20.28
REE		140.85	271.99	197.03	130.17	196.72	132.62	213.55	113.87	189.33	229.94	181.61
LREE/HREE		8.90	8.54	8.85	7.44	8.38	6.19	8.09	6.48	8.29	7.83	7.96
Normalized to Chondrite Average												
∂Ce		1.01	1.01	1.01	1.00	1.00	1.00	1.01	1.01	1.00	1.00	1.01
∂Eu		0.75	0.81	0.76	0.83	0.74	0.81	0.82	0.91	0.82	0.85	0.81
Yb/Tb|n		0.77	0.57	0.51	0.67	0.65	0.62	0.71	0.74	0.67	0.60	0.65
Normalized to NASC												
∂Eu		0.52	0.76	0.67	1.07	0.63	0.82	0.82	1.41	0.82	0.87	0.84
∂Ce		0.99	1.01	1.01	0.96	0.94	0.93	1.00	0.95	0.95	0.95	0.97
Yb/Tb|NASC		1.00	0.75	0.66	0.87	0.85	0.80	0.92	0.96	0.87	0.78	0.85

Appendix III-2.7 REE data of the migmatites occurring in the larger Hetai area

Elements	Chondrite	S-02	S-03	S-06	P4-4-1*	P4-4-3*	Average migmatite	Average schists	Migmatie/Schist	TiO2-normalized
La	0.329	46.68	41.90	19.09	22.3	20.0	35.89	40.40	0.89	1.25
Ce	0.865	84.38	70.80	35.32	65.1	51.3	63.50	77.91	0.82	1.15
Pr	0.116									
Nd	0.63	29.17	24.15	12.03	29.1	23.3	21.78	28.01	0.78	1.10
(Pm)										
Sm	0.203	6.10	4.80	3.20	6.7	3.4	4.70	6.69	0.70	0.99
Eu	0.077	1.05	0.96	0.44	0.6	0.7	0.82	1.09	0.75	1.05
Gd	0.276									
Tb	0.047	0.88	0.68	0.60	1.4	1.0	0.72	0.91	0.80	1.12
Dy	0.325									
Ho	0.073									
Er	0.213									
Tm	0.03									
Yb	0.22	3.41	2.62	2.01	0.80	1.10	2.68	2.68	1.00	1.41
Lu	0.0339	0.57	0.44	0.34	0.20	0.20	0.45	0.46	0.99	1.40
LREE		175.18	149.24	73.29	129.89	103.76	132.57	161.34	0.82	1.16
HREE		21.41	16.51	13.93	24.18	18.29	17.28	20.28	0.85	1.20
REE		196.59	165.75	87.22	154.07	122.06	149.86	181.61	0.83	1.17
LREE/HREE		8.18	9.04	5.26	5.37	5.67	7.67	7.96	0.96	1.36
Normalized to Chondrite Average										
∂Ce		1.00	0.99	1.01	1.06	1.04	1.00	1.01	0.99	
∂Eu		0.82	0.86	0.65	0.56	0.72	0.80	0.81	0.98	
Yb/Tb|n		0.83	0.88	0.73	0.12	0.24	0.56	0.65	0.86	
Normalized to NASC										
∂Eu		0.84	1.04	0.38	0.30	0.62	0.64	0.84	0.76	
∂Ce		0.93	0.90	0.96	1.19	1.09	1.02	0.97	1.05	
Yb/Tb|NASC		1.07	1.15	0.94	0.16	0.31	0.73	0.85	0.86	

Sources: * from Huang (1988); Others from the present study
Notes: The total REE does not include Sc and Y

Appendix III-2.8 Chemical compositions of the granites occurring in the Hetai area

Samples	Granites	SiO2	TiO2	Al2O3	Fe2O3	FeO	MnO	MgO	CaO	Na2O	K2O	P2O5
WC-01	WC	71.77	0.26	14.45	0.41	1.31	0.06	0.50	1.70	3.46	5.38	0.19
WC-2	WC	71.47	0.37	14.10	0.91	1.59	0.09	0.80	2.80	3.60	3.81	0.15
W35	WC(1)	71.11	0.33	14.22	0.85	1.35	0.05	0.71	1.84	3.21	4.50	0.15
W36	WC(1)	71.88	0.28	14.35	0.85	1.13	0.06	0.42	1.61	3.17	4.70	0.16
W88	WC(1)	70.30	0.42	14.48	1.07	1.89	0.09	0.85	2.59	3.36	3.90	0.15
W100-1	WC(1)	69.83	0.37	13.91	0.44	1.97	0.08	0.67	2.05	3.27	5.17	0.13
G70-3	WC(1)	70.92	0.38	13.84	1.50	2.63	0.08	0.70	2.32	2.87	3.54	0.07
253	WC(2)	71.58	0.31	13.88	0.87	2.39	0.07	0.61	2.02	3.28	4.19	0.12
YL-01	YL	66.29	0.71	15.64	1.10	3.35	0.07	1.80	5.20	3.06	1.99	0.21
G49	YL(1)	71.07	0.29	14.22	0.46	2.64	0.06	1.17	2.34	2.86	3.96	0.03
G96-6	YL(1)	65.59	0.56	12.16	1.06	3.33	0.05	2.00	0.55	1.17	2.87	0.12
P3-88	YL(1)	68.72	0.40	14.89	0.50	3.43	0.15	1.81	2.52	2.92	2.76	0.00
P3-90	YL(1)	66.70	0.51	14.94	1.40	2.98	0.08	1.21	1.18	2.08	3.54	0.03
P3-91-1	YL(1)	65.00	0.53	14.86	0.13	4.16	0.13	2.23	3.43	3.00	2.46	0.01
P3-95	YL(1)	70.79	0.34	13.22	0.72	3.10	0.07	1.08	1.15	3.41	3.16	0.05
P3-96	YL(1)	69.18	0.38	14.76	0.54	3.69	0.15	1.44	1.22	2.03	3.58	0.01
P3-97	YL(1)	68.42	0.50	14.68	0.71	3.51	0.15	1.58	3.10	3.09	2.97	0.01
15162	YL(2)	68.44	0.45	14.76	1.05	4.05	0.09	1.91	3.11	3.54	1.98	0.07
15169	YL(2)	68.59	0.50	14.83	0.95	3.53	0.06	1.72	3.22	2.94	2.40	0.19
11153	YL(2)	68.86	0.35	14.74	0.96	2.92	0.08	1.45	2.92	3.40	3.11	0.13
SG-02	SD	70.46	0.35	14.76	0.63	1.79	0.05	0.80	2.80	3.24	4.51	0.13
SG-03	SD	67.35	0.53	16.02	1.23	2.66	0.08	1.10	4.00	4.13	2.29	0.20
SG-06	SD	74.41	0.13	13.44	0.16	0.96	0.04	0.30	0.70	3.60	4.99	0.05
G93	SD(1)	73.15	0.25	13.43	0.12	2.35	0.03	0.60	1.14	2.48	4.66	0.12
G94-1	SD(1)	69.26	0.50	14.51	0.29	3.64	0.03	1.44	3.02	2.52	2.56	0.08
P4-4-1	SD(1)	72.56	0.33	13.39	0.50	1.59	0.08	0.51	0.78	2.40	5.08	0.00
P4-4-3	SD(1)	68.01	0.55	15.20	0.34	3.58	0.15	2.00	2.78	3.34	2.30	0.00
P4-4-5	SD(1)	69.01	0.45	15.01	0.41	3.33	0.15	1.86	2.52	3.60	2.51	0.05
P4-4-6	SD(1)	70.85	0.33	14.89	0.27	2.77	0.10	1.35	1.49	3.55	2.77	0.00
W51	SD(1)	68.16	0.51	15.17	0.43	3.23	0.06	1.77	3.22	3.18	3.10	0.14
WC average		71.11	0.34	14.15	0.86	1.78	0.07	0.66	2.12	3.28	4.40	0.14
YL average		68.14	0.46	14.48	0.80	3.39	0.10	1.62	2.50	2.79	2.90	0.07
SD average		70.32	0.39	14.58	0.44	2.59	0.08	1.17	2.25	3.20	3.48	0.08
UA		70.69	0.49	14.16	· 0.75	3.02	0.06	1.61	1.28	1.99	3.62	0.11

Sources: (1) from Huang (1988); (2) from No.719 Geological Team (1987); Others from the present study.

UA stands for the element abundance of the regional background rock;

WC = Wucun granite; YL = Yunluogan granite; SD = Shidong granite.

Appendix III-2.9 Concentrations of trace elements of the granites occurring in the Hetai area

Samples	Granites	Ag	As	Au	Ba	Bi	Co	Cr	Cs	Cu	Hf	Hg	Li	Nb	Ni	Pb
WC-01	WC	3.3	0.8	0	522	2.3	2.5	22	24	4	3.1	10.85		16	33.3	57
WC-2	WC	30	1	8	348	1	4.4	29	28	10	4.1	5.63		21	33.3	57.2
W35	WC(1)						14.0	32.0		2.5			70	17.0	7.0	46.0
W36	WC(1)						7.0	8.0		2.5			60	14.0	2.5	42.0
W88	WC(1)						12.0	3.5		2.5			70	13.0	2.3	37.0
YL-01	YL	106.6	0.9	1	555	5.6	11	43	8.7	24	5.5	15.26		13	25	38.5
P3-88	YL(1)						8.6	75.9		35.0			60	17.0	26.5	21.0
P3-89	YL(1)						9.2	49.2		31.2			44	14.0	25.3	20.0
P3-97	YL(1)						9.3	53.8		25.9			75	14.0	9.2	27.0
SG-02	SD	26.6	0.6	1	864	0.7	4.8	45	4.7	12	4.3	13.97		8.4	16.7	57.7
SG-03	SD	60	0.4	3	417	6.4	6.3	45	10	12	5.3	2.83		14.7	58.3	38
SG-06	SD	16.6	1	2	694	0.5	1.3	39	4.4	2	3.5	0.74		8.4	41.7	76.9
P4-4-1	SD(1)						3.9	16.5		26.5			25	15.0	1.5	37.0
P4-4-3	SD(1)						9.7	42.7		23.2			59	13.0	19.6	21.0
P4-4-6	SD(1)						6.3	55.0		30.1			44	12.0	19.5	32.0
WC average		16.65	0.9	4	435	1.7	8.0	18.9	26	4.3	3.6	8.24	67	16.2	15.7	47.8
YL average		106.6	0.9	1	555	5.6	9.5	55.5	8.7	29.0	5.5	15.26	59	14.5	21.5	26.6
SD average		34.4	0.7	2	658	2.5	5.4	40.5	6.4	17.6	4.4	5.85	43	11.9	26.2	43.8
UA		93.3	24.3	4.5	522	4.9	9.2	64.1	13.7	25.0	6.1	5.1		11.8	48.9	42.8

UA stands for the element abundance of the regional background rock; WC = Wucun; YL = Yunluogan; SD = Shidong.

Sources: (1) from Huang (1988); Others from the present study.

(continued)

Samples	Granites	Rb	Sb	Sc	Se	Sn	Sr	Ta	Te	Th	U	V	W	Zn	Zr
WC-01	WC	276	0.019	3.9	0.05	3.5		3.17	0.042	16.8	9.5	23	1.2	50	76
WC-2	WC	211	0.11	5.4	0.048	4.3		3.27	0.042	20.7	15.2	15	1	70	77
W35	WC(1)	240.0		6.0		6.2	215	3.5	.			24.0	3.5	55	
W36	WC(1)	262.0		6.0		8.5	186	7.0				19.0	3.5	46	
W88	WC(1)	236.0		6.0		8.7	261	3.5				41.0	3.5	64	
YL-01	YL	140	0.005	11	0.055	4		0.86	0.04	10.7	4.9	19	1.5	115	265
P3-88	YL(1)	181.0		11.0		15.5	112	3.0				69.5	0.7	68	
P3-89	YL(1)	146.0		12.0		18.6	157	0.0				70.7	0.4	88	
P3-97	YL(1)	135.0		20.0		13.4	124	0.0				68.5	0.1	64	
SG-02	SD	144	0.094	5.8	0.05	4		1.11	0.05	29	4.4	34	0.8	95	150
SG-03	SD	121	0.041	8.3	0.062	9		1.31	0.038	23.8	2.9	32	1	125	214
SG-06	SD	207	0.078	4.4	0.055	8		0.51	0.04	13	3.2	24	1.2	58	165
P4-4-1	SD(1)	232.0		4.0		8.4	73	0.0				23.0	0.2	48	
P4-4-3	SD(1)	188.0		14.0		10.1	88	1.0		.		74.9	0.1	89	
P4-4-6	SD(1)	185.0		6.0		17.7	161	3.5	.			46.0	0.2	46	
WC average		245	0.065	5.5	0.049	6.2	221	4.1	0.042	18.75	12.4	24.4	2.5	57	77
YL average		150.5	0.005	13.5	0.055	12.9	131	1.0	0.040	10.7	4.9	56.9	0.7	84	265
SD average		179.5	0.071	7.1	0.056	9.5	107	1.2	0.043	21.9	3.5	39.0	0.6	77	176
UA		188.8	0.094	9.5	0.056	7.5		1.1	0.043	19.9	4.1	30.0	1.0	102	221

Appendix III-2.10   REE data of the granites occurring in the Hetai area

Elements	Chondrite	WC-01 WC	WC-02 WC	G70-3 WC(1)	W100-1 WC(1,2)	YL-01 YL	P3-93 YL(1)	P3-96 YL(1)	P3-88 YL(2)	P3-93- YL(2)	P3-93-2 YL(2)	P3-97 YL(2)
La	0.329	28.25	29.18	27.3	13.8	29.06	16.5	12.6	17.1	24.2	11.9	17.9
Ce	0.865	51.55	50.59	42.3	51.8	52.67	58.6	55.4	40.9	67.6	55.4	91.2
Pr	0.116											
Nd	0.63	15.79	17.17	13.7	13.9	17.23	22.9	14.4	18.9	30.2	15.8	18.5
(Pm)												
Sm	0.203	4.63	5.10	3.8	4.5	3.90	5.3	8.7	4.7	7.4	3.4	3.9
Eu	0.077	0.85	0.92	0.4	0.7	1.10	0.7	0.4	0.4	0.5	0.3	0.6
Gd	0.276											
Tb	0.047	0.48	0.77	1.2	1.4	0.45	1.4	0.9	1.1	1.5	0.8	0.9
Dy	0.325											
Ho	0.073											
Er	0.213											
Tm	0.03											
Yb	0.22	1.24	2.24	1.40	1.70	1.23	1.10	1.30	0.50	2.60	1.40	1.20
Lu	0.0339	0.24	0.43	0.20	0.20	0.23	0.50	0.40	0.30	0.60	0.40	0.40
LREE		107.15	109.23	92.62	90.41	110.37	111.80	97.51	87.92	139.52	93.10	140.84
HREE		9.42	15.36	33.34	37.76	8.91	53.69	21.91	69.18	33.01	17.61	23.04
LREE/HREE		11.37	7.11	2.78	2.39	12.38	2.08	4.45	1.27	4.23	5.29	6.11
REE		116.57	124.59	125.97	128.18	119.28	165.49	119.42	157.10	172.53	110.70	163.88
Normalized to Chondrite Average												
∂Eu		0.69	0.56	0.21	0.31	1.00	0.27	0.16	0.18	0.17	0.21	0.36
∂Ce		1.05	0.98	0.92	1.77	1.02	1.50	1.99	1.09	1.23	2.00	2.38
Yb/Tb|n		0.56	0.62	0.25	0.26	0.59	0.17	0.31	0.10	0.37	0.37	0.28
Normalized to NASC												
∂Eu		1.03	0.84	0.31	0.46	1.49	0.41	0.24	0.26	0.26	0.31	0.54
∂Ce		0.99	0.92	0.87	1.67	0.96	1.42	1.88	1.03	1.16	1.89	2.25
Yb/Tb|NASC		0.72	0.81	0.32	0.34	0.76	0.22	0.40	0.13	0.48	0.49	0.37

Sources: (1) from Huang (1988); (2) from Fu (1988); Others from the present study.
UA stands for the element abundance of the regional background rock;
WC = Wucun granite; YL = Yunluogan granite; SD = Shidong granite

(continued)

Elements	SG-02 SD	SG-03 SD	SG-06 SD	P4-4-1 SD(1)	P4-4-3 SD(1)	P4-4-9 SD(1)	P4-4-9' SD(1)	Average WC	YL	SD	UA
La	47.68	42.37	19.19	22.3	20.0	53.7	24.7	24.63	18.47	32.85	39.44
Ce	84.38	69.80	35.32	65.1	51.3	74.1	42.3	49.06	60.25	60.33	74.82
Pr											
Nd	29.17	23.15	12.03	29.1	23.3	48.9	28.6	15.14	19.70	27.75	26.68
(Pm)											
Sm	·6.10	4.66	3.20	6.7	3.4	9.3	5.3	4.51	5.33	5.52	6.26
Eu	1.05	0.96	0.29	0.6	0.7	1.0	0.7	0.72	0.57	0.76	1.03
Gd											
Tb	0.88	0.64	0.62	1.4	1.0	1.7	1.3	0.96	1.01	1.08	0.87
Dy											
Ho											
Er											
Tm											
Yb	3.41	2.63	2.10	0.80	1.10	2.20	1.00	1.64	1.33	1.89	2.68
Lu	0.57	0.44	0.35	0.20	0.20	0.50	0.20	0.27	0.40	0.35	0.46
LREE	178.94	149.49	74.42	133.06	106.06	199.81	109.00	99.85	111.58	135.83	155.2
HREE	19.61	14.85	12.85	70.97	29.06	44.13	50.51	23.97	32.48	34.57	19.64
LREE/HREE	9.13	10.07	5.79	1.87	3.65	4.53	2.16	5.91	5.12	5.31	7.9
REE	198.55	164.34	87.28	204.04	135.12	243.94	159.52	123.83	144.06	170.40	174.81
Normalized											
∂Eu	0.56	0.70	0.26	0.20	0.42	0.28	0.28	0.44	0.34	0.39	0.55
∂Ce	0.98	0.95	1.02	1.26	1.15	0.67	0.77	1.18	1.60	0.97	1.02
Yb/Tb|n	0.83	0.88	0.73	0.12	0.24	0.28	0.16	0.42	0.31	0.46	0.60
Normalized											
∂Eu	0.84	1.04	0.38	0.30	0.62	0.42	0.42	0.66	0.50	0.58	
∂Ce	0.93	0.90	0.96	1.19	1.09	0.64	0.73	1.12	1.52	0.92	
Yb/Tb|NAS	1.07	1.15	0.94	0.16	0.31	0.36	0.21	0.55	0.41	0.60	

Appendix III-3.1 Results of correspondence analysis of the Zd bedded cherts at Gusui
(Major elements)

Elements/ Samples	Masses	Distances	Coordinates			Absolute contributions			Squared correlations		
			F1	*F2*	*F3*	*F1*	*F2*	*F3*	*F1*	*F2*	*F3*
SiO2	0.943	0.01	0.10	0.01	0.00	4.4	1.0	0.0	0.99	0.01	0.00
TiO2	0.001	2.45	-1.55	0.01	-0.21	1.3	0.0	1.1	0.98	0.00	0.02
Al2O3	0.028	5.09	-2.26	0.04	-0.07	68.2	0.4	3.3	1.00	0.00	0.00
FeO	0.011	1.71	-1.14	-0.37	0.52	6.8	18.2	66.3	0.76	0.08	0.16
Fe2O3	0.007	0.49	-0.03	-0.61	-0.31	0.0	32.4	15.4	0.00	0.76	0.19
MnO	0.001	0.16	0.25	-0.19	-0.07	0.0	0.3	0.1	0.40	0.22	0.03
MgO	0.001	2.54	-0.08	-1.54	-0.30	0.0	42.0	2.9	0.00	0.94	0.03
CaO	0.001	1.17	-0.17	-0.36	-0.63	0.0	1.2	6.7	0.02	0.11	0.33
Na2O	0.000	3.96	-1.97	0.17	-0.12	0.5	0.1	0.1	0.98	0.01	0.00
K2O	0.006	6.29	-2.50	0.23	-0.08	18.6	3.8	0.9	0.99	0.01	0.00
P2O5	0.001	1.41	0.02	-0.30	-0.51	0.0	0.6	3.2	0.00	0.06	0.18
GS-01	0.092	0.06	0.07	-0.21	-0.07	0.2	49.3	9.4	0.09	0.78	0.08
GS-02	0.091	0.03	0.08	-0.07	-0.11	0.3	5.4	27.3	0.20	0.16	0.43
GS-03	0.092	0.02	0.13	0.00	0.08	0.7	0.0	11.7	0.66	0.00	0.24
GS-04	0.091	0.04	-0.01	-0.13	0.16	0.0	17.7	49.9	0.00	0.40	0.59
GS-05	0.092	0.04	0.17	0.08	-0.01	1.3	6.4	0.1	0.81	0.17	0.00
GS-06	0.091	0.04	0.20	0.05	0.01	1.7	3.2	0.1	0.92	0.07	0.00
GS-07	0.092	0.03	0.16	0.06	-0.02	1.2	3.9	1.0	0.84	0.11	0.01
GS-08	0.092	0.05	0.20	0.08	0.00	1.8	6.3	0.0	0.86	0.13	0.00
GS-09	0.091	0.04	0.20	0.05	-0.01	1.8	2.9	4.0	0.92	0.06	0.00
GS-10	0.091	0.04	0.19	0.06	0.00	1.6	3.4	0.0	0.91	0.08	0.00
GS-11	0.087	2.13	-1.46	0.04	-0.01	89.5	1.4	2.0	1.00	0.00	0.00

Appendix III-3.2 Results of correspondence analysis of the Zd bedded cherts at Gusui
(Trace elements)

Elements/ Samples	Masses	Distances	Coordinates				Absolute contributions				Squared correlations			
			F1	F2	F3	F4	F1	F2	F3	F4	F1	F2	F3	F4
Bi	0.018	2.56	-1.40	-0.31	-0.57	0.24	19.2	3.6	14.1	2.6	0.77	0.04	0.13	0.02
Cu	0.005	8.27	-0.21	-1.39	1.04	-0.24	12.7	20.8	13.6	0.8	0.53	0.23	0.13	0.01
Pb	0.002	0.80	-0.34	0.27	-0.12	0.01	0.1	0.3	0.1	0.0	0.14	0.09	0.02	0.00
Zn	0.005	2.85	-1.36	-0.42	0.71	-0.04	5.4	1.9	6.4	0.0	0.65	0.06	0.18	0.00
Ni	0.005	4.51	-1.77	-0.29	0.57	0.32	8.4	0.9	3.8	1.3	0.69	0.02	0.07	0.02
Co	0.003	1.94	-1.28	0.43	0.08	0.14	3.0	1.2	0.1	0.2	0.84	0.09	0.00	0.01
Cr	0.004	5.37	-1.29	-0.43	1.03	0.85	3.7	1.5	10.3	7.5	0.31	0.03	0.20	0.13
V	0.002	3.72	-1.44	-0.07	-0.96	0.58	1.9	0.0	3.7	1.5	0.55	0.00	0.25	0.09
As	0.005	5.94	-1.41	0.30	-0.52	-1.84	5.3	0.9	3.2	42.9	0.33	0.01	0.05	0.57
Nb	0.001	2.27	-1.26	0.30	0.08	0.29	0.7	0.1	0.0	0.2	0.70	0.04	0.00	0.04
Ta	0.001	3.45	-0.98	1.33	0.57	0.47	0.3	1.9	0.4	0.3	0.28	0.51	0.09	0.06
Se	0.000	2.78	-0.97	1.18	0.49	0.38	0.1	0.8	0.2	0.1	0.34	0.50	0.09	0.05
Sb	0.000	1.76	-0.92	0.83	0.06	0.05	0.1	0.4	0.0	0.0	0.48	0.39	0.00	0.00
Hg	0.001	1.54	-1.03	-0.22	-0.48	-0.07	0.9	0.1	0.8	0.0	0.69	0.03	0.15	0.00
W	0.001	2.59	-1.54	0.22	0.10	-0.38	1.3	0.1	0.0	0.4	0.91	0.02	0.00	0.06
Sn	0.005	7.10	-1.63	0.39	-1.50	1.15	7.6	1.6	28.1	17.6	0.38	0.02	0.32	0.19
Au	0.002	6.72	-1.41	0.58	-0.72	-1.85	2.4	1.5	2.8	19.8	0.30	0.05	0.08	0.51
Ag	0.000	8.07	-1.80	-0.41	-0.72	-0.01	0.2	0.0	0.1	0.0	0.40	0.02	0.06	0.00
Zr	0.012	2.02	-1.32	0.33	0.10	-0.25	11.9	2.9	0.3	2.1	0.86	0.06	0.01	0.03
Ba	0.915	0.02	0.13	-0.01	0.00	0.00	8.0	0.3	0.0	0.0	0.99	0.01	0.00	0.00
Rb	0.008	4.24	-0.79	1.73	0.69	0.27	2.9	52.2	9.8	1.6	0.15	0.71	0.11	0.02
Cs	0.001	4.16	-0.78	1.70	0.69	0.34	0.2	3.3	0.6	0.2	0.15	0.70	0.11	0.03
Hf	0.000	3.13	-1.20	0.93	0.82	0.16	0.1	0.3	0.3	0.0	0.46	0.28	0.21	0.01
Sc	0.002	2.71	-1.55	-0.02	0.20	-0.40	2.9	0.0	0.2	0.9	0.88	0.00	0.02	0.06
Th	0.001	3.03	-0.94	1.26	0.69	0.26	0.4	2.9	1.0	0.2	0.29	0.52	0.16	0.02
U	0.000	1.62	-0.46	1.02	0.42	0.28	0.0	0.4	0.1	0.0	0.13	0.64	0.11	0.05

(continued)

Elements/ Samples	Masses	Distances	Coordinates				Absolute contributions				Squared correlations			
			F1	F2	F3	F4	F1	F2	F3	F4	F1	F2	F3	F4
GS-01	0.027	2.62	-1.27	-0.72	0.61	0.05	24.7	29.0	24.9	0.2	0.62	0.19	0.14	0.00
GS-02	0.232	0.05	0.21	-0.04	-0.01	0.00	5.9	0.7	0.1	0.0	0.91	0.03	0.00	0.00
GS-03	0.263	0.06	0.21	-0.04	-0.04	-0.07	6.3	0.9	1.2	3.8	0.75	0.03	0.03	0.10
GS-04	0.022	2.87	-1.30	0.21	-0.27	-1.01	20.3	2.0	3.8	58.2	0.59	0.02	0.02	0.36
GS-05	0.008	3.60	-1.55	-0.23	-0.56	0.27	10.6	0.9	6.0	1.2	0.67	0.01	0.09	0.02
GS-06	0.008	2.13	-1.13	-0.23	-0.61	-0.15	5.9	0.9	7.4	0.5	0.60	0.02	0.17	0.01
GS-07	0.022	1.09	-0.64	-0.22	0.19	0.39	5.0	2.3	1.9	8.9	0.37	0.05	0.03	0.14
GS-08	0.012	3.59	-1.11	0.05	-1.21	0.82	8.1	0.1	42.2	21.0	0.34	0.00	0.41	0.19
GS-09	0.054	0.06	0.01	-0.13	0.02	0.10	0.0	1.8	0.0	1.3	0.00	0.28	0.00	0.16
GS-10	0.217	0.06	0.22	-0.06	-0.02	0.00	6.1	1.7	0.2	0.0	0.89	0.07	0.01	0.00
GS-11	0.136	0.36	-0.31	0.46	0.19	0.11	7.1	59.8	12.2	4.5	0.26	0.59	0.10	0.40

Appendix III-3.3 Results of factor analysis of major elements in the Gusui cherts

Factor Analysis for try: X_1 ... X_{11}

Summary Information

Factor Procedure	Principal Component Analysis
Extraction Rule	Method Default
Transformation Method	Orthotran/Varimax
Number of Factors	3

Note: your correlation matrix is Singular.

Eigenvalues and Proportion of Original Variance

	Magnitude	Variance Prop.
Value 1	6.145	.559
Value 2	2.81	.255
Value 3	1.425	.13
Value 4	.358	.033
Value 5	.225	.02
Value 6	.026	.002

Orthogonal Transformation Solution-Varimax

	Factor 1	Factor 2	Factor 3
SiO2	-.995	-.054	-.055
TiO2	.982	.026	.087
Al2O3	.996	-.009	.045
FeO	.88	.178	-.098
Fe2O3	.016	.96	.202
MnO	-.658	.608	-.066
MgO	.051	.932	.195
CaO	.105	.251	.956
Na2O	.985	-.051	.006
K2O	.989	-.085	.057
P2O5	-.064	.107	.978

(to be continued)

Oblique Solution Primary Pattern Matrix-Orthotran/Varimax

	Factor 1	Factor 2	Factor 3
SiO2	-1.004	-.077	2.075E-4
TiO2	.984	.039	.041
Al2O3	.998	.011	.003
FeO	.922	.245	-.188
Fe2O3	.126	.988	.002
MnO	-.574	.652	-.176
MgO	.158	.961	-.001
CaO	.04	.038	.973
Na2O	.986	-.024	-.03
K2O	.98	-.074	.033
P2O5	-.152	-.128	1.038

Oblique Solution Reference Structure-Orthotran/Varimax

	Factor 1	Factor 2	Factor 3
SiO2	-.982	-.07	1.875E-4
TiO2	.963	.035	.037
Al2O3	.976	.01	.003
FeO	.901	.221	-.17
Fe2O3	.123	.891	.002
MnO	-.561	.588	-.159
MgO	.155	.866	-.001
CaO	.039	.035	.879
Na2O	.964	-.021	-.027
K2O	.958	-.067	.03
P2O5	-.149	-.116	.938

Primary Intercorrelations-Orthotran/Varimax

	Factor 1	Factor 2	Factor 3
Factor 1	1		
Factor 2	-.124	1	
Factor 3	.105	.399	1

Appendix III-3.4 Results of factor analysis of the trace elements in the Gusui cherts

Factor Analysis for Trace+Major.Gusui: X_1 ... X_{26}

Summary Information

Factor Procedure	Principal Component Analysis
Extraction Rule	Method Default
Transformation Method	Orthotran/Varimax
Number of Factors	6

Note: your correlation matrix is Singular.

Eigenvalues and Proportion of Original Variance

	Magnitude	Variance Prop.
Value 1	15.491	.596
Value 2	3.132	.12
Value 3	2.235	.086
Value 4	2.179	.084
Value 5	1.123	.043
Value 6	1.002	.039
Value 7	.354	.014
Value 8	.231	.009
Value 9	.175	.007
Value 10	.079	.003
Value 11	6.983E-17	2.686E-18
Value 12	6.983E-17	2.686E-18
Value 13	6.983E-17	2.686E-18

(to be continued)

Oblique Solution Primary Pattern Matrix-Orthotran/Varimax

	Factor 1	Factor 2	Factor 3	Factor 4	Factor 5	Factor 6
Bi	.734	-.136	.003	.438	-.231	-.015
Cu	-.365	-.009	-.305	1.138	-.088	.028
Pb	.017	.393	-.104	-.02	-.102	.778
Zn	.347	-.082	.064	.757	-.092	.066
Ni	.54	-.199	-.15	.485	.444	-.044
Co	.958	.026	.012	.078	-.005	-.044
Cr	.372	-.495	-.08	.453	.626	.256
V	1.12	-.187	.002	-.441	-.343	-.219
As	-.223	1.038	-.004	.011	-.022	.023
Nb	.94	-.065	-.018	.043	.152	.062
Ta	1.026	-.058	-.011	-.057	.018	.039
Se	.976	.011	-.043	-.044	.025	.112
Sb	.881	.16	-.002	-.113	.007	.209
Hg	.152	-.002	1.076	-.228	.089	-.175
W	.758	.297	-.02	.228	.077	-.182
Sn	.984	.001	-.566	-.223	-.529	-.054

Oblique Solution Primary Pattern Matrix-Orthotran/Varimax

	Factor 1	Factor 2	Factor 3	Factor 4	Factor 5	Factor 6
Au	.042	1.028	.005	-.143	-.009	-.062
Ag	-.055	.18	.056	-.294	.877	-.17
Zr	.89	.123	.26	.088	.017	-.303
Ba	-.084	-.006	.729	-.187	-.021	.563
Rb	1.042	-.02	.071	-.119	.035	-.009
Cs	1.042	-.032	.067	-.122	.038	.009
Hf	.943	-.013	-.039	.11	.033	.013
Sc	.617	.265	.15	.394	-.003	-.317
Th	1.005	-.023	.047	-.04	.041	.023
U	.87	.043	.116	-.124	.014	.299

(to be continued)

Oblique Solution Reference Structure-Orthotran/Varimax

	Factor 1	Factor 2	Factor 3	Factor 4	Factor 5	Factor 6
Bi	.598	-.119	.002	.367	-.196	-.013
Cu	-.298	-.008	-.251	.953	-.075	.025
Pb	.014	.344	-.085	-.017	-.087	.683
Zn	.283	-.072	.053	.634	-.078	.058
Ni	.44	-.174	-.124	.406	.377	-.039
Co	.78	.023	.01	.065	-.004	-.038
Cr	.303	-.433	-.066	.38	.532	.225
V	.912	-.164	.001	-.369	-.291	-.192
As	-.182	.907	-.003	.009	-.019	.02
Nb	.766	-.057	-.015	.036	.129	.055
Ta	.836	-.051	-.009	-.047	.015	.035
Se	.795	.01	-.035	-.036	.021	.098
Sb	.718	.14	-.001	-.095	.006	.183
Hg	.124	-.002	.884	-.191	.075	-.153
W	.618	.259	-.016	.191	.065	-.16
Sn	.802	.001	-.465	-.186	-.45	-.047

Oblique Solution Reference Structure-Orthotran/Varimax

	Factor 1	Factor 2	Factor 3	Factor 4	Factor 5	Factor 6
Au	.034	.899	.004	-.12	-.007	-.054
Ag	-.045	.158	.046	-.246	.745	-.149
Zr	.725	.108	.214	.073	.014	-.266
Ba	-.068	-.005	.599	-.157	-.018	.494
Rb	.849	-.018	.059	-.1	.03	-.008
Cs	.849	-.028	.055	-.102	.032	.008
Hf	.768	-.011	-.032	.092	.028	.011
Sc	.503	.232	.123	.33	-.003	-.278
Th	.819	-.02	.039	-.034	.035	.021
U	.709	.038	.095	-.104	.012	.262

Appendix III-3.5 Correlation coefficients between elements of the Gusui cherts
(n =11)

	SiO2	TiO2	Al2O3	Fe2O3	FeO	MnO	MgO	CaO	Na2O	K2O	P2O5	Bi
SiO2	1.00	-0.98	-1.00	-0.08	-0.88	0.60	-0.10	-0.17	-0.98	-0.99	0.00	-0.85
TiO2	-0.98	1.00	0.99	0.08	0.80	-0.61	0.06	0.21	0.99	0.99	0.01	0.86
Al2O3	-1.00	0.99	1.00	0.02	0.84	-0.64	0.03	0.15	0.99	1.00	-0.02	0.84
Fe2O3	-0.08	0.08	0.02	1.00	0.09	0.56	0.91	0.45	-0.01	-0.05	0.27	0.35
FeO	-0.88	0.80	0.84	0.09	1.00	-0.49	0.24	0.02	0.80	0.82	-0.08	0.74
MnO	0.60	-0.61	-0.64	0.56	-0.49	1.00	0.40	0.03	-0.63	-0.67	0.07	-0.38
MgO	-0.10	0.06	0.03	0.91	0.24	0.40	1.00	0.41	-0.04	-0.04	0.29	0.34
CaO	-0.17	0.21	0.15	0.45	0.02	0.03	0.41	1.00	0.11	0.14	0.94	0.22
Na2O	-0.98	0.99	0.99	-0.01	0.80	-0.63	-0.04	0.11	1.00	1.00	-0.07	0.83
K2O	-0.99	0.99	1.00	-0.05	0.82	-0.67	-0.04	0.14	1.00	1.00	-0.02	0.81
P2O5	0.00	0.01	-0.02	0.27	-0.08	0.07	0.29	0.94	-0.07	-0.02	1.00	-0.04
Bi	-0.85	0.86	0.84	0.35	0.74	-0.38	0.34	0.22	0.83	0.81	-0.04	1.00
Cu	-0.13	0.13	0.08	0.88	0.22	0.52	0.79	0.06	0.07	0.01	-0.14	0.43
Pb	-0.34	0.32	0.33	-0.14	0.44	-0.16	-0.22	0.14	0.33	0.34	0.09	0.19
Zn	-0.70	0.70	0.67	0.68	0.64	-0.05	0.62	0.37	0.65	0.62	0.11	0.88
Ni	-0.69	0.70	0.70	0.32	0.59	-0.28	0.24	-0.17	0.69	0.67	-0.38	0.69
Co	-0.99	0.98	0.99	0.08	0.87	-0.62	0.10	0.11	0.98	0.97	-0.09	0.90
Cr	-0.51	0.54	0.53	0.28	0.33	-0.10	0.07	-0.12	0.55	0.52	-0.31	0.50
V	-0.70	0.78	0.74	-0.14	0.44	-0.75	-0.09	0.29	0.74	0.75	0.13	0.59
As	-0.20	0.07	0.15	-0.06	0.61	-0.09	0.14	-0.11	0.09	0.13	-0.03	0.05
Nb	-0.97	0.97	0.97	0.08	0.80	-0.55	0.04	0.12	0.98	0.97	-0.06	0.78
Ta	-0.98	0.99	0.99	-0.02	0.80	-0.64	-0.04	0.11	1.00	1.00	-0.07	0.82
Se	-0.98	0.98	0.99	-0.04	0.83	-0.64	-0.06	0.08	0.99	0.99	-0.10	0.81
Sb	-0.94	0.93	0.95	-0.11	0.85	-0.62	-0.11	0.10	0.95	0.96	-0.03	0.74
Hg	-0.22	0.17	0.18	0.19	0.17	-0.11	0.29	0.80	0.12	0.17	0.85	0.25
W	-0.94	0.89	0.92	0.21	0.96	-0.47	0.29	0.03	0.89	0.89	-0.14	0.83
Sn	-0.66	0.73	0.70	-0.20	0.53	-0.67	-0.16	-0.08	0.72	0.71	-0.27	0.58
Au	-0.38	0.24	0.33	-0.16	0.73	-0.23	0.06	-0.13	0.27	0.32	-0.04	0.13
Ag	0.06	-0.09	-0.04	-0.19	-0.02	-0.16	-0.17	-0.31	-0.07	-0.03	-0.19	-0.42
Zr	-0.95	0.91	0.93	0.23	0.87	-0.58	0.33	0.29	0.89	0.90	0.12	0.88
Ba	-0.11	0.10	0.09	-0.01	0.08	-0.09	-0.06	0.72	0.08	0.11	0.74	0.11
Rb	-0.99	0.99	1.00	-0.04	0.82	-0.67	-0.04	0.15	1.00	1.00	-0.01	0.81
Cs	-0.99	0.99	1.00	-0.05	0.81	-0.67	-0.05	0.15	1.00	1.00	-0.02	0.81
Hf	-0.99	0.99	0.99	0.10	0.85	-0.57	0.09	0.09	0.99	0.98	-0.10	0.87
Sc	-0.85	0.81	0.81	0.48	0.87	-0.34	0.58	0.27	0.76	0.76	0.08	0.86
Th	-0.99	0.99	1.00	0.01	0.83	-0.64	0.00	0.14	1.00	1.00	-0.03	0.84
U	-0.93	0.93	0.93	-0.08	0.79	-0.62	-0.12	0.25	0.93	0.94	0.10	0.74

(continued)

	Cu	Pb	Zn	Ni	Co	Cr	V	As	Nb	Ta	Se	Sb	Hg
SiO2	-0.13	-0.34	-0.70	-0.69	-0.99	-0.51	-0.70	-0.20	-0.97	-0.98	-0.98	-0.94	-0.22
TiO2	0.13	0.32	0.70	0.70	0.98	0.54	0.78	0.07	0.97	0.99	0.98	0.93	0.17
Al2O3	0.08	0.33	0.67	0.70	0.99	0.53	0.74	0.15	0.97	0.99	0.99	0.95	0.18
Fe2O3	0.88	-0.14	0.68	0.32	0.08	0.28	-0.14	-0.06	0.08	-0.02	-0.04	-0.11	0.19
FeO	0.22	0.44	0.64	0.59	0.87	0.33	0.44	0.61	0.80	0.80	0.83	0.85	0.17
MnO	0.52	-0.16	-0.05	-0.28	-0.62	-0.10	-0.75	-0.09	-0.55	-0.64	-0.64	-0.62	-0.11
MgO	0.79	-0.22	0.62	0.24	0.10	0.07	-0.09	0.14	0.04	-0.04	-0.06	-0.11	0.29
CaO	0.06	0.14	0.37	-0.17	0.11	-0.12	0.29	-0.11	0.12	0.11	0.08	0.10	0.80
Na2O	0.07	0.33	0.65	0.69	0.98	0.55	0.74	0.09	0.98	1.00	0.99	0.95	0.12
K2O	0.01	0.34	0.62	0.67	0.97	0.52	0.75	0.13	0.97	1.00	0.99	0.96	0.17
P2O5	-0.14	0.09	0.11	-0.38	-0.09	-0.31	0.13	-0.03	-0.06	-0.07	-0.10	-0.03	0.85
Bi	0.43	0.19	0.88	0.69	0.90	0.50	0.59	0.05	0.78	0.82	0.81	0.74	0.25
Cu	1.00	-0.04	0.73	0.44	0.17	0.32	-0.21	0.06	0.15	0.06	0.06	-0.01	-0.17
Pb	-0.04	1.00	0.21	0.02	0.32	0.01	0.12	0.64	0.32	0.34	0.44	0.60	0.03
Zn	0.73	0.21	1.00	0.63	0.72	0.44	0.34	0.09	0.67	0.64	0.63	0.57	0.22
Ni	0.44	0.02	0.63	1.00	0.75	0.88	0.35	-0.01	0.74	0.69	0.70	0.58	-0.18
Co	0.17	0.32	0.72	0.75	1.00	0.56	0.70	0.18	0.95	0.97	0.98	0.93	0.16
Cr	0.32	0.01	0.44	0.88	0.56	1.00	0.16	-0.20	0.63	0.55	0.55	0.43	-0.18
V	-0.21	0.12	0.34	0.35	0.70	0.16	1.00	-0.17	0.66	0.74	0.71	0.66	0.21
As	0.06	0.64	0.09	-0.01	0.18	-0.20	-0.17	1.00	0.09	0.09	0.19	0.34	0.07
Nb	0.15	0.32	0.67	0.74	0.95	0.63	0.66	0.09	1.00	0.98	0.97	0.92	0.06
Ta	0.06	0.34	0.64	0.69	0.97	0.55	0.74	0.09	0.98	1.00	0.99	0.95	0.11
Se	0.06	0.44	0.63	0.70	0.98	0.55	0.71	0.19	0.97	0.99	1.00	0.98	0.09
Sb	-0.01	0.60	0.57	0.58	0.93	0.43	0.66	0.34	0.92	0.95	0.98	1.00	0.13
Hg	-0.17	0.03	0.22	-0.18	0.16	-0.18	0.21	0.07	0.06	0.11	0.09	0.13	1.00
W	0.33	0.30	0.75	0.77	0.94	0.53	0.52	0.37	0.90	0.89	0.90	0.86	0.10
Sn	-0.06	0.23	0.31	0.37	0.69	0.26	0.75	0.02	0.68	0.72	0.72	0.66	-0.21
Au	-0.03	0.62	0.12	0.05	0.33	-0.15	-0.02	0.96	0.28	0.28	0.36	0.50	0.07
Ag	-0.20	-0.11	-0.32	0.24	-0.10	0.27	-0.17	0.09	0.07	-0.05	-0.04	-0.05	-0.36
Zr	0.23	0.15	0.77	0.67	0.94	0.43	0.67	0.19	0.87	0.89	0.87	0.81	0.36
Ba	-0.21	0.58	0.16	-0.35	0.06	-0.25	0.06	0.22	0.04	0.08	0.11	0.23	0.69
Rb	0.01	0.33	0.62	0.66	0.97	0.52	0.75	0.12	0.97	1.00	0.99	0.95	0.18
Cs	0.01	0.34	0.62	0.66	0.97	0.52	0.76	0.11	0.97	1.00	0.99	0.95	0.18
Hf	0.20	0.32	0.73	0.76	0.99	0.59	0.67	0.14	0.98	0.99	0.98	0.93	0.09
Sc	0.50	0.17	0.86	0.70	0.85	0.42	0.51	0.32	0.77	0.76	0.75	0.70	0.28
Th	0.08	0.35	0.67	0.70	0.98	0.54	0.73	0.13	0.98	1.00	0.99	0.95	0.16
U	-0.03	0.62	0.60	0.53	0.90	0.42	0.67	0.27	0.91	0.94	0.96	0.98	0.23

(continued)

	W	Sn	Au	Ag	Zr	Ba	Rb	Cs	Hf	Sc	Th	U
SiO2	-0.94	-0.66	-0.38	0.06	-0.95	-0.11	-0.99	-0.99	-0.99	-0.85	-0.99	-0.93
TiO2	0.89	0.73	0.24	-0.09	0.91	0.10	0.99	0.99	0.99	0.81	0.99	0.93
Al2O3	0.92	0.70	0.33	-0.04	0.93	0.09	1.00	1.00	0.99	0.81	1.00	0.93
Fe2O3	0.21	-0.20	-0.16	-0.19	0.23	-0.01	-0.04	-0.05	0.10	0.48	0.01	-0.08
FeO	0.96	0.53	0.73	-0.02	0.87	0.08	0.82	0.81	0.85	0.87	0.83	0.79
MnO	-0.47	-0.67	-0.23	-0.16	-0.58	-0.09	-0.67	-0.67	-0.57	-0.34	-0.64	-0.62
MgO	0.29	-0.16	0.06	-0.17	0.33	-0.06	-0.04	-0.05	0.09	0.58	0.00	-0.12
CaO	0.03	-0.08	-0.13	-0.31	0.29	0.72	0.15	0.15	0.09	0.27	0.14	0.25
Na2O	0.89	0.72	0.27	-0.07	0.89	0.08	1.00	1.00	0.99	0.76	1.00	0.93
K2O	0.89	0.71	0.32	-0.03	0.90	0.11	1.00	1.00	0.98	0.76	1.00	0.94
P2O5	-0.14	-0.27	-0.04	-0.19	0.12	0.74	-0.01	-0.02	-0.10	0.08	-0.03	0.10
Bi	0.83	0.58	0.13	-0.42	0.88	0.11	0.81	0.81	0.87	0.86	0.84	0.74
Cu	0.33	-0.06	-0.03	-0.20	0.23	-0.21	0.01	0.01	0.20	0.50	0.08	-0.03
Pb	0.30	0.23	0.62	-0.11	0.15	0.58	0.33	0.34	0.32	0.17	0.35	0.62
Zn	0.75	0.31	0.12	-0.32	0.77	0.16	0.62	0.62	0.73	0.86	0.67	0.60
Ni	0.77	0.37	0.05	0.24	0.67	-0.35	0.66	0.66	0.76	0.70	0.70	0.53
Co	0.94	0.69	0.33	-0.10	0.94	0.06	0.97	0.97	0.99	0.85	0.98	0.90
Cr	0.53	0.26	-0.15	0.27	0.43	-0.25	0.52	0.52	0.59	0.42	0.54	0.42
V	0.52	0.75	-0.02	-0.17	0.67	0.06	0.75	0.76	0.67	0.51	0.73	0.67
As	0.37	0.02	0.96	0.09	0.19	0.22	0.12	0.11	0.14	0.32	0.13	0.27
Nb	0.90	0.68	0.28	0.07	0.87	0.04	0.97	0.97	0.98	0.77	0.98	0.91
Ta	0.89	0.72	0.28	-0.05	0.89	0.08	1.00	1.00	0.99	0.76	1.00	0.94
Se	0.90	0.72	0.36	-0.04	0.87	0.11	0.99	0.99	0.98	0.75	0.99	0.96
Sb	0.86	0.66	0.50	-0.05	0.81	0.23	0.95	0.95	0.93	0.70	0.95	0.98
Hg	0.10	-0.21	0.07	-0.36	0.36	0.69	0.18	0.18	0.09	0.28	0.16	0.23
W	1.00	0.58	0.51	0.02	0.93	-0.05	0.89	0.89	0.94	0.93	0.91	0.81
Sn	0.58	1.00	0.16	-0.16	0.58	-0.13	0.71	0.71	0.69	0.45	0.70	0.64
Au	0.51	0.16	1.00	0.14	0.34	0.18	0.31	0.31	0.31	0.40	0.31	0.41
Ag	0.02	-0.16	0.14	1.00	-0.10	-0.35	-0.04	-0.04	-0.05	-0.10	-0.05	-0.10
Zr	0.93	0.58	0.34	-0.10	1.00	0.11	0.90	0.90	0.92	0.94	0.91	0.80
Ba	-0.05	-0.13	0.18	-0.35	0.11	1.00	0.11	0.12	0.04	0.02	0.11	0.37
Rb	0.89	0.71	0.31	-0.04	0.90	0.11	1.00	1.00	0.98	0.77	1.00	0.94
Cs	0.89	0.71	0.31	-0.04	0.90	0.12	1.00	1.00	0.98	0.76	1.00	0.94
Hf	0.94	0.69	0.31	-0.05	0.92	0.04	0.98	0.98	1.00	0.83	0.99	0.91
Sc	0.93	0.45	0.40	-0.10	0.94	0.02	0.77	0.76	0.83	1.00	0.79	0.68
Th	0.91	0.70	0.31	-0.05	0.91	0.11	1.00	1.00	0.99	0.79	1.00	0.94
U	0.81	0.64	0.41	-0.10	0.80	0.37	0.94	0.94	0.91	0.68	0.94	1.00

Appendix III-5.1 Factor analysis for trace elements of the altered rocks occurring in the Hetai gold field

Oblique Solution Primary Pattern Matrix-Orthotran/Varimax

	Factor 1	Factor 2	Factor 3	Factor 4	Factor 5	Factor 6
Ag	.958	-.161	-.051	-.076	-.042	-.029
As	.97	.333	.036	.062	-.103	-.015
Au	.863	-.262	-.131	-.037	-.05	-.042
Ba	-.071	.568	.088	-.452	.238	.341
Bi	.774	.023	-.064	-.335	.354	-.02
Co	.818	.161	-.273	.123	.05	-.189
Cr	.033	.963	-.547	.309	-.155	-.188
Cs	.047	.81	.237	-.312	-.071	-.426
Cu	.417	-.344	-.37	.062	.218	-.191
Hf	-5.595E-3	.082	-.162	-.103	-.905	-.033
Hg	.921	-.055	.201	.098	-.177	.243
Nb	-.131	.436	.728	.208	-.088	-.204
Ni	.512	.825	.151	.128	.164	.175
Pb	.867	.332	.514	-.023	.063	-.176
Rb	-.064	.565	.334	-.53	.493	-.046
Sb	.995	-6.749E-3	-3.888E-3	-.017	7.942E-3	.165

Oblique Solution Primary Pattern Matrix-Orthotran/Varimax

	Factor 1	Factor 2	Factor 3	Factor 4	Factor 5	Factor 6
Sc	-6.789E-3	.951	-.056	.116	-.041	.09
Se	.088	.127	-.026	.865	.216	-.039
Sn	-.35	-.061	-.394	-.656	.537	-.039
Ta	-.028	-.175	.963	.244	.082	-.03
Te	-.044	.023	.271	.95	.101	.278
Th	-.028	.823	-.209	-.021	-.344	.05
U	-3.506E-4	-.179	1.024	-.051	.124	.107
V	-.4	-.031	-.069	.612	.375	-.507
W	-.014	.039	-.113	.142	-.021	.951
Zn	.333	.181	-.35	.109	.617	.013
Zr	-.033	.038	-.174	.01	-.945	.046

Oblique Solution Reference Structure-Orthotran/Varimax

	Factor 1	Factor 2	Factor 3	Factor 4	Factor 5	Factor 6
Ag	.835	-.134	-.048	-.07	-.038	-.025
As	.846	.277	.033	.057	-.092	-.013
Au	.753	-.217	-.122	-.034	-.045	-.037
Ba	-.062	.472	.082	-.419	.213	.298
Bi	.675	.019	-.059	-.311	.317	-.018
Co	.714	.133	-.253	.114	.045	-.165
Cr	.029	.8	-.507	.286	-.139	-.164
Cs	.041	.672	.22	-.289	-.064	-.371
Cu	.363	-.286	-.343	.058	.195	-.167
Hf	-4.880E-3	.068	-.15	-.096	-.81	-.029
Hg	.803	-.046	.187	.091	-.158	.212
Nb	-.114	.362	.675	.192	-.079	-.178
Ni	.447	.685	.14	.119	.147	.152
Pb	.756	.276	.476	-.022	.056	-.153
Rb	-.056	.469	.31	-.491	.441	-.04
Sb	.868	-5.604E-3	-3.605E-3	-.016	7.104E-3	.144

Oblique Solution Reference Structure-Orthotran/Varimax

	Factor 1	Factor 2	Factor 3	Factor 4	Factor 5	Factor 6
Sc	-5.921E-3	.79	-.052	.108	-.036	.079
Se	.076	.106	-.024	.802	.193	-.034
Sn	-.305	-.051	-.365	-.607	.481	-.034
Ta	-.024	-.145	.893	.226	.074	-.026
Te	-.038	.019	.252	.88	.09	.242
Th	-.024	.684	-.194	-.019	-.307	.043
U	-3.058E-4	-.149	.949	-.047	.111	.094
V	-.349	-.026	-.064	.567	.335	-.442
W	-.013	.032	-.105	.131	-.019	.829
Zn	.29	.15	-.325	.101	.552	.011
Zr	-.029	.032	-.161	9.437E-3	-.846	.04

Primary Intercorrelations-Orthotran/Varimax

	Factor 1	Factor 2	Factor 3	Factor 4	Factor 5	Factor 6
Factor 1	1					
Factor 2	-.25	1				
Factor 3	-.31	.223	1			
Factor 4	.303	-.181	-.102	1		
Factor 5	.346	-.306	-.165	.234	1	
Factor 6	-.121	.432	-.032	-.21	-.036	1

Variable Complexity-Orthotran/Varimax

	Orthogonal	Oblique
SiO_2	1.913	1.831
TiO_2	1.397	1.18
Al_2O_3	1.247	1.044
Fe_2O_3	1	1.092
FeO	1.082	1.038
MnO	2.716	2.858
MgO	2.004	1.526
CaO	1.319	1.23
Na_2O	1.412	1.458
K_2O	1.049	1.01
Average	1.514	1.427

Appendix III-5.2 Correlation coefficients between trace elements of the altered rocks occurring in the Hetai Are
(N = 12)

	Ag	As	Au	Ba	Bi	Co	Cr	Cs	Cu	Hf	Hg	Nb	Ni	Pb
Ag	1.00	0.79	0.99	-0.42	0.83	0.92	-0.09	-0.39	0.81	-0.28	0.75	-0.50	0.18	0.56
As	0.79	1.00	0.71	-0.11	0.54	0.83	0.30	0.05	0.45	-0.11	0.61	-0.13	0.54	0.62
Au	0.99	0.71	1.00	-0.51	0.79	0.92	-0.14	-0.49	0.87	-0.30	0.70	-0.59	0.07	0.46
Ba	-0.42	-0.11	-0.51	1.00	-0.07	-0.42	0.28	0.61	-0.66	0.13	-0.23	0.27	0.51	-0.02
Bi	0.83	0.54	0.79	-0.07	1.00	0.73	-0.10	-0.29	0.67	-0.44	0.63	-0.49	0.26	0.56
Co	0.92	0.83 ·	0.92	-0.42	0.73	1.00	0.20	-0.30	0.81	-0.31	0.66	-0.49	0.31	0.50
Cr	-0.09	0.30	-0.14	0.28	-0.10	0.20	1.00	0.38	-0.20	0.33	0.04	0.12	0.56	0.06
Cs	-0.39	0.05	-0.49	0.61	-0.29	-0.30	0.38	1.00	-0.63	0.31	-0.28	0.61	0.33	0.28
Cu	0.81	0.45	0.87	-0.66	0.67	0.81	-0.20	-0.63	1.00	-0.50	0.39	-0.73	-0.23	0.19
Hf	-0.28	-0.11	-0.30	0.13	-0.44	-0.31	0.33	0.31	-0.50	1.00	-0.17	0.24	-0.01	-0.30
Hg	0.75	0.61	0.70	-0.23	0.63	0.66	0.04	-0.28	0.39	-0.17	1.00	-0.20	0.41	0.71
Nb	-0.50	-0.13	-0.59	0.27	-0.49	-0.49	0.12	0.61	-0.73	0.24	-0.20	1.00	0.31	0.22
Ni	0.18	0.54	0.07	0.51	0.26	0.31	0.56	0.33	-0.23	-0.01	0.41	0.31	1.00	0.43
Pb	0.56	0.62	0.46	-0.02	0.56	0.50	0.06	0.28	0.19	-0.30	0.71	0.22	0.43	1.00
Rb	-0.36	-0.19	-0.45	0.79	0.02	-0.37	0.00	0.57	-0.57	-0.05	-0.17	0.40	0.49	0.09
Sb	0.94	0.90	0.90	-0.23	0.76	0.90	0.05	-0.29	0.68	-0.30	0.78	-0.41	0.39	0.60
Sc	-0.37	0.12	-0.47	0.69	-0.24	-0.19	0.81	0.62	-0.65	0.31	-0.02	0.49	0.72	0.14
Se	0.36	0.38	0.37	-0.50	0.20	0.52	0.21	-0.41	0.45	-0.37	0.28	-0.01	0.27	0.20
Sn	-0.15	-0.39	-0.15	0.24	0.23	-0.23	-0.16	-0.18	0.06	-0.13	-0.23	-0.38	-0.27	-0.32
Ta	-0.22	-0.10	-0.27	-0.12	-0.27	-0.35	-0.41	0.14	-0.35	-0.14	-0.02	0.78	0.01	0.29
Te	0.07	0.13	0.07	-0.27	-0.01	0.18	0.12	-0.26	0.09	-0.33	0.27	0.22	0.29	0.25
Th	-0.41	0.04	-0.49	0.64	-0.34	-0.26	0.80	0.62	-0.69	0.63	-0.10	0.40	0.57	-0.05
U	-0.30	-0.17	-0.37	0.18	-0.25	-0.48	-0.49	0.30	-0.50	-0.12	-0.08	0.76	0.04	0.28
V	0.01	-0.20	0.09	-0.64	-0.04	0.17	-0.08	-0.29	0.40	-0.51	-0.04	-0.02	-0.31	0.07
W	-0.16	0.08	-0.20	0.59	-0.06	-0.14	0.28	0.01	-0.29	-0.01	0.07	-0.14	0.35	-0.08
Zn	0.60	0.56	0.60	-0.23	0.57	0.71	0.15	-0.43	0.70	-0.64	0.40	-0.51	0.25	0.23
Zr	-0.31	-0.20	-0.32	0.12	-0.44	-0.32	0.35	0.33	-0.49	0.88	-0.04	0.16	-0.08	-0.15

a

	Rb	Sb	Sc	Se	Sn	Ta	Te	Th	U	V	W	Zn	Zr
Ag	-0.36	0.94	-0.37	0.36	-0.15	-0.22	0.07	-0.41	-0.30	0.01	-0.16	0.60	-0.31
As	-0.19	0.90	0.12	0.38	-0.39	-0.10	0.13	0.04	-0.17	-0.20	0.08	0.56	-0.20
Au	-0.45	0.90	-0.47	0.37	-0.15	-0.27	0.07	-0.49	-0.37	0.09	-0.20	0.60	-0.32
Ba	0.79	-0.23	0.69	-0.50	0.24	-0.12	-0.27	0.64	0.18	-0.64	0.59	-0.23	0.12
Bi	0.02	0.76	-0.24	0.20	0.23	-0.27	-0.01	-0.34	-0.25	-0.04	-0.06	0.57	-0.44
Co	-0.37	0.90	-0.19	0.52	-0.23	-0.35	0.18	-0.26	-0.48	0.17	-0.14	0.71	-0.32
Cr	0.00	0.05	0.81	0.21	-0.16	-0.41	0.12	0.80	-0.49	-0.08	0.28	0.15	0.35
Cs	0.57	-0.29	0.62	-0.41	-0.18	0.14	-0.26	0.62	0.30	-0.29	0.01	-0.43	0.33
Cu	-0.57	0.68	-0.65	0.45	0.06	-0.35	0.09	-0.69	-0.50	0.40	-0.29	0.70	-0.49
Hf	-0.05	-0.30	0.31	-0.37	-0.13	-0.14	-0.33	0.63	-0.12	-0.51	-0.01	-0.64	0.88
Hg	-0.17	0.78	-0.02	0.28	-0.23	-0.02	0.27	-0.10	-0.08	-0.04	0.07	0.40	-0.04
Nb	0.40	-0.41	0.49	-0.01	-0.38	0.78	0.22	0.40	0.76	-0.02	-0.14	-0.51	0.16
Ni	0.49	0.39	0.72	0.27	-0.27	0.01	0.29	0.57	0.04	-0.31	0.35	0.25	-0.08
Pb	0.09	0.60	0.14	0.20	-0.32	0.29	0.25	-0.05	0.28	0.07	-0.08	0.23	-0.15
Rb	1.00	-0.27	0.43	-0.39	0.28	0.15	-0.22	0.36	0.39	-0.35	0.10	-0.21	-0.11
Sb	-0.27	1.00	-0.15	0.36	-0.20	-0.19	0.12	-0.23	-0.24	-0.13	0.09	0.69	-0.34
Sc	0.43	-0.15	1.00	-0.08	-0.13	-0.05	0.07	0.93	0.01	-0.35	0.48	-0.11	0.32
Se	-0.39	0.36	-0.08	1.00	-0.41	0.16	0.84	-0.26	-0.14	0.62	-0.09	0.50	-0.40
Sn	0.28	-0.20	-0.13	-0.41	1.00	-0.32	-0.55	-0.08	-0.20	-0.15	0.02	0.22	-0.22
Ta	0.15	-0.19	-0.05	0.16	-0.32	1.00	0.34	-0.20	0.93	0.18	-0.27	-0.27	-0.22
Te	-0.22	0.12	0.07	0.84	-0.55	0.34	1.00	-0.15	0.13	0.56	0.17	0.16	-0.19
Th	0.36	-0.23	0.93	-0.26	-0.08	-0.20	-0.15	1.00	-0.12	-0.51	0.40	-0.30	0.60
U	0.39	-0.24	0.01	-0.14	-0.20	0.93	0.13	-0.12	1.00	-0.07	-0.11	-0.39	-0.18
V	-0.35	-0.13	-0.35	0.62	-0.15	0.18	0.56	-0.51	-0.07	1.00	-0.47	0.24	-0.34
W	0.10	0.09	0.48	-0.09	0.02	-0.27	0.17	0.40	-0.11	-0.47	1.00	0.10	0.11
Zn	-0.21	0.69	-0.11	0.50	0.22	-0.27	0.16	-0.30	-0.39	0.24	0.10	1.00	-0.70
Zr	-0.11	-0.34	0.32	-0.40	-0.22	-0.22	-0.19	0.60	-0.18	-0.34	0.11	-0.70	1.00

Appendix III-5.3 REE data and related reference values of the altered rocks in the Hetai gold field

Element	Chondrite	Ma-04	G-10	G-11	GZ-31	GZ-31-1	GZ-34A	CM17-03	Sk-s	GZ-32	CM17-05	G-13	G-14
La	0.329	32.26	43.22	33.19	36.88	30.00	42.28	28.14	35.35	13.97	3.90	25.28	27.05
Ce	0.865	64.71	83.30	62.37	70.18	58.32	84.19	56.28	65.68	26.50	7.39	46.57	48.31
Pr	0.116												
Nd	0.63	22.79	30.92	24.05	26.68	20.59	27.74	19.84	27.19	8.00	2.85	17.80	19.31
(Pm)													
Sm	0.203	5.22	6.99	5.29	5.75	4.97	6.98	4.78	5.76	2.21	0.90	4.10	4.45
Eu	0.077	0.83	1.14	0.93	1.09	1.03	0.96	0.93	1.01	0.27	0.13	0.56	0.69
Gd	0.276												
Tb	0.047	0.73	0.95	0.61	0.78	0.66	1.07	0.67	0.80	0.28	0.23	0.60	0.72
Dy	0.325												
Ho	0.073												
Er	0.213												
Tm	0.03												
Yb	0.22	2.43	2.85	2.34	2.61	1.97	2.91	2.18	2.41	0.75	0.65	1.61	2.30
Lu	0.0339	0.42	0.49	0.40	0.45	0.37	0.51	0.40	0.43	0.13	0.11	0.27	0.41
LREE		131.66	173.48	131.95	147.37	120.24	169.44	115.06	141.77	53.15	15.90	98.88	104.75
HREE		16.97	21.28	14.73	18.05	14.86	23.43	15.40	17.94	6.10	5.12	13.11	16.50
REE		148.63	194.76	146.68	165.42	135.11	192.87	130.46	159.70	59.25	21.02	111.99	121.24
LREE/HREE		7.76	8.15	8.96	8.17	8.09	7.23	7.47	7.90	8.71	3.10	7.54	6.35
Normalized by Chondrite Average													
∂Ce		1.06	1.02	0.99	1.00	1.04	1.08	1.06	0.96	1.08	0.99	0.98	0.94
∂Eu		0.53	0.55	0.66	0.64	0.71	0.43	0.65	0.58	0.42	0.35	0.44	0.48
Yb/Tb|n		0.71	0.64	0.83	0.72	0.64	0.58	0.70	0.65	0.43	0.59	0.57	0.68

AA is the average of all altered rocks including ore rocks with pegmatites excluded;

AP, the average of altered pegmatites; AO, the average of ore rocks; AA-O, equal to AA but ore rocks excluded

US is the average of unaltered schists; UM, the average of unaltered migmatites; UA, the average of all unaltered rocks

(continued)

Element	G-05	G-07	G-12	GZ-34B	AA-O	AO	AP	AA	US	UM	UA	AA/UA
La	3.93	2.17	1.70	6.46	35.17	17.55	2.60	29.29	40.40	35.89	39.44	0.74
Ce	6.60	5.14	3.61	13.42	68.13	32.19	5.12	56.15	77.91	63.50	74.82	0.75
Pr												
Nd	0.60	0.39	0.91	3.91	24.98	11.99	0.63	20.65	28.01	21.78	26.68	0.77
(Pm)	.											
Sm	3.04	2.02	1.59	2.45	5.72	2.91	2.21	4.78	6.69	4.70	6.26	0.76
Eu	0.10	0.07	0.20	0.37	0.99	0.41	0.12	0.80	1.09	0.82	1.03	0.77
Gd												
Tb	0.33	0.11	0.19	0.18	0.78	0.46	0.21	0.67	0.91	0.72	0.87	0.78
Dy												
Ho												
Er												
Tm												
Yb	2.79	0.93	1.05	0.77	2.46	1.33	1.59	2.08	2.68	2.68	2.68	0.78
Lu	0.53	0.20	0.22	0.19	0.43	0.23	0.32	0.37	0.46	0.45	0.46	0.80
LREE	14.51	9.95	8.27	27.67	141.37	68.17	10.92	116.97	161.3	132.6	155.2	0.75
HREE	11.14	3.65	5.30	4.58	17.84	10.21	6.70	15.29	20.28	17.28	19.64	0.78
REE	25.65	13.60	13.57	32.25	159.21	78.38	17.62	132.27	181.61	149.86	174.81	0.76
LREE/HREE	1.30	2.73	1.56	6.05	7.93	6.68	1.63	7.65	8.0	7.7	7.9	0.97
Normalized												
∂Ce	1.49	1.98	1.24	1.16	1.03	0.98	1.49	1.02	1.03	0.99	1.02	1.00
∂Eu	0.13	0.21	0.49	0.75	0.58	0.44	0.25	0.55	0.55	0.56	0.55	1.00
Yb/Tb|n	1.79	1.85	1.94	0.92	0.68	0.57	1.86	0.64	0.56	0.65	0.60	1.08

华南河台金矿田的地球化学及成矿机理
(摘要)

河台金矿田地处华南广东省西部,是八十年代在粤西、桂东南地区(金省)发现的最大金矿田。已初步探明的金矿床和矿化点包括高村、云西、太平顶、尚台、坑尾、桃子山、后经和河海等。本论文的主要目的在于详细描述该矿田的地质、地球化学特征,了解元素金在整个成矿过程中的地球化学行为,最后,以上述为基础,建立一个合理的成矿模型。

从区域构造上讲,该矿田位于诗洞 — 伍和 — 石洞 — 河台混合岩田的边缘带,属于华南云开变质地体的一部分。北东向延伸的吴川 — 四会断裂及广宁 — 罗定断裂对该地区的地质发展起了重要的控制作用。云开变质地体的基本地质构架形成于加里东期。

矿田范围内,主要的赋矿地层是已遭受变质作用的震旦系。在北和西北侧分别有伍村和云楼岗花岗岩体侵入。再往西北方向,则为诗洞花岗岩体。

一、区域变质岩和花岗岩

在河台地区,片岩类(包括片状石英岩)和混合岩是分布最广的区域变质岩。它们构成了金矿床的直接围岩。片岩的特征矿物组合是石英 + 白云母 + 黑云母 +

（十字石）＋（矽线石）＋（钙铝榴石）。它们形成的温压范围大致是550° - 670° C和2.5 - 6千巴，是中 — 中低压变质相系演化的阶段性产物。原岩可能主要是各种泥质岩石，夹杂沉积硅岩等。

混合岩代表了区域变质作用的高级阶段。它的形成与SiO_2、K_2O和Na_2O的逐步带入有关。其中许多金属元素，尤其是亲硫元素，属于亏损元素（与相同地区的片岩为参考标准）。然而，一些大离子亲石元素和高场强元素，如Rb、Ta、Nb、Hf、Zr、Sc等，则保持不变或甚至显示富集之特征。这种微量元素亏与富集特征是两种不同地球化学过程平衡的结果。一是在普通地质热场中，微量元素倾向于从高温区域向低温区域迁移；另一是在原岩部分融熔和熔体注入结晶过程中，不相容元素倾向于富集。

稀土元素的活动规律与其它微量元素一致，但作为一个整体，混合岩继承了片岩的稀土元素配分模式。

诗洞花岗岩 —> 云楼岗花岗岩 —> 伍村花岗岩代表了一个完整的原地 —> 半原地 —> 侵入花岗岩演化系列。诗洞花岗岩形成于加里东期，与同期的混合岩有紧密的成因联系。而云楼岗和伍村花岗岩形成于海西—印支期。锶和氧同位素研究表明，云楼岗花岗岩的物质来源于上地壳，而伍村花岗岩则可能包含了部分更深源的物质。

二、层状沉积硅岩及其地球化学特征和成因

震旦系Z^d组层状硅岩沉积建造在粤西地区零星出露，但分布范围广泛。本研究的重点在于解剖古水剖面。该剖面震旦系Z^d组硅岩建造的硅岩矿物成分简单，主要由微晶石英组成。次要矿物包括粘土、赤铁矿，偶见重晶石。沉积构造以层状、纹层状、块状、假角砾状为特征。其中，纹层状构造由微晶石英和富铁氧化物两种纹层韵律交替出现而成；假角砾状构造实质上是原生的半固结硅质沉积物被稍后期的网状细小硅质脉所分割，形似厘米级的红 — 棕 — 白色燧石小块悬浮在以绿 — 白色为基调的微晶石英基质中。各种岩性特征表明，这套层状硅岩是震旦时期古地热

系热水沉积的产物。

地球化学特征同样支持上述硅岩热水成因这一认识。总体上，古水硅岩与世界上已被证明是热水成因的硅岩具有明显的地球化学相似性：a) 常量元素以TiO_2、Al_2O_3和K_2O一致地低为特征。在Al-Fe-Mn三元图上，几乎所有的古水硅岩样品都落在前人圈定的热水成因硅岩范围内；b) 大部分微量元素含量偏低（与地壳克拉克值相比），但Ba、As、Sb、Hg和Se偏高。而这些含量偏高的元素恰恰是热水沉积的特征元素。

特征的元素组合可以通过对应分析和因子分析有效地获得。在所鉴定出的有意义的元素组合中，{As, Au, -Cr}，{Ba, Hg, -Sn} 和 {Ba, Pb} 是热水沉积物的特征组合。大部微量元素在表征热水淋滤作用的因子上有显著的体现。热水淋滤因子进一步由两个元素组合组成。一是华南地球化学异常基底的特征元素组合 {Rb, Cs, Nb, Ta, U, Zr, Hf, W, Sn, …}；另一则是包括了Bi、Ni、Zr、Cr等过渡族元素和亲硫元素，它们在华南地区属于亏损元素。

根据稀土元素总量，古水硅岩可以区分为两个端元：纯热水沉积硅岩和正常沉积页岩。前者以低的稀土元素含量为特征，而不纯硅岩的稀土元素含量则依赖于被混入的正常沉积页岩的比例。

在对北美页岩组合样标准化后，古水硅岩稀土配分模式落在已知的典型热水沉积物的上、下限之间。Ce可以出现正异常，但也可以是负异常。这反映了正常沉积作用对热水作用的混染。混染方式有二：一是正常沉积作用和热水沉积作用交替出现；另一是它们俩同时出现，但作用的强度不同。

根据Z^d层状硅岩建造在粤西地区的分布及古水硅岩的岩性、地球化学特征推断，在震旦期间，古地热系曾广泛地在华南冒地槽中发育。层状硅岩形成的机理如下：

在开始阶段，稠密且冷的海水沿地槽中深断裂系或裂谷下渗。在下渗的过程中，海水不断地被加热和还原，并与所通过的基底岩石进行化学反应。后来，这些热水流体上升并继续从围岩中淋滤出SiO_2和许多微量元素。最后，这些富SiO_2的热水溶液在泉口位置附近，与周围的冷海水相混合。这时，部分SiO_2以非晶质二氧化

硅或玉髓矿物形式快速沉积，另一部分则可以迁移到海底其它地区，和正常沉积结合在一起。目前所观察到的微晶石英是原始的非晶质SiO₂和玉髓重结晶的结果。

三、热事件中微量元素的迁移行为：多层次扩散陷井镶嵌模型

尽管流体流动和渗滤对元素迁移常常很有效，但扩散作用更具普遍性。在流体流动和渗滤不存在的地质区域里，扩散作用尤其显得重要。

自然界中，所有岩石和地质体里都存在着许多薄弱部位（软弱面），比如颗粒边界、微细裂隙或大断裂等，并且后者还常常可能充填着水溶液（膜）。这些软弱面可被数学地抽象为"无限深"的扩散陷井。微量的杂质原子在固体里的迁移实际上是一系列随机的跳跃，但当它们一旦遇到陷井后，它们将被后者所捕捉。也就是说，这些原子将不再返回原来的"固体单元"里，代之，只能沿着这些软弱面继续运动，因为微量元素沿着这些软弱面迁移毫不例外地比相邻的结构相对完整的固体单元有效得多（扩散系数可差好几个数量级）。

另一方面，所谓"无限深"的扩散陷井又是分层的。根据前人的实验和理论计算，多数金属元素在结构完整的块状固体和水溶液中的扩散系数分别是10^{-14}至10^{-18}量级和$10^{-5}\text{cm}^2\text{sec}^{-1}$量级。沿着软弱面的扩散系数应该在块状固体和水溶液这两个极端之间，并在很大程度上取决于扩散陷井的等级和是否有水溶液充填。在每个特定的层次上，纵横交错的扩散陷井和被它们所分割的固体单元形似一个精致的镶嵌图案。这种图案具有结构自相似性，因而是一种分形结构。级别低的扩散陷井（如亚颗粒或颗粒边界）可以变成级别更高的固体单元（如由微细裂隙所限定的岩石部分）的内部。本文所定义的多层次扩散陷井镶嵌结构就是用来表征这种由不同等级组成的镶嵌图案的。它能够说明一些成矿元素，特别是金从地层中活化或扩散出来的基本原理。

多层次扩散陷井镶嵌模型表明，微量元素在岩石和各种地质块体中存在两种迁移倾向。一是倾向于从块状固体单元内部和级别低的陷井中往级别高的陷井迁移。具体路径是从矿物颗粒、亚颗粒内部—> 颗粒边界 —> 显微裂隙 —>…—>到充满

流体的大断裂。微量元素的另一个迁移倾向则是从高温区域到低温区域。温度升高和温度梯度增大有助于上述迁移倾向的实现。

扩散是一种重要的元素活化形式。元素的扩散活化常在固体单元和低级别的陷井范围内进行。它本质上是一种发生在矿源岩中的短程、定向质量迁移运动。其路径与多层次扩散陷井镶嵌模型的一致。

共扼地球化学异常现象是区域地球化学封闭体系演化的必然结果。温度分布反差的大地区（如变质中心及其邻域）和大断裂系统是共扼地球化学异常带出现的有益场所。当这些共扼异常带迭加在区域地球化学异常时，对找矿和矿床远景评价具有特殊意义。

四、控矿构造与围岩热液蚀变作用

河台金矿田的矿体分布和产状严格受控于近乎北东向的塑性剪切构造带及与之结合的热液蚀变作用。这些构造带形成于海西—印支期，具有如下特征：

1) 剪切带内部的几何图案与剪切带在空间的分布图案非常相似。从显微镜下观察到地质图分析，特征的图案是菱形格子状构造，即高度变形的构造岩呈网络带状，中间分隔着变形程度较低或甚至未变形的菱形状块体。

2) 构造分布具有明显的分带性。在剪切变形带的中心部，常常发育着糜棱岩，甚至超糜棱岩。往外逐渐过渡为初糜岩和未变形的原岩。

围岩热液蚀变作用在时空上完全与构造岩带相伴随。绿泥石、绢云母、石英、硫化物和铁白云石是主要的蚀变矿物。蚀变岩中的石英可分为三个世代，它们是构造岩前石英、早期热液石英和晚期热液石英。晚期热液石英与硫化物共生。硫化物又可以进一步细分出两代。第一代以中粗粒、自形黄铁矿为特征，第二代以细粒、它形黄铁矿和黄铜矿共生为特征。

金的沉淀是热液蚀变体系中不可分割的一部分。含金蚀变糜棱岩是最主要的矿石类型。有用的工业矿物包括自然金、黄铜矿和黄铁矿，它们呈浸染状分布在矿石中。

在热液蚀变过程中，TiO_2是一个保守组分。因此，TiO_2正规化值可以用来度量其他元素的带入或带出程度。依据蚀变和未蚀变岩石的化学成分所进行的质量平衡计算表明，热液蚀变作用导致围岩质量的净增加，增加的平均质量系数是 1：0.92。这种质量增加在以黄铜、黄铁矿化为特征的强烈热液蚀变带达到最大值（平均质量系数为1：0.84）。

被带入的组份包括SiO_2和亲硫元素Bi、Cu、Hg、Sb、Te、Zn、Co、(Se)等。但Na_2O和大部分亲石元素（华南基底的特征异常组合），如Cs、Hf、Zr、Nb、Sc、Th、Ba和REE等，属于迁出组份。

矿石（含金蚀变糜棱岩）的球粒陨石化稀土元素配分模式与未被蚀变的赋矿地层基本一致，但位置已稍稍下移。相反，矿区内的蚀变花岗质伟晶岩脉具有完全不同的稀土元素配分模式，且稀土总量非常低。

五、流体包裹体地球化学

在河台金矿床里，与矿化作用有关的热液流体包裹体可分为三个组：a) 低盐度（约1.5-6%重量等值NaCl）的H_2O-CO_2包裹体；b) 中盐度（6-14%重量等值NaCl）水溶液包裹体；c) 富CO_2包裹体。三组包裹体的形成具有同时性。

各种盐度的包裹体具有一致的均一化温度范围，主要分布在130°-310°C之间。在245°和170°C附近分别出现两个明显的频率峰。根据计算，流体包裹体在捕获时的围压近似在500-1700巴之间。

低盐度的H_2O-CO_2包裹体本质上是一个以$H_2O-NaCl-CO_2$为主的热水化学体系。它们代表了原始的成矿热液。

中等盐度的水溶液包裹体和几乎不含盐的富CO_2包裹体的形成与原始成矿热液的不混溶作用和CO_2发泡作用有关。低盐度的原始成矿溶液在上升期间，由于压力的突然释放或温度的突然下降，可以发生不混溶现象，结果造成大部分CO_2分离形成富CO_2的流体相，而NaCl等盐类物质残余下来，在被捕获后形成中等盐度的水溶液包裹体。

六、矿床形成机理

河台金矿田是多元地质地球化学过程演化的产物。沉积作用、区域变质作用、花岗岩浆作用、构造作用及后期热液活动都分别在该矿田矿床的形成过程中起了一定的作用。

微量元素、稀土元素和同位素的证据表明，震旦系和寒武系地层是主要的金源层。对金源层中热水成因硅岩的研究进一步建议了，金的初步沉积富集可能与古地热系热水活动有关。

在加里东期间，由于受区域变质作用的影响，矿源层中的金曾被活化和转移。当时存在着两个基本的迁移方向。一是从矿源岩固体单元或成岩矿物中迁出，向各种软弱面（如颗粒界面，微裂隙等）转移。另一个基本方向是从高温区域迁出，向相对低温地带转移。

海西 — 印支期是金矿化的主要阶段。该期的构造岩带和与之紧密结合的围岩热液蚀变作用严格控制了金矿床的定位。金的沉淀与黄铁矿化、黄铜矿化关系最为密切。温度下降、压力的突然释放及由此引起的原始低盐度含CO_2成矿溶液不混溶作用是金从热液中析出的主要诱发因素。热液与围岩中的铁反应可能也是一个重要因素。依据矿相分析，金的沉淀在第二世代硫化物形成期间达到最高峰。

云楼岗和伍村花岗岩不是主要的金源，但它们所对应的岩浆作用已为成矿热水溶液的形成和循环提供了必要的驱动力 —— 热源。热水溶液可能主要是大气降水和变质水的混合。